

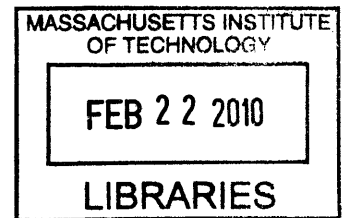
# Time-Variied Daylighting Performance to Enable a Goal-Driven Design Process

by

Siân Alexandra Kleindienst

B.A. Physics (2003)  
Harvard University

M.S. Building Technology (2006)  
Massachusetts Institute of Technology



Submitted to the Department of Architecture  
In Partial Fulfillment of the Requirements for the Degree of

DOCTOR OF PHILOSOPHY IN ARCHITECTURE: BUILDING TECHNOLOGY  
at the  
MASSACHUSETTS INSTITUTE OF TECHNOLOGY

February 2010

**ARCHIVES**

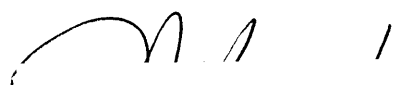
© 2010 Siân A. Kleindienst. All rights reserved.

The author hereby grants to MIT permission to reproduce  
and to distribute publicly paper and electronic  
copies of this thesis document on whole or in part  
in any medium now known or hereafter created.


Author: \_\_\_\_\_

Building Technology Program  
January 8<sup>th</sup>, 2010

Certified by: \_\_\_\_\_

  
Marilyn Andersen  
Associate Professor of Building Technology  
Thesis Supervisor

Accepted by: \_\_\_\_\_

  
Julian Beinart  
Professor of Architecture  
Chairman, Committee for Graduate Students





Thesis Supervisor.....  
Marilyne Andersen  
Associate Professor of Building Technology  
Department of Architecture, MIT

Thesis Reader.....  
Leslie K. Norford  
Professor of Building Technology  
Department of Architecture, MIT

Thesis Reader.....  
Christoph Reinhart  
Associate Professor of Architectural Technology  
Graduate School of Design, Harvard



# Time-Variied Daylighting Performance to Enable a Goal-Driven Design Process

by

Siân A. Kleindienst

Submitted to the Department of Architecture on January 8<sup>th</sup>, 2010  
in Partial Fulfillment of the Requirements of the Degree of  
Doctor of Philosophy in Architecture: Building Technology

## ABSTRACT

Due to the overwhelming number of decisions to be made during early stage design, there is a need for intuitive methods to communicate data so that it is quickly and easily understood by the designer. In daylighting analysis, research has been moving towards dynamic daylighting metrics, which include both annual performance indicators and local climate conditions. Temporally-based graphics are one method of annual data display which shows great promise for use in the early design stage. Not only can temporal data be easily connected to time-dependent environmental variables like weather and solar angle, but non-spatial quantities related to solar heat gain can be compared on the same terms with spatial quantities like illuminance.

This thesis demonstrates methods for quickly calculating annual data sets for which temporal maps are the intended display format. Metrics are then developed in order to display goal-based performance information for an entire area of interest on a single temporal map. This process is demonstrated first by reducing the number of simulations necessary to produce reliable annual illuminance data, the results of which are compiled into a metric based on a user-given illuminance range, known as Acceptable Illuminance Extent (AIE). Similarly, a geometry-based glare approximation method is developed and validated for quick annual calculations of Daylight Glare Probability, and the results are condensed to a single number representative of glare perception within the model, known as Glare Avoidance Extent (GAE). Finally, a simple solar heat gain indicator is demonstrated using the Balance Point calculation method and the metric Solar Heat Scarcity/Surplus (SHS) is used to convey the urgency of allowing more direct solar gain or shading it.

This thesis is part of the Lightsolve project, which aims to specifically address the needs of the architect during early design stages. Specifically, Lightsolve aims to produce fast, unique design analyses, based on local annual climate data with reasonably accurate and intuitive outputs to promote good decision-making. Such resources could enable a desirable shift in schematic stage design practices and move daylighting analysis one step closer to achieving "best practice" recognition.

Thesis Supervisor: Marilyne Andersen

Title: Associate Professor of Building Technology

# Acknowledgements

The work in this thesis was accomplished as all large projects are: by learning from those who preceded me and by the unending patience and support of family and friends.

In particular I would like to thank Marilyne Andersen for her excellent advice, guidance, understanding, and sense of humor. I would like to thank Les Norford and Christoph Reinhart for their advice (and helpful criticisms), and I would especially like to acknowledge Les Norford for his help in during development of the Solar Heat Scarcity/Surplus metric. I would also like to thank Jan Wienold for conversations and advice regarding his work with *evalglare* and the Daylight Glare Probability metric.

I would like to thank the MIT Department of Architecture Building Technology Program and the Martin Family fellowship for funding this work, and Google for providing brief educational SketchUp licenses to those who tested it.

I would like to thank Angela Watson for allowing us to use her studio as the first test of Lightsolve, and all those students who have given us feedback on early versions of the software. I would like to thank Les Norford and John Ochsendorf for allowing me to give a survey in their classes.

Finally, I would like to thank all of my friends and family. I would especially like to thank Jaime for her heroic dealings with Lightsolve issues, Stephen and Nick for their understanding, David for enabling an obsession with tea, and everyone else in the Building Technology Lab. I would like to thank my Ashdown family – you know who you are – for providing an enjoyable and somewhat balanced social life. Last but far from least, I would like to thank my parents, sister, and Evan for their love and support.

# Table of Contents

<b>1 Introduction</b>	<b>10</b>
1.1 Motivating Daylight in Design	10
1.2 Problem Statement	11
1.3 The Lightsolve Concept	14
<b>2 State of the Art</b>	<b>16</b>
2.1 Lighting Metrics	16
2.1.1 Quantity Metrics	16
2.1.2 Existing Annual Illuminance Calculations	18
2.1.3 Light Contrast Metrics	20
2.1.4 Daylight Glare Probability	21
2.1.5 Existing Annual Glare Calculations	23
2.1.6 Solar Heat Gain	24
2.2 Graphical Displays of Numerical Information	25
2.3 Existing Solutions for Early-Stage Analysis	28
2.3.1 Allowed Model Complexity	28
2.3.2 Sky Luminance Distribution	30
2.3.3 Calculation and Simulation	31
2.3.4 Annual Calculations and Metrics	33
2.3.5 Light Quantity, Glare, and Heat Gain	33
2.3.6 Goal-based Performance Metrics	34
2.3.7 Visualizations	34
2.3.8 Summary of Existing Solutions	35
<b>3 Simulation Reduction for Temporal Graphics</b>	<b>38</b>
3.1 Data Reduction Methodology	39
3.1.1 Representative Annual Periods	40
3.1.2 Sky Models Choice and Discussion	42
3.2 Validation of Data Reduction Method	44
3.3 External Sky and Weather Variability Test	45
3.3.1 Temporal Map Visual Similarities	47
3.3.2 Numerical Pixel-Based Comparison	50
3.4 Interior Illuminance Test for Simple Geometry	53
3.4.1 Temporal Map Visual Similarities	54
3.4.2 Numerical Pixel Comparison	55
3.5 Interior Illuminance Data for Complex Geometry	58
3.6 Summary of Data Reduction Method	62

<b>4</b>	<b>Acceptable Illuminance Extent</b>	<b>63</b>
4.1	Definition of a Temporal Illuminance Metric	64
4.2	Temporal Map Visual Similarities using Acceptable Illuminance Extent	66
4.2.1	Simple Geometry Case	66
4.2.2	Classroom Iterations Case	69
4.2.3	Complex Geometry Case	71
4.3	Summary of New Temporal Illuminance Metric	71
<b>5</b>	<b>Glare Avoidance Extent</b>	<b>73</b>
5.1	Daylight Glare Probability in Depth	73
5.2	Deriving a Model-Based DGP Approximation	76
5.3	Glare Simulation Parameters	79
5.4	Validation of Model-Based DPG Approximation	81
5.4.1	Vertical Windows Classroom Case	81
5.4.2	Skylights Classroom Case	83
5.4.3	Cases Involving Contrast Glare	84
5.5	Definition of a Temporal Glare Metric	87
5.6	Visual Comparisons using Glare Avoidance Extent	88
5.6.1	Classroom Model Comparisons	88
5.6.2	Frame Model Comparisons	90
5.7	Summary of New Temporal Glare Metric	90
<b>6</b>	<b>Solar Heat Surplus and Scarcity</b>	<b>93</b>
6.1	Balance Point Method	93
6.2	User Inputs and Defaults for Balance Point Analysis	96
6.3	Definition of a Temporal Solar Energy Metric	97
6.4	Solar Heat Surplus/Scarcity Feasibility Study	100
6.4.1	Comparison of Daily Total Loads	102
6.4.2	Visualizing Solar Heat Scarcity/Surplus	108
6.5	An Alternate Daily Totals Visualization	112
6.5	Summary of New Solar Energy Metric	112
<b>7</b>	<b>Temporal Maps and Design Analysis</b>	<b>114</b>
7.1	Iterative Example of Improving Illuminance Performance	114
7.2	Spatial and Temporal Analysis	118
7.2.1	Classroom Example	118
7.2.2	Hospital Room Example	122
7.2.3	Church of Light Example	124
7.2.4	Combining Temporal Maps with Renderings	125
7.3	Analyzing Options Using All New Metrics	127
7.4	Daylight Analysis Surveys	130
7.4.1	Survey Results	131

7.4.2 Survey Discussion .....	132
7.5 Design Analysis Summary .....	134
<b>8 Conclusion .....</b>	<b>135</b>
8.1 Main Achievements .....	135
8.2 Applications .....	137
8.3 Future Work .....	138
<b>9 References .....</b>	<b>140</b>
<b>Appendix A .....</b>	<b>153</b>
<b>Appendix B .....</b>	<b>154</b>
<b>Appendix C .....</b>	<b>155</b>
<b>Appendix D .....</b>	<b>157</b>

# Chapter 1

## Introduction

### 1.1 Motivating Daylight in Design

*Architecture is the learned game, correct and magnificent, of forms assembled in the light. ~ Le Corbusier*

Throughout history, natural light has played a large role in the shaping of buildings. From dramatic stained-glass cathedral windows (such as in Figure 1-1) pushing the surrounding stone structures towards slimmer efficiency, to utilitarian ties between window height and room depth, light has acted both as an artistic medium and a design constraint. In England, the importance of daylight has been recognized legally for over a century. A building's "right to light" (otherwise known as "ancient lights") can prevent a new construction which would block light-access of another building – provided that light access has existed for twenty years – and is granted under the Prescription Act of 1832 [Act, 1832; Chynoweth, 2004]. Access to both light and view also has a social status, which can be seen in the desirability of the penthouse apartment or the corner office [Leslie, 2003]. Furthermore, daylight is the near black-body standard to which we compare the spectral quality of certain color temperatures of artificial light using the Color Rendering Index.

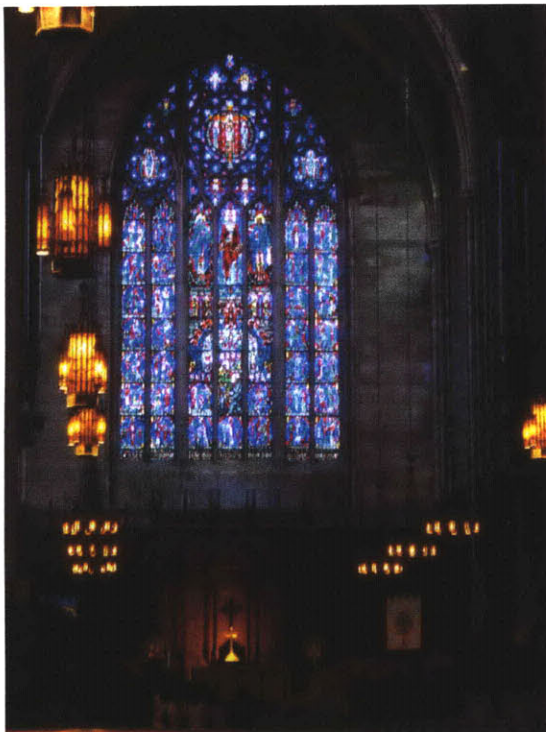


**Figure 1-1. Light in worship: stained glass in the Princeton University Chapel (photograph by author).**

More recently, the health benefits of daylight have gained wider acceptance. We now recognize that lack of light in the daylight spectrum can cause lower serotonin levels, contributing to Seasonal Affective Disorder and depression [Levitt *et al.*, 2002; Lambert *et al.*, 2002]. Similarly, it takes a large amount of light in the blue and violet range (high frequency) to promote daytime alertness and reset the endogenous circadian rhythm, which both contribute to hormonal balance and illness recovery [Rea *et al.*, 2002; Cajochen *et al.*, 2000; Joseph, 2006; Pechacek, 2008]. One Swedish study of hormones in school children linked healthy levels to daylight [Küller & Lindsten, 1992], and a very famous, although debated, study by the Heschong Mahone Group attributed higher grades to daylit schools and higher sales to daylit stores [Heschong *et al.*, 1999; Boyce, 2004].

On the energy side, the Department of Energy estimates that electric lighting



consumes 38% of electricity used in US commercial buildings [DOE-EIA, 2008], and that doesn't account for the cooling load generated by active light bulbs. Proper daylighting can offset a significant fraction of that energy demand, and well-controlled solar gains can positively impact the heating and cooling demands [Li & Lam, 2001; Bodart & De Herde, 2002; Nicklas & Bailey, 1996].

The motivations for good daylighting design are numerous and compelling, ranging from aesthetics to health to energy, but creating a good daylighting design is not always straightforward. The quantity, color, diffusivity, and angle of natural light change with latitude, weather, building orientation, and time of day. Although both old and new rules of thumb exist for rectangular rooms with windows on one wall [IESNA, 2000; Reinhart, 2005a], more complex needs and building forms require more complex modeling.

## **1.2 Problem Statement**

The quality and quantity of daylight available in an architectural space depends on a three part process: collection, transportation, and distribution. These steps are contained in the simplicity of a window and the complexity of a tracking heliostat system, and every design choice has a different level of impact on these three aspects of daylighting. Decisions that impact daylight access and collection are usually very influential because it is, metaphorically, the first link in the chain. These include choices made about building orientation, form, and exterior shading, and on a lesser level, window area and complex façade systems. Decisions impacting daylight transport might include wall thickness, glazing type, complex façade systems, reflector systems, and light ducts, and daylight distribution is affected mainly by window positions, interior geometry, interior reflectivity, and interior shading. Design features which have the greatest impact – orientation, form, and space distribution – are all governed by choices made in the earliest or schematic stages of design. It may be impractical for an expert to be called in at this stage, due to tight schedules or financial constraints, and therefore it often falls to architects to make the decisions that have the greatest effect on daylighting.

Unfortunately, as several recent surveys have revealed, daylighting design explorations do not often happen during schematic design. Two of these surveys were given by the National Research Council (NRC) of Canada and less comprehensive one by a Harvard design student, which was administered a few months after the second NRC survey [Reinhart & Fitz, 2004; Reinhart & Fitz, 2006; Galasiu & Reinhart, 2008; Lawrence, 2005]. Although each survey had a different participant group – the NRC queried members of software mailing lists in one survey and practitioners interested in sustainable design in the other, while the Harvard survey targeted students and practitioners in the Boston area who had no obvious bias for or against daylighting software – each survey found similar trends. Although both NRC surveys found daylighting software use to be around 75% among architects, both also found that tools were largely used in design development or later stages [Reinhart & Fitz, 2004; Reinhart & Fitz, 2006; Galasiu & Reinhart, 2008]. The earlier NRC survey drew this conclusion because the majority of users reported using tools to resize windows and shading systems and to prove code compliance. The later survey asked directly and found that less than 50% of designers who use software tools use it during schematic design. In that survey, “prior experience” and “rules of thumb” were the more popular choices during schematic design at just under 80% and 60% respectively [Galasiu & Reinhart,

2008]. In Lawrence's less specific group of participants, over one third did not use daylight design tools of any kind. In fact, only 22% of Lawrence's participants used 3D modeling software (not necessarily daylight-specific) in the schematic design exploration, preferring to use hand drawings and physical models [Lawrence, 2005].

There may be many reasons why software tools are not used in the earliest stages of design. Reasons given in the later NRC survey included lack of software experience, client not paying for it, and lack of time, although a conviction that experience and rules of thumb are sufficient for early decision can also be implied [Galasiu & Reinhart, 2008]. Another culprit could be the lack of exposure in architectural education. A survey given by Sarawgi in 2006 to educators at American accredited architectural schools revealed that "computer software packages" was the least used method for teaching lighting design [Sarawgi, 2006]. The other choices were "rules of thumb", "manual calculation methods", "manufacturer's literature", and "scale physical models", all of which were more popular. Unfortunately, simple calculations are inaccurate at best and only really work with box-like spaces. Physical models can vary widely in accuracy, depending on the care given to detail and the choice of light source [Thanachareonkit *et al.*, 2005], and any model flexibility must be designed in from the start. Furthermore, the latter NRC survey found most architects' rules of thumb to be non-standard and home-grown [Galasiu & Reinhart, 2008], and while prior experience is useful for developing intuition, it cannot be used as a proof of concept for new designs, and it does not always translate well between different climates. "Prior experience" is also limited to the collective lighting experience of the design team, which could be extensive or limited depending on those involved. For these reasons, and to meet the growing interest in good daylighting, there needs to be a shift in the accepted exploration techniques in the earliest stages of design.

Since current popular rules of thumb and simplified analytic methods are of variable accuracy or are non-transferable to new situations, more useful methods, including appropriate computer simulation tools, should be given greater prominence in the schematic toolbox. Architects need the resources to produce fast, unique design analyses, based on local annual climate data with reasonably accurate and intuitive outputs to promote good decision-making.

In early-stage daylighting analysis, speed is of the utmost importance, or there is no chance for exploration, iteration, and comparison. This means that defining a model and performing calculations in any medium should be relatively quick, and that resulting data should be easily understood by the user. In the case of computer simulation, although hardware is constantly improving, making design truly iterative may still require shortening the computation time. It also makes sense to focus on improvements to modeling and intuitive data outputs.

The goal of schematic analysis is for the designer to acquire all data necessary to make decisions. Because this stage is one of seemingly infinite possibility, the amount and breadth of data involved necessary to understand "the factual constraints, without unduly restricting the designer's freedom, and without prejudicing the solution" can seem overwhelming [Koenigsberger *et al.*, 1975]. Koenigsberger *et al.* state the problem very succinctly:

*In the synthesis, the designer must consider a wide range of factors simultaneously. The capacity of his mind is limited. It is therefore*

*essential to present the information in a readily comprehensible form. It should not be excessively detailed, but it should still take into account all that is relevant [Koenigsberger et al., 1975].*

Herbert Simon also describes the limits of memory in the context of pattern recognition and design process in his book *The Sciences of the Artificial*. The “bottleneck”, as he puts it, is in the short-term memory required to hold all information simultaneously while a solution can be synthesized from the disparate pieces [Simon, 1969]. Both books suggest that mental processing time can be improved if the data is pre-processed or otherwise arranged. Simon points out the benefits of grouping information into associative “chunks” while Koenigsberger *et al.* suggest data can be conveyed in the form of performance specifications [Simon, 1969; Koenigsberger *et al.*, 1975].

The main questions involved in creating a design analysis process for the earliest stage of design are therefore:

- 1) What daylighting information is necessary for informed design decisions?
- 2) How can that information be calculated quickly, but with reasonable accuracy?
- 3) How, if at all, should that information be pre-processed for the designer?
- 4) What output formats should be used to convey the information?
- 5) What metrics are appropriate for those output formats?

There is not always a consensus regarding which daylighting information is “necessary” to make informed design decisions, but research has been moving towards dynamic daylighting metrics which include both annual performance indicators and local climate conditions. Daylight Autonomy (DA) [Reinhart & Walkenhorst, 2001] and Useful Daylight Illuminance (UDI) [Mardaljevic & Nabil, 2006; Mardaljevic, 2009], are existing metrics which use annual climate data to find the percentage of time that a sensor point is above or between given illuminance benchmarks. Another direction research has taken is graphing data as it changes over time, often together with spatial data. One benefit of a time-based graph is the implicit correlation to solar angle and climate, which, for each location, are dependant on time of day and year. These environmentally based variables have a large impact on design orientations, window size, and basic form, which are all important aspects of daylight access, as discussed above. Mardaljevic and Glaser have separately published papers on temporal and spatial graphics, which will be discussed at greater length in Chapter 2 [Mardaljevic, 2001; Glaser & Ubbelohde, 2001].

Regarding what *kind* of information should be given in annual data sets, the performance of daylight can be quantified in three main ways: the quantity of light on a surface (such as illuminance), the contrast caused by neighboring luminous sources (of which glare is the negative result), and the solar heat gain associated with light penetration. Because these aspects of performance can often be conflicting, it’s essential to convey each kind of information in the same format so that the benefits and tradeoffs are easily comparable. This can be accomplished using a temporal graphic format so that non-spatial quantities like solar heat gain may be compared with more spatially oriented performance data like illuminance. The comparability of different data types can also be enhanced by using similar goal-based metrics to convey each quantity.

Goal-based metrics can also help reduce the data interpretation and synthesis required by the user. Dynamic data sets involving both temporal and spatial data are by nature very large. The greatest challenge involved in producing such an immense quantity of

information is the problem of transferring it to designers without overwhelming them, as discussed above. Some of this difficulty can be alleviated if the data is given, not as pure numbers, but as a relationship between the calculated data and the user's design goals. Goal-driven metrics could show the varying success of a certain design rather than numerical results, which would reduce the time needed to interpret the data. Furthermore, goal-driven results can be compiled over either time or space to reduce the number of graphs required to convey the same results.

This thesis demonstrates methods for quickly calculating annual data sets for which temporal maps are the intended display format. Metrics are then developed in order to display goal-based performance information for an entire area of interest on a single temporal map. This process is demonstrated first in Chapter 3 by reducing the number of simulations necessary to produce reliable annual illuminance data, the results of which are compiled in Chapter 4 into a new metric based on a user-given illuminance range, known as Acceptable Illuminance Extent (AIE). Similarly, in Chapter 5, a geometry-based glare approximation method is developed and validated for quick annual calculations of Daylight Glare Probability, and the results are condensed to a single number representative of overall glare perception within the model, introduced as Glare Avoidance Extent (GAE). In Chapter 6, a simple solar heat gain indicator is demonstrated using the Balance Point calculation method, and a new metric called Solar Heat Scarcity/Surplus (SHS) is used to convey the urgency of allowing more direct solar gain or shading it. Finally, in Chapter 7, several examples are used to demonstrate the conclusions which can be drawn from temporal graphics and the new metric forms described above. The chapter concludes with the results of a small user survey given to a group of students in the architecture department of the Massachusetts Institute of Technology.

One important note is that the simulations in this thesis do not involve models of occupant behavior regarding blinds control. Large energy impacts (and certainly lighting impacts) can be attributed to the predicted use of blinds [Bourgeois *et al.*, 2006], however there is also a school of thought which suggests "that a design evaluation should always begin with the intrinsic daylighting performance of the space, and only then should the simulations be repeated with behavioral models added" [Mardaljevic *et al.*, 2009]. In the development of an analysis for the earliest stages of design, this thesis focuses on the building daylight potential, rather than simulations including probabilistic occupant behavior models.

### **1.3 The Lightsolve Concept**

This thesis is part of the Lightsolve project, which was initiated with the object of meeting the needs described in the previous section while promoting a greater understanding of daylighting strategies [Andersen *et al.*, 2008]. The current version of Lightsolve acts as a plug-in to SketchUp, receiving geometric and material files from that program and producing data and renderings with an in-house radiosity engine [Cutler *et al.*, 2007]. Annual results – which take local climate conditions into account – are presented graphically along side renderings on a highly visual GUI, designed for architects by architects [Yi, 2008; Seaton, 2009].

The data outputs of Lightsolve will be graphical in format, due not only to the general appeal of visual information (and the increased appeal for architects), but because graphics can display trends and patterns in data more succinctly and intuitively than numerical outputs [Tuft, 1983]. Lightsolve aims to produce fast, unique design analyses, based on local annual climate data with reasonably accurate and intuitive outputs to promote good decision-making. Such resources could enable a desirable shift in schematic stage design practices and move daylighting analysis one step closer to achieving “best practice” recognition.

# Chapter 2

## State of the Art

### 2.1 Lighting Metrics

Good daylighting is not easily quantifiable. There are too many variables to consider, and judging some of them can be a highly subjective process. However, most light measurements can be considered from one of three perspectives: measurements of light quantity, measurements of light contrast, and measurements of the heat gain associated with light.

#### 2.1.1 Quantity Metrics

Light quantity measurements are the most numerically quantifiable ways to judge lighting performance, which also makes them the most commonly used. Illuminance, a physical measurement of incident luminous flux per area, is the most ubiquitous of these and it is the metric around which many other quantity metrics are based – for instance, building codes and recommendations are nearly always in terms of illuminance on the work plane or important surfaces [IESNA, 2000]. Luminance, a physical measurement of luminous flux emitted per area per solid angle, is another common quantity measurement, but the metrics based on luminance generally fall into the light contrast category. Both illuminance and luminance are photometric measurements, meaning that they are energy values that have been weighted according to the spectral sensitivity of the eye [CIE, 1926].

Because illuminance is an objective quantity, it can be difficult to use it to judge the architectural use of daylight. Sunlight and skylight are highly variable in intensity, diffusivity, color, and direction of incidence, and because our eye is a very adaptive sensor, there is a range of possibilities that could be determined “successful”, which could adjust according to the situation. Therefore, other metrics have been developed which convert illuminance values to something which relates more specifically to the architectural use of daylight.

The Daylight Factor (DF) has been in existence through most of the 20<sup>th</sup> century, although it evolved greatly over time. Its modern form consists of a sum of three components: the direct component, the externally reflected component, and the internally reflected component. The direct component, originally the only one considered, started purely as a measure of the fraction of the sky vault visible from the window. It was also sometimes called “sky factor,” and that term is still used today when describing this sky vault view [Wu & Ng, 2003]. This direct component went through several iterations of correction factors for CIE overcast sky luminance distribution, glass transmittance, and other factors [Collins, 1984], until it was put in its final form in 1968 by J. A. Lynes, who added weighting corrections based on the measurement position in a rectangular room [Lynes, 1968]. The externally reflected component, like the direct component, was calculated by angular view, and then divided by 5, under the assumption that the ground and all building materials have an average reflectance factor of 20% [Collins, 1984]. For the internally reflection component, there was no good

calculation until Hopkinson, *et al.*, published what they called the “split-flux method” in 1954. This method divides the light flux entering a rectangular room into two parts: one seen by the upper part of the room and affected by the average reflectance factors from the higher spaces, and one seen by the lower part of the room and affected by the reflectance factors of the floor and lower walls [Hopkins *et al.*, 1966]. All together, these three components add to produce the total daylight factor, which is defined, for any point in a space, as the fraction of the illuminance that one would receive on a horizontal plane under an unobstructed view of a CIE overcast sky.

The Daylight Factor has been the dominant method of analyzing daylight for the better part of a century. It analyzes the geometry of a building without reference to location, orientation, or weather, but these characteristics are seen more as a weakness than a strength. In his 1968 book *Principals of Natural Lighting*, Lynes notes that DF only applies “when the *pattern* of sky luminance is static... The use of daylight factors is therefore restricted in practice to solidly overcast weather,” [Lynes, 1968]. Then in 1980, Tregenza’s study of the internal illuminances of several models found DF to be unreliable under real skies. This was mainly because the CIE overcast sky distribution is idealized and uncommon [Tregenza, 1980]. More recently, Reinhart did a study in which several daylight analysis methods were compared, and his data shows DF often vastly underestimated the illuminance values in comparison with other analysis tools [Reinhart & Herkel, 2000]. Mardaljevic also published a paper which compared standard daylight factors to those measured in life. He found that the standard DF tended to underestimate the real DF by at least 20% (and in many cases as much as 40-77%) [Mardaljevic, 2004]. One of the primary reasons given for this discrepancy was again the difference between the CIE overcast sky and real skies. In essence, DF is an idealized worst-case scenario, and its application promotes the design of fully-glazed buildings [Reinhart *et al.*, 2006]. The use of only overcast skies also precludes any mechanism for studying automatic or occupant shading control.

Because DF represents only one rather uncommon sky possibility, Mardaljevic, Reinhart, and other experts are now advocating metrics which takes into account weather, statistical realistic skies, location, and building occupancy over the period of a full year. Both men developed similar dynamic metrics at approximately the same time in Europe and North America respectively. Mardaljevic tackled the problem by doing a set of hourly illuminance simulations, and graphing illuminance ranges every 50 lux against the frequency of occurrence in that range. This approach is called “Annual Daylight Profiles (ADP), and each graph represents the information from a single sensor [Mardaljevic, 2000]. Reinhart’s method involves finding illuminance data at various points hourly, or even sub-hourly, and finding the percent of yearly occupied hours when the illuminance is above a user-defined threshold [Reinhart & Walkenhorst, 2001; Walkenhorst *et al.*, 2002]. This became known as Daylight Autonomy (DA), since it represented the percent of time when a building was autonomous from electric lighting. A few years later, Nabil and Mardaljevic introduced the idea of Useful Daylight Illuminance (UDI), which is similar to daylight autonomy, except it uses a pre-defined illuminance range of 100 to 2500 lux (the original range was 100 to 2000 lux) to find the percent autonomy instead of a user-defined lower threshold [Nabil & Mardaljevic, 2005; Nabil & Mardaljevic, 2006; Mardaljevic, 2009]. UDI takes into account the times when lighting is too high, but lacks the flexibility of DA to conform to a designer’s specific goals.



Daylight Autonomy has gained some acceptance in North America. Most notably, the California High Performance Schools program (CHPS) uses Daylight Autonomy to judge the success of a daylighting design [Rogers, 2006]. During the development of daylighting strategies for that program, Rogers created a modified version of DA which gives partial credit for illuminances below the threshold, and called it Continuous Daylight Autonomy [Rogers, 2006]. Along with this modified daylight autonomy, Rogers suggests calculating the Maximum Daylight Autonomy, which he sets the DA threshold to ten times the design illuminance threshold. This number is meant, like UDI, to indicate possible glare situations when lighting levels are too high. Similarly, changes have been suggested for UDI which would divide the range into two parts – the illuminances between 100 and 500 lux would represent “supplementary” UDI (meaning that supplementary electric lighting might be necessary), and those between 500 and 2500 lux would represent “autonomous” UDI [Nabil & Mardaljevic, 2006; Mardaljevic, 2009]. Reinhart, Mardaljevic, and Rogers co-wrote a paper comparing Daylight Autonomy, Continuous Daylight Autonomy, and Useful Daylight Illuminance with Daylight Factor. For every design scenario tested, which included variations of shading type and user control, DF merely supported the design letting in the most light, whereas the dynamic metrics disagreed with DF, were more nuanced in their conclusions, and generally agreed with each other [Reinhart *et al.*, 2006].

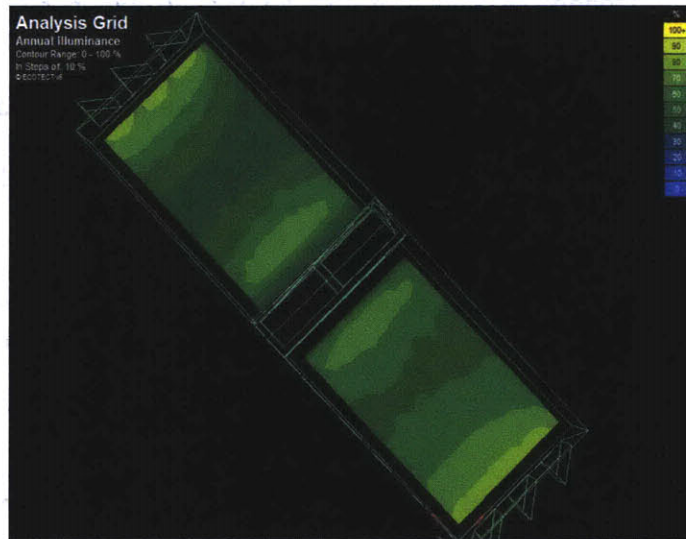
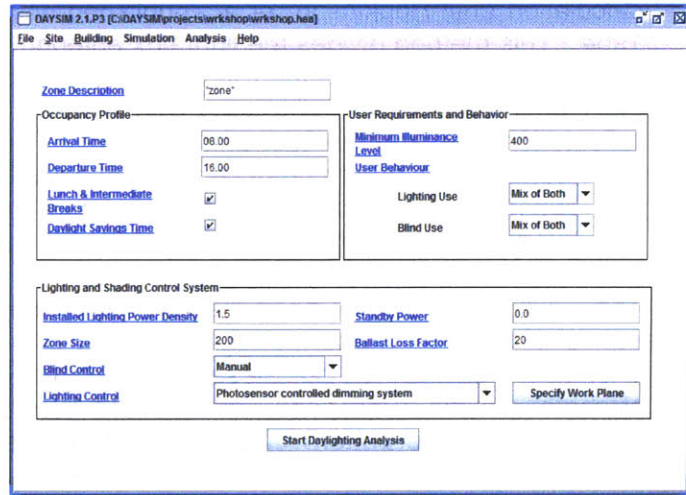


**Figure 2-1. Screenshot of Daysim analysis interface (above) and Daylight Autonomy on a workplane (below), as visualized through Ecotect.**

### 2.1.2 Existing Annual Illuminance Calculations

Dynamic metrics requiring annual data sets, like DA or UDI, can be calculated by brute force repetition of illuminance calculations, however the sheer number of iterations needed for an accurate data set makes this method prohibitively time-intensive. Therefore, Daysim, a program written for the sole purpose of calculating DA [Walkenhorst *et al.*, 2002], uses daylight coefficients to aid its calculations. Proposed by Tregenza and Waters in 1983, this method assigns to each “sensor” location a



coefficient, or weight, dependent upon room geometry, reflectivity, sky visibility, etc, similarly to the concept of daylight factor [Tregenza & Waters, 1983]. Unlike DF, however, these coefficients can take small changes in each angular segment of the sky into account. After the daylight coefficients are calculated for a particular model, the sky can be defined by any brightness and luminance distribution, and each additional moment is merely one more set of weighted sums rather than a time-intensive simulation. Mardaljevic suggested a daylight coefficient method based on 145 diffuse sky patches (as was Tregenza's), but also on 100,366 direct sun positions and an indirect sun component from each of the 145 diffuse patches [Mardaljevic, 2000]. Daysim uses the Radiance ray-tracing program *rtrace* to calculate daylight coefficients based on 145 different diffuse sky patches, 3 ground segments, and 65 sun positions (sunlight from between these 65 points are extrapolated from the four nearest) [Reinhart & Walkenhorst, 2001; Reinhart, 2005]. A more recent synthesis of both of these ideas, called Dynamic Daylight Simulations or DDS, has been suggested in which daylight coefficients are based again on 145 diffuse sky patches, 2596 direct solar positions (in which the one nearest to the actual sun position is used in each calculation), and also indirect solar calculations from the center of the 145 sky patches, where the indirect contribution is weighted similarly to the direct solar contribution in Daysim [Bourgeois & Reinhart, 2006; Bourgeois *et al.*, 2008].

Another strategy is a method based on "daylight factor" interpolation and originally developed for the energy simulation program DOE-2 [Winkelmann & Selkowitz, 1985]. This method was later adopted for the LBNL daylighting tool DELight (and therefore also Building Design Advisor, which uses the DELight simulation engine) [Hitchcock & Carroll, 2003; LBNL, 2001]. This method finds the daylight factor and clear-sky illuminance ratios (although it also refers to these ratios as "daylight factors") for a pre-determined set of 20 solar positions and then interpolates the illuminance ratios for all hourly points in between. These 20 data points are fixed for all latitudes, so the clear skies created using them are sometimes theoretical rather than realistic. Using the interpolated ratios, this method finds interior illuminances based on the hourly horizontal illuminances from TMY type weather files. The relationship of hourly calculations to a small set of predetermined sun positions recalls the strategies from both Daysim and the DDS discussed above, however the daylight factor interpolation method has far less proven accuracy [Reinhart & Herkel, 2000; Hitchcock & Carroll, 2003].

If less detail is required in the set of annual data, one could try to reduce the possible combinations of sky types and sun positions to a smaller representative set. This was the approach used by Wittkopf *et al.* in their comparative study of anidolic ceilings in Sheffield and Singapore, where they did simulations on the solstices and equinox at five times of day [Wittkopf *et al.*, 2006]. They used a virtual sky dome to try to represent the local climate as closely as possible. This situation, although more advanced, is reminiscent of the common practice of doing illuminance calculations at 9am, noon, and 3pm on the solstices and equinoxes under a clear sky plus one overcast sky simulation. Although it may seem that a range of dates and times is represented, this strategy showcases only the extremes of both sun positions and conditions and is not annually representative.

A more complicated strategy for making a subset of annual calculations was suggested by Herkel at the 1997 IBPSA conference. Herkel's method uses the similarity of 3 factors – direct irradiance, diffuse irradiance, and solar altitude – to separate a series of annual lighting simulations into "bins", reducing thousands of simulation moments to a

few hundred [Herkel, 1997]. But because the objective is only to reduce calculation time, this method discards information such as solar azimuth. Solar azimuth plays a critical role in the internal distribution of daylight and greatly affects the choice of building orientation. This method also precludes the possibility of producing realistic, chronological renderings which might be of use to the designer.

### 2.1.3 Light Contrast Metrics

In measuring both the quality and quantity of light, there are few factors that are more difficult to quantify, more subjective, and yet more important to visual comfort, than glare. There are at least seven recognized glare indexes: British Glare Index, Discomfort Glare Rating, Visual Comfort Probability, CIE Glare Index, Unified Glare Rating, Daylight Glare Index, and Daylight Glare Probability [Hopkinson, 1957; Hopkinson, 1963; Eble-Hankins & Waters, 2004; Rubiño *et al.*, 1994; Nazzal, 2001; Wienold & Chrisoffersen, 2006]. These algorithms are the result of half a century of research involving user studies and simulations of various types of glare sources, although the majority were created in reference to electrically-produced glare sources. For this reason, they work with unequal accuracy for electric and daylight sources [Hopkinson, 1963; Iwata & Tokura, 1998; Nazzal, 2001; Nazzal & Cutarat, 2004], and it has been suggested that it is less practical to use them to predict daylight glare [Österhaus, 2005]. In addition, glare varies with observer position, view direction, and the adaptability of the eye, so it is no wonder that glare calculations are not standard in lighting design tools (see Section 2.3). A commonly adopted glare control analysis in practice is to evaluate it either based on renderings generated for at most one or two viewpoints and a few moments in time, or to not evaluate it at all. As a result, interior blinds are often required after construction. Yet proper control of glare is essential to ensure visual comfort, and some occupants' passive habits – which involves pulling the blinds at the first sign of glare, and then leaving them drawn interminably [Rea, 1984; Reinhart, 2004] – can ruin a daylighting strategy and increase lighting loads [Newsham, 1994; Reinhart, 2004].

Just as most light quantity metrics are based on illuminance, most light contrast metrics are based on luminance, because luminance is what our eye sees. In fact, one can think of the human eye as an organic luminance meter with a pre-defined angular aperture and the ability to adapt to different light levels [Hopkinson, 1957; Jameson & Hurvich 1961]. There is a perceptible range of luminances for every adaptation luminance level, and this range gets more restrictive the closer we get to the center of our visual field. Therefore if the difference between two luminances within our field of view is greater than the range that our eye can handle, we experience a visual discomfort known as “disability glare” [Vos, 2003]. Another form of glare is “discomfort glare”, which is defined generally as “glare that causes discomfort”, although Vos has suggested breaking this further into a new definition of discomfort glare – which would encompass glare that is severe enough to be distracting – and “dazzling glare”, in which there is actually organic, not just visual, discomfort caused by bright light [Vos, 2003].

Despite their differences, most glare metrics agree that quantifying glare depends on some combination or subset of these variables: glare source angular size, glare source luminance, glare source position in viewfield, background luminance, adaptation luminance, and vertical illuminance at the eye. Although research in glare dates back to the first decade of the 20<sup>th</sup> century [Vos, 2003], the first recognizable glare metric came from the research of Hopkinson and Pretherbridge in the 1950's and was later known as

the British Glare Index, or BGI [Hopkinson, 1957; Hopkinson, 1972; Rubiño *et al.*, 1994]. The BGI ranges from 0 to above 30, with 10 representing imperceptible glare and 28 representing intolerable glare. At around the same time, Lukiesh and Guth began studies that would turn into the Discomfort Glare Rating (DGR) and Visual Comfort Probability, or VCP. The DGR was based on Lukiesh's work on glare sensation in the 1920's, and it formed the basis of the VCP, which is defined as the probability that a person will find the visual environment comfortable, and was based on participant studies [Eble-Hankins & Waters, 2004; Rubiño *et al.*, 1994]. All of these metrics were based on point-source glare, and are not easily applicable to large-area glare situations caused by daylight.

The CIE Glare Index, or CGI, was proposed in 1978 by a CIE committee led by Einhorn. It did not attempt to create new human subject studies, but used the current metrics and the information available to create a synthesized metric which would also account for the effect of the glare source on the adaptation level (thus making it better suited to larger area glare sources) [Österhaus, 2005; Eble-Hankins & Waters, 2004]. The next CIE committee decided then to remove the new detailed definition of adaptation level and created a compromise rating in 1995, the Unified Glare Rating (UGR), which was simplified to appeal to a wider audience; it produces results very similar to the BRI [Österhaus, 2005; Eble-Hankins & Waters, 2004]. Like the BRI, the UGR has a scale ranging from 0 to 30 with the same thresholds, and each step in the scale is meant to be a uniform change in glare perception. Another attempt to correct the weaknesses of the original glare equations is known as the Cornell equation or the Daylight Glare Index (DGI). Despite its name, it was formulated with user studies that employed direct and diffuse electric light sources, and has been shown less accurate for actual daylight sources [Wienold & Chrisoffersen, 2006]. There have been more recent suggestions regarding changes to the DGI which involve actual daylight sensor readings, but no further human studies [Nazzal, 2001; Nazzal & Chutarat, 2004]. DGI also uses the scale from 0 to 30.

#### **2.1.4 Daylight Glare Probability**

The latest glare metric to emerge is the only one to date which was formulated from daylight-based human studies, and it is called Daylight Glare Probability, or DGP. Similarly to the VCP, the metric measures the disturbance probability in a general population. However, the metric represents the percent of persons disturbed by (not those comfortable with) the scenario, and it has demonstrated good correlation with human responses to daylight environment [Wienold & Chrisoffersen, 2006; Wienold, 2007]. So far, it is the most promising glare metric for daylighting, since it is the only one based on user response to actual daylight scenarios. It can be calculated using the program *evalglare*, which performs pixel analyses on Radiance renderings to locate and define glare sources. A sample output from *evalglare* is shown in Figure 2-2.

The DGP may also have some weaknesses, however, due to the limited scenarios used to gather the data on which the metric is based. In the study's defense, any user-based equation is necessarily limited by location and available test room facilities, and it would require a great deal of time and money to cover all possibilities. However, the possible biases of the DGP equation must be understood. First, the equation for the DGP has not been validated lower than 20% or higher than 80%. Seen in a qualitative light, this is not much of a limitation, since beyond these limits there is almost no glare or a large

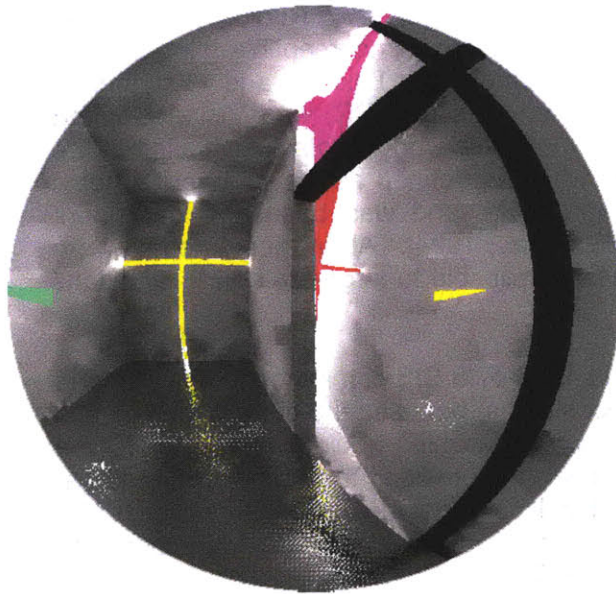


Figure 2-2. Pixel analysis output of a DGP calculation done in the program *evalglare*.

amount of glare, respectively. Also, although the DGP follows the same basic format for contrast glare analysis – all the formulas described above have similarities to the original Glare Index which became the BGI – the DGP has only been validated in moderately sized rooms with unilateral openings and non-extreme light levels. There is a reasonably heavy dependence in the equation on vertical illuminance which might cause the metric to recognize high-illuminance glare more readily than low-illuminance glare caused only by contrast levels. However, if further data sets were later assimilated, the DGP could be either validated for low-illuminance glare situations or modified to account for them. The circumstances of the user tests which resulted in the DGP are listed in Table 2-1, and the DGP itself is discussed in further detail in Chapter 5.

Table 2-1. Characteristics of tests used to develop DGP.

<b>Location</b>	Hoersholm, Denmark	Freiburg, Germany
<b>Latitude</b>	55.86°N	48.01°N
<b>Dimensions</b>	3.5m x 6m x 3m	3.65m x 4.6m x 3m
<b>Floor Reflectance</b>	11%	34%
<b>Wall Reflectance</b>	62%	56%
<b>Ceiling Reflectance</b>	88%	80%
<b>Visual Transmittance</b>	72%	54%
<b>Glass Fraction</b>	25%, 44%, 85%	21%, 45%, 89%
<b>Shading Types</b>	White Venetian Blinds Specular Venetian Blinds Vertical Foil System	White Venetian Blinds Specular Venetian Blinds Vertical Foil System
<b>Blind Tilt</b>	Direct Sun Cutoff, Variable	Direct Sun Cutoff, Variable
<b>Test Times</b>	1hr 45 min long, Variable Start Time	1hr 45 min long, Variable Start Time
<b>Test Dates</b>	Sept 2003 → Dec 2004	Sept 2003 → Dec 2004
<b>Sun Angles</b>	Near perpendicular to Façade, Variable	Near perpendicular to Façade, Variable

### 2.1.5 Existing Annual Glare Calculations

If one desires to determine annual glare potential, the calculation intensity issue becomes an even greater problem than it is for annual illuminance calculation. Glare is based, not only on one's position, but also on the view direction, and that may increase the necessary simulations. Furthermore, simulating a single glare measurement is more time-intensive than calculating illuminance. This is due to the rendering and/or pixel processing required by most full glare analyses. There have been a few attempts to reduce this calculation intensity by approximating various parts of the analysis.

One annual glare calculation technique was developed for DOE-2 in the 1980's. Winkelmann and Selkowitz used internal illuminances and known building geometry to find glare at given reference points using Hopkinson's Glare Index equation (see Appendix X) [Winkelmann & Selkowitz, 1985]. The variables needed to calculate this glare index are background luminance, window luminance, the solid angle of the window as seen from the reference point, and a view-dependant empirical excitation factor which decreases from 1 to 0 the further it is from the middle of the view field [Winkelmann & Selkowitz, 1985]. In this method, the background luminance was found by multiplying an average wall illuminance by the average room reflectance factor, and both the solid angle and excitation factor are based on available room geometry. The only variable left unexplained by the paper is the window luminance. Due to the very quick annual illuminance calculations performed by the same program (see Section 2.1.2), annual glare calculations could also be performed in a matter of seconds [LBNL, 2001]. The method used to calculate annual illuminances, however, has been validated only within 15% of results from the program SuperLite and physical model simulations under artificial CIE clear and overcast skies. Because SuperLite has less demonstrated accuracy than other tools [Ubbelohde, 1998], because most carefully made physical models can produce errors of 20% or more [Cannon-Brookes, 1997; Thanachareonkit *et al.*, 2005], and because parallax and other errors are introduced by using an artificial sky [Mardaljevic, 2002], one must assume that the errors involved in this method could be significantly greater than 15%.

In 1997, Mardaljevic and Lomas used what they called a "brute force" method to analyze the annual glare possibilities for a food court hall in Manchester, England [Mardaljevic & Lomas, 1998]. They were able to reduce the necessary calculations to half by simulating only six months of the year (eliminating duplicate solar positions), after analyzing the local weather file to make sure there were sufficient similarities in cloud cover and brightness between the two halves of the year. They further reduced the computation time by disregarding internal reflections from diffuse sky light, which brought the time for 1,820 simulations down to approximately 22 hours. Although this elimination of internal reflections might have caused errors in background luminance or vertical illuminance in the calculation of any accepted glare metric, they chose instead to profile the size, brightness, and frequency of high luminance patches [Mardaljevic & Lomas, 1998]. The result is similar to the format of Annual Daylight Profiles (discussed in Section 2.1.1).

Most recently, Wienold, the creator of Daylight Glare Probability, has proposed a simplified, linear version of the DGP based only on vertical illuminance, which would allow annual glare simulations in the time it takes to calculate annual illuminance values. This equation, called DGPs, shows remarkable correlation with the DGP in situations where there is both no direct sun hitting the eye/sensor and where the cause of glare is

caused by high vertical illuminances [Wienold, 2007; Wienold 2009]. Situations where glare may be caused by luminance contrasts rather than peak luminances were again less present in the analysis, as the test case was the model of a small office with a large window. Within the last year, Wienold has also proposed integrating DGPs with the program Daysim (a program discussed in Section 2.3) which would benefit from Daysim's quick daylight coefficient-based illuminance calculations and improve DGPs accuracy by adding an analysis of quick and simple renderings [Wienold, 2007; Wienold, 2009].

### 2.1.6 Solar Heat Gain

Solar heat gain is not a measure of "light" as we define it, nor does it have a visual aspect, but light and heat are so tightly tied together that one cannot afford to ignore the thermal consequences of daylighting. Despite the fact that solar gain is an important tradeoff, few lighting simulation programs even mention it. The problem is one of practicality. While it would be reasonably easy to find the energetic solar influx in Watts using current lighting simulation techniques, this number alone could not be used to make design decisions – or even to understand the consequences of the tradeoff. The same value in watts could, under different circumstances, have a very different effect on indoor temperature and HVAC loads. For instance, solar gains might be welcome in winter, but detrimental to the same building in summer. A heavily occupied building might find solar gains harmful during the week, but beneficial when it is empty on the weekend, and the existence of thermal mass only complicates the issue by delaying the thermal effects. The only information suitable for judging the impact of solar gains is the indoor temperature change as a result of those gains. From this value, HVAC loads can either be calculated or inferred.

Finding the indoor temperature requires an energy simulation. Energy and lighting simulations require different inputs from the user, which means that a combined model would have to include both sets of information. Fortunately, the industry has been moving in the direction of combined simulation tools and Building Information Models incorporating multiple building characteristics [Ibrahim & Krawczyk, 2003; Papamichael *et al.*, 1998]. However, few tools focused primarily on lighting include this still important effect of using natural light.

A few people have addressed the issue of accounting for solar gains in design without the need for energy models, but these methods tend to be more primitive in scope. Work done by Littlefair in the 1980's and 1990's resulted in a set of recommendations for maximum obstruction angles depending on European latitudes and climates [Littlefair, 2001]. The goal of making sure certain solar angles are not masked is to preserve the psychological and winter heating benefits of direct sun in buildings.

Because it is located in a tropical climate, the government of Hong Kong took the opposite approach. In 1995, they included a maximum Overall Thermal Transfer Value (OTTV) in the building codes which limits the average thermal transfer (including transfer through the envelope and solar gain) of facades based on height from the ground [Building Authority, 1995]. For building facades within 15m of the ground, the OTTV was capped at 80 W/m<sup>2</sup>, while higher facades were capped at 35 W/m<sup>2</sup> (changed later to 30 W/m<sup>2</sup>), since they generally have greater sun exposure. Hong Kong was the fifth Southeast Asian government to adopt OTTV regulations, which are developed from



detailed energy analysis, specific location climate data, and economic factors [Hui, 1997]. However, critics claim that such codes restrict façade innovation, disregard tradeoffs between higher OTTV and electric lighting savings due to daylight use, and cannot take internal heat gains and building layout into account [Hui, 1997; Li *et al.*, 2002; Yik & Wan, 2005].

Recommendations and regulations regarding solar gain are generally based on previous energy analyses, and are therefore specific to location and assumptions made about building variables. For a simple, yet more general approach, one can use various hand calculations based on tables of sun angles and solar incident radiation, although even these require information from the user about the heat transfer of the building envelope [ASHRAE, 2001; Stephenson, 1957; Stephenson, 1965]. Also, since these tables are forced to make assumptions and simplify the building in question, they are less accurate than the more detailed computer simulations. Some hand calculation methods for thermal assessment include steady-state heat balance equations, the lumped capacitance model, radiant time series, and the balance point model, the last of which will be discussed at greater length in Chapter 6 [ASHRAE, 2001; McQuiston *et al.*, 2005; LBNL, 2001].

## 2.2 Graphical Displays of Numerical Information

In the introduction to his book, *The Visual Display of Quantitative Information*, Edward Tufte observes that “of all methods for analyzing and communicating statistical information, well-designed data graphics are usually the simplest and at the same time the most powerful,” [Tufte, 1983]. Successful graphics take a large data set and communicate it in such a way that the patterns and trends in the numbers are instantly and intuitively understood by the reader. The larger and more complex the data set, the greater the benefit of communicating via graphics, which makes it a perfect medium for large annual daylighting data sets. Unfortunately, it is impossible to put every useful piece of information in the same graph. Some choices must be made regarding which data to show and how to convey it, or different data trends may devolve into unreadable noise.

The greatest difficulty with daylighting data is in attempting to simultaneously show how performance varies over both time and space. To display a four-dimensional data set in a static two-dimensional medium is complicated at best and near impossible at worst, so at least one or two aspects are usually condensed in pre-processing. The most common way to display quantitative daylighting data is by disregarding the time-variation of performance and focusing on the spatial variation. Contour-line renderings or workplane illuminance plots representing a single moment in time are the only available outputs of nearly every daylighting tool that supports graphics. Although a few tools will show animations of sun penetration and shadows [Ecotect web] or renderings tacked together to represent time passing [AGI32 web], analyzing annual daylight performance using only these graphics is computationally intense, time-consuming, and requires expertise to choose which moments to simulate (and which skies to simulate them under) and mental processing to fill the inevitable information gaps.

A more efficient option for annual analysis is to output data in the form of Daylight Autonomy or Useful Daylight Illuminance, which were both discussed in Section 2.1.1 [Reinhart & Walkenhorst, 2001; Nabil & Mardaljevic, 2006]. Both metrics, which

condense temporally-based performance to a single number, are calculated at specific points in space and can be displayed in a work plane contour map, as is often done with Daylight Factor or single-moment illuminance measurements.

Knowing the spatial variation of performance data is important, since architecture is, in essence, the shaping of man-made spaces. However, many practical daylighting problems are caused by not anticipating the effects of changing sun angles and weather conditions – variables which are largely dependant on time of year and day. To fully understand these factors and to best judge the cause of a design’s success or failure requires lighting data in a “fourth” dimension.

A very efficient way to view time-based information is by using temporal maps – color- or grey-scaled graphs on which the x-axis represents the year and the y-axis represents the day [Mardaljevic, 2002]. Although they are not often seen in the world of architecture, the use of temporal maps to display daylighting-related data is not a new idea. Tufte reproduced a sample temporal map showing “moments of sunshine” which was originally printed in 1971 by Monkhouse and Wilkinson [Tufte, 1983]. Both Mardaljevic and Glaser have suggested displaying daylighting data in temporal maps and associated spatial maps simultaneously. Mardaljevic called this combination Spatio-Temporal Irradiance Maps, or STIMAPs, and one example of his, shown in Figure 2-3, displays the cumulative annual irradiance in  $Wh/m^2$  spatially, while the temporal graph point out times of higher and lower irradiance influx using a relative scale [Mardaljevic, 2001; Mardaljevic, 2003]. The Building Design Advisor tool by the Lawrence Berkeley National Laboratory also displays both illuminance and glare in temporal map and spatial formats (see Figure 2-4) [LBNL, 2001]. Each temporal map represents a single reference sensor, and each spatial grid represents a single moment in time.

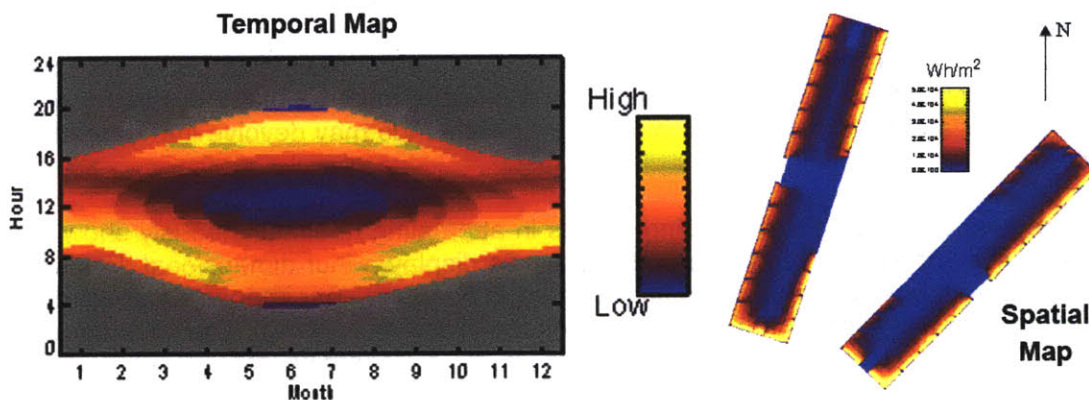


**Figure 2-3. STIMAP figure from [Mardaljevic, 2003]. The spatial map shows cumulative irradiance at different points on the workplane, while the temporal map highlights low and high points of irradiance influx.**

Glaser’s temporal and spatial maps both show illuminance data, but there is a more interactive link between them. When viewed using a computer interface, the user can change the moment in time shown on the spatial graph by clicking on the temporal map and vice versa [Glaser & Ubbelohde, 2001; Glaser & Ubbelohde, 2002; Glaser *et al.*, 2003a]. Glaser calls this interactive connection “brushing and linking” (see Figure 2-5). He has also explored the idea of “tessellating” daylighting plots, which is arranging tiny temporal maps spatially or tiny spatial graphs in a temporal format [Glaser & Ubbelohde,



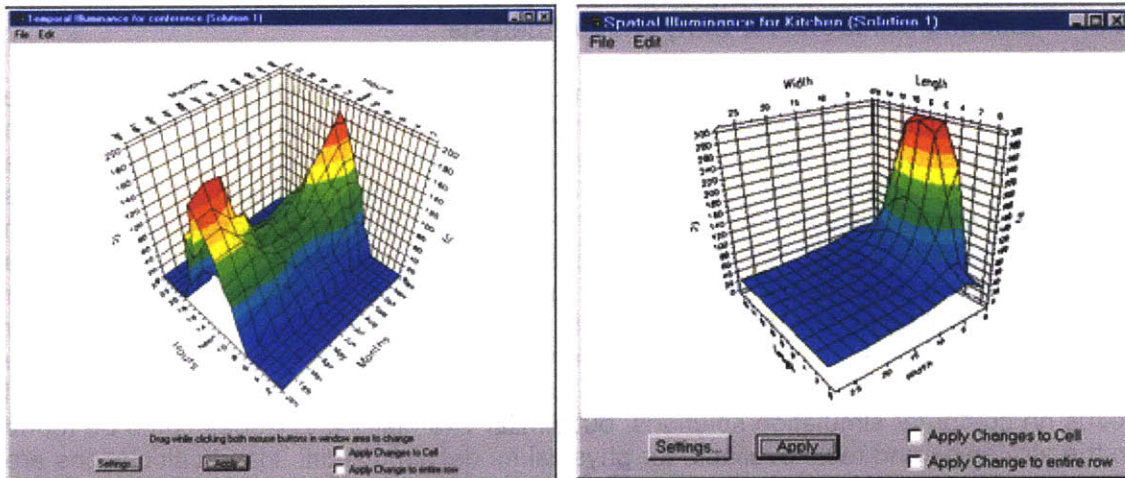


Figure 2-4. Temporal (left) and Spatial (right) illuminance graphs from Building Design Advisor interface [LBNL, 2001].

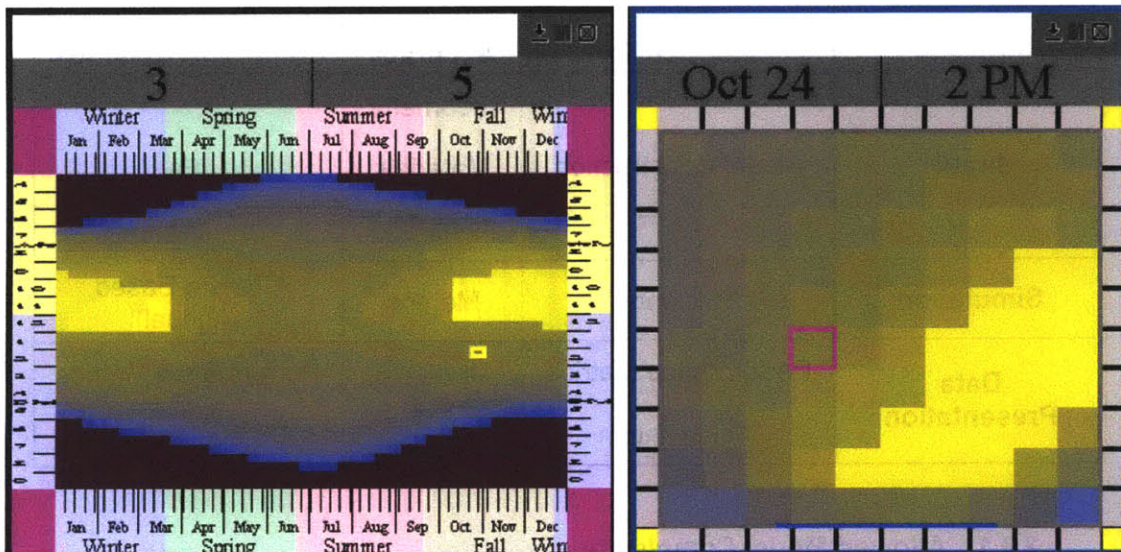


Figure 2-5. A temporal (left) and spatial (right) illuminance map joined by “brushing and linking”, figure from [Glaser *et al.*, 2003a].

2001; Glaser & Ubbelohde, 2002; Glaser *et al.*, 2003a]. The most unusual of Glaser’s graphics studies is one meant to show both temporal and spatial data in the same graph. Dubbed “Space Series”, this graph starts as a temporal map of the maximum illuminances in a room, but the user can click on different parts of the map and add “focus points”, which give the maximum illuminance in different north-south or east-west zones [Glaser & Hearst, 1999; Glaser *et al.*, 2003a]. In this way, a large amount of information is provided in one map, but the detail gets overwhelming and the map difficult to read. Unlike DA and UDI, temporal maps have not been widely accepted by non-researchers, but this may have more to do with their lack of general availability in the daylighting tools of today.

## 2.3 Existing Solutions for Early-Stage Analysis

Early-stage daylighting analysis is a balancing act between conflicting agendas. The analysis should be fast and easy enough to be used in an iterative process, which suggests a need for simplicity. On the other hand, the analysis should be accurate enough to be useful in making decisions for a unique design scenario. This suggests some level of complexity in the aspects of the model that have the greatest impact on daylighting simulation (or calculation) accuracy. The analysis should also result in a data set with all necessary information for making informed design decisions. In other words, all useful types of lighting data should be calculated at all moments necessary for a complete understanding of design performance. The following sections will explore some of the current solutions that exist for each analysis feature individually. They will focus on computer simulation solutions, but similar examples and issues could be found in the strategies and tools available for physical model simulation. Hand calculations are at least partially represented in the computer tools exploration below, since some tools use hand calculations as their primary analysis method.

**Table 2-2. The analysis process and the features important to early-stage analysis.**

Process	Interactivity	Accuracy	Comprehensiveness
Input	Model Construction	Geometry Materials Sky Model	n/a
Simulation	Efficiency	Method	Climate-Based (Annual)
Data Presentation	Performance Metrics Visualization	n/a	Performance Metrics Visualization

### 2.3.1 Allowed Model Complexity

Table 2-2 is a breakdown of the analysis process and the features important to each aspect of a good early stage analysis. For instance, simulation, in the second row, simulation efficiency promotes interactivity, and the choice of simulation method can aid the accuracy of results. In this table, “model construction”, “geometry”, and “materials”, are related and can be grouped together as “model complexity”. In creating a model for analysis, there are two competing ideals which must be addressed. First, in order to promote iterative explorations, the model in question should be quick and easy to build. For instance, building a model using drop-down menus in the MIT Design Advisor [Lehar & Glicksman, 2007] is much quicker than building one in the command-line version of Radiance [Ward & Shakespeare, 1998], however that kind of speed is only possible if one sacrifices all control over model complexity. The MIT Design Advisor assumes that all spaces are rectangular with unilateral daylighting (and that all rooms in a building are the same size), and gives a limited set of options for shading devices, window types, building orientation, and even location. Wall, floor, and ceiling reflectances are assumed by the program and cannot be changed. On the other hand, all model inputs for



Radiance must be entered by hand using a Radiance-specific coding language; however, any geometry or material description which can be mathematically described can be modeled. Model complexity has some correlation to simulation accuracy, because a design which cannot be accurately modeled cannot be accurately simulated. The other determining factor for simulation accuracy is the type of calculation performed, which is discussed in Section 2.3.3.

Radiance and MIT Design Advisor are extremes on the spectrum of model complexities, as is apparent from Figure 2-6, but many computer simulation tools seem to cluster at the extremes and are often either limited but quick, such as DELight, DIAL-Europe, Building Design Advisor, and Daylight 1-2-3, or detailed but slower, like AGI32, IES, 3ds Max Design, Maxwell, and Inspirer [Hitchcock & Carroll, 2003; de Groot *et al.*, 2003; Papamichael *et al.*, 1997; Reinhart *et al.*, 2007; AGI32 web; IES web; Autodesk, 2009; Maxwell web; Inspirer web]. The last four tools mentioned are commercial tools popular with architects for their realistic renderings, however they are used less often (or cannot be used at all) for numerical lighting analysis. The only exception to this is 3ds Max, which has recently been numerically validated by the National Research Council of Canada [Reinhart & Breton, 2009; Reinhart & Breton, 2009a].

Although most of the simple analysis tools available were created with early-stage design explorations in mind, those which limit too many aspects of the model end up defeating the purpose. For instance, many of the simple tools listed above allow only box-like, sometimes only unilateral models. While this makes the modeling process quicker, it restricts creativity, use of advanced technologies, and most other things which might make the design unique. Similarly, while simpler models can be created using complex modeling tools, the modeling process is often slower, and there is always a temptation to add more detail. What is needed in early stage analysis is something in the middle ground between too restricted and too complex, but unfortunately, very few tools exist between these extremes – with Ecotect as a notable exception [Ecotect web]. Ecotect handles unique shapes and materials, moderately complex models (too many components and the program tends to crash), and the internal CAD function is intuitive and easy to use. The Adeline/SuperLite pairing is also one in which unique models may



**Figure 2-6. A detailed Radiance rendering by the author (left) and a sample rendering done for the MIT Design Advisor [Lehar & Glicksman, 2007].**

be made in the internal Scribe Modeler, but its complexity is stunted by the limited number of allowed surfaces and objects [Erhorn *et al.*, 1998; Adeline web ; Ubbelohde, 1998]. This strategy is useful for keeping modeling simple, however the limitation on external shading objects could be too restrictive for the sake of necessary model accuracy [Ubbelohde, 1998].

Although it is limited, the Building Design Adviser approaches moderate model complexity [Papamichael *et al.*, 1997; Papamichael *et al.*, 1998; LBNL, 2001]. While it restricts the user to rectangular spaces, these can be grouped in any way, and each space can be moved to as a unit to a different place in the building plan. The Schematic Graphic Editor makes liberal use of drop-down menus and default values, but allows any default to be changed.

Finally, there are a few “sketch” modeling tools which could be considered quick, intuitive, and moderately complex. Space Pen [Jung *et al.*, 2002], which is the modeling tool used in Spot! [Bund & Do, 2005], and LightSketch [Glaser *et al.*, 2003] are both tools in which the modeling is done by interpolating user sketches using a pre-conceived set of symbols. Both tools came out of the Carnegie Mellon Computational Design Lab and can handle unique, but not detailed shapes, and at least LightSketch is restricted to a default diffuse wall material. There is great potential in the possible development of tools such as these, but unfortunately, both projects seem to have halted, or at least paused.

### 2.3.2 Sky Luminance Distribution

Sky luminance distribution is one model input which requires a higher level of necessary accuracy for daylight analysis. The sky and sun are the primary sources of light, and if the source is modeled incorrectly, the simulated data will probably also be erroneous [Mardaljevic, 2004], and any daylighting tool should be able to model a variety of skies, since every location on earth has a variety of weather. At the very least, one “in between” option should be offered apart from overcast and clear sky extremes, so a model offering the CIE clear, intermediate, and overcast skies should be the minimum acceptable accuracy [CIE, 1973; Nakamura *et al.*, 1985; Moon & Spencer, 1942]. Unfortunately, while the CIE clear and overcast skies are ubiquitous in the existing computer tools set, the intermediate sky is less so – Radiance, AGI32, Ecotect, and IES are some of the tools which can model CIE intermediate skies [Ward & Shakespeare, 1998; AGI32 web; Ecotect web; IES web].

Because real skies are infinite in variety, it is better to be able to model a spread of different intermediate skies. Darula and Kittler have defined many individual steps between the CIE clear and overcast skies [Darula & Kittler, 2002] while Igawa *et al.* have made a similar set of distinct sky distributions based on their intermediate sky model [Igawa *et al.*, 1999]. Unfortunately, the author knows of no current analysis tool which can automatically create either of these sets of sky definitions.

The Perez All-Weather sky distribution uses a single equation which, given brightness and clearness index inputs, can define any number of realistic sky distributions [Perez *et al.*, 1993]. Although this sky model has been validated to a reasonably high accuracy, only Radiance and 3ds Max Design can easily be used to model a Perez All-Weather sky [Ward & Shakespeare, 1998; Reinhart & Breton, 2009]. This model will be

discussed at greater length in Chapter 3, as will another sky distribution by Perez et al. known as the ASRC-CIE model [Perez *et al.*, 1992].

### 2.3.3 Calculation and Simulation

Some tools which strive for speed choose to find illuminances and other light quantities using simplified approximate algorithms. Analyses like the lumen method or the split flux method [ASHRAE, 2001; Lynes, 1968] were developed before the widespread use of computer simulations and could be done with a calculator, prepared numerical tables, and view protractors. With the speed of today's computers, any one of these algorithms can be calculated in under a few seconds, making any computer tool that uses them very quick. Unfortunately, they are approximations of the way light reacts in specific common situations, and many were developed for rectangular rooms with unilateral side-lighting. The further one gets from that geometric base case, the less accurate the calculation.

The alternate option, available only as faster computers have become ubiquitous, are physical simulations which attempt to imitate the behavior of light in reality. The two most common physical light simulation methods are ray-tracing and radiosity, both of which encompass a few different methodologies based on the same idea. The software with best known accuracy is Radiance, which is a Monte Carlo backwards ray-tracing program valid to within 5.6% of life measurements [Mardaljevic, 1995]. Each sensor or pixel point sends a user-determined number of light rays in a spread of directions according to a randomized Monte Carlo algorithm, and when these rays hit objects, they bounce and split (again according to user-defined parameters) until some of them have traced a path backwards from the sensor point to a light source [Ward & Shakespeare, 1998]. Ray tracing software can theoretically handle any model geometry and any material definition. Because of its proven robustness, flexibility, and accuracy, Radiance has gained a great deal of trust from the daylighting simulation world. In fact, in two recent surveys given by the National Research Council of Canada found that, among a spread of many tools, about 50% of participants chose to use a tool with a Radiance simulation engine [Reinhart & Fitz, 2006; Galasiu & Reinhart, 2008]. The drawback to this famous accuracy is that Radiance is one of the slower simulation tools with no user interface to speak of. Its renderings are also view-dependant, so rendering two different views of the same scene would take twice as long. Two ray-tracing tools which produce quicker results than Radiance are Daysim [Reinhart & Walkenhorst, 2001], which uses a modified version of Radiance to run annual simulations, and 3ds Max Design [Autodesk, 2009], which uses a ray-tracing engine called mental ray. Both tools have been validated by Christoph Reinhart and the National Research Council of Canada [Reinhart & Breton, 2009]. Other tools which include ray-tracing engines are Genelux, FormZ, and Inspirer [Mitanchey et al., 1997; FormZ web, Inspirer web].

The other common physical simulation method is radiosity. Radiosity is calculated in a similar way to radiant heat transfer between surfaces, and because of this, radiosity is restricted to diffuse materials only. (Although some radiosity programs add a single bounce ray tracing at the end of rendering simulations [AGI32 web] this is merely for aesthetic purposes, and it makes little or no difference to numerical calculations.) However, materials definitions are the only real restriction to radiosity. In a thorough comparison between Radiance and Lightscape, the most prominent radiosity tool in 2001, Altmann and Apian-Bennewitz found comparable results as long as specular



materials were not a large part of the light transport and distribution and the radiosity simulations were allowed to continue for simulation times which were also comparable to Radiance [Altmann & Apian-Bennewitz, 2001]. The benefits of radiosity are that the renderings look good before the program has reached a point of high numerical accuracy and that as soon as a simulation is complete, the model may be viewed from any angle in real time, since Radiosity is not view-dependant. Unfortunately, Lightscape is no longer available, but other currently available examples radiosity tools are AGI32, Adeline/SuperLite, DELight, IES FlucsDL, and the MIT Design Advisor [AGI32 web; Adeline web; Papamichael *et al.*, 1997; IES web; MIT Design Advisor web; Lehar & Glicksman, 2007].

With a simulation spectrum spanning from split-flux to Radiance, the level of “necessary accuracy” for early stage design tools is not immediately obvious. Hand calculations are really not accurate enough due to the model restrictions they impose. The internal simulation engine in Ecotect, which is based on the split-flux method, deploys a Monte Carlo distribution of rays from each sensor point in order to help weight the different components of the split-flux according to the unique shape of the model [Ecotect web]. This should improve the performance of calculations in non-rectangular rooms, however there is still a significant difference between Ecotect’s internal results and similar results computed by Radiance (see Figure 2-7).

Another promising method is that used by Daysim to make annual Radiance calculations in a reasonable amount of time. As mentioned in Section 2.1.2, Daysim uses daylight coefficients to make thousands of Radiance simulations with similar accuracy and in the same order of time it would take to produce a single one in Radiance [Reinhart & Herkel, 2000]. Finally, the reason that many of the programs meant for early-stage design use radiosity, is that it’s possible to produce quicker numerical results and renderings at a lesser, though possibly acceptable, accuracy.

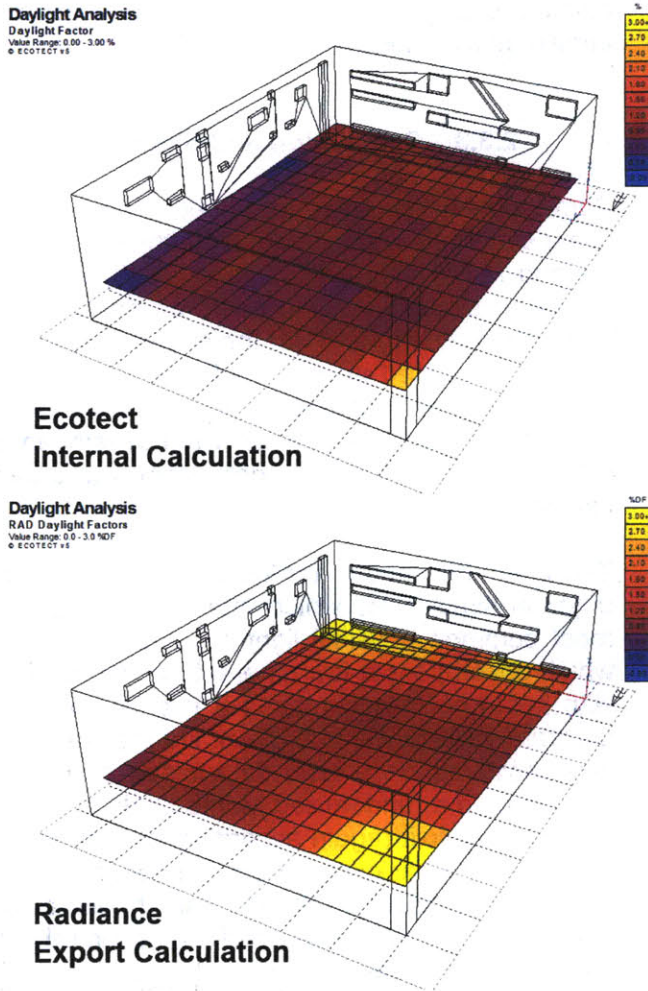


Figure 2-7. Daylight Factor calculations for the same model in Ecotect, using the internal calculation engine (top) and Radiance export (bottom).

### 2.3.4 Annual Calculations and Metrics

As discussed in Section 2.1.1, understanding the performance of a space over the full year for a correct climatic representation of sky-types is an important part of making an informed design decisions. Therefore, the ability to automatically perform annual simulations and convey them to the user using annual metrics is a “necessary accuracy” required in early-stage design tools. Unfortunately, it is also rare in the set of available tools. MIT Design advisor performs annual calculations using radiosity, and the annual (or monthly) impacts on lighting, heating, and cooling energy are the output [Lehar & Glicksman, 2007, MIT Design Advisor web]. The Building Design Advisor originally used the split-flux method and now uses the DELight radiosity engine to produce annual sets of illuminance and glare data [Papamichael *et al.*, 1997; LBNL, 2001; Hitchcock & Carroll, 2003; Winkelmann & Selkowitz, 1985]. It does not output data using any special annual metrics but rather, keeps it in the form of illuminance or Daylight Glare Index. As mentioned several times previously, Daysim was written in order to perform annual Radiance calculations using the daylight coefficients method [Reinhart & Herkel, 2000]. It outputs data in the form of Daylight Autonomy, as do Daylight 1-2-3 [Reinhart *et al.*, 2003; Reinhart *et al.*, 2007] and the Sensor Placement Optimization Tool (S.P.O.T.) [Rogers, 2006]. LightSketch seems also to have been meant for annual calculations [Glaser *et al.*, 2003], but similarly to Building Design Advisor, only illuminances are output.

### 2.3.5 Light Quantity, Glare, and Heat Gain

When it comes to making informed decisions, especially during schematic design, it is important to understand the tradeoffs between light quantity, glare, and solar heat gain. Every software created for the express purpose of light simulation calculates data in terms of light quantity, usually as illuminance, although many of these also calculate Daylight Factor. Those which output Daylight Autonomy were listed in the previous section. Far fewer tools additionally calculate some form of glare; these include Adeline (using the Radiance engine), AGI32, Building Design Advisor, DIALux, Genlux, IES, and Radiance [Erhorn *et al.*, 1998; AGI32 web; Papamichael *et al.*, 1997; GmbH, 2009; Mitanchey *et al.*, 1997; IES web; Ward & Shakespeare, 1998]. Of these, only Radiance with the plug-in program *evalglare* can calculate the Daylight Glare Probability, although there is currently plan for implementing *evalglare* within Daysim [Wienold & Christoffersen, 2006; Wienold, 2009].

Only those tools which also have some (if simple) thermal modeling abilities (Dial-Europe, MIT Design Advisor, Building Design Advisor, Daylight 1-2-3, Ecotect, and IES) provide any sort of dedicated solar heat gain indicators [de Groot *et al.*, 2003; Urban & Glicksman, 2007; Reinhart *et al.*, 2007; Ecotect web, IES web]. Of these tools, only Dial-Europe includes the thermal modeling solely for the purposes of assessing solar heat gain rather than energy loads. Both Dial-Europe and MIT Design Advisor predict the number of days or hours when the space may overheat, and MIT Design Advisor includes thermal comfort as dependant on proximity to the window. Solar heat gain, though a crucial part of balancing daylight performance, is not included in many lighting analysis tools, since it takes an energy model to truly find the effects of solar heat gain.

### 2.3.6 Goal-based Performance Metrics

Koenigsberger *et al.* suggested that data could be more easily communicated to a designer if it was preprocessed to reflect the relationship between the data and the user's performance specifications [Koenigsberger *et al.*, 1975]. Indeed, it is not difficult to see how a decision process would be made easier if the information available was tailored to answer specific questions. Therefore, metrics that reflect the user's lighting goals would be a great asset to an early-stage design tool.

Daylight Autonomy is a goal-driving metric, since the user must input the illuminance threshold with reference to which the DA is calculated. Useful Daylight Illuminance is a similar metric, although the thresholds for UDI are pre-determined, not user-selected. IES FluxDL (the IES radiosity program) will calculate the work plane area above 2% Daylight Factor. Like UDI, this is a goal-based processing feature, however the goal (for the work plane to be above 2% DF) is pre-determined for the user. These metrics show how daylight performance varies over a spatial grid. Although DA and UDI depict annual data, the variation in annual performance is condensed to a single number, and Daylight Factor is defined under an ideal overcast sky and does not change with climatic conditions, so neither metric could be displayed in a temporal format.

### 2.3.7 Visualizations

Although some tools output numerical results only as tables or text files, many display numerical results graphically as well in either two or three dimensions. Often two dimensional graphics are in the form of contour maps of data (usually illuminance or Daylight Factor) on the work plane, while three dimensional graphics include renderings in which colors or contour lines indicate the data value on visible model surfaces. Spatial graphics are a good way to show how performance varies within a space, to assess lighting uniformity (or lack thereof), and to identify problem spots, all in a single glance.

A more qualitative way to understand the spatial performance of daylighting is to view photorealistic renderings. Tools that allow greater complexity in model input and perform either ray-tracing or radiosity simulations will usually output renderings as well as numerical data. In fact, a few of the popular tools output only renderings and do not allow the user to make a quantitative assessment of the space (Maxwell Render and FormZ, for example) [Maxwell web; FormZ web]. Renderings are a good way to bridge the gap and form an intuitive link between data-driven performance assessments and the visual reality of light quality and aesthetics. By nature, they represent only a single moment in time, although several chronological renderings can be strung together to form an animation.

One other way to graphically arrange numerical data is to display it in a two-dimensional graph where the x- and y-axes represent time passing over the year and the day respectively. These graphs, known as temporal maps, were discussed at greater length in Section 2.2, and they allow the user to understand the annual variation in performance. Temporal maps highlight the performance variations between occupied and non-occupied times, and help identify problem moments – which can then be correlated with typical weather patterns and sun positions.



Spatial and temporal graphics and photorealistic renderings each help the user analyze data from a different angle, although there is some information overlap between spatial graphics and renderings. Because so many critical decisions are made in the early stages of design, a strong analysis would include two of the three, preferably including some kind of temporal information. The ideal would be to have access to all three types of visualizations, since each has its own strengths and weaknesses. Again, Building Design Advisor and LightSketch are two tools which communicate data using both temporal and spatial illuminance graphs [Papamichael *et al.*, 1997; Papamichael *et al.*, 1998; Glaser *et al.*, 2003]. Unfortunately, they both display data only in terms of illuminance, so each temporal map can only show the data from one sensor point at a time and each spatial grid can only display one moment in time. LightSketch does something called “brushing and linking” (see Section 2.2) which allows these graphics to be explored in an intuitive and interactive way, but there is still no way to understand the performance of the whole space at once.

Spot!, which is a sun-only daylighting tool, also conveys spatial information (in the form of 3-dimensional models), and temporal information as a percent of the time when reference points are illuminated by direct sun [Bund & Do, 2005]. The time periods over which these percents are calculated are usually the same few hours every day over the course of one month. Again, each temporal map displayed the data from only one reference point. Daysim and other programs which calculate Daylight Autonomy also supply both spatial and temporally-based information, however in that case, temporal performance is condensed to a single number and displayed on a spatial grid, a bar graph, or in tabulated charts [Reinhart, 2005; Rogers, 2006]. Daylight Autonomy is valuable for allowing the user to assess a space using a single, or at most two, contour maps, but DA cannot be displayed on a temporal map.

### **2.3.8 Summary of Existing Solutions**

There are many daylighting design tools available, ranging from research-oriented tools produced by universities to professionally made commercial tools. The previous sections lean more towards a discussion of tools produced by researchers, partially because these are usually the tools in which new concepts are first applied. The features and existing tools and tool packages mentioned in Section 2.3 are summarized in Table 2-3 below. The conclusions in this section and on the chart were formed through a literature review plus the author’s personal experience with a handful of the tools.

This thesis is concerned with providing an appropriate analysis method for the earliest stages of architectural design. The ideal analysis for the this stage needs to balance the need for interactivity with the need to produce comprehensive and reasonably accurate data. It is most crucial to find this balance in the simulation strategy and in the model construction, including geometric, material, and sky distribution inputs. The analysis should present data in such a way that the user can easily understand the quantitative and qualitative performance data with respect to variations over time and within the model space. The most complete data output is one generated by annual, climate-based simulations and displayed using qualitative renderings and graphs where both the spatial and temporal variation of performance is apparent.

Table 2-3. A Summary of the aspects of early design stage analysis and a few of the tools that offer existing solutions.

	3ds Max Design	Adeline (Superlite)	Adeline (Radiance)	AGI32	Building Design Advisor (DELIGHT)	Daylight 1-2-3 <sup>a</sup>	Daysim	DIAL-Europe <sup>b</sup>	DIALux	Ecotect	FormZ	Genelux	IES FlucsDL	IES Radiance	Inspirer	LightSketch	Maxwell Render	MIT Design Advisor	Radiance (Linux)	S.P.O.T.	Spot!	Package: Ecotect/Radiance/Daysim
<b>Model: Intuitive Construction<sup>d</sup></b>	✓	✓	✓		✓	✓		✓	✓	✓			✓	✓		✓		✓		✓	✓	✓
<b>Model: Unique Geometry</b>	✓	✓	✓	✓			✓		✓	✓	✓	✓	✓	✓	✓	✓	✓		✓		✓	✓
<b>Model: Unique Reflectances</b>	✓	✓	✓	✓	✓		✓		✓	✓	✓	✓	✓	✓	✓		✓		✓	✓		✓
<b>Model: Includes Intermediate Skies<sup>e</sup></b>	✓		✓	✓		✓	✓			✓		✓	✓	✓	✓				✓	✓		✓
<b>Simulation: Sufficient Accuracy<sup>f</sup></b>	✓	✓*	✓	(✓)		✓	✓		(✓)			(✓)	(✓)	✓	(✓)	(✓)		✓*	✓	✓		✓
<b>Simulation: Annual, Climate-Based</b>	✓				✓	✓	✓	✓								✓		✓		✓	✓	✓
<b>Metrics: Light Quantity</b>	✓	✓	✓	✓	✓	✓	✓	✓	✓	✓		✓	✓	✓		✓			✓	✓		✓
<b>Metrics: Glare</b>			✓	✓	✓			✓				✓		✓					✓			
<b>Metrics: Thermal<sup>g</sup></b>		✓*	✓*		✓*	✓*		✓		✓*								✓				✓*
<b>Metrics: Goal-Based</b>						✓	✓													✓		✓
<b>Graphics: Spatial Variation<sup>h</sup></b>	✓	✓	✓	✓	✓	✓	✓	✓	✓	✓		✓	✓	✓	✓	✓				✓		✓
<b>Graphics: Temporal Variation<sup>i</sup></b>					✓											✓					✓	
<b>Graphics: Renderings</b>	✓		✓	✓					✓		✓	✓		✓	✓	✓	✓	✓	✓	✓		✓

#### NOTES:

- a) The prototype for Daylight 1-2-3 was previously named The Lightswitch Wizard. Thermal, geometric, and other features were added to Daylight 1-2-3.
- b) DIAL-Europe was previously named LESO-DIAL.
- c) Viz is the result of Autodesk purchasing and significantly changing Lightscape.
- d) For tools with which the author has no personal experience, this judgement is based on literature and website reviews.
- e) This includes CIE Intermediate skies [Nakamura et al., 1985] and Perez All-Weather skies [Perez et al., 1993], but not averaged skies or user-defined distributions.
- f) For the most part, any tool using radiosity or ray-tracing is considered sufficient. (√) indicates tools for which the author cannot find a validation of accuracy, and √\* indicates tools which demonstrate less accuracy in published papers [Ubbelohde; Lehar].
- g) √\* indicates tools which perform energy simulations (which include solar thermal effects) internally or as a convenient export, but do not have specific solar thermal metrics.
- h) This includes both 2-dimensional contour maps and falsecolor renderings.
- i) This does not include the ability to produce animations.

# Chapter 3

## Simulation Reduction for Temporal Graphics

Temporal and spatial graphics convey different information to the designer, and a further exploration of their complementary natures can be found in Chapter 7. However, temporal graphics were chosen as the primary mode of conveying numerical data throughout this thesis and in the Lightsolve project [Andersen *et al.*, 2008]. This is due in part to the close connection between the passage of time and environmental daylighting variables, and in part to the ease by which one can compare spatial and non-spatial quantities using temporal graphics (see Section 1.2).

Because it is important to give the user both temporal and spatial information, a correlated set of representative renderings provides both spatial information and an opportunity for qualitative assessment (see Section 7.2.4). Spatial renderings, rather than spatial numerical graphics, were chosen partially due to the work of Lu Yi, who did a master's thesis for the MIT architecture department. Yi's work was the development of a user interface design, the idea of which was to strongly link the numerical rigor of the analysis software preferred by engineers to the highly interactive and visual displays preferred by architects [Yi, 2008]. The centerpiece of these daylighting visual outputs, and one of the most striking results of any daylighting analysis software, is the realistic rendering.

The relationship between the temporal map and renderings in the proposed Lightsolve interface is similar to the "brushing and linking" method described in Section 2.2 [Glaser & Ubbelohde, 2001] – as the mouse travels over different points in the temporal map, the nearby renderings update in real time to display the one closest to the time of day and year indicated by the cursor. In this way, temporal data and spatial renderings are intuitively linked to form a more informative whole. Other features of the interface allow the user to watch animations of the changing light patterns over a day or over a year for a specific hour. Renderings can also be displayed according to dominant weather type, or as clear, clear-turbid, intermediate, or overcast renderings only, and they can be shown simultaneously in a tiled table rather than as chronologically linked with the temporal maps. The model's object file can also be viewed and manipulated from the interface and new views chosen for rendering [Yi, 2008]. Although the aesthetics and navigation functions have been updated since Yi completed her thesis [Seaton, 2009], the ideas and principals behind it have been preserved in the new incarnation. Figure 3-1 shows a screenshot of both Yi's and Seaton's interface which links the temporal numerical data to spatial renderings.

This chapter develops and validates a method to reduce the number of simulations necessary to produce an annual data set which will be displayed using a temporal graphic format. The year is first divided into periods of similar seasonal and daily moments, which are then analyzed for sky type frequency and average brightness of each sky type. The choice of sky model, the ASRC-CIE model by Perez *et al.* [Perez *et al.*, 1992], was influenced by the decision to associate renderings with the numerical data in the temporal map (see Section 3.1.2). Finally, the data reduction method is validated against a far more detailed data set for sensors under unobstructed skies, inside a simple room, and inside more a complex architectural model.

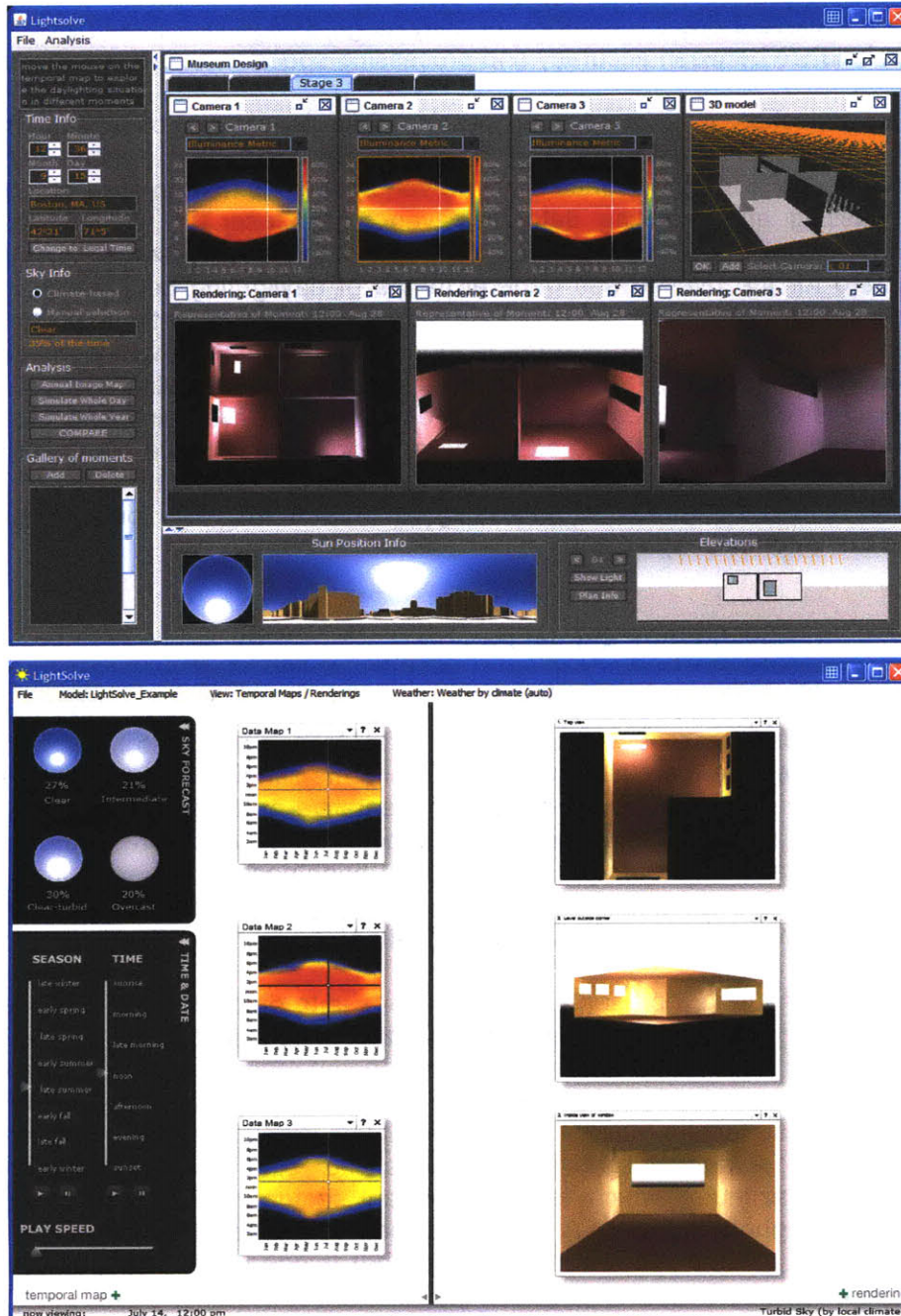


Figure 3-1. Two incarnations of the Lightsolve interface: the earlier version above [Yi, 2008], and the most recent version below [Seaton, 2009].

### 3.1 Data Reduction Methodology

To produce climate-based temporal maps and renderings that update in real time, all calculations and simulations must be done prior to analysis and exploration. To make a tool iterative for schematic design, it is important that the process be as quick as possible without giving up too much relevant detail – and that the end product is not

inundated in irrelevant detail. In short, an early-stage design tool should strive to strike the perfect balance between accuracy and processing speed.

Although a reduction in computer processing time is always beneficial, inevitable hardware improvements will eventually make any data reduction method outdated, if computation speed is the only concern. However, speed it is not the greatest advantage of pre-processing and reducing data displayed to the user. If daylighting data is presented one small piece at a time, or if the detail of the data presented is very high, it might be hard for the user to see general trends of daylighting behavior in the noise caused by the minute fluctuations of external conditions. If data is pre-processed correctly, the noise disappears, and the responsibility of choosing which moments and weather conditions to simulate is lifted from the user. In the methodology presented below, two types of pre-processing occur: temporal data averaging and reduction is done before the simulations to expose general trends and improve computation time, and spatial data is subject to goal-based pre-processing in order to assist the user in analysis and reduce the number of necessary temporal maps. The former is presented below, and the latter in Chapter 4.

### **3.1.1 Representative Annual Periods**

One way to simultaneously reduce the computation time and to emphasize daylighting performance trends is to reduce the frequency simulations meant to represent a year. However, the more time there is between the moments simulated, the more crucial it is to ensure that the simulated “moment” is representative of the whole temporal region. For example, a single illuminance measurement must incorporate the compiled influences of sun angles, weather types, and sky brightness for all surrounding times, and for the sake of creating realistic renderings, it must do this without resorting to a single unrealistic averaged sky luminance distribution.

The first step in ensuring representative simulations is to divide the year into periods of similar conditions. The sun should be at approximately the same position in the sky, and weather should be reasonably consistent. This concept resembles in some aspects the method presented by Herkel at the 1997 IBPSA conference [Herkel, 1997], which uses the similarity of three factors – direct irradiance, diffuse irradiance, and solar altitude – to separate a series of annual lighting simulations into “bins”. That strategy, however, disregards solar azimuth, which is an important factor in determining daylighting performance throughout the day. A preferable method is one which takes into account both solar altitude and azimuth, which among other things implies temporal groupings limited to similar times of day and year.

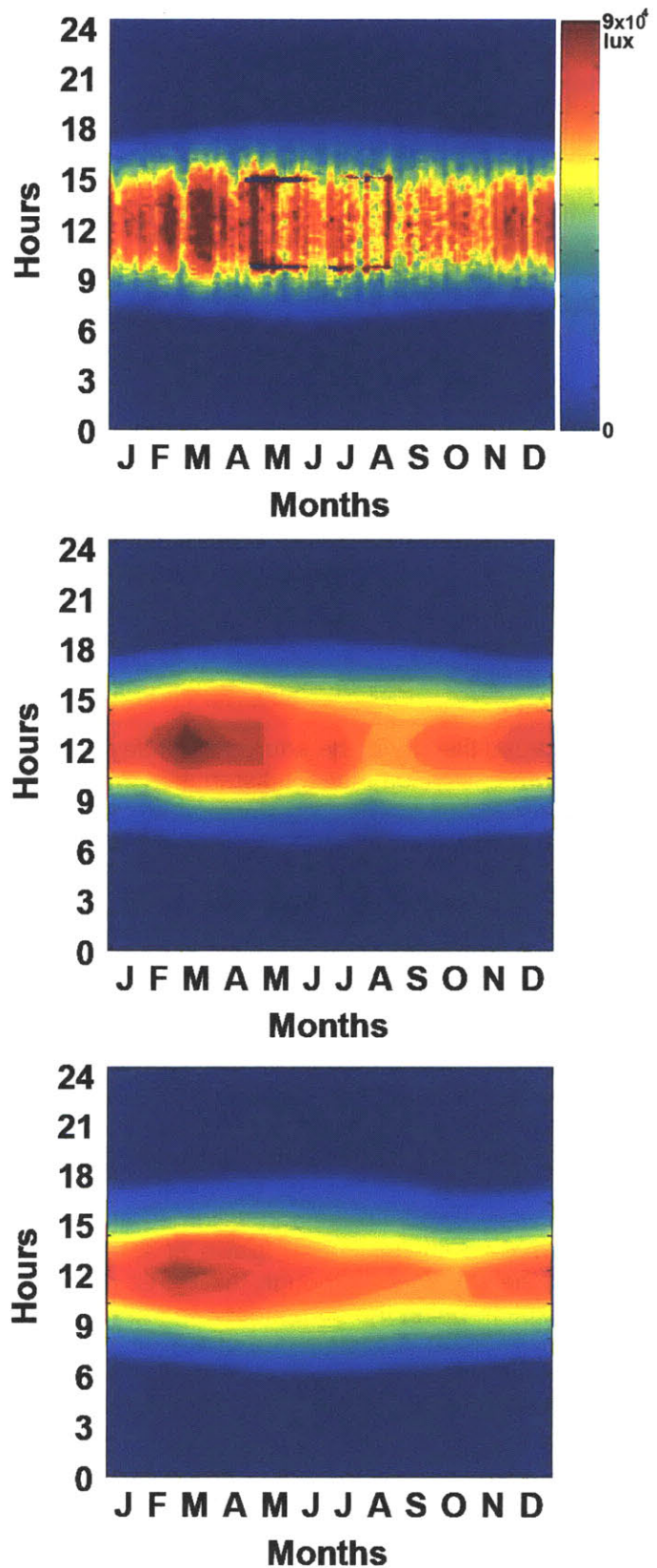
For the test cases shown below, the year is divided into 56 periods: the day is divided into 7 intervals, and the year into 8. All times of day are in solar time, and since noon is an important solar day benchmark, it was decided preferable to divide the day into an odd number of intervals. The seven daily intervals are spaced equally from sunrise to sunset, and the fourth interval is always solar noon. This choice was made so that representation of the passing day does not change seasonally or by latitude – so that short days are not underrepresented and long days are not overrepresented. The year is divided in an even number of sections, so that both solstices may serve as interval limits, not interval centers. Because of this, extreme sky conditions contribute but do not have an overwhelming influence on the period which includes them.



The number of periods, 56, was decided after a visual exploration of different numbers of divisions; Figure 3-2 illustrates the a very detailed Daysim illuminance temporal map, and the similarities between a map divided into 132 temporal periods (11 diurnal and 12 annual divisions) and one divided into 56 temporal periods (7 diurnal and 8 annual divisions). Temporal maps divided into less than 7 diurnal or 8 annual sections did not provide enough visual definition of data trends, and the validation will show that 56 annual data points is sufficient for diffuse illuminance analysis, however the data reduction methodology is applicable to any temporal distribution of periods.

Because there is only one illuminance result given per period, only one sun position (the central point within that time period by both hour and day) can be realistically represented. The division of periods results in 28 unique sun positions and 56 annual periods, as shown in Figure 3-3. Since the Daysim tool is instrumental in subsequent validations, the spatial difference between the 28 sun positions and Daysim's solar simulation points (usually around 60 in number) [Reinhart & Walkenhorst, 2001; Reinhart, 2005] is also illustrated in Figure 3-3.

**Figure 3-2. Temporal representations of horizontal outdoor illuminance in Bangkok. From top to bottom, the temporal maps were created using 105,120 discrete illuminances, 132 representative illuminances, and 56 representative illuminances.**





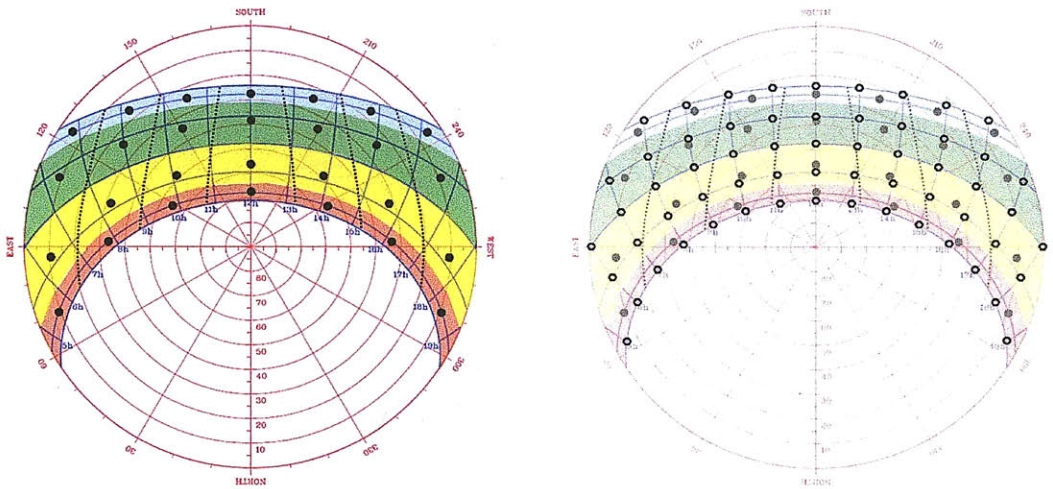


**Figure 3-3. Sun course diagram [University of Oregon web] overlaid with the 56 periods (left), and the hourly sun positions at which Daysim performs direct sun contribution calculations (right). The colored bands show the proposed division of the year, and the dotted lines show the proposed division of the day.**

### 3.1.2 Sky Models Choice and Discussion

Because the sky is the source of all daylight, it is important perform simulations using an accurate sky luminance distribution model. Two of the most accurate existing sky models were created by Perez and others: the All-Weather sky model [Perez *et al.*, 1993] and the ASRC-CIE sky model [Perez *et al.*, 1992].

The All-Weather sky model was developed by Perez *et al.* in two steps. The first step was the proposition of a luminous efficacy model relating the three basic radiation components – direct, global and diffuse irradiance – to their photopic equivalents – direct, global and diffuse illuminance. Together with this efficacy model, Perez proposed a model predicting the sky’s zenith luminance and a model predicting the sky dome luminance distribution as an extrapolation of CIE standard skies [Perez *et al.*, 1990]. The second step was the development of Perez’s own sky luminance distribution model based on the date and time and on horizontal direct and diffuse illuminance. This model is called the All-Weather model, or sometimes just the Perez model [Perez *et al.*, 1993].

The Perez model has been validated and compared with several other models [Perez *et al.*, 1992; Littlefair, 1994; Igawa *et al.*, 2004]. Results differ with the climate conditions and the sky zone, although the Perez model often gives good results, with one notable exception being the comparison made by Littlefair using the BRE data and the climate of Garston (UK) [Littlefair, 1994] for which it performed badly at low sun altitudes. In general, however, the Perez model is recognized as one of the more reliable sky luminance distributions.

The ASRC-CIE sky model, also created by Perez *et al.*, is one of the most accurate existing sky models [Perez *et al.*, 1992]. It integrates the four standard CIE sky models into one sky luminance angular distribution. The models used are the standard CIE

overcast sky [Moon & Spencer, 1942], the CIE averaged intermediate sky [Nakamura *et al.*, 1985], the standard CIE clear sky and a high turbidity formulation of the latter (CIE clear sky for polluted atmosphere) [CIE, 1973; Darula & Kittler, 2002].

This sky model has been validated for diverse climate and sky zones (sun proximity) [Perez *et al.*, 1992; Littlefair, 1994] and compared with several other models. Comparison results vary from one study to another, but the ASRC-CIE model always gives good results (sometimes even better results than the more complex All Weather sky model) and was validated with several other models [Littlefair, 1994]. It was declared most likely to be adaptable to a wide range of climate zones.

The ASRC-CIE model is the one used in simulations populating the 56 periods temporal maps. The choice was made due not only to the validated accuracy of the model, but more importantly because the simulation of discrete sky types is inherent in its definition. Ultimately, a temporal map is formed using one data result (one illuminance, for example) per each of the 56 temporal periods. A sky model which provides the needed ability to weight the contributions of different sky types within one period is an asset to the process.

One change was made to the ASRC-CIE methodology. In order to preserve the realism of renderings under different skies, the weighted sum of weather conditions is performed after illuminances are calculated rather than applying them to the distribution of sky luminance used in the simulations. Therefore, the governing equation is:

$$E = b_c E_c + b_t E_t + b_i E_i + b_o E_o \quad (3.1)$$

Where  $E$  is the illuminance at the considered point and  $E_c$ ,  $E_t$ ,  $E_i$  and  $E_o$  are, respectively, the luminance at the considered point for a standard CIE clear sky, a CIE clear turbid sky, a CIE intermediate sky and a CIE overcast sky. The  $b_j$  coefficients are found using equations 3.2-3.6 below.

The luminance definition of each of the four sky types includes a zenithal luminance which must be determined before simulation. Representative zenithal luminances for each of the 56 periods are found by processing a Typical Meteorological Year weather file for a given location and finding the average zenithal luminance for each of the four sky types per temporal period. This processing also finds the frequency of occurrence of the different sky types during each temporal period.

The frequency of different sky conditions becomes the weighting factors  $b_c$ ,  $b_t$ ,  $b_i$ ,  $b_o$ , which were adapted by Perez in 1992, depend on the sky clearness  $\varepsilon$  and brightness  $\Delta$  [Perez *et al.*, 1992]. The sky  $\varepsilon$  and  $\Delta$  are calculated using the horizontal diffuse irradiance ( $E_{diff}$ ), the normal incident irradiance ( $E_{norm}$ ) and the solar zenith angle ( $Z$ ) expressed in radians:

$$\varepsilon = \frac{(E_{diff} + E_{norm}) / E_{diff} + 1.041 \cdot Z^3}{1 + 1.041 \cdot Z^3} \quad (3.2)$$

$$\Delta = \frac{m \cdot E_{diff}}{E_{norm.ex}} \quad (3.3)$$

where  $E_{norm.ex}$  is the normal incident extraterrestrial irradiance and  $m$  the relative optical airmass.

For any given date and time, two of the four skies are selected depending on the prevailing value of the sky clearness  $\epsilon$ . The  $b_j$  coefficients are thus linked in pairs and calculated as follows:

$$\begin{aligned} &\text{If } \epsilon \leq 1.4 \\ &b_i = \max(0, \min\{1, (\Delta - 0.15)/0.6 + (\epsilon - 1)/0.4\}) \\ &b_o = 1 - b_i \text{ and } b_c = b_{cl} = 0 \end{aligned} \quad (3.4)$$

$$\begin{aligned} &\text{If } 1.4 < \epsilon \leq 3 \\ &b_{cl} = (\epsilon - 1.4)/1.6, b_i = 1 - b_{cl} \text{ and } b_o = b_c = 0 \end{aligned} \quad (3.5)$$

$$\begin{aligned} &\text{If } \epsilon > 3 \\ &b_c = \min[1, (\epsilon - 3)/3], b_{cl} = 1 - b_c \text{ and } b_i = b_o = 0 \end{aligned} \quad (3.6)$$

By using the ASRC-CIE model and a Typical Meteorological Year weather file, an annual illuminance data set can be approximated under realistic skies using the results from only 224 simulations (4 weather conditions times 56 periods). This can be reduced to 169 simulations if only one overcast rendering is done and the remaining overcast illuminances and renderings are scaled in reference to that one. The result either way is a single weighted illuminance per annual period, which can then be made into a temporal map.

### 3.2 Validation of Data Reduction Method

Because illuminance is the most common daylighting metric, and because it is the basic value from which every metric in Section 4 is calculated, the validation of the “56 periods” data reduction method was conducted using single-sensor illuminance measurements. The temporal maps are contour graphs of the resulting 56 data points. Points set to zero were added at sunrise and sunset in order to keep the daily extremes contours from falling off too quickly.

The reference cases for the Temporal Maps validation are similar maps created using data calculated at 5 minute intervals in Daysim. The 105,120 values calculated by Daysim make a good reference set in validating the data reduction approach to be used in Lightsolve. They allow one to compare a highly detailed set of data points to a set of weighted points which, though hopefully representative of the full year, is only 0.05% as large. The comparison is further strengthened by the fact that Daysim’s calculation engine is based on Radiance algorithms, since the 56 weighted moment values are calculated using Radiance.

Figure 3-4 shows a single-sensor illuminance temporal map made from 56 weighted data points with a corresponding detailed temporal map, in this case, for an unobstructed horizontal sensor in Boston. Figure 3-4a is a contour graph of the 56 weighted data points, and figure 3-4b is a surface graph representing the illuminances calculated by Daysim. Its data density requires no contour interpolation between points, although the graphs were smoothed slightly to make them easier to read.



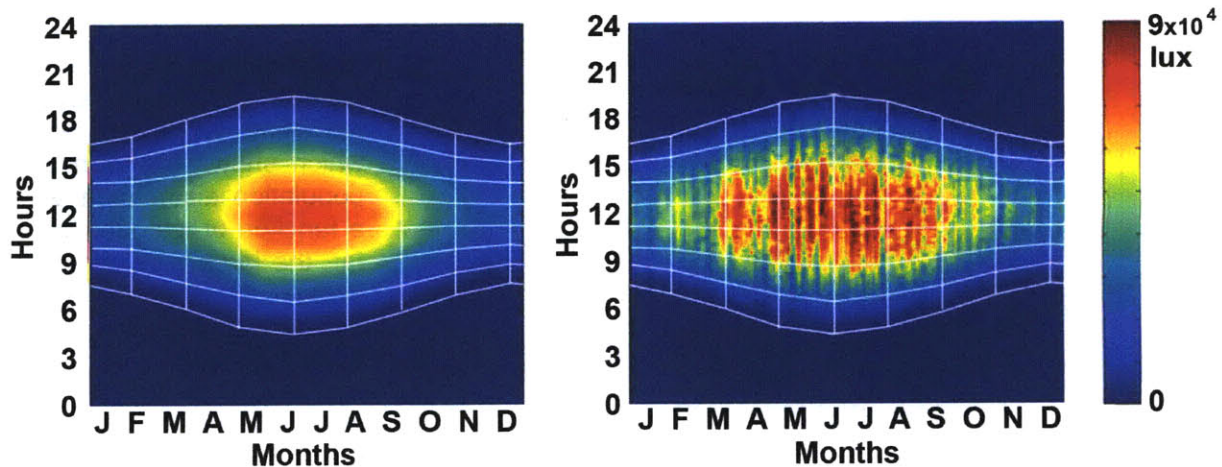


**Figure 3-4. Comparison of temporal maps for an exterior horizontal sensor under Boston skies: (left) the data reduction approach versus (right) the corresponding Daysim reference case. Overlaid on both maps is the division of the year into 56 periods.**

The validation, which involves both a numerical Mean Bias Error and a visual comparison, was performed on three models representing increasing levels of architectural complexity. The first level of validation was performed with five unobstructed sensors under an open sky – one vertical sensor facing each cardinal direction and one horizontal sensor facing upwards. The purpose of comparing illuminance values taken with an unobstructed sky view is to validate the temporal data reduction and averaging method against the far more detailed Daysim data set from a weather representation standpoint, without adding an architectural variable. This group of simulations was performed for a wide range of climates and latitudes, chosen to be a representative sample of conditions found through out larger human population centers.

The second level of validation was performed using a box-like model with large windows. Although the illuminances in this model are influenced by the surrounding architecture, there is still a very large and unbroken connection to the sky itself through the model's windows. This validation was performed for two distinctly different climates: Boston and Harare. The final level of validation was performed in Boston only using a museum model made by Yi [Yi, 2008]. The window openings in this complex model are very small and further obscured by many louvers, which means that the interior illuminances are heavily influenced by the surrounding architecture and much less by the sky luminance distribution. These three validation cases are presented in Sections 3.3 through 3.5.

### **3.3 External Sky and Weather Variability Test**

To validate any proposal that depends heavily on weather and solar position, one needs to perform this validation for a group of locations representative of different climate types and latitudes. Ideally, a group of test locations would encompass a wide range of latitudes and a similarly wide spread of climate types. It would be heavy on those latitudes and climates most relevant to the majority of the world's population, which is distributed unevenly over the globe. The cities chosen should also be ones for which annual data is readily available.

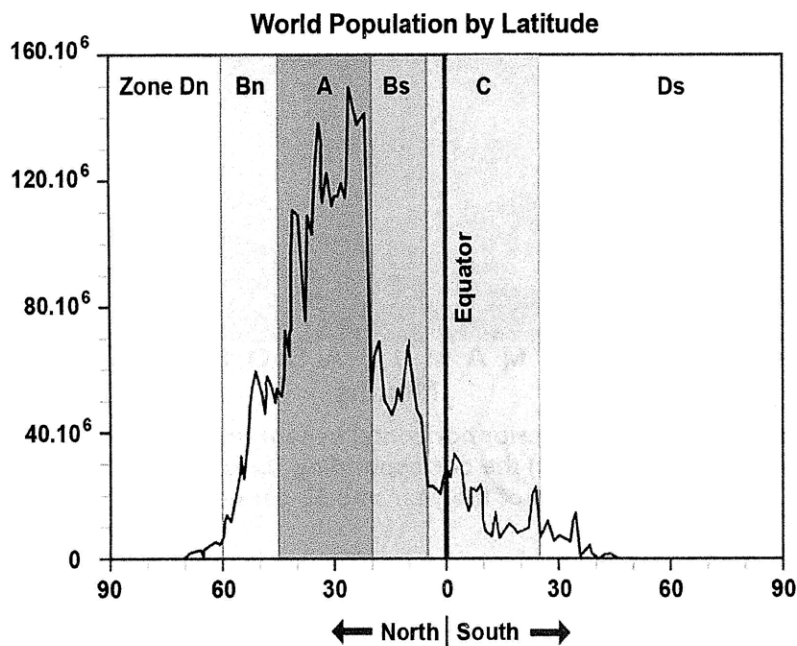


**Figure 3-5. An illustration of world population as a function of latitude (graph source: [Tobler, 1999]), divided into approximate population density zones.**

Assisting in the choice of latitude distribution was the chart in Figure 3-5, which shows the world's population distribution as a function of latitude. By far, the largest density of world population falls between 20° N and 45° N. Latitude ranges between 5° N and 20° N and between 45° N and 60° N have about half the population density as the previous range, and the latitudes between 25° S and 5° N have about one sixth. In latitudes north of 60° N and south of 25° S, the population density falls off very quickly. This distribution resulted in a greater number of cities representing the northern

hemisphere than southern: three cities were chosen from the most populous zone "A", two each from the northern and southern halves of zone "B", two again from the much larger zone "C", and one from the southern part of zone "D", which represents everything else. In this way, the large range of latitudes was preserved and concentrated slightly in the higher population latitudes while still including a few cities at extreme latitudes and two from the southern hemisphere. Each location was also chosen with regard to its climate and average number of average sun hours available [BBC web; Houghton Mifflin web].

The final ten cities in Table 1 (listed in order of distance from the equator) represent both hemispheres, 5 continents, 5 climate types, a range of average sun hours per day, and a wide spread of latitudes. All have TMY2-type data (or similar) available on the Energy Plus website, and all are reasonably populous.

In the illuminance simulations, the sensors for the external validation were arranged so that one vertical sensor was facing each cardinal direction and one horizontal sensor was facing upwards. Because this arrangement is reminiscent of the five exposed surfaces of a box, this validation model was nicknamed "cube". All graphs presented in this and the following sections were produced using MATLAB. All illuminance simulations for the data reduction method were done using Radiance, and all reference simulations were done using Daysim. The parameters used in the simulations are as follows: -ab 7, -ar 128, -aa .1, -ad 2048, -as 256, -dp 4096, -ds .15, -dt .05, -dc .75, -dr 3, -ms 0.066, -sj 1, -st .01, -lr 12, -lw .0005, -l+, -h.

**TABLE 3-1. Ten locations for simulation, listed in order of distance from the Equator.**

City	Latitude	Climate	Sun hrs/day	Pop. Zone
Singapore	1.2	Tropical	5.6	C
Addis Ababa	9	Highland	7	B <sub>south</sub>
Bangkok	13.8	Tropical	7.2	B <sub>south</sub>
Harare	-17.8	Hot Arid	8.3	C
Hong Kong	22.1	Warm Temperate	5.5	A
Phoenix	33.4	Hot Arid	11.1	A
Sydney	-33.8	Warm Temperate	6.7	D <sub>south</sub>
Boston	42.3	Cool Temperate	7.4	A
London	51.5	Warm Temperate	4	B <sub>north</sub>
St. Petersburg	59.9	Cool Temperate	4.5	B <sub>north</sub>

### 3.3.1 Temporal Map Visual Similarities

The weighted temporal maps produced using the data reduction method will ultimately be used as visual displays of data, intended to help architects make design decisions. Hence, it is important to confirm a visual similarity as well as numerical accuracy between the weighted and the detailed reference case temporal maps. A critical validation point is also to ensure that the “main visual features” of a very detailed temporal map would also be observed in a contour map based on 56 representative moments. These main visual features refer to those aspects of the map which, if lost, would cause the architect to misjudge the performance of the design and may typically refer to the general level of illuminance, the way that illuminance levels change with time of day or season, indications of sun penetration, or indications of weather patterns.

As shown in Figure 3-6, the biggest visual difference between the weighted temporal maps and the Daysim temporal maps is the effect of averaging. The Daysim maps, which have a resolution of 5 minutes, can show minute changes in weather and the “scan-line” striations of back-to-back clear and cloudy days, the result of which is a busy temporal map. The Daysim map can show the exact illuminance at each sensor point at any time of the day or year, but on the smoother weighted map, general trends through time are also revealed clearly - and without what could be perceived as noise.

However, the weighted maps also show high illuminance values that are less extreme than those in the Daysim maps, which is the logical effect of averaging illuminances over a certain period of time. Because this might become a critical oversimplification in some cases, especially in terms of pointing out high illuminance risks, it was concluded that an overlay with direct-sun data, described in Section 3.5, was necessary.

Unsurprisingly, the visual effects of averaging are more pronounced in maps of cities in which the weather is highly changeable – in other words, those cities which have a balanced number of clear and cloudy periods in quick succession with each other. Boston (Figures 3-4 and 3-6) is one such city, as are Hong Kong and Addis Ababa to an even greater degree. Harare (Figure 3-7) and Phoenix, two hot arid climates, tend towards more consistently sunny days, resulting for the most part in a higher visual correlation between the two maps. Likewise, although Sydney (Figure 3-8) and Bangkok



(Figure 3-2) have average sun hours that are closer to Boston's, the weather in those cities seems to change more slowly, causing less discrepancy between the two maps.

On the other extreme are cities such as London (Figure 3-9), St. Petersburg, and Singapore, which are largely overcast climates. The visual correlation between the weighted and detailed Daysim maps for these cities is good, because the sunny "peaks" in the Daysim maps are so few and far between that the averaging effect is less noticeable. The temporal maps shown above are typical of the variety of the whole group, rather than representing only the best correlations. In fact, the south-facing Boston map is one of the worst visual correlations produced by this method. Yet even in Figure 3-6, the most important weather features were maintained. It can be seen that the general illuminance level on the south face increases around midday during fall and spring, and decreases in the middle of summer and winter (presumably because of the steeper sun angles of the former season, and because of the overcast weather of the latter season). The other maps only increase in visual accuracy.

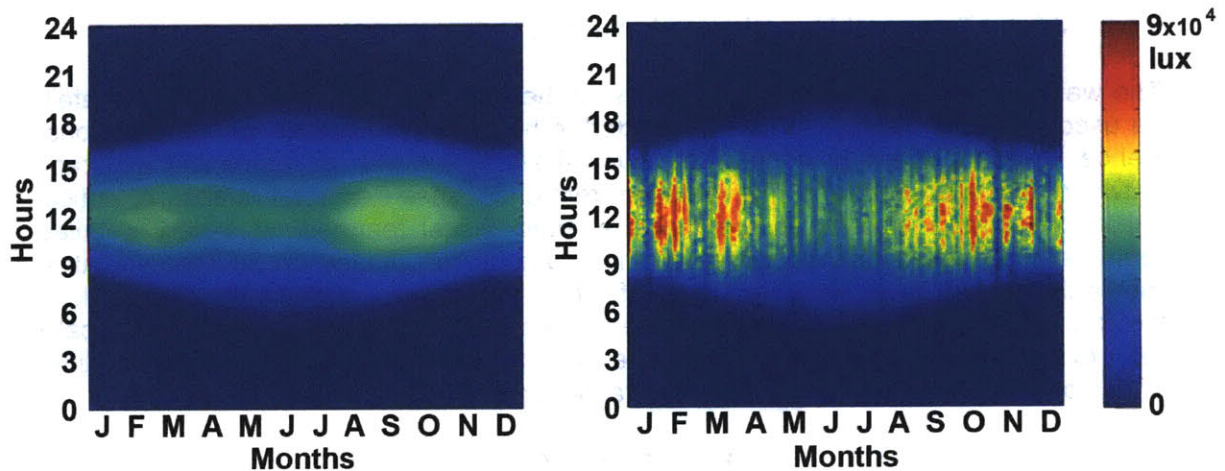


Fig 3-6. Temporal maps comparison for exterior conditions: Boston south-facing sensor. The saturation illuminance is 90,000 lux. Left) data reduction method; Right) Daysim.

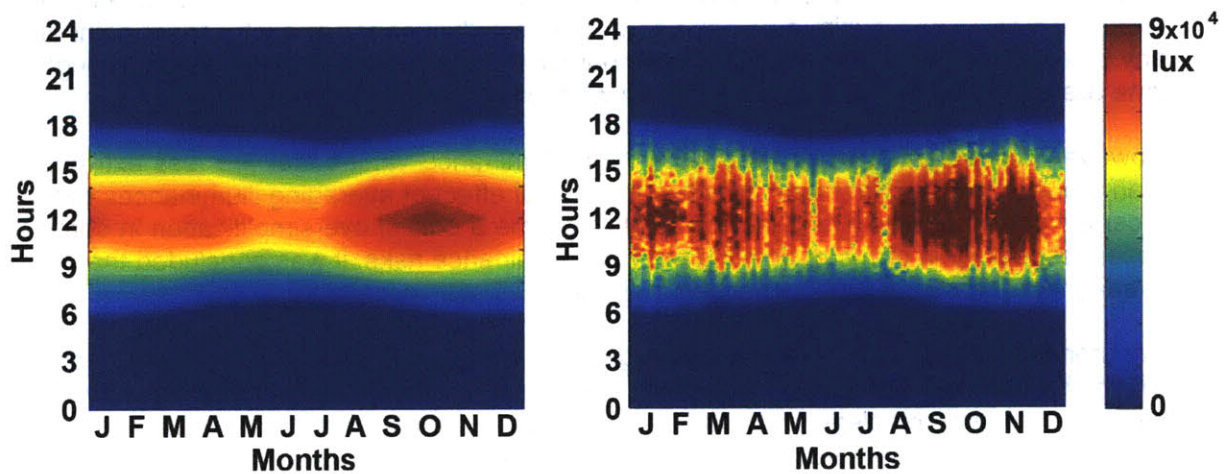


Fig 3-7. Temporal maps comparison for exterior conditions: Harare horizontal sensor. The saturation illuminance is 90,000 lux. Left) data reduction method; Right) Daysim.

Harare's horizontal weighted map, for instance, faithfully reproduces high-illuminance spots during the spring and early summer (September through December at Harare's southern latitude), and London's South-facing map shows a lack of those high-illuminance peaks, while indicating that the late summer is the brightest time of year (however marginally). These time-dependent patterns of illuminance could be vital to design decisions and are clearly marked on every weighted temporal map. One could even argue that the smoother presentation of the weighted maps is preferable to the busy detailed maps, because they are less distracting and show general trends more clearly.

One analogy which can be drawn here is the practice of leaving nonessential and peripheral details out of a rendering or architectural model. For instance, a rendering in grey tones prevents clients from complaining about the wallpaper when they're supposed to be judging the building form. In the case of a temporal map, it is much more important for an architect to understand that there's too much light at midday

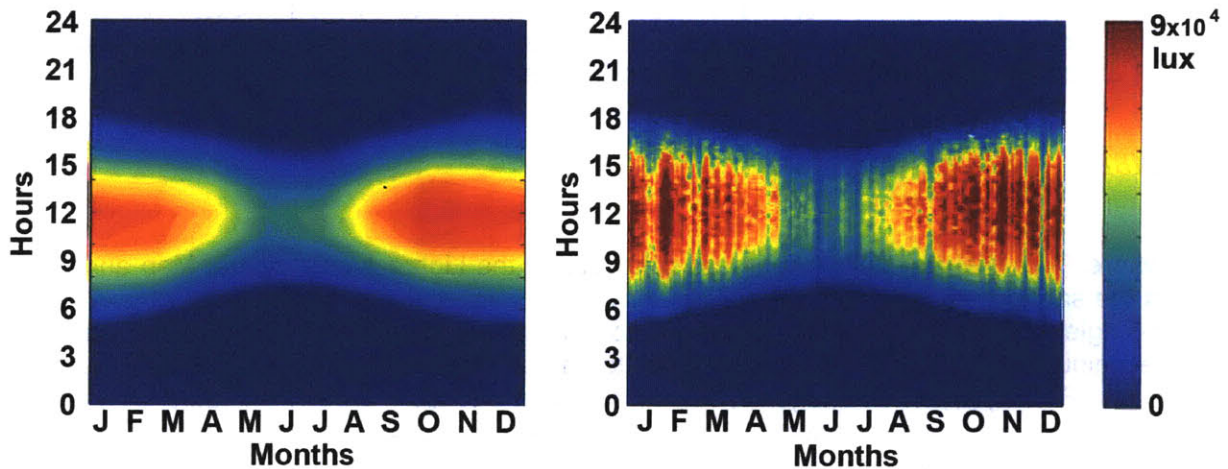


Fig 3-8. Temporal maps comparison for exterior conditions: Sydney horizontal sensor. The saturation illuminance is 90,000 lux. Left) data reduction method; Right) Daysim.

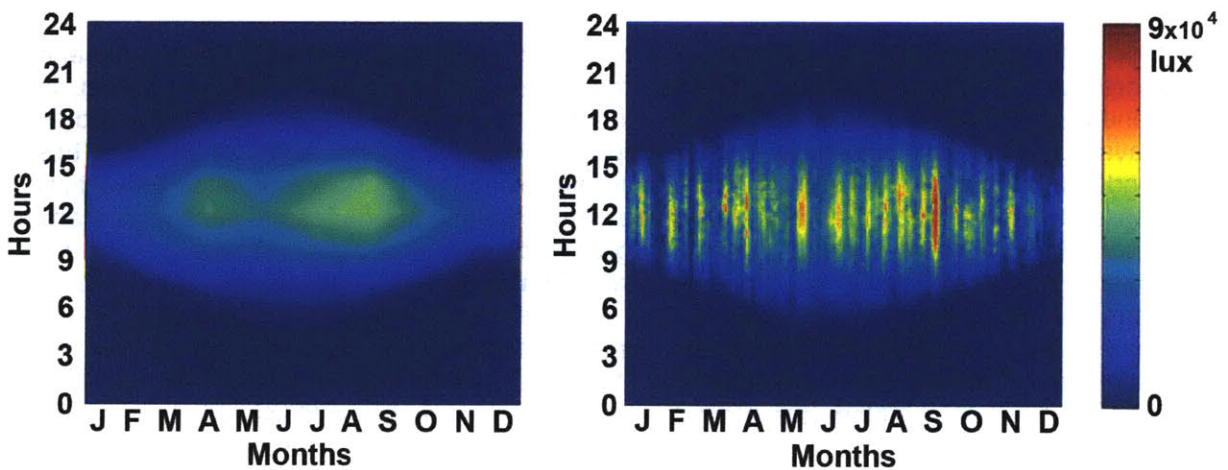


Fig 3-9. Temporal maps comparison for exterior conditions: London south-facing sensor. The saturation illuminance is 90,000 lux. Left) data reduction method; Right) Daysim.

during the summer than to focus on the fact that it's cloudy on March 17<sup>th</sup> in the afternoon during the theoretical "Typical Meteorological Year".

The most prominent piece of information not captured in the weighted maps is that of changeable weather and the greater averaging of those illuminance extremes. For less changeable climates (like London and Harare), a few peaks or troughs may still be lost, but since they are not the norm, they probably should not have a great weight in design decisions, and may even serve to confuse matters.

### 3.3.2 Numerical Pixel-Based Comparison

Pixel-by-pixel analyses were undertaken on grayscale versions of the temporal maps: after dividing both weighted and detailed Daysim maps into areas corresponding with the 56 annual divisions (shown in Figure 3-4), an average illuminance, determined by the average grayscale pixel brightness, was found for each of the 56 periods. The Mean Bias Error (MBE) between the weighted and Daysim temporal maps, was then analyzed for each of the 56 periods. The Mean Bias Error is given as:

$$MBE = \frac{1}{N} \sum_{i=1}^N \frac{(P_{iL} - P_{iD})}{P_{iD}} \quad (3.7)$$

where  $P_{iL}$  is the greyscale brightness of a pixel in the Lightsolve Temporal Map and  $P_{iD}$  is the same pixel in the Daysim map. They are summed and averaged over all pixels in a single period. These graphs allow one to analyze the similarity between the 56 period technique and the detailed data on a per temporal area basis. The Root Mean Square Error (RMSE) was not analyzed, because in this situation, a high standard deviation would not indicate a correlation failure. The method being presented is not intended to match the reference data perfectly, but to be a reasonable averaging process, in which case the effect of averaging peaks and troughs in the Daysim data would skew the RMSE artificially high and would not inform the appropriateness of the simplification methodology.

One definable discrepancy between the weighted and Daysim maps is systematic and more evident from a pixel analysis than from visual comparison. It was found that, in general, the weighted maps estimate illuminances that are lower than those produced by Daysim. Furthermore, there is a strong correlation between solar angle and this "underestimation" – for instance, there is greater evidence of underestimation on vertical sensor temporal maps than between maps produced with the horizontal sensor, and any differences seem more pronounced during the local winter season. In fact, it is for this reason that the Boston south-facing map (Figure 3-6) is one of the worst visual correlations; Boston is at a high enough latitude to have very low sun angles in the winter, yet gets enough winter sun (unlike London and St. Petersburg) that the illuminance difference between the temporal maps is visible. Since this "underestimation" problem is systematic and dependent on sun altitude, it is tempting to try to artificially correct for it. However, according to the study done by Littlefair [Littlefair, 1994], it may actually be at least partially caused by an overestimation on the part of the Daysim maps produced using the Perez All Weather skies.



In a comparison study involving carefully recorded measurements and seven different sky models, Littlefair found that both the ASRC-CIE model (used in the data reduction scheme) and the Perez All-Weather sky model (used in Daysim) overestimated sky luminance in comparison with actual measurements, and that the All-Weather model overestimation was significantly greater in certain circumstances [Littlefair, 1994]. Specifically, the All-Weather Mean Bias Error (MBE) was significantly higher than the ASRC-CIE MBE for low solar altitudes, as was the Root Mean Square Error (RMSE, which is a standard deviation from the measurements, not the mean). Particular trouble spots for the All-Weather model were cloudy and intermediate skies near the sun (at low sun altitudes) and the sky areas opposite the sun (at any altitude) for intermediate and clear skies. Consequently, the south-facing winter illuminances, the morning east-facing illuminances, and the afternoon west-facing illuminances produced for the weighted maps might seem much lower than those produced by Daysim, and these problems should only increase with latitude. Visual observation supports this supposition, and the pixel analysis (see below) supports it even more strikingly. However, since the Daysim maps are used as a reference for validation, this discrepancy appears in the numbers as an error of the weighted maps.

Figure 3-10 supports the phenomenon discovered by Littlefair. In the top of Figure 3-10, the average illuminance was found over all periods – except those in the early morning and late evening, which were disregarded in order to keep the erratic errors associated with very small illuminances from dominating the data. The difference (the MBE) between the weighted and Daysim values was plotted as a function of absolute latitude (southern hemisphere latitudes were made positive). There is a general decrease in correlation between the weighted and Daysim maps as one gets further from the equator, which, if Littlefair is correct, is at least partially due to the All-Weather model's tendency to overestimate illuminances at the lower sun angles found at such latitudes. The linear correlation (in the bottom of Figure 3-10) between those locations with a moderate to large number of average sun hours (excluding Singapore, Hong Kong, London, and St. Petersburg) is extremely strong. This further supports Littlefair's discovery since it is based on sky luminances near the sun.

This tendency is also seen in Figure 3-10 (bottom), which shows the percent error between the vertical, south-facing weighted moments and Daysim temporal maps over the 8 annual periods. (For southern-hemisphere cities, Harare and Sydney, the north-facing sensor is used.) Again, the extremes of the day were disregarded to prevent unpredictable low-illuminance errors. During the summer, the time with the highest solar altitudes, all cities remain within a 0% to 15% difference, regardless of latitude. During the winter, however, the error usually increases, especially for the higher latitudes as solar angles get lower. Since the sensor facing the equator is vertical and facing the sun, it is the most affected by the accuracy of the sky model around these low sun angles, and as such, any differences would be emphasized.

In short, there is a documentable difference between the weighted and detailed Daysim maps, especially at lower sun angles, but there is not enough evidence to support artificially correcting for a higher correlation between the two. In fact, Littlefair's evidence suggests that the weighted maps are using the more accurate sky model and may be closer to the measured values than Daysim. Taking this phenomenon partially into account by ignoring the most extreme low sun angles of the day (times 1 and 7, nearest sunrise and sunset), there is still a good correlation between the weighted maps and Daysim. The MBE for every city at a non-extreme time of day falls between 0 and -22%,

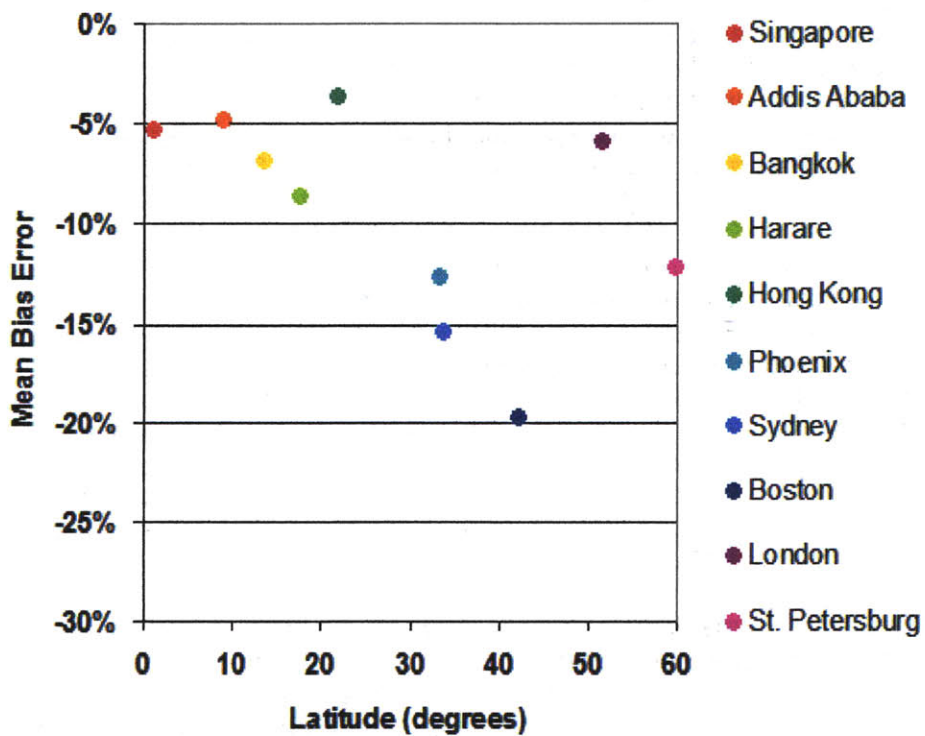
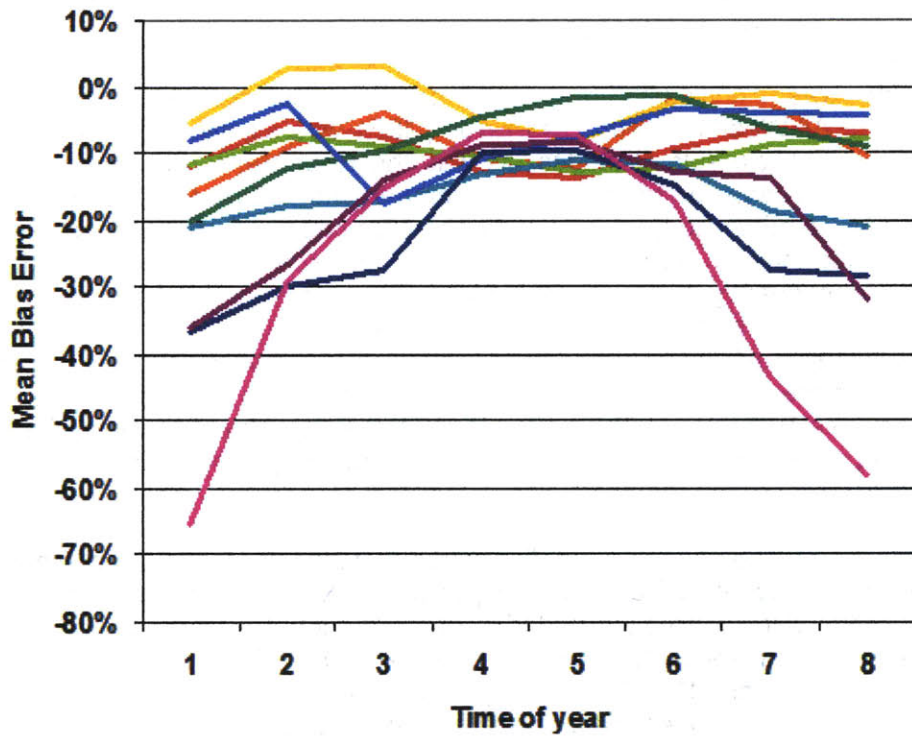


Figure 3-10. MBE averaged over all 56 periods of the horizontal sensor map, for each city (top). MBE between all south-facing (or north-facing for southern latitudes) weighted and Daysim temporal maps as a function of time of year (bottom).

while in the first and last months of the year, that range stretches to about -40% except for a few outliers. This November through February increase in error is because most of the cities are in the northern hemisphere, some at high enough latitudes, that even midday sun angles can be reasonably low.

### 3.4 Interior Illuminance Test for Simple Geometry

Having shown that the weighted temporal maps are a reasonable correlation to those produced by Daysim under an unobstructed sky, one must demonstrate that restricting the access to the sky (via architecture) does not seriously change this correlation. To this end, two simple shoebox-like rooms were constructed and tested under Boston and Harare skies, respectively among the worst and best correlating cities from the previous section. The Radiance model consists of a rectangular room, 10m x 7.5m x 3m, in which the shorter facades face north and south. There is one south-facing window, 1.5 m tall and 5.5m wide, with a head height of 2.5m, rendered without glass. The idea behind this model was to restrict access to the sky but still provide a large, unbroken, direct connection. A modified version of the “shoebox” model was also tested in the Boston and Harare environments: a diffuse light shelf was added to the south window of the shoebox model as well as strip window on the north wall a third the area of it’s opposite (flush with the ceiling with a height of 0.5m). All shoebox models were rendered using a 3x4 grid of 12 horizontal sensor points at the height of one meter to simulate a work plane. Although Harare is located south of the equator, making the north façade the “sunny” side in comparison with the south, the orientation of the models was not changed between climates. The Radiance simulation parameters for this model are the same as in the previous section. All opaque materials are perfectly diffuse grey tones. The ceiling reflectance is 83%, walls 65%, floors 5%.

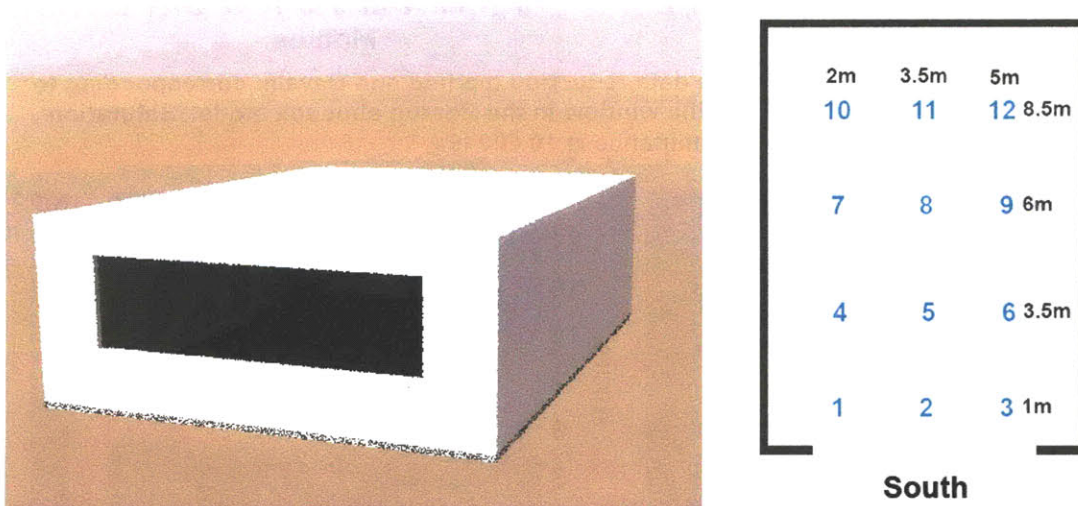


Figure 3-11. Rendering of the shoebox model (Radiance) and a diagram showing the points layout.



### 3.4.1 Temporal Map Visual Similarities

Because the sensors within the shoebox model can “see” a large swath of the southern sky, many of the visual correlations and discrepancies are similar to those found for the south-facing “cube” model sensors. The south-facing cube sensor for Boston (Figure 3-6), being vertical, facing the sun, and at higher latitude, was susceptible to a high MBE between the ASRC-CIE and All-Weather sky models, and this was very visually perceptible in the winter moments. Likewise, the lower winter illuminance occurs also in the Boston shoebox model (Figures 3-12 and 3-13), and is most striking at the points 6m from the window (Figure 3-13), although the actual illuminance difference is only a few hundred lux. The window on the Harare model, on the other hand, is facing away from the sun and only receives diffuse light (see Figures 3-14 and 3-15). Like its north-facing “cube” model counterpart, these graphs show a high visual correlation and smooth, easily definable temporal illuminance features. With a window this large, there is a pronounced visual similarity between the unobstructed “cube” model sensors and the shoebox model sensors.

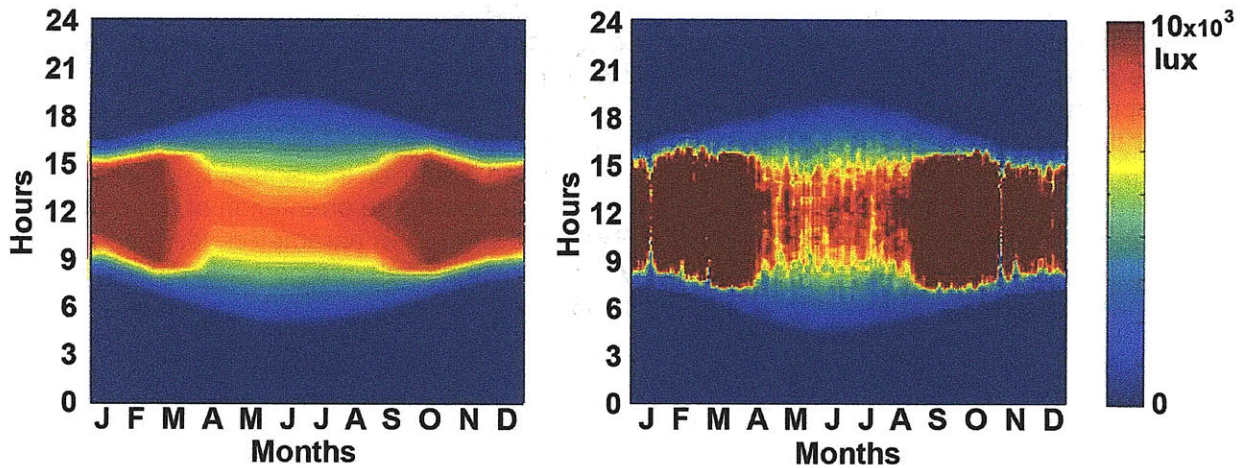


Figure 3-12. Temporal maps for the data reduction method and Daysim corresponding to a sensor point situated 1 m from the window in the Boston shoebox model. Saturation illuminance is 10,000 lux.

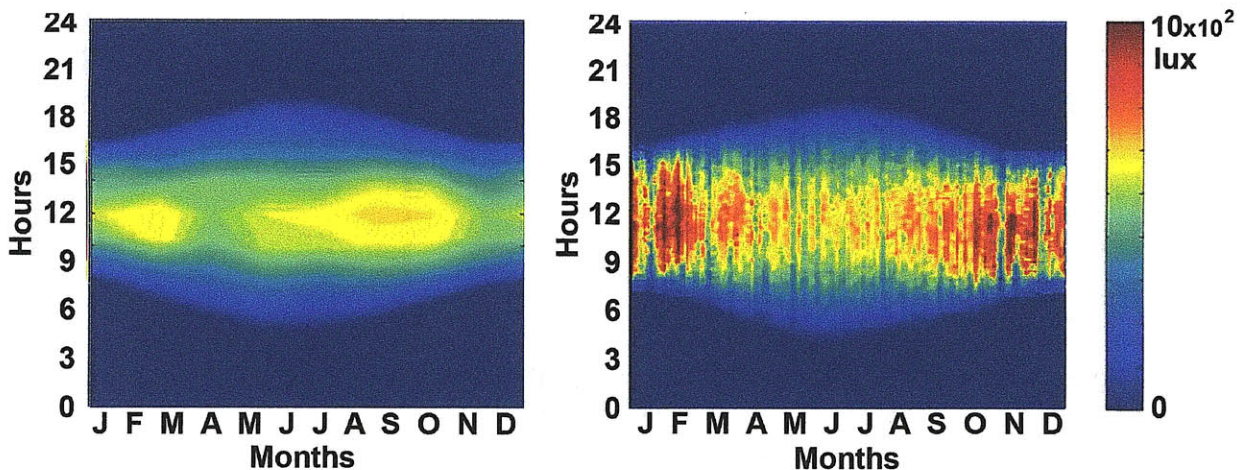


Figure 3-13. Temporal maps for the data reduction method and Daysim corresponding to a sensor point situated 6 m from the window in the Boston shoebox model. Saturation illuminance is 1000 lux.



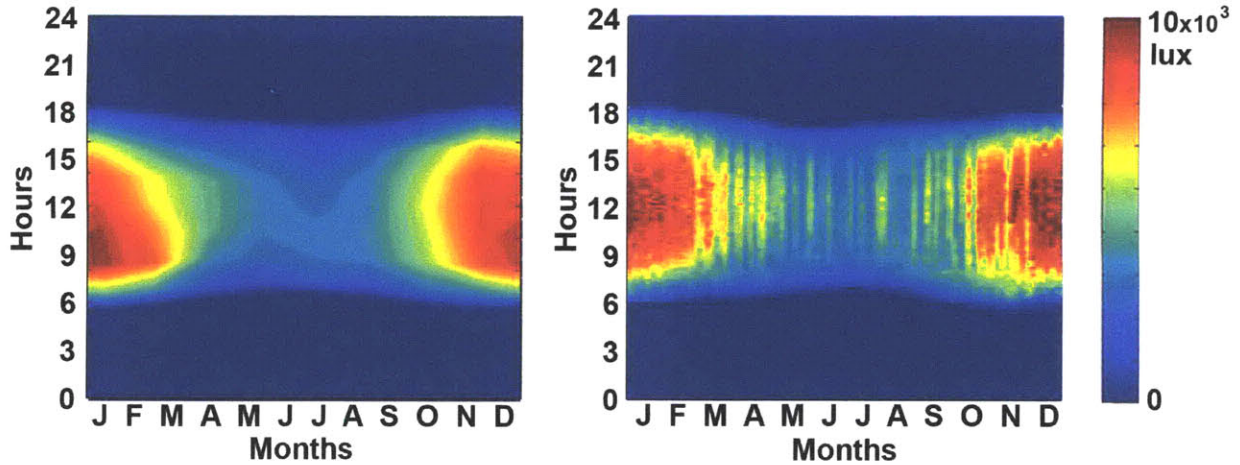


Figure 3-14. Temporal maps for the data reduction method and Daysim corresponding to a sensor point situated 1 m from the window in the Harare shoebox model. Saturation illuminance is 10,000 lux.

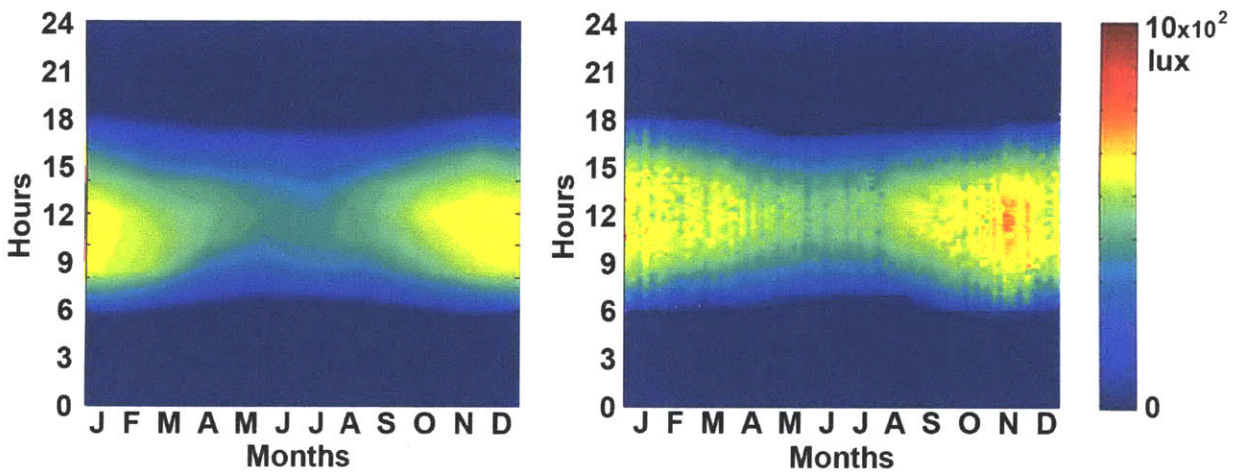


Figure 3-15. Temporal maps for the data reduction method and Daysim corresponding to a sensor point situated 6 m from the window in the Harare shoebox model. Saturation illuminance is 1000 lux.

The modified shoebox model for Boston is similar in many respects (see Figures 3-16 and 3-17). There is definitely a lessening of direct sunlight near the window in the spring, fall, and summer, which is the point of a light shelf, and is also apparent in the Daysim-produced maps. The middle of the room is a bit darker as well, and the points near the northern wall benefit from their new window proximity, especially in summer.

### 3.4.2 Numerical Pixel Comparison

Just as the visual analysis correlates to the “cube” model sensor which sees the same swath of sky, the numerical correlations and discrepancies are also similar between the open sky and the large-windowed shoebox. Sensor points numbered 1, 2, and 3 in Figures 3-18, 3-19, and 3-20 below are closest to the south window, and points 10, 11, and 12 are furthest north. Pixel analyses, similar to those done for the outdoor “cube” model, were applied to the shoebox model.



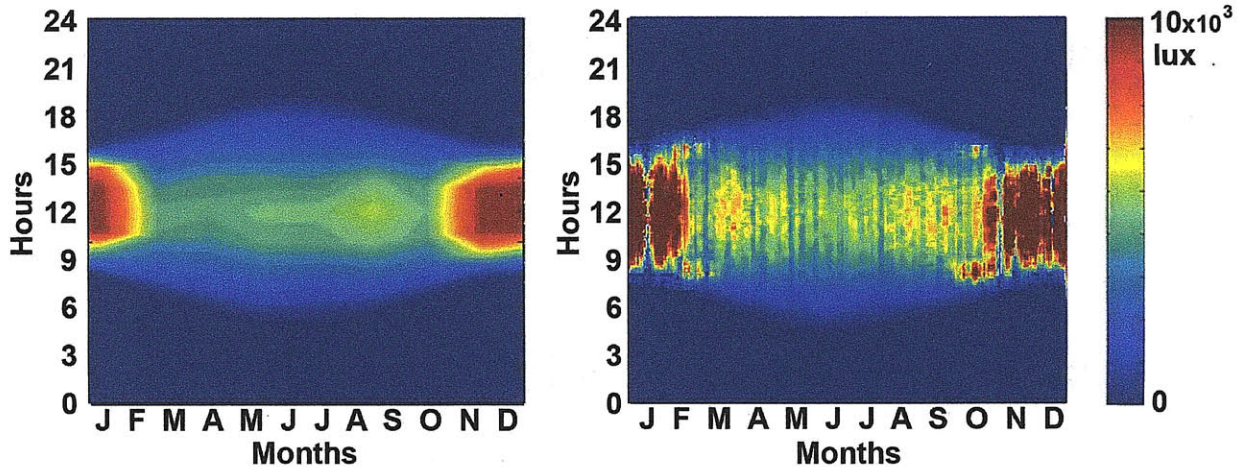


Figure 3-16. Temporal maps for the data reduction method and Daysim corresponding to a sensor point situated 1 m from the window in the Boston modified shoebox model. Saturation illuminance is 10,000 lux.

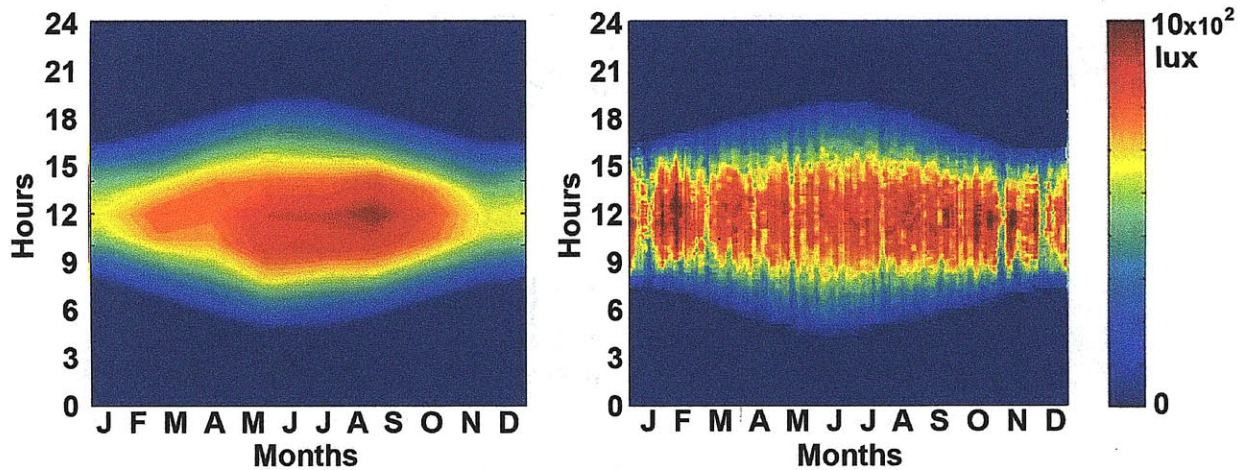


Figure 3-17. Temporal maps for the data reduction method and Daysim corresponding to a sensor point situated 6 m from the window in the Boston modified shoebox model. Saturation illuminance is 1000 lux.

Figure 3-18 shows that the nature of the period-based MBE in the Boston shoebox model is similar to the error for an unobstructed view of the sky. There is a larger difference between weighted moments and detailed Daysim maps for the lower sun angles in Boston's winter and less error in summer. This is somewhat true of Harare (Figure 3-19) also, although the sun is on the north side of the building in that case, and the error curve is flatter throughout the year. In the modified Boston shoebox model (Figure 3-20), there is also a smaller north-facing window, and the shape of the north-facing error curve for the cube model is a visible influence in the three most northerly points (10, 11, and 12). There is one anomalous curve for the normal shoebox model in Boston, which falls between -50% and -70%, the peak of which is barely visible on the graph in Figure 3-18.

One interesting observation to make is that the error between weighted and detailed Daysim maps can be as much as 10% less for the shoebox model than for the

unobstructed sensors, and some points tend slightly positive rather than negative. It is encouraging that this simplification method moves even closer to the Daysim temporal map's performance when one adds architecture into the model, especially since much of the validation done for Daysim was done using interior sensor points [Reinhart & Walkenhorst, 2001]. The systematic "underestimation" as a function of solar altitude, which was discussed in Section 3.3, can clearly be seen still, but most of the MBE curves have shifted closer to zero.

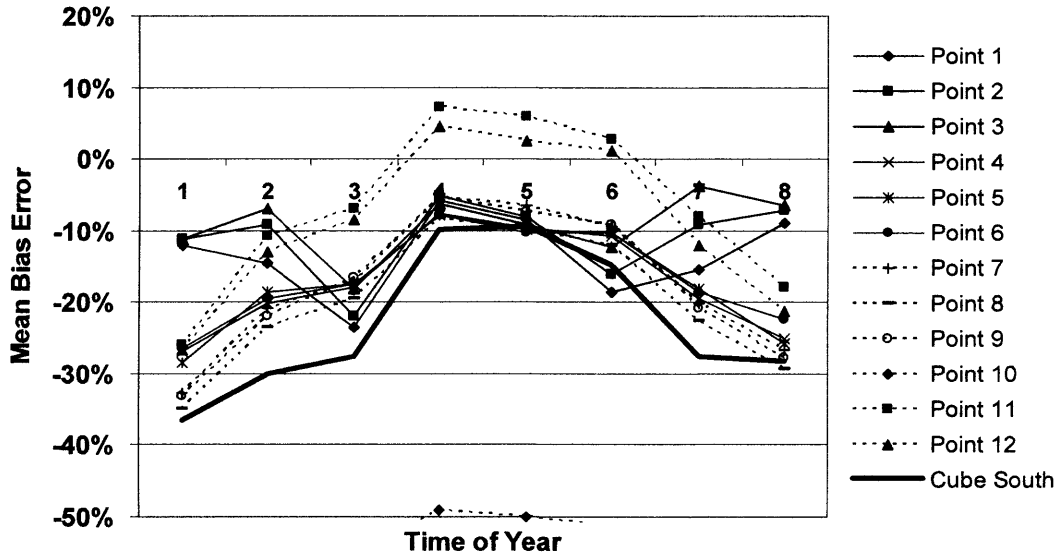


Figure 3-18. Shoebox model MBE between data reduction method and Daysim maps as a function of time of year in Boston. The thick black lines represent the MBE for the south-facing vertical cube model sensor, included for comparison.

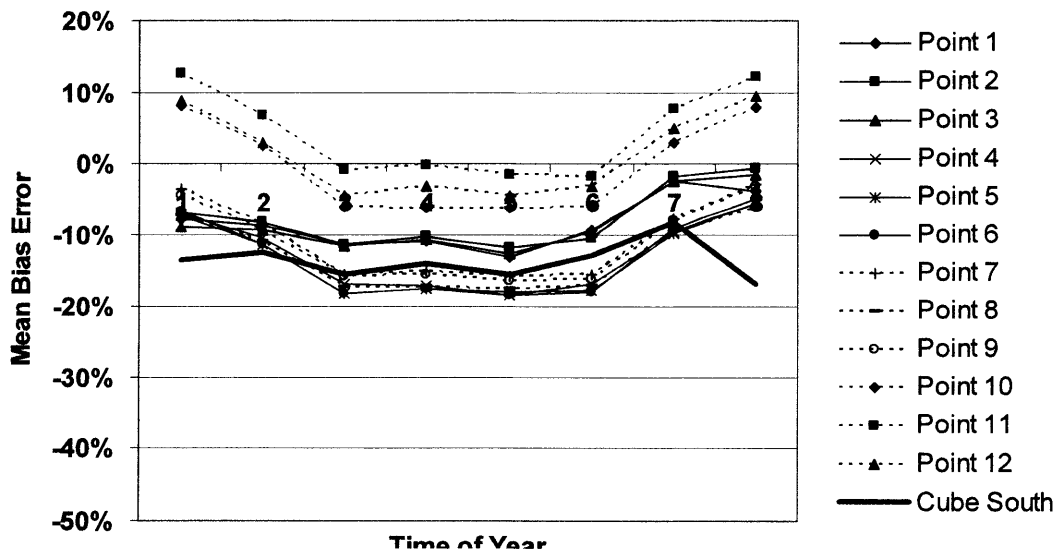


Figure 3-19. Shoebox model MBE between data reduction method and Daysim maps as a function of time of year in Harare. The thick black lines represent the MBE for the north-facing vertical cube model sensor, included for comparison.

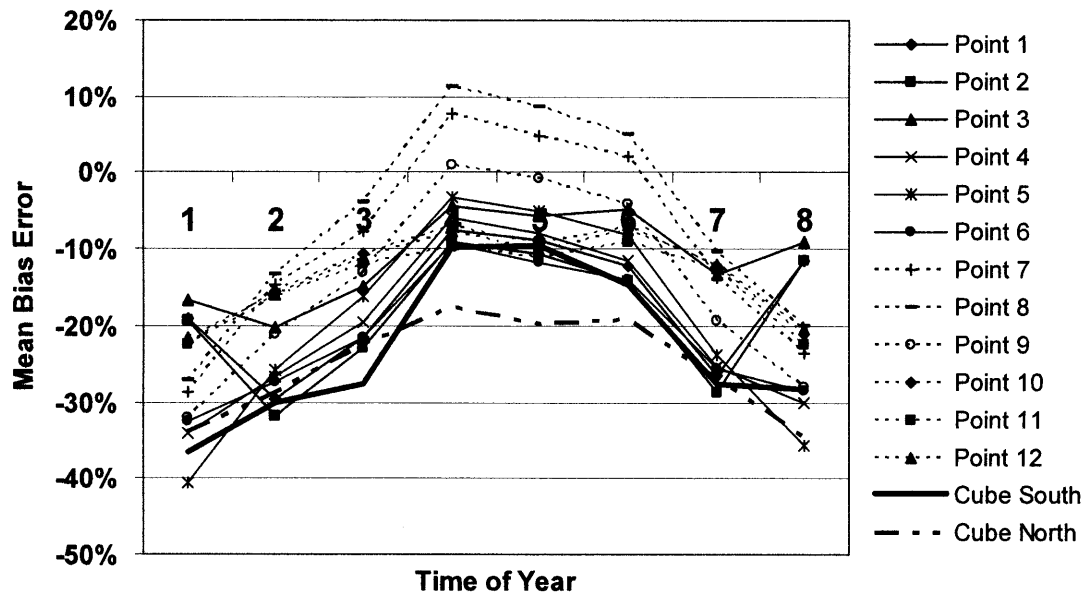


Figure 3-20. Modified shoebox model MBE between data reduction method and Daysim maps as a function of time of year in Boston. The thick black lines represent the MBE for the south- and north-facing vertical cube model sensors, included for comparison.

### 3.5 Interior Illuminance Test for Complex Geometry

The third validation case is based on a four-room museum. Designed by an architecture student at MIT [Yi, 2008], it is a building of much higher complexity than the shoe box model and includes features such as louvers, small windows, divided skylights, and lattices. The walls are 70% reflective (diffuse), and the ceiling and skylight wells are about 80% reflective. The object of this case study was to see if the complex geometry changed the level of visual correlation between the weighted and detailed Daysim maps. Figure 3-21 shows an exterior and two interior shots of the museum model.

Two areas of interest were chosen in the museum: a horizontal area in the center of the southwest room at table height (1m from the floor), represented by 9 sensor points spaced 1.5m apart, and a vertical area along the north and east walls in the northeast room, represented by ten sensor points (four on one wall and six on the other, at heights 0.65m and 2.5 m). Weighted maps and Daysim-based maps were then produced for each sensor point in each area under Boston skies. The Radiance simulation parameters used in this case were -ab 5, -ar 256, -aa .15, -ad 1024, -as 256, -dp 1024, -ds .15, -dt .1, -dc .75, -dr 3, -ms 0.1, -sj 1, -st .1, -lr 12, -lw .01, -l+, -h. The increase in the resolution parameter in this case is due to the vast decrease in size of the architectural elements.

The first important observation one could make was that for general illuminance levels, the same high level of visual correlation could be observed between the weighted and detailed Daysim maps, which was a satisfying result considering the complexity of the building model. One big difference, however, was that there were also small stripes or patches of direct sunlight moving around the rooms which were only intermittently



captured using the data reduction method. This was due to the fact that most of the sensor points never see the sky directly, or if they do, it is as tiny patches scattered over the hemisphere. To make matters more complex, the reference maps were produced by Daysim, another program which limits the number of sun angles it simulates (see Section 3.1.1). According to the Daysim tutorial, the program only simulates 60-65 independent sun angles (over 100 per year), and extrapolates the sun's contribution at all other moments from the nearest 3 or 4 sun positions rendered (Reinhart 2005). Unfortunately, this technique produces a result similar to that of using only 28 sun positions, the only difference being that there are about twice as many sun positions accounted for and they are in different locations. Both methods extrapolate sun contribution in the surrounding moments where there might be none, and both methods might miss smaller sun spots.

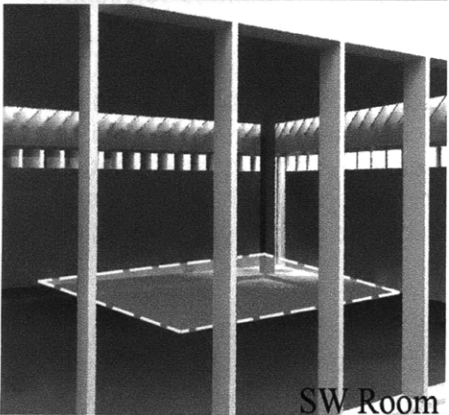
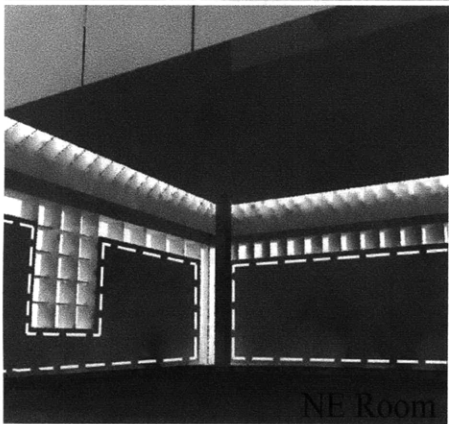
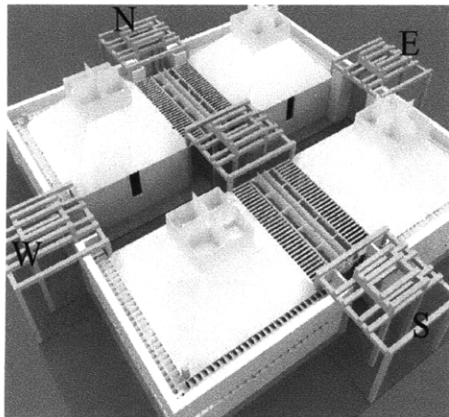


**Figure 3-21. Museum model in Boston. Top) Exterior rendering with cardinal directions indicated. Middle) Interior rendering of the NE room. Bottom) Interior rendering of the Southwest room. Dotted lines represent areas of interest.**

Based on these findings, it was deemed necessary to include an additional zero-bounce sun penetration data set to the proposed data reduction method, calculated at 15 times per day and 80 times per year, or 1200 moments and 600 separate sun angles. This dataset is calculated by doing illuminance calculations in Radiance similar to those done for the 56 annual periods, using the ASRC-CIE sky model and the TMY2 weather data, but at a much greater number of sun angles and discarding interior reflections. The result is that with this fast calculation, the sensor will only record the direct sky component of the illuminance. Whenever it exceeds the illuminance level of the original map, for example, whenever the direct sky component is the dominant one, the new illuminance value should be considered in lieu of the original one because it better reflects the risk of direct sun penetration. When the original map value exceeds the direct sun calculation, global diffuse illuminances is dominant. The direct sun data is thus overlaid onto the general illuminance temporal maps only during the moments where they exceed the original illuminance values.

In a recent paper by Bourgeois, Reinhart, and Ward [Bourgeois *et al.*, 2008], a new format for dynamic daylighting simulation (DDS) was proposed that calculates 2305 direct daylight coefficients per sensor point, which is the number of non-zenithal Tregenza sky patches [Tregenza, 1987] multiplied by a factor of 16. While the DDS sun positions account for the full sky dome rather than just the annual sun path lines (in order to more easily change latitudes between simulations), their research indicates the need for much higher frequency direct sun contribution than is

accounted for by dividing the year into 56 moments. The number 1200 was considered sufficient in comparison with the DDS scheme, since these sun angle test points are all concentrated within the actual angles of a location's specific sun path, rather than over the full sky dome as in DDS. The decision to limit the daily divisions to 15 stems from the fact that for most climates there are not many days which exceed 15 hours, and the TMY2 climate data available has a resolution of only one hour per day.

Figure 3-22 shows examples of general illuminance temporal maps overlaid with direct-sun data. The shoebox model graph in Figure 3-22 (top) is an example of an overlay which does not greatly change the general illuminance temporal map. This is because the large connection to the sky afforded by the shoebox window causes large, consistent, and long-lasting sun spots. On the other hand, the "museum" model graph in Figure 3-22 (bottom) illustrates a situation in which there are many small sun patches flitting around the room. In this extreme case, the general illuminance temporal map did not catch any of these points of direct sunlight, whereas the higher-frequency direct-sun checks did. Weather was taken into account in both cases of finding direct sun spots by weighing and averaging  $b_i$  coefficients as discussed in Section 3.1.2. Although ignoring internal reflections will result in a slight underestimation of illuminance values, this process is only meant to pinpoint moments in which direct sun may be an issue; the general illuminance is still calculated by the 56 periods averaging method.

Unfortunately, when there are many small sun spots, the 56 periods graphs (with or without direct sun overlays) and the normal Daysim results are no longer directly comparable, since each method may perceive or miss different spots. There is another Daysim setting (requiring text manipulation of the header file) which performs a quick shadow casting check to keep track of those points which see direct sun and those which don't. The shadow casting setting recognizes points which catch direct sunlight when the surrounding measured sun contributions do not, but the result of this occurrence is a zero illuminance error from Daysim. The result is that, in a situation where there are many small sun spots, the Daysim shadow casting mode barely recognizes any direct sun contribution, causing an underestimation of illuminances. As

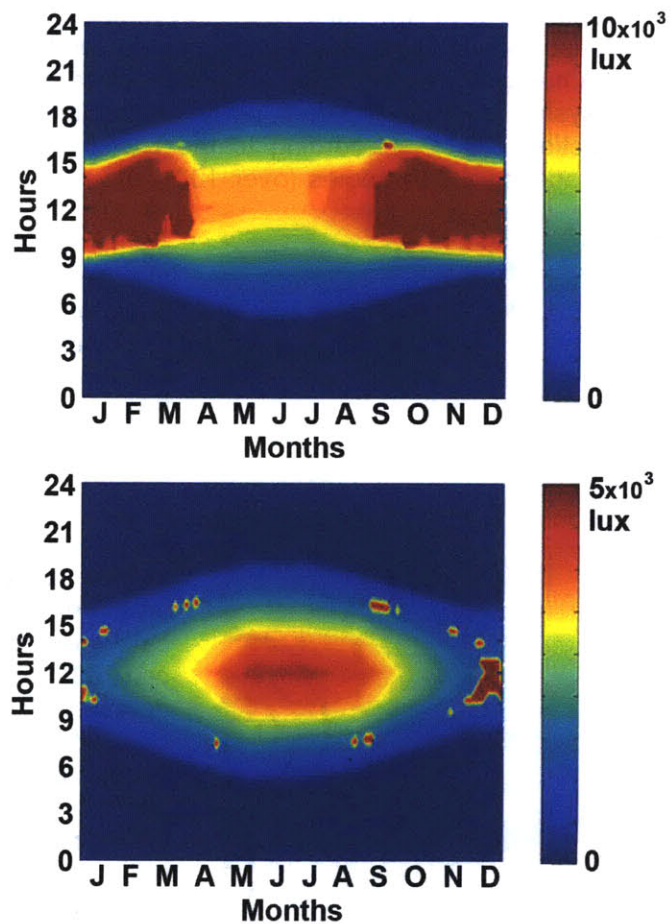


**Figure 3-22. Direct sun overlay examples for a horizontal sensor point in the "shoebox" model (top) and the museum model (bottom). Saturation illuminance for the shoebox point is 10,000 lux, and for the museum point is 5,000 lux.**



**56 periods +  
1200 Moments  
Direct Solar Overlay**

**Daysim  
Normal Operation**

**Daysim  
Shadow-Check Mode**

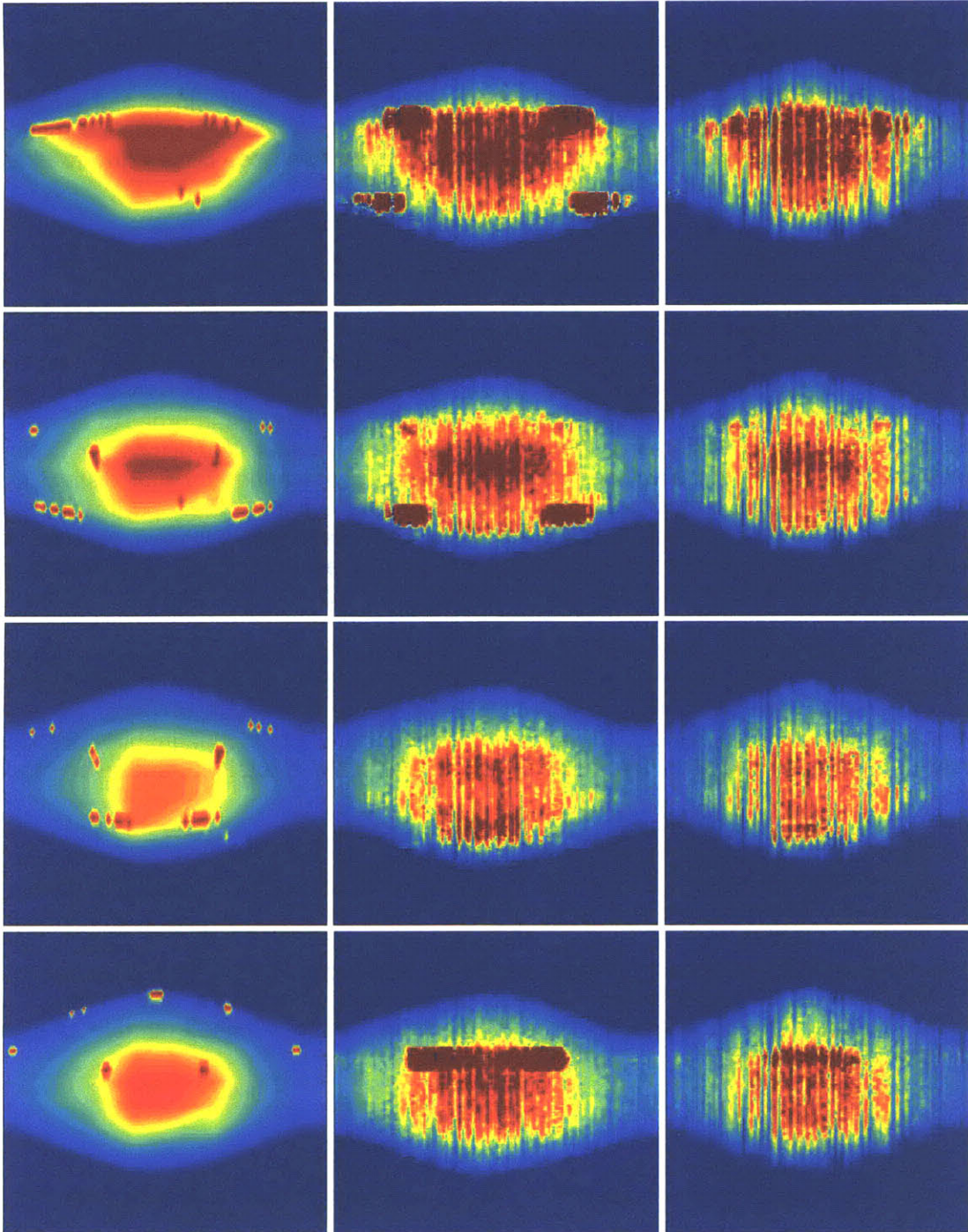


**Figure 3-23. Temporal maps for four representative sensor points in the Northeast room of the Museum model: left column, 56 periods plus 1200 points direct solar overlay; middle column, normal Daysim simulations overestimate direct sun contributions; right, shadow casting Daysim simulations underestimate them.**

this calculation must be performed for one sensor point at a time, only four points in the museum model were tested using shadow casting. As shown through a sample of points in Figure 3-23 (one point per row), every sensor using the shadow-check method records a drop in direct sun contribution in comparison with conventional Daysim simulations. However, a visual comparison suffices to show the good correlation between the shadow casting Daysim temporal maps and the general illuminances levels of the weighted temporal maps. The combination of the simplified annual performance analysis with this detailed direct sun penetration check allows a designer to grasp, at a glance, how lighting conditions will vary over time for that particular location's climate – and also to point out when there might be comfort or performance issues due to direct sunlight.

### **3.6 Summary of the Data Reduction Method**

The overwhelming amount of information possible in an annual data set and the computation time of producing large numbers of renderings are arguments in favor of using a small number of simulations to represent a full year. However, the sky conditions used in these simulations must be very carefully chosen in order to ensure a reasonably accurate representation of the annual weather conditions. Typical Meteorological Year data was used to define average luminances for four distinct sky types over each of 56 temporal periods, and these skies became the input for realistic simulations. The simulated illuminances were then weighted by the frequency of occurrence of each type of sky. Results were compared numerically and visually to detailed data for the cube (external), shoebox (simple), and museum (complex) models.

The comparisons show a strong visual and numerical correlation between temporal maps produced using the data reduction method and those produced using detailed illuminance data extracted from the program Daysim. The result of data reduction method is that small details and the sense of immediate weather changeability are lost, while the changeability of performance on an annual scale is retained, and even made clearer.

However, validation studies found this to be insufficient for accurately depicting the effect of direct sunlight in more complex structures. Therefore, a much greater number of direct sun-only simulations are included and the more detailed information overlaid on the diffuse light-based temporal maps. This extra step is less necessary in cases where areas of interest are large, as a modest change in sun angle can still be captured by the larger sensor plane. As areas of interest, or sensor planes, get smaller, there is a greater chance that direct light will miss the sensors if such a limited number of solar positions are simulated.

# Chapter 4

## Acceptable Illuminance Extent

The data reduction method described and validated in Chapter 3 makes it possible to easily display useful illuminance data as it varies over time. However, there are also spatial dimensions to consider, since daylighting analysis almost always involves more than one or two reference sensor points. Because of the physical limitations of the short term memory [Simon, 1969], we are only able to imperfectly assimilate a few graphs before the amount of data involved becomes overwhelming. Therefore, a single graphic which encompasses both spatial and temporal data at once would be a great asset to the design process – and this is the reason why Daylight Autonomy (DA) (see Section 2.1) is such a valuable metric. Unfortunately, although its calculation involves annual data sets, DA is primarily a spatial metric, whereas this thesis has argued that it is important to know the temporal variation in daylighting performance (Chapter 3).

Section 2.2 discussed the existing research on displaying daylighting data using temporal maps, which includes work done by Mardaljevic [Mardaljevic, 2003] and the simulation tools LightSketch and Building Design Advisor [Papamichael, 1998; Glaser *et al.*, 2003]. All use single point illuminance data to populate their spatial and temporal graphics, and the author has found little precedent for including spatial information in a temporal map format. Glaser's work on "space series" graphs starts in a temporal format and attempts to overlay instances of spatial data [Glaser & Hearst, 1999], however this method is very limited in the complexity of model it can handle, and the resulting images are very confusing. In fact, the only successful precedents for combining temporal and spatial information in a single graphic are the spatially-based Daylight Autonomy and Useful Daylight Illuminance (UDI) [Reinhart & Herkel, 2000; Nabil & Mardaljevic 2005].

DA and UDI sacrifice an understanding of the time-based variability of performance in favor of retaining the spatial variability of performance. In other words, DA can show that for 70% of annual working hours, a particular point has adequate daylight, but it cannot show whether this point is underperforming in the morning hours, or letting in too much light in the summer. Understanding how daylighting data varies over an architectural space can help a designer identify problems in light distribution, which might relate to wall reflectance or room shape. Understanding how daylighting data varies over time can help a designer identify problems in light access, such as building orientation, building form, and window size. Both temporal and spatial formats are crucial to an ultimate assessment of daylighting performance, but schematic design is one of easiest times to fix problems with light access, which are more easily linked with temporal data.

Reversing DA's approach, this chapter describes a metric which condenses the portion of a pre-defined area, in which the illuminance stays within a user-given range, to a single percent and displays the variation of that percent over time. Because this metric is, in essence, defining the amount of space which stays within acceptable limits, it is called the Acceptable Illuminance Extent, or AIE. The first part of this chapter introduces the concept of AIE, and the second part visually compares temporal graphs of AIE



produced using the data reduction method to similar AIE temporal graphs produced using the detailed illuminance data acquired from Daysim.

#### 4.1 Definition of a Temporal Illuminance Metric

The main idea of Acceptable Illuminance Extent is to preprocess spatial illuminance data in terms of given design goals. In most design problems, there are codes or other benchmarks which prescribe minimum illuminance thresholds or illuminance ranges associated with an area of interest (such as the work plane). The IESNA Handbook gives minimum illuminance recommendations for various types of spaces [IESNA, 2000], and the US Green Building Council's LEED rating system gives a daylighting point to buildings where 75% of the work plane is over 2% Daylight Factor. Because of this, DA uses a threshold minimum illuminance value in its calculation, and IES FlucsDL has a feature which calculates the percent of a model work plane that exceeds 2% DF [IES web].

DF cannot be calculated under any except an ideal overcast sky, so for AIE to be truly representative of a given climate, illuminance values relating to codes or the designer's own requirements should provide the thresholds of performance by which to judge a daylighting design. Given an array of illuminances over an area of interest (AOI), the number of sensors, (or sensor patches, in the case of Lightsolve), which falls within the desired range is found, as well as the number of sensors where illuminances are too high or too low. The percent of total sensors which falls within the goal range is the Acceptable Illuminance Extent.

In reality, illuminances which fall outside the prescribed range may still have value; it is difficult to argue that one cannot read just as well with 390 lux as one can with 400 lux, and from this perspective, a hard cut-off seems unreasonable. For this reason, Rogers developed Continuous Daylight Autonomy, which gives partial credit for all illuminances less than the minimum threshold [Rogers, 2006]. For AIE, a "buffer zone" can also be applied, so that models with many sensors reading just below the minimum threshold do not generate the same results as those in which the sensors are far below the minimum threshold. The upper and lower buffer zones can be any size (although the minimum buffer illuminance cannot be below zero), and they do not have to be the same size as each other. Figure 4-1 shows how partial credit can be applied on a linear

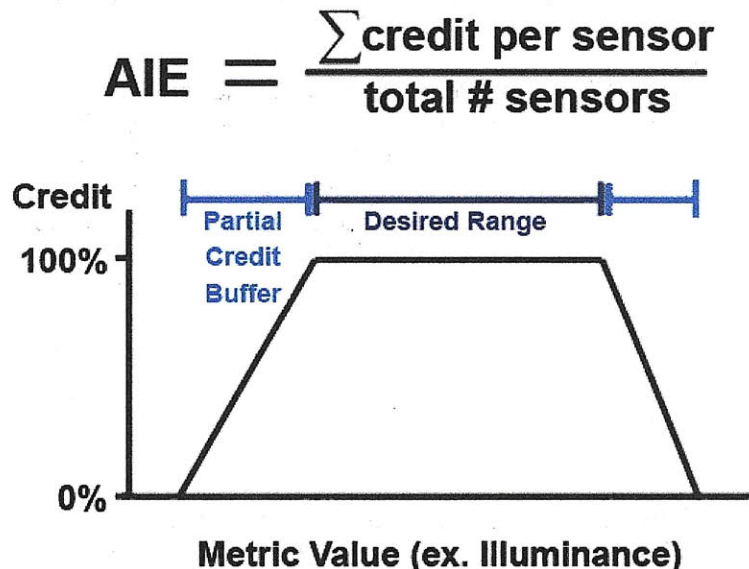


Figure 4-1. This figure illustrates the system of credit and partial credit for AIE. Values within the desired range get full credit, and those in the buffer zone get partial credit.

scale for sensors which fall between the buffer threshold and the actual threshold.

When an area of interest has been divided into AIE and the corresponding high illuminance and low illuminance areas, the next problem is how to display them graphically. It is certainly possible to create a temporal map using a color scale to indicate the AIE from 0% to 100%. The issue with this is that information is lost. It is impossible to tell, using a linear color scale, whether the percent of the plane which is not acceptable is caused by high illuminances, low illuminances, or both, and this information would certainly help diagnose the cause of a performance issue. Of course, the high and low areas could easily be displayed in their own temporal maps, such as in Figure 4-2, however this increases the number of necessary temporal maps when the goal was to reduce their number.

Because of this, the temporal maps displaying AIE are based on a color scale created by mixing the three primary colors. In the triangular (as opposed to linear) scale, yellow represents 100% AIE, blue represents 100% low illuminance extent, and red represents 100% high illuminance extent, as shown in Figure 4-3. Following from this, orange represents a moment when only part of the plane is too high (which might be caused by direct sun spots), greenish represents a moment when only part of the plane is too low, and purple represents a moment when the plane has excessive high and low illuminances. Any color on the triangle is a possible outcome, based on the portions of the plane which are in range, high, and low. The sample temporal map in Figure 4-4

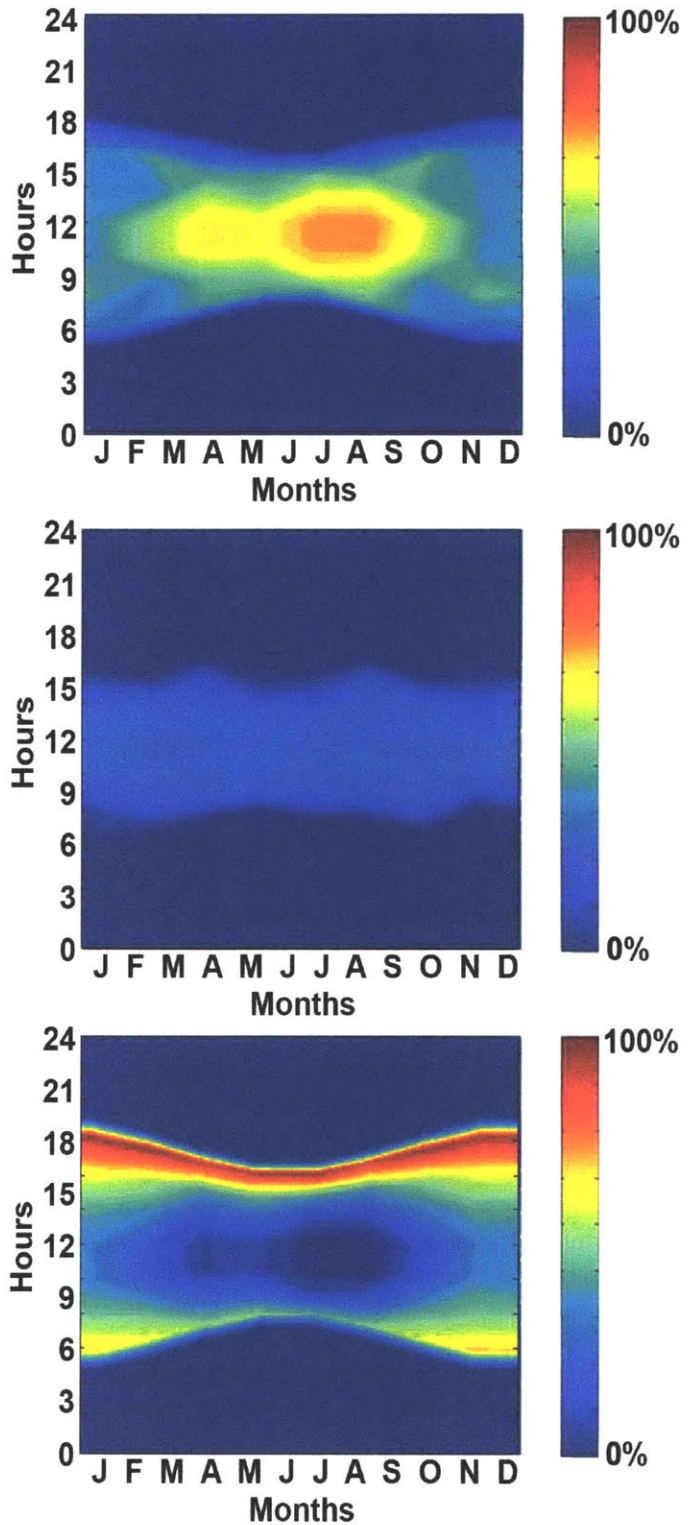
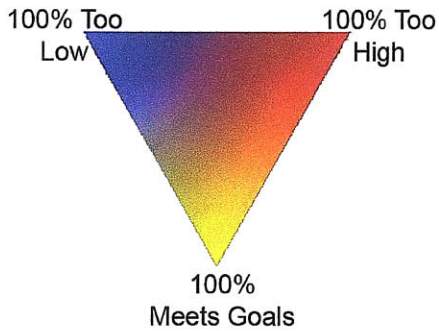


Figure 4-2. Three temporal maps showing the percent in range or AIE (top), percent of the plane which is high (middle), and percent which is low (bottom) for a sample model discussed in Chapter 7.





**Figure 4-3. Color key for goal-based illuminance metrics.**

illustrates this interpretation of color. The great advantage of using a triangular color scale is therefore that three pieces of crucial information (representing compliance with goals, not reaching goals, and overstepping goals) can be displayed simultaneously on the same graph. Furthermore, these three colors represent, not raw data, but goal compliance for any metric, which makes very different metrics comparable.

Previous attempts to convey the same information using a linear scale involved the use of three graphs, similar to those in Figure 4-2, or scroll-over information which would give the percent of the data which was too high or too low. For instance, numbers or figures to the side of a temporal map displaying 0% to 100% goal compliance would describe non-compliant data and would change as the user scrolled over the temporal graph. However, the most elegant solution, and the only way to perceive all data in a single glance (and a single graph), was the triangular color scale.

## 4.2 Temporal Map Visual Similarities using Acceptable Illuminance Extent

Chapter 3 validated a data reduction approach to making temporal maps both numerically and visually, but all of these validations were done for single point illuminances. Because this temporal preprocessing will be used in the formation of illuminance values for AIE, it is necessary to at least do a visual comparison of the AIE processing combined with the data reduction method. This is done in the following sections by comparing weighted AIE temporal maps and AIE maps made with detailed Daysim data. The comparison cases include two instances of simpler architecture – the shoebox model described in Section 3.4 and a similar series of classroom models located in Sydney, Australia – and one exploration of the complex museum model described in section 3.5.

### 4.2.1 Simple Geometry Case

The goal range for the Shoebox model comparison case was derived from the most recent definition of Useful Daylight Illuminance (UDI) [Mardaljevic, 2009]. The illuminance goal range is 500 – 2000 lux, the fully “autonomous” range of the UDI as defined by [Mardaljevic, 2009], although with the upper illuminance limit of the original UDI definition [Nabil & Mardaljevic, 2006]. Partial credit is given down to 100 lux (the “supplemental” range of the UDI) and up to 2500 lux (the new upper limit of the UDI) [Mardaljevic, 2009]. In the figures below, the weighted illuminance method graphs are all on the left hand side, and the figures derived from Daysim data are on the right. A visual comparison makes sense in this case, because the temporal graphic is meant to be the primary information source for design decisions. If the graphs look the similar enough to encourage the same design decisions, it does not matter if the numbers forming them are slightly different.

The graphs in Figures 4-5 and 4-6 represent the original Shoebox model (with one very large unshaded south window) and the modified Shoebox model (with southern

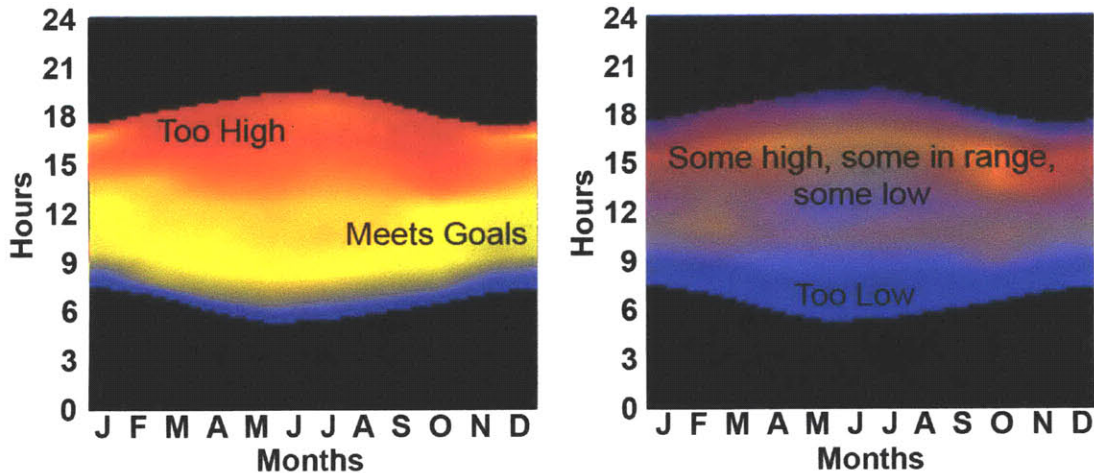


Figure 4-4. Example AIE goal-based temporal maps using the triangular color scale.

overhang plus smaller north window). The area of interest covers most of the workplane (1m from the ground) and is represented by twelve point sensors (see Figure 3-11). The temporal maps below show very close visual correlation, especially considering that the south-facing Boston sensor was one of the worst performing exterior illuminance validations in section 3.4. Indeed, the weighted illuminances graph shows slightly less high illuminances (less orange) in the winter midday as compared with the Daysim data, but it is a less noticeable difference in the goal-based graphs than it was in the pure illuminance graphs.

The orange-yellow color of the main part of the graph in Figure 4-5 represents a sensor plane of which a large portion is within the desired illuminance range, and a smaller portion has illuminances which are too high (probably the area of the plane right next to the window). The graph gets more orange in the winter (especially morning and evening), as the low sun angles penetrate further into the room and make more of the sensor plane too bright. There is also a small blue tinge to the whole graph, but mostly in the early morning and late evening, which indicates that a small part of the sensor plane is usually too low (probably the area in the back of the room). The fact that we are forced to make guesses concerning the location of the problem areas shows the importance of having a spatial reference as well as the temporal maps.

The graphs in figure 4-6 show the improvements made by adding the southern overhang and the north window; the overhang shades the work plane area near the window from direct sun, bringing it back into the acceptable illuminance range, and the north-facing window lights the darker back of the room. There is still an orange tinge to parts of the graph indicating that some sun might still enter, or that the diffuse illuminance is very bright at times.

The graphs in Figures 4-7 and 4-8 represent the same models located in Harare. One should note that the modified Shoebox model represented by Figure 4-8 has not been rotated despite the fact that Harare is in the southern hemisphere (the overhang is still to the south, and the small window was added to the north, despite the fact that the sun is largely to the north). The resulting temporal maps show very bad performance and make an interesting contrast to Figure 4-7.



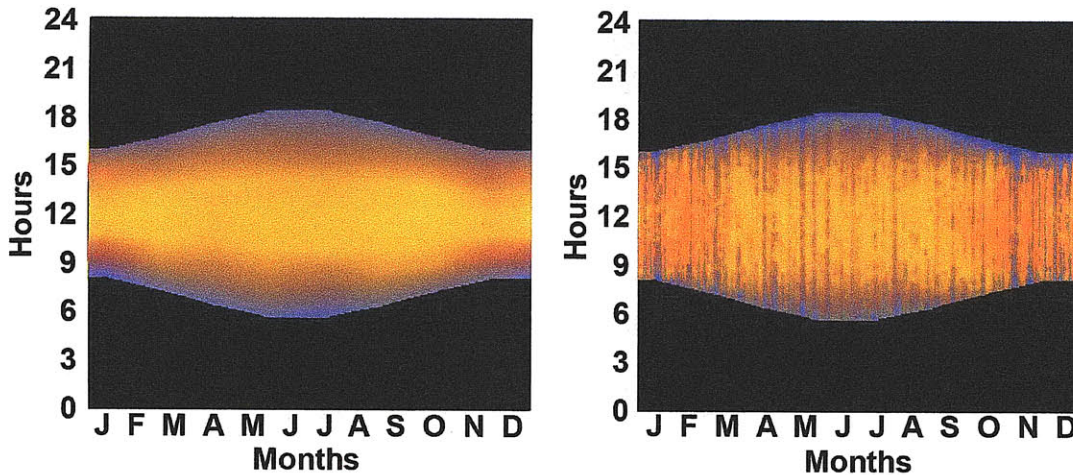


Figure 4-5. AIE temporal maps for the Shoebox model in Boston, range 500-2000 lux, buffer 100-2500 lux. Map created using the data reduction method on the left, and Daysim on the right.

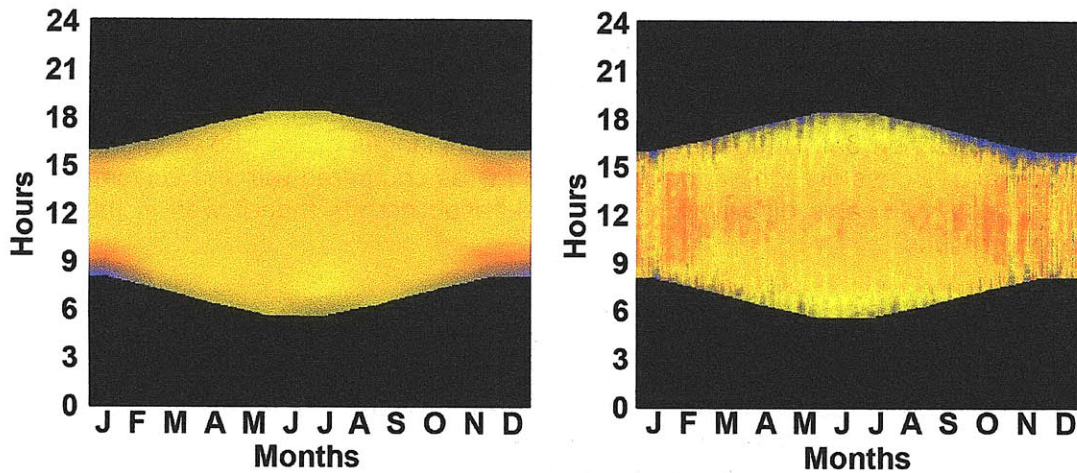


Figure 4-6. AIE temporal maps for the modified Shoebox model in Boston, range 500-2000 lux, buffer 100-2500 lux. Map created using the data reduction method on the left, and Daysim on the right.

In the original shoebox model (Figure 4-7), the greater part of the graph is yellow, indicating that the large south-facing window is letting in a lot of diffuse light. The purple tinges in the early mornings and evenings indicate times which are getting darker, but at Harare's latitude, some glancing sun might penetrate the south-facing window during daily extremes in the summer. (Again, this is when spatial information is useful to have as well.) When the overhang and the unshaded window are added to the "wrong" sides of the model, its performance worsens in every respect. The entire graph takes on a slight blue hue, indicating that shading the diffuse light hurt the total influx into the room, and the addition of the small northern window was not enough to make up for it. Furthermore, the northern window introduces some direct light and bright sun spots during the day in the warmer months.



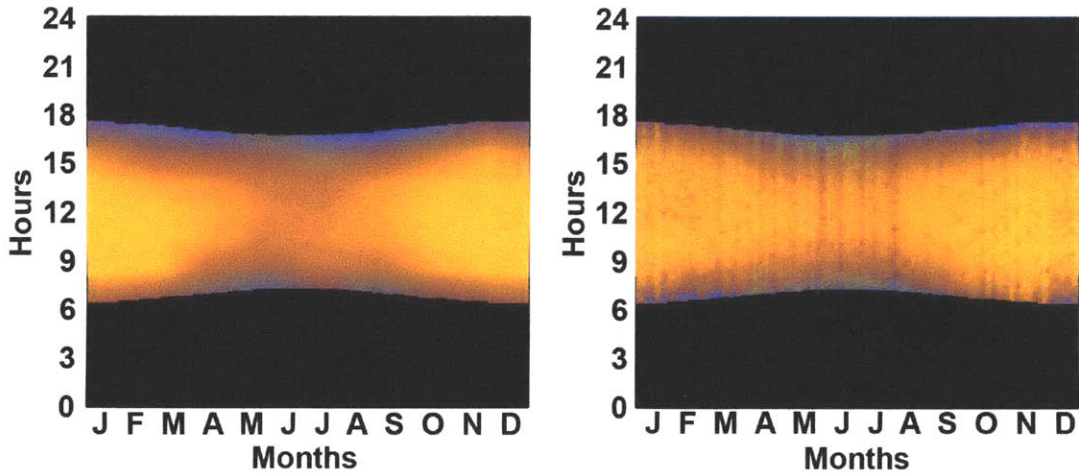


Figure 4-7. AIE temporal maps for the Shoebox model in Harare, range 500-2000 lux, buffer 100-2500 lux. Map created using the data reduction method on the left, and Daysim on the right.

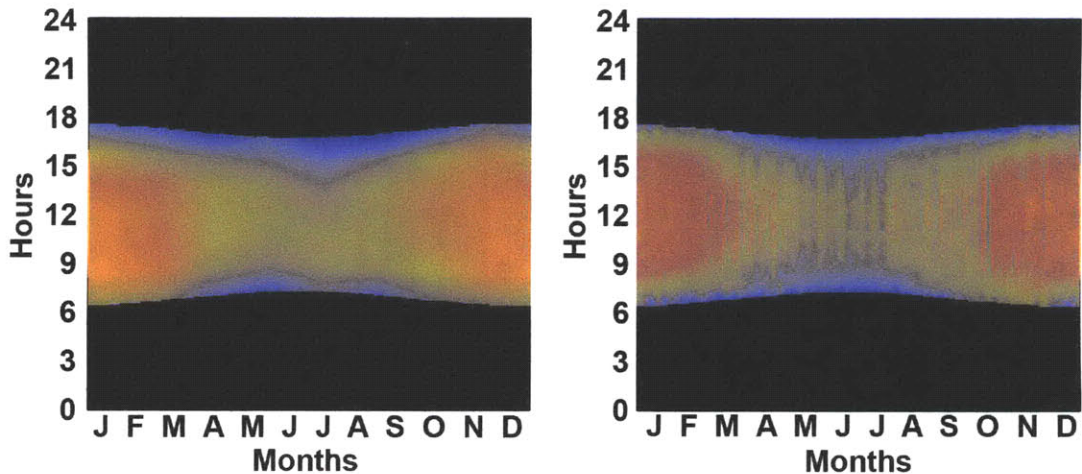


Figure 4-8. AIE temporal maps for the modified Shoebox model in Harare, range 500-2000 lux, buffer 100-2500 lux. Map created using the data reduction method on the left, and Daysim on the right.

Each feature described above shows clearly in both the weighted temporal maps and the detailed Daysim maps, making them directly comparable for the purposes of design analysis.

#### 4.2.2 Classroom Iterations Case

The three classroom models represented in figures 4-9, 4-10, and 4-11 are part of a mock design process meant to show a progression from a bad model to one that fulfills the illuminance design goals. The design goal range is tighter than the one in the previous model, which means that it is less forgiving of inconsistencies. The model and its iterations will be described at greater length in Section 7.1, and figures representing these models appear there as well. This section will focus on the graph comparison.

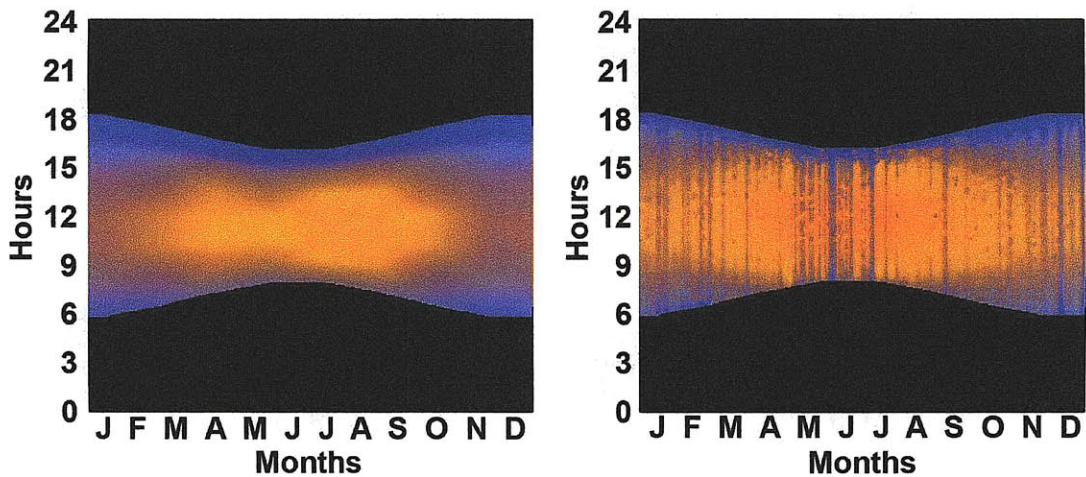


Figure 4-9. AIE temporal maps for the first iteration of the mock design process (Chapter 7) in Sydney, range 400-1000 lux, buffer 200-2000 lux. Map created using the data reduction method on the left, and Daysim on the right.

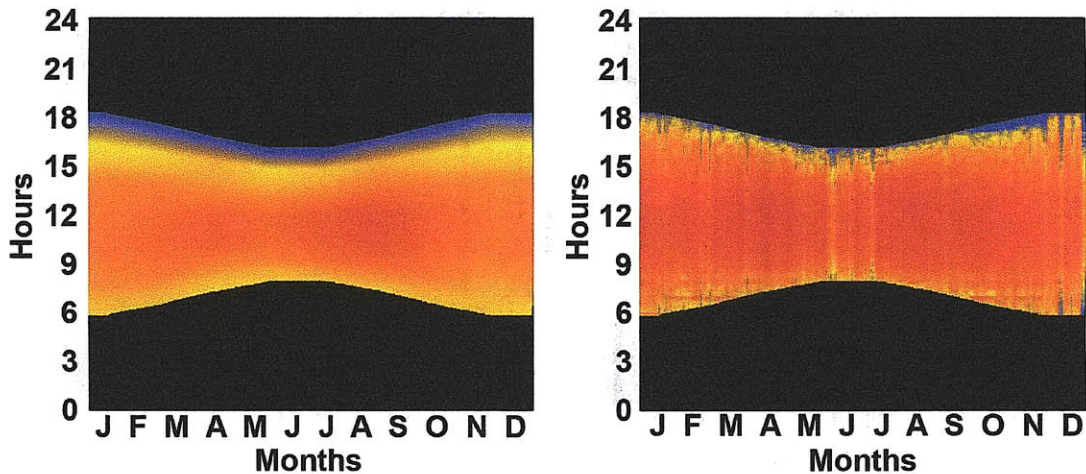


Figure 4-10. AIE temporal maps for the second iteration of the mock design process (Chapter 7) in Sydney, range 400-1000 lux, buffer 200-2000 lux. Map created using the data reduction method on the left, and Daysim on the right.

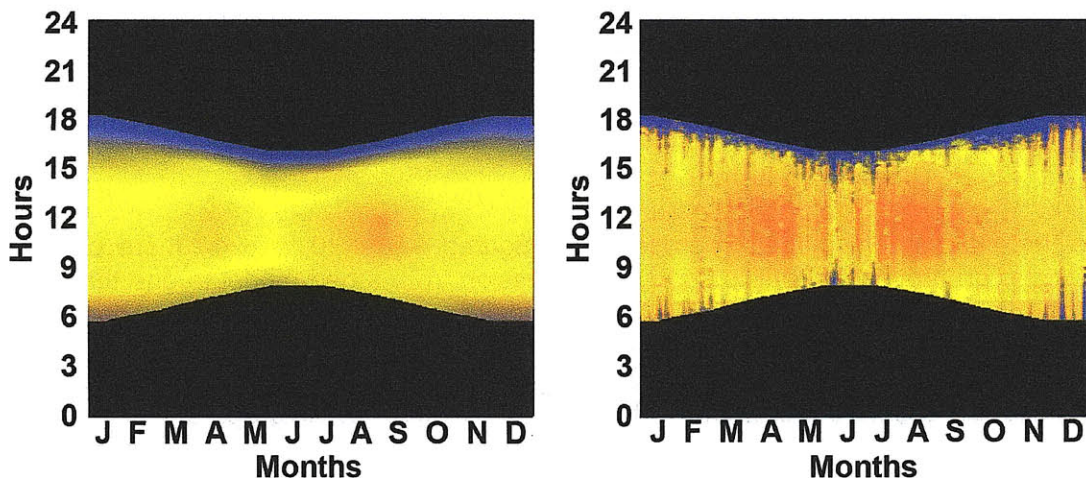


Figure 4-11. AIE temporal maps for the third iteration of the mock design process (Chapter 7) in Sydney, range 400-1000 lux, buffer 200-2000 lux. Map created using the data reduction method on the left, and Daysim on the right.



In all iterations, a slight bias towards lower illuminances can be seen in the weighted illuminances model – the most noticeable ones in the first iteration on summer mid-days, and in the third iteration in winter mid-days. The illuminances in these periods are probably on the cusp between being in range and being either too low or too high respectively. All features of each Daysim graph are visible in each weighted illuminances graph, however.

One should note that both the Shoebox and Classroom series of models are simulated here without the benefit of the high-frequency direct sun overlay discussed in Section 3.5, which would be generally beneficial to the final version calculation of AIE. Because it was demonstrated that the temporal maps of models with large-area windows were virtually identical whether or not the direct sun overlay was used (see Section 3.4), the extra Radiance processing was deemed unnecessary for the current demonstration. The high-frequency sun overlay is used in the next comparison case, however.

### **4.2.3 Complex Geometry Case**

One instance of the complex museum model is shown below, including high-frequency direct sun overlay (see Section 3.5). The points in question are vertical sensors arranged on the north and east walls of the northeast room of the museum model in figure 3-21 from Chapter 3, and two illuminance goal ranges are demonstrated in figures 4-12 and 4-13 for the same set of data points. The tighter range, in figure 4-12, is 400-800 lux preferably, but with partial credit down to 200 and up to 1000 lux. It is meant to represent the stricter illuminance requirements applied to works of art. Obviously, in this iteration of the model, the wall is too bright for displaying sensitive artwork. The broader goal range, in figure 4-13, is the UDI-based range of 500-2000 lux with a buffer zone down to 100 and up to 2500 lux. The contributions of the direct sun overlay are more evident in this weighted illuminance graph, however they don't register with any strength, because the sun spots are small and infrequent. They appear as slightly more orange spots within the yellow expanse. The largest discrepancy between any of the comparisons in this chapter occurs in figure 4-13. The chronic lower illuminances of the Boston-based weighted metric in comparison with Daysim (see Section 3.3.2) may play a part in the difference.

### **4.3 Summary of New Temporal Illuminance Metric**

Acceptable Illuminance Extent (AIE) describes the portion of an area of interest which meets a set of given illuminance goals. Full credit is given to sensors which fall within the illuminance goal range, and partial credit is given on a sliding linear scale to sensors which fall between the range extremes and the buffer illuminances. In this way, the AIE, the low illuminance extent, and the high illuminance extent can all be found. Using a triangular scale based on the mixture of three primary colors, all three values can be displayed on a single temporal map.

On the whole, AIE temporal maps of both simple and complex models show a very good visual correlation between the weighted illuminance metric and Daysim. Tight illuminance goal ranges have the most potential for misrepresentation, since the range is less forgiving of illuminance calculation error. In most cases, however, the act of

condensing the information in the space to one number actually lessens the visual discrepancies found in single sensor point illuminance temporal maps.

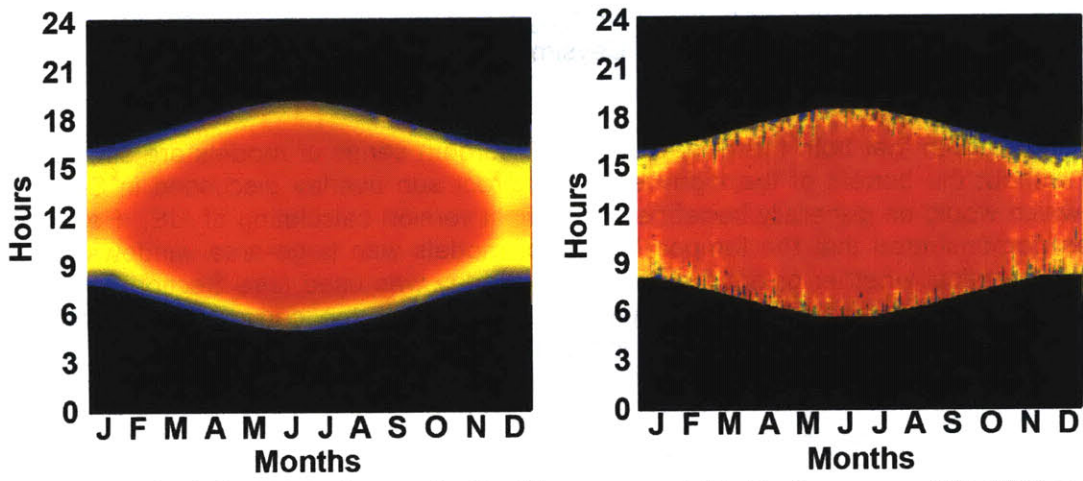


Figure 4-12. AIE temporal maps for the Museum model in Boston, range 400-800 lux, buffer 200-1000 lux. Map created using the data reduction method on the left, and Daysim on the right.

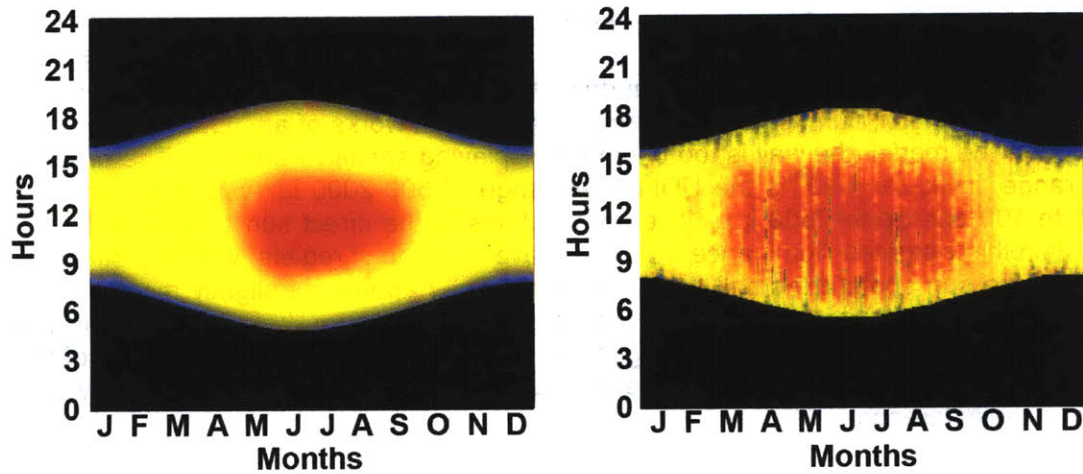


Figure 4-13. AIE temporal maps for the Museum model in Boston, range 500-2000 lux, buffer 100-2500 lux. Map created using the data reduction method on the left, and Daysim on the right.



# Chapter 5

## Glare Avoidance Extent

In early-stage architectural design, temporal graphics can help determine if and when lighting design goals have been met. Chapter 4 was concerned with condensing spatial illuminance data to a single number so that it can be displayed on a temporal map. In that case, the color of each point on the map represents the percentages of a sensor plane which meet, overstep, or remain below some user-defined illuminance goals (see Figure 5-1). The same principal could be applicable to the portion of a space in which one perceives glare, but to be realistically applied, the methods for computing glare must be made more efficient. High-speed annual glare evaluations would be a valuable tool, and there is enough information in the computer models themselves to create a viable approximation method for all scenarios.

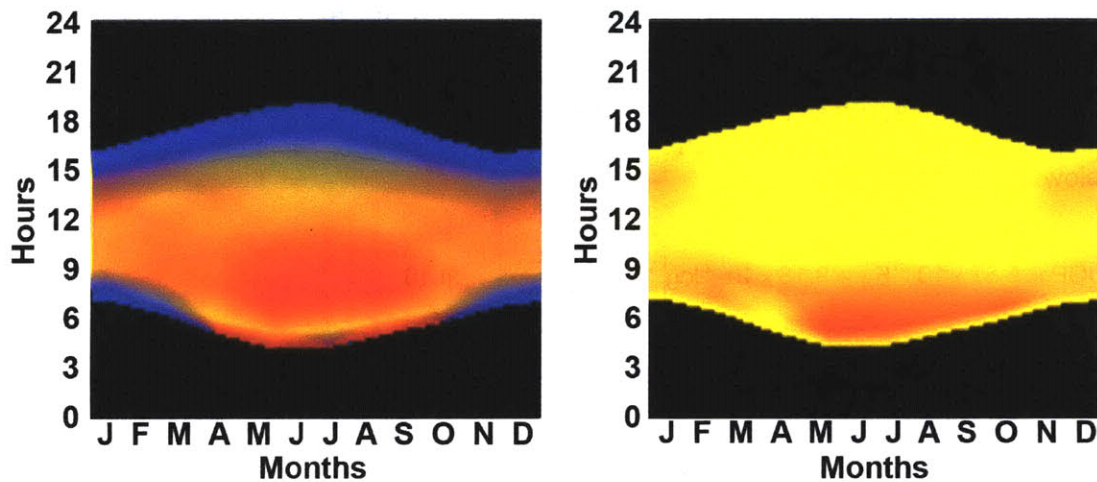


**Figure 5-1. The temporal map on the left represents the percent of a sensor plane which has met (yellow), overstepped (red), or not reached (blue) a user's illuminance goals. The temporal map on the right represents the percent of a vertical sensor array which perceives glare (red) or no glare (yellow).**

This chapter develops a new method for computing the Daylight Glare Probability using only illuminance values and geometric model information provided by the user. The results of this approximation are validated numerically against traditional DGP calculations and also with the existing simplified DGPs calculation, both developed by Jan Wienold [Wienold & Christoffersen, 2006; Wienold, 2007]. The results of these various methods of calculating DGP are then compiled into a new goal-based metric called "Glare Avoidance Extent" and compared visually using the temporal map format.

### 5.1 Daylight Glare Probability in Depth

The earliest glare metrics were not intended for the variable, diffuse area sources common to daylighting. The Daylight Glare Index was an attempt to correct this, and the

studies contributing to its formation were performed using artificial diffuse area sources [Österhaus, 2005], but because the view through a clear window is not uniform, discrepancies have been discovered between DGI and user responses to real daylight [Iwata & Tokura, 1998]. Several more recent glare studies have focused on developing glare indices which accurately represent daylight glare [Iwata & Tokura, 1998; Wienold & Christoffersen, 2006]. One of the most promising new metrics for daylighting is Daylight Glare Probability (DGP), developed by Wienold and Christoffersen [Wienold & Christoffersen, 2006], which represents “percent of people disturbed” and is based on human reactions to daylight-based glare in a side-lit office environment with venetian blinds. The down-side of relying on user studies is that the metric may be biased towards the ranges of sky conditions, architecture, window types, and user demographics which were available over the course of the study. The potential biases of the DGP are discussed in Section 2.1.4; however the advantages of a metric based on human responses to daylight environments are greater than the potential disadvantages. At the very least, the DGP has not been proven inaccurate (the one study which seemed to prove inaccuracies was shown later to have been invalidated by a computer coding error [Painter *et al.*, 2009]), which makes it unique thus far in the realm of glare metrics.

Finding DGP requires the vertical illuminance at the eye and, like most glare calculations, the size, position, and luminance of the source, as shown in the equation below:

$$DGP = 5.87 \times 10^{-5} E_v + 9.18 \times 10^{-2} \log \left( 1 + \sum_j \frac{L_{s,j}^2 \omega_{s,j}}{E_v^{1.87} P_j^2} \right) + 0.16 \quad (5.1)$$

where  $E_v$  is the vertical illuminance at the eye,  $L_s$  is the luminance of the glare source,  $\omega_s$  is the solid angle of the source, and  $P$  is the Guth position index of the source [Wienold & Christoffersen, 2006]. The variable values are usually found by pixel-processing an HDR photograph, rendering, or CCD image.

For predictive computer models, creating the necessary HDR renderings can be prohibitively time consuming, especially when considering multiple positions, viewpoints, and times of day and year. This makes it difficult to predict the glare potential of a whole space on an annual basis. One solution is to find a reliable way to predict glare by performing illuminance calculations only, which take much less time to compute.

There are two existing examples of annual glare calculation methods, both of which use illuminance measurements in the calculation as opposed to luminances found during a pixel analysis. This vastly decreases the computation time required for an annual glare calculation, since there are several efficient ways to find an annual set of illuminances (see Section 2.1.2). The more recent of these annual glare calculation methods is a simplified, linear version of the DGP equation, called “DGPs”, which depends only on the vertical illuminance at the eye [Wienold, 2007; Wienold, 2009]. This is possible because DGP is heavily influenced by the vertical illuminance component. The linear equation is the simplified DGP (or DGPs) as defined by Wienold:

$$DGPs = 6.22 \times 10^{-5} E_v + 0.184 \quad (5.2)$$

and it demonstrated a remarkable correlation with DGP for instances when  $E_v$  is composed only of indirect and diffuse light [Wienold, 2007]; the very clear linear relationship between these diffuse light DGPs and the vertical illuminance can be seen in Figure 5-2. Miss-predicting direct sun glare is not an insurmountable weakness, however, since many daylight simulation programs can distinguish indirect from direct sunlight, and it is reasonable to assume that there will be a glare issue whenever direct sunlight hits the eye.

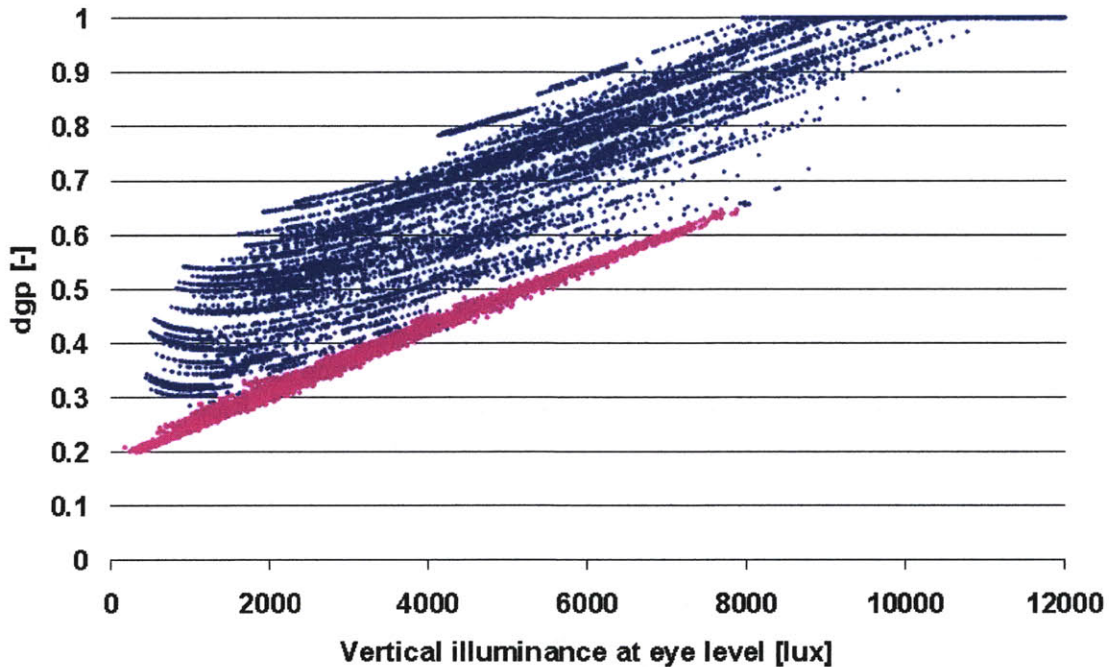


Figure 5-2. A scatter plot of the data from which DGPs was derived; the data points involving no direct sun are highlighted in pink. Figure source: [Wienold, 2007].

As Wienold recognized [Wienold & Christoffersen, 2006; Wienold, 2009], the aspect of glare not addressed in this equation is that of luminance contrast. The data set from which equation (5.2) was derived was based on a two-person office model where a large window took up much of the view. In that scenario, glare caused by luminance contrast would not be nearly as common as glare caused by high luminance levels, so disregarding the logarithm term, which is the contrast component of the glare equation, is less of a problem. On the assumption that other models would require the contrast component to accurately predict DGP, however, an approximation method which includes that aspect of equation (5.1) would be an asset.

Because the DGPs neglects peak glare sources, Wienold has developed an enhanced simplified DGP. The “enhancement” is a return to image-based processing of DGP, but the images are themselves simplified radiance pictures created quickly by a modified version of Daysim. They are meant to have enough luminance accuracy to roughly represent the peak glare sources, but no more than that. The enhanced simplified method accomplishes quick renderings partly by leaving the internal reflective component of daylight out of the renderings (although they are still included in the calculation of vertical illuminances). This methodology, though a promising study, is

currently still a work in progress. It is also limited by its dependence on renderings, however quick. Not only does it still take time to process each image, the renderings are still position and view dependent, which means that simulating glare over an array of sensors would somewhat increase the computation involved.

The other annual glare calculation method is the one employed by the Building Design Advisor [Papamichael *et al.*, 1998]. Originally developed by Winkelmann and Selkowitz for use with DOE-2, it computes the Daylight Glare Index (see Section 2.1.3) from reference points using illuminance values and building geometry to approximate the appropriate variables [Winkelmann & Selkowitz, 1985]. Specifically, the DGI formula depends on source luminance ( $L_s$ ), background luminance ( $L_b$ ), solid angle of the source ( $\omega$ ), and the solid angle of the source modified by its deviation from the line of sight ( $\Omega$ ) (see Appendix A). Building Design Advisor assumes that each full window is a glare source.  $\Omega$  and  $\omega$  are both geometric properties, which can be found using the model's geometric data, and the program already calculates annual sets of illuminance values [Hitchcock & Carroll, 2003].  $L_b$ , which is measured in  $\text{cd}/\text{m}^2$ , is found using the equation  $L_b = E_b \rho_b$ , where  $E_b$  represents the average illuminance falling on the walls and other surfaces near the window, and  $\rho_b$  is the average surface reflectance of the whole room [Winkelmann & Selkowitz, 1985]. One inexplicable factor in this approximation is that the relationship (in SI units) between luminance and illuminance for a lambertian surface usually includes a factor of  $\pi$  in the denominator, or  $L_{\text{surf}} = E_{\text{surf}} \rho_{\text{surf}} / \pi$ . Finally, Winkelmann and Selkowitz do not specify how  $L_s$  is found.

Although approximation based on illuminance and known geometry is a promising idea, this uncertainty in the definition of luminance values lends some doubt to the accuracy of the method, since the luminance values (especially source luminance) have great impact on the outcome of the glare index. Furthermore, the method by which Building Design Advisor finds illuminance already includes substantial approximation (see Section 2.1.2). The author was not able to find any validation done for this glare approximation method.

## 5.2 Deriving a Model-Based DGP Approximation

Any method using pixel analysis to find glare is inevitably still limiting the number of view points and directions which can be processed at each moment, since a separate image must be created for each view. On the other hand, any number of reference point illuminances may be found in a single simulation, and in the case of radiosity, with almost no impact on computation time. Because of this, and because the geometry and sky distribution are all mathematically defined in the model, there should be a reasonably accurate way to calculate the original DGP equation using approximated variables. To get any kind of accuracy, however, each variable approximation needs to be done carefully and as accurately as possible.

The variables that must be found to complete the DGP equation (5.1) are the luminance of each glare source ( $L_s$ ), the solid angle of each source ( $\omega_s$ ), and the position of each source ( $P$ ). Vertical illuminance ( $E_v$ ) is calculated directly in the simulation. The glare sources must be identified and defined, a task which can be a challenge even for traditional daylight glare analysis. On the other hand, if one is working inside a daylight modeling program, there are certain inherent advantages. The approximation method presented below is based on variables that are already defined in any daylighting model, so it is called the model-based DGP, or DGPm.



First and foremost, any daylighting model includes a definition of the model's geometry. The sensor position and view direction are known, and if the sources of glare could be attached to physical objects in the model, the solid angle  $\omega_s$  and position index P, which are merely geometric quantities, are easy to find. Aside from the geometric variables, the two necessary assumptions involve locating glare sources and approximating their luminances.

The first necessary assumption deals with the identification of glare sources. When inside a building, the most common sources of glare are direct or indirect light transmitted through windows, specular reflections, and electric light fixtures. Because the primary focus of this research is daylighting, not electric lighting, and because the Lightsolve LSV radiosity-based rendering engine does not yet include specular material definitions [Cutler *et al.*, 2007], the focus here will be on windows as the probable source of glare. However, since electric lights and specular materials must have a defined directional exitance, one may presume that a similar methodology could be applied to them.

The LSV radiosity program takes a triangular-meshed object file, like the visualization in Figure 5-3, which divides all surfaces into similarly sized patches with assigned material definitions. The initial supposition, therefore, is that any window patch is a possible glare source when viewed from the interior. One can sort through them by assigning an approximate adaptation luminance to each view position and direction, as represented by a vertical illuminance sensor, and comparing this to the assumed luminance of each triangular glass patch (see below). A constant luminance integrated over a hemisphere, weighted by the cosine to the normal, is related to illuminance by a factor of  $\pi$ , so we will take  $E_v/\pi$  as a working value for adaptation luminance. Because it is based on all illuminance reaching the eye (including glare sources), this approximation does carry the risk of being higher than the actual background luminance. Because the LSV engine distinguishes between diffuse and direct illuminance, this background luminance overestimation might be mitigated by disregarding any direct illuminances. It should also be noted that the background luminance does not appear in the DGP equation at all, and that it is used by both this method and the DGP calculation program *evalglare* as a way to weed out glare sources, a job for which it does not need the highest accuracy.

The second assumption involves assigning illuminances to all window patches. All rendering programs require sky luminance distribution data, which is generally defined using a well-known

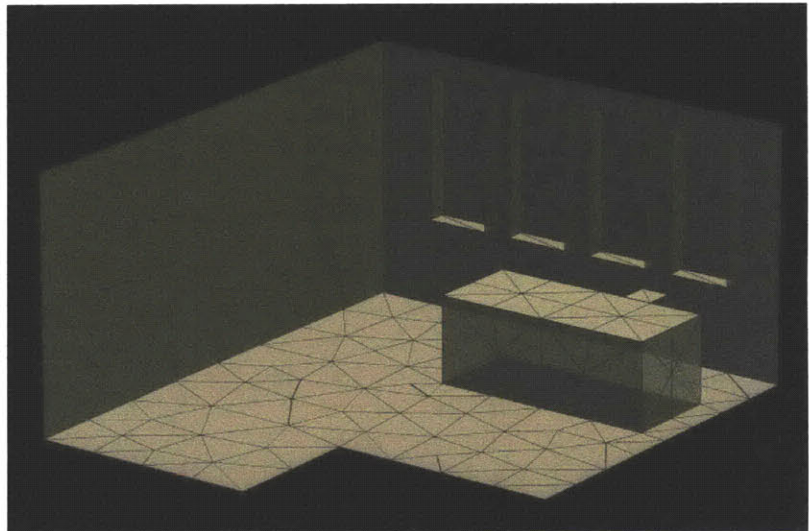
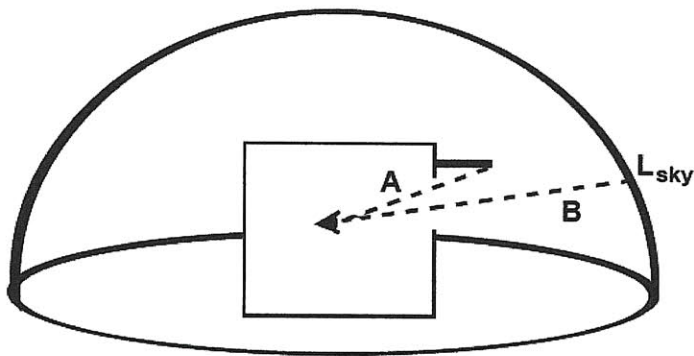


Figure 5-3. A visualization of the object file mesh structure for a simple room.





**Figure 5-4.** A geometric representation of the line of sight between a sensor and the sky dome. The weighting factor would be 0 for Line A and the transmissivity of the window for Line B.

would be 40%. Because the validation for this method was done using Radiance simulations (see Section 5.3), the equations governing the sky distributions for CIE clear, clear-turbid, intermediate, and overcast skies were copied from the program code of *gensky* and can be found in Appendix B [Radiance web].

All of this is done assuming a diffuse-sky luminance is seen through the glass patch. If there is direct sun hitting the sensor, the *gensky* equation for direct sun luminance (see Appendix B) is used to define the source luminance [Radiance web], and the angular size of the source is defined as 0.009 steradians. This way, the very bright luminance source of the sun is treated separately from the larger area diffuse sky luminances seen through the full glass patch. A conceptual visualization of glass patches as glare sources is given in Figure 5-5.

A threshold luminance of four times the adaptation luminance was set to keep lower-illuminance glass patches from being considered glare sources. This is the default background luminance multiplication factor in the program *evalglare*, because it represented a middle ground between over-detecting and under-detecting glare sources [Wienold, IP]. (Wienold also found that basing the glare luminance threshold on the task area's luminance is preferable, but that is impossible to find given the available information for this approximation.) If the vector between the eye and any glass patch is below the horizontal, it is given a ground luminance, since disregarding the ground as a source might cause glare underestimation in some circumstances. The ground

luminance distribution equation, so by creating a line of sight between the sensor and the window patch and applying the known sky distribution, one can figure out the luminance of the sky as seen through that window patch (see Figure 5-4). LSV also provides a weighting factor based on whether other opaque or transparent objects are between the sensor and the sky. For instance, if there was a solid wall blocking the view of the sky, the weighting factor would be 0%. If there were two transparent objects with transmissivities of 80% and 50% respectively, the weighting factor

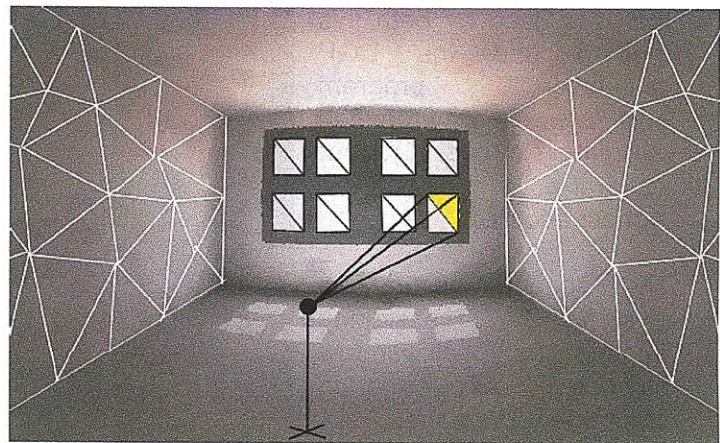


**Figure 5-5.** Conceptual picture of object meshing and glare source identification.

luminance is defined by the equations for ground glow found in the Radiance scripts, which can be found in Appendix B [Radiance web]. Finally, since DGPs is only valid for indirect light, simulations were done under the CIE clear, clear-turbid, intermediate, and overcast sky models, with sun and without sun to make all data points viable for comparison.

The LSV object file is a list of all vertex coordinates and material names of every triangular patch in the model. This file can be easily parsed into a list of central points, normal vectors, and areas for each non-opaque material patch. The angular size of each patch is then defined using the equation below:

$$\omega = \frac{A_p \cos(\beta)}{d_p^2} \quad (5.3)$$

where  $A_p$  is the area of the patch,  $d_p$  is the distance from the sensor to the center of the patch, and  $\beta$  is the angle between the patch normal and the vector from the patch to the sensor.

The position index for points above the line of sight can be found in the IESNA Handbook [IESNA, 2000] and is defined below:

$$P = \exp\left[\left(35.2 - 0.31889\tau - 1.22e^{-2\tau/9}\right)10^{-3}\sigma + \left(21 + 0.26667\tau - 0.002963\tau^2\right)10^{-5}\sigma^2\right] \quad (5.4)$$

where  $\tau$  and  $\sigma$  are defined in Figure 5-6. Below the line of sight, the DGP position index is based on the study by Iwata and Tokura as expressed mathematically by Einhorn [Wienold & Christoffersen, 2006]:

$$\begin{aligned} P &= 1 + 0.8 \times \frac{R}{D} && \{R < 0.6D\} \\ P &= 1 + 1.2 \times \frac{R}{D} && \{R \geq 0.6D\} \\ R &= \sqrt{H^2 + Y^2} \end{aligned} \quad (x)$$

where  $D$ ,  $H$ , and  $Y$  are also defined in Figure 5-6. These calculations are repeated for every non-opaque patch which has a luminance higher than the threshold defined above, and the position index, angular source sizes, source luminances, and the calculated vertical illuminance at the eye are then plugged into the DGP equation (5.1).

### 5.3 Glare Simulation Parameters

Because the goal is to use this method with the LSV radiosity-based engine mentioned in the last section (both this method and the LSV are being developed in the framework of the Lightsolve project described in [Andersen *et al.*, 2008]), the geometry of each

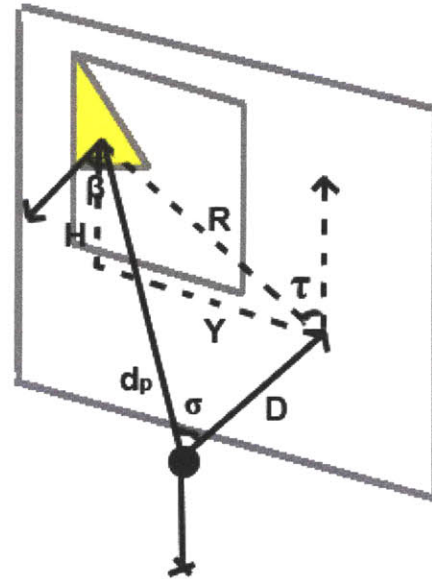


Figure 5-6. Diagram of the geometry involved in finding source angular size and position index.



model tested is in the form of a triangular-meshed object file. However, all simulations of illuminance or DGP were done using an identical Radiance model with interior and glass sensor points derived from the object file. The reasons for this are that the *evalglare* program – used to find the control DGP values for comparison – only works with the Radiance simulation engine, which is a validated and trusted simulation program [Mardaljevic, 1995]. Data from four models will be presented here: “Classroom”, “Skylights”, “Frame”, and “Simple Corbusier”.

The Classroom model is a rectangular room located in Sydney, Australia, with two big punched windows to the south, six smaller punched windows to the north, and an external overhang over the lower three windows to the north. The Skylights model is the same size, shape, and location as the Classroom model, but it has two large skylights instead of the punched windows. The Simple Corbusier model is again the same size and shape as the previous two, but it has many scattered small windows on the south and east and a tall window to the northwest. It was inspired by the Chapel of Notre Dame du Haut by Le Corbusier, but the simulation location is Boston. The Frame model is a slightly smaller rectangular room located in Boston. It has one large window divided into pieces with a thick dark window frame and facing 20 degrees south of east.

Classroom and Skylights were analyzed in the initial set of explorations in which nine view positions with eight view directions each were simulated. In subsequent model simulations, for the sake of time, only a few view points and view directions were chosen. Sample renderings of each model can be found in Figure 5-7, and their dimensions, reflectances, and Radiance parameters are listed in Table 5-1.

Several other models were also made in an attempt to simulate glare due more to contrast than illuminance levels, including a detailed model of Ando’s Church of Light in Osaka, Japan, and a very simplified model inspired by Safdie’s Yad Vashem museum in Jerusalem, Israel. However, DGP is not valid for low illuminances [Wienold, 2007], and it is difficult to find contrast-based glare situations at higher illuminances. Both the DGPs and DGPm approximations seemed to fail for these other models (the former by underestimation, the latter by overestimation), but since the DGP itself is invalid, the results are inconclusive. The Church of Light model is used in Chapter 7 as a conceptual example, but its results are not numerically validated.

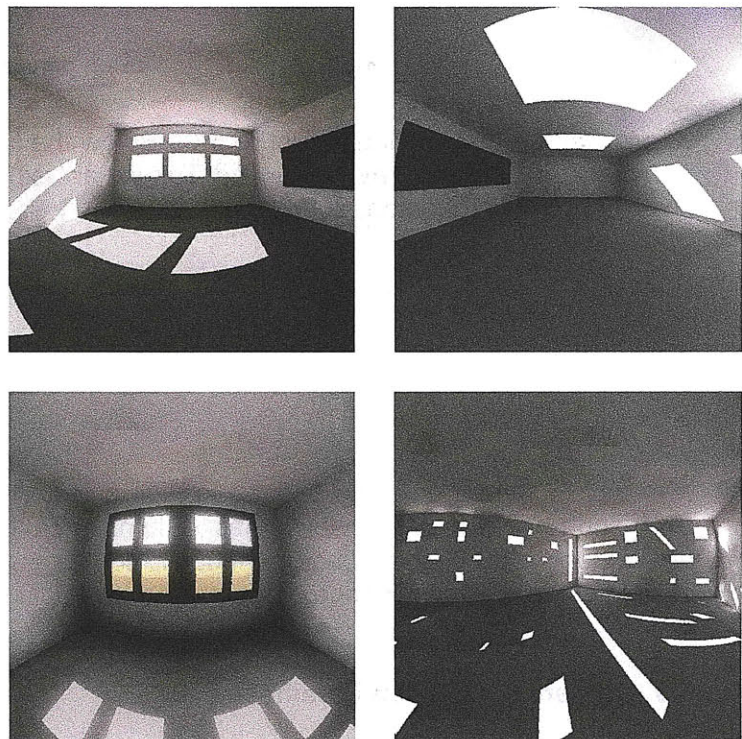


**Figure 5-7. Rendered interior views of the models. Top left -- Classroom, top right -- Skylights, bottom left -- Frame, and bottom right -- Simple Corbusier.**



For each model, point, and view direction, a picture was rendered with Radiance, and DGP was measured using the program *evalglare* [Wienold & Chrisoffersen, 2006]. The illuminance at each point and at the glass patch positions was either taken from the detailed *evalglare* output files or from an identical Radiance calculation of point illuminance.

**Table 5-1. Geometric and simulation parameters of the four models**

Model	Classroom	Skylights	Frame	Simple Corbusier
Dimensions (m)	7.5 x 10 x (3 to 4)	7.5 x 10 x 3	5 x 7 x 3	7.5 x 10 x 3
Wall Reflectance	0.65	0.65	0.5	0.5
Ceiling Reflectance	0.83	0.83	0.5	0.65
Floor Reflectance	0.2	0.2	0.2	0.2
Chalboard Reflectance	0.05	0.05	n/a	n/a
Frame Reflectance	n/a	n/a	0.15	n/a
Glass Transmissivity	0.8	0.8	0.8	0.8
# Sensor Positions	9	9	1	1
# Views per Position	8	8	1	3
<b>Radiance Parameters:</b>				
ab	5	5	5	5
ad	512	512	512	512
ar	128	128	128	128
as	128	128	128	128
dp	512	512	512	512

#### 5.4 Validation of Model-Based DPG Approximation

Results for both the DGPm and the DGPs are given in the form of percent error from the corresponding DGP output of *evalglare*. Both scatter plots and histograms of the errors are provided for each model.

##### 5.4.1 Vertical Windows Classroom Case

The Classroom model is the one closest to the data on which equation (5.2) is based, in the sense that it has large areas of vertical windows and the glare situations are mostly illuminance-based, rather than contrast-based. For this reason, Figure 5-8 shows that this the simplified DGP method performs very well in the Classroom model, with most errors occurring between -10% and 0%. The proposed DGPm approximation performs similarly well, with most errors occurring between -5% and +10%. In most vertical-window cases, this is typical of each approximation method; DGPs has a tendency to underestimate, and DGPm tends to overestimate glare. In the sense that glare is something one wishes to avoid, this makes the latter the more conservative method when the relative errors are the same.

The graphs in figure 5-8 show a scatter plot and histogram of the error between each approximation method and the DGP – DGPs is shown in blue and DGPm in pink. Both sets of data represent simulations with no direct sun involved, however, the dotted line

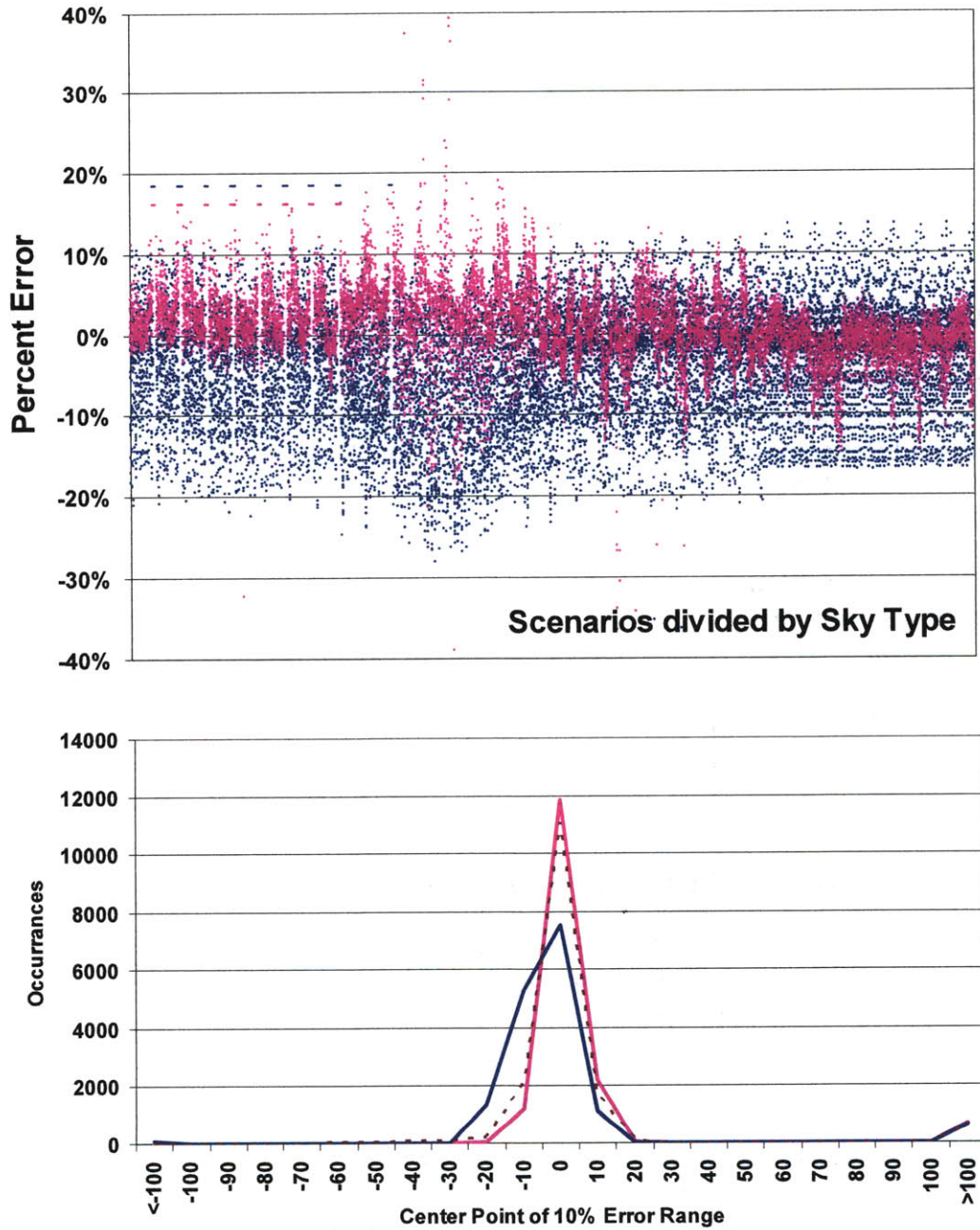


**Figure 5-8. Error scatter plot (top) and histogram (below) for the Classroom model, showing DGPs errors in blue and DGPm errors in pink.**

on the histogram graph shows a similar performance for the model-based method in full-sun simulations.

The scatter plot shows simulation results for clear, clear-turbid, intermediate, and overcast skies in order from right to left (within each group, simulation results are arranged annually). This highlights the slightly different error tendencies for simulations under each sky type. These differences could be caused by inconsistencies between

the sky distribution equations in Radiance and the DGPm, although the sky distribution equations were copied very carefully from Radiance.

### 5.4.2 Skylights Classroom Case

The Skylights model is the only one shown in which the DGPs approximation overestimates the actual DGP. (Similar results occurred in another skylight-dominated model which was not included due to many data points being below the valid range for

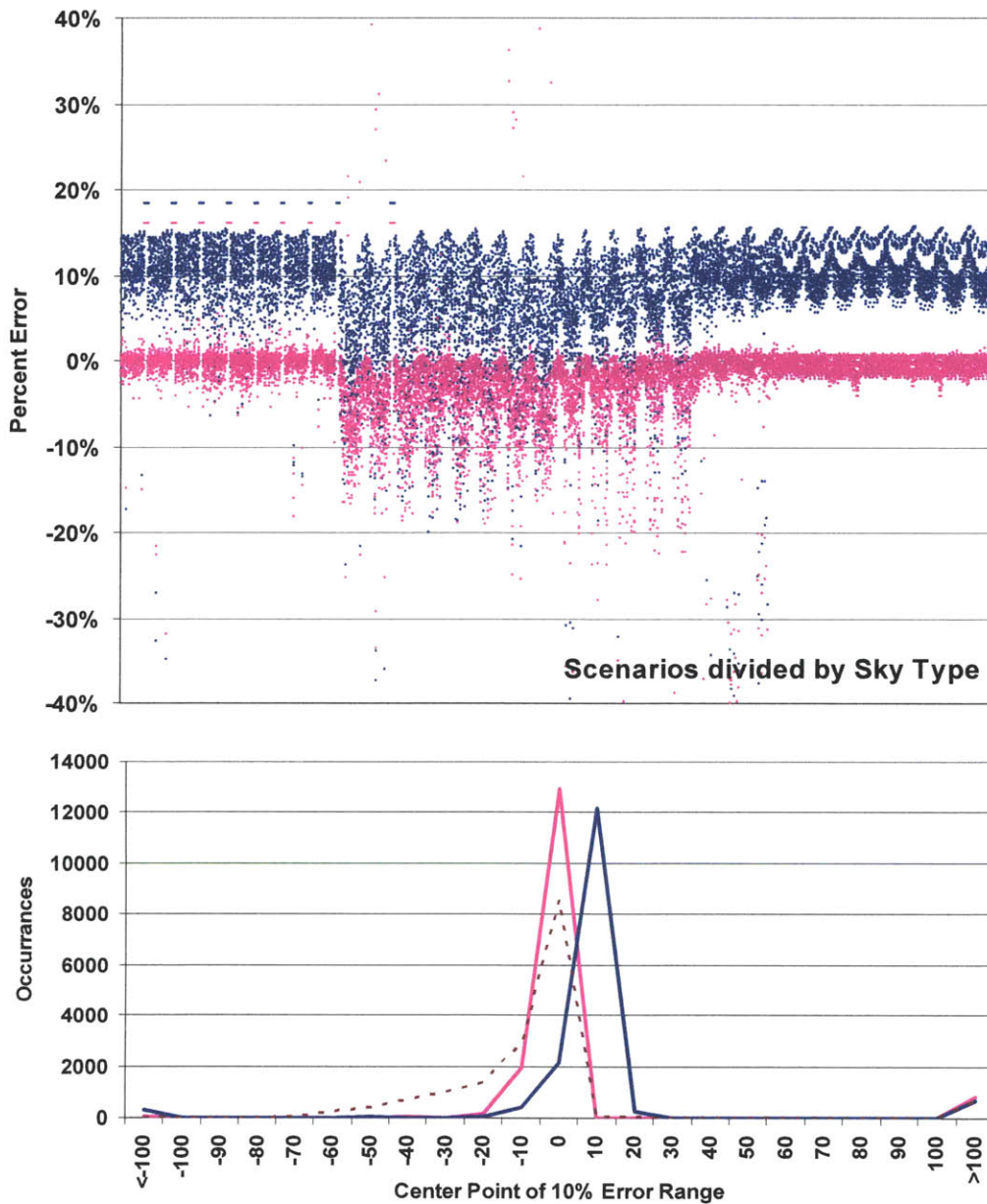
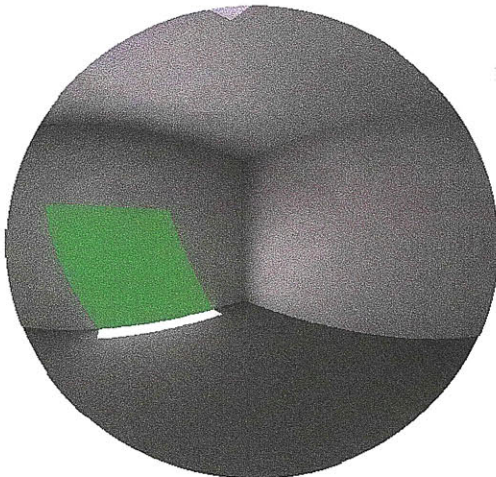


Figure 5-9. Error scatter plot (top) and histogram (below) for the Skylights model, showing DGPs errors in blue and DGPm errors in pink.



the DGP equation.) As shown in Figure 3, DGPs hovers largely around +10% error, while the model-based approximation ranges between -10% and 0%, with many points near 0% error. One possible reason for the unusual overestimation on the part of the DGPs approximation might be that, while illuminances in the room remain high due to the large skylights, the possible sky-based glare sources are mostly at the very edges of the visual range. This means they not only contribute a lower illuminance to the vertical illuminance, but they also cause less glare, due to lower contrast sensitivity in the outer regions of the visual field.

The error plot and histogram for the Skylight model are shown in Figure 5-9. There is a less consistent performance of both the DGpm and the DGPs under clear-turbid and intermediate skies, however the worst errors in the DGpm approximation don't go beyond -15%. The clear and overcast sky DGpm approximations have nearly zero error and are therefore very close to the DGP found using *evalglare*.



**Figure 5-10. *Evalglare* output depicting a glare source (in green) on a diffuse wall.**

The results under skies simulated with sun (the dotted line in Figure 5-9) for the model-based approximation are worse in this scenario than any other. Further analysis of the raw data revealed that the largest errors were not associated with the high DGP levels caused when there is direct sun hitting the sensor. It is more likely caused by bright sun spots on the diffuse wall being perceived as glare by *evalglare*. For instance, the scene shown in Figure 5-10 has a DGP of 56%, yet no windows are present in the view range and the only glare source is a bright sun-spot on the wall. Glare from diffuse surfaces is the one scenario that it would be impossible to predict using the model-based approximation, even if specular materials and electric light sources were later taken into account. This is because, in order to narrow down the possible surface patches which might cause glare, all diffuse opaque surfaces are disregarded as

possible sources in the DGpm method. In most situations, this would not be a problem, but since there are no windows at eye-level in the Skylights model, a diffuse surface illuminated by direct sunlight can easily become the brightest object in the room.

### 5.4.3 Cases Involving Contrast Glare

The Frame and Simple Corbusier models are attempts to create contrast-glare situations (with a high enough illuminances such that the DGP itself is still valid). Of the four validation cases, the Frame model is the only one for which the DGpm systematically underestimates – although it still gives closer results than the DGPs method. In Figures 5-11 and 5-12, the DGPs approximation constantly underestimates glare probability by around 20% for all sky types. Both Frame and Simple Corbusier produce lower-illuminance results in general, with higher contrast points such as a bright glass pane against a very dark frame or small windows scattered over the visual field. Since DGPs is dependent entirely on vertical illuminance, it misses the instances of contrast-based



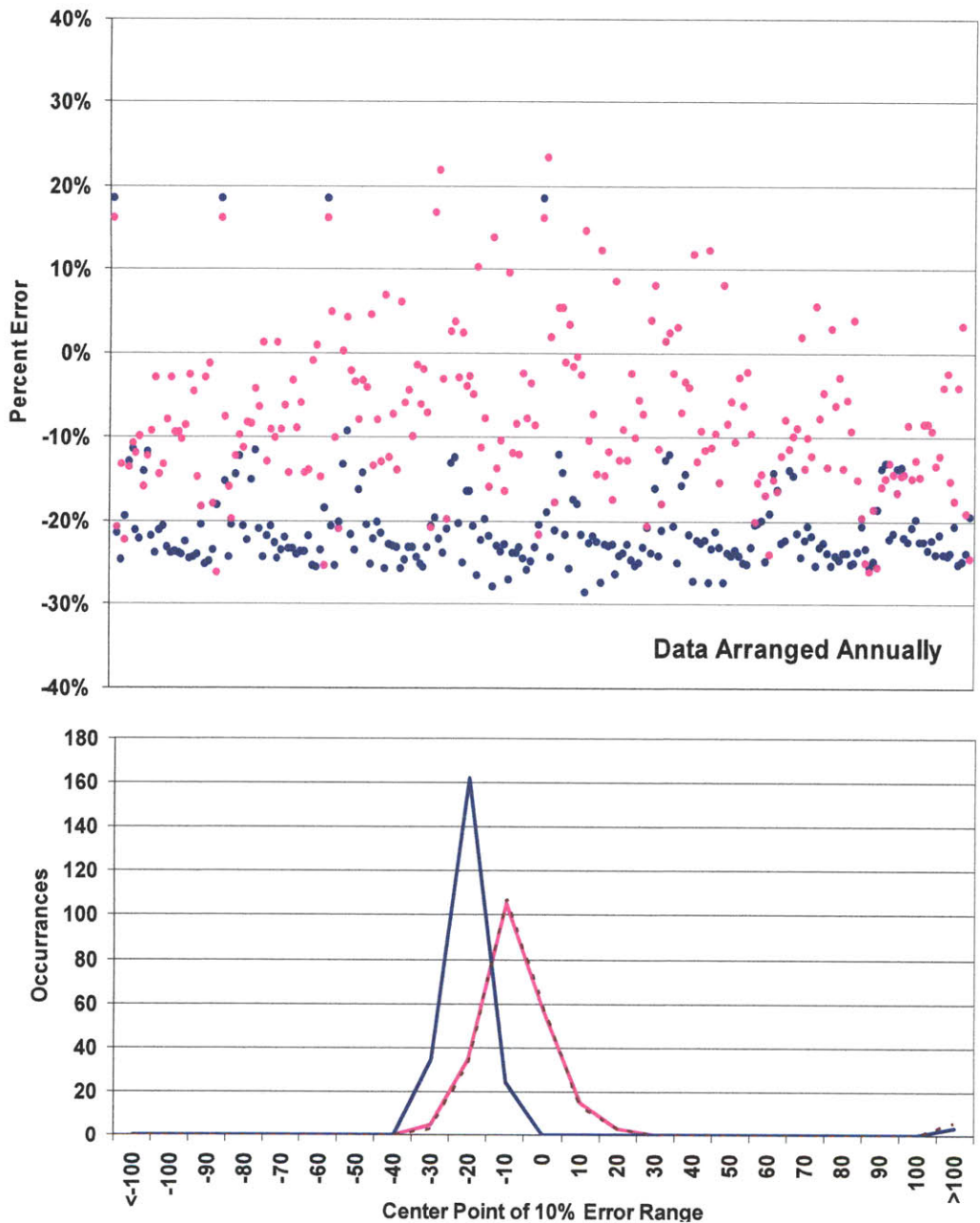
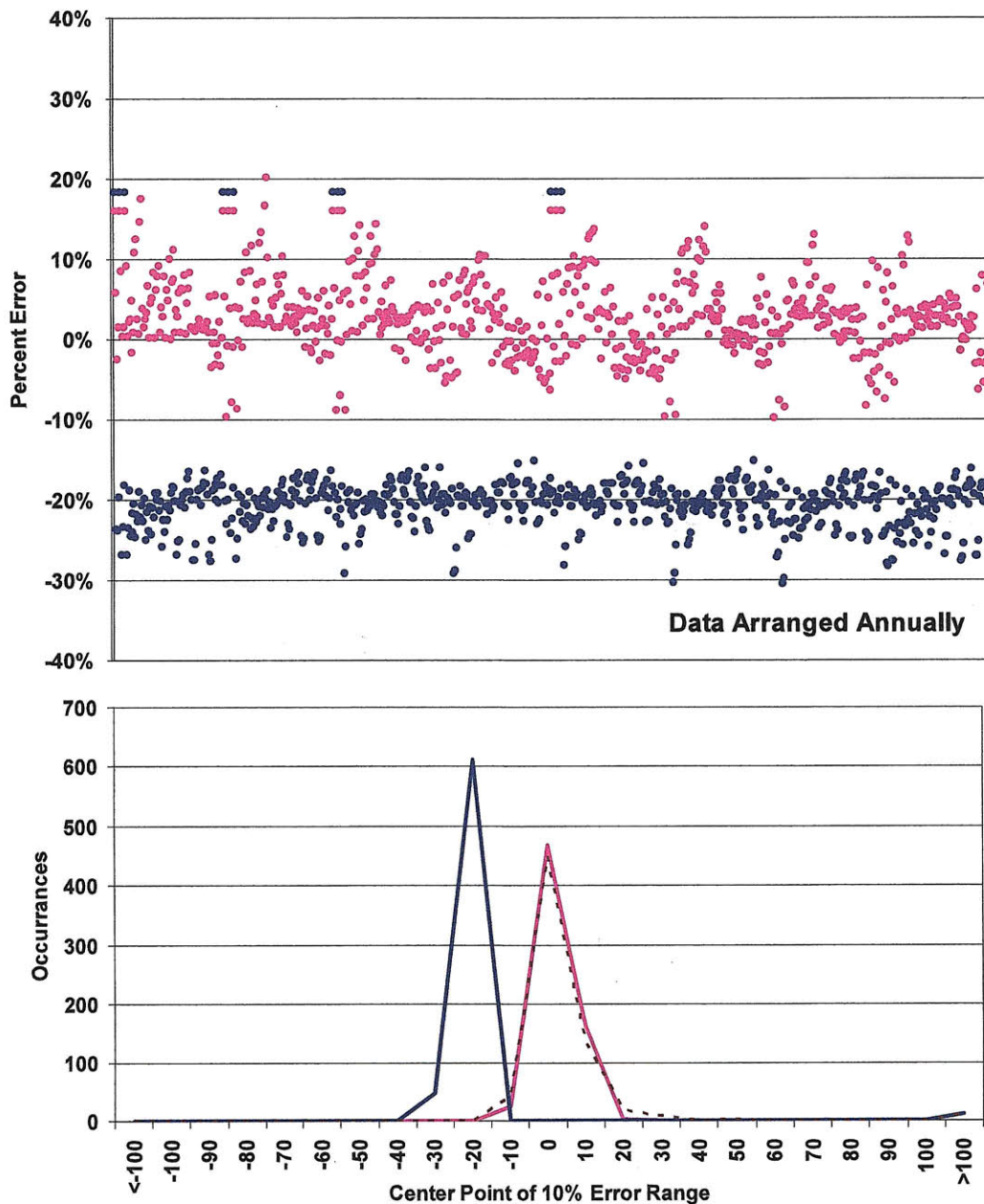


Figure 5-11. Error scatter plot (top) and histogram (below) for the Frame model, showing DGPs errors in blue and DGPM errors in pink.

glare. For the DGPM, the results for Frame stay mostly between -20% and 10% error, and those for Simple Corbusier range between 0% and +10%.

Overall, the model-based method is potentially valid for more scenarios than DGPs because it allows for the approximation of contrast-based glare and non-vertical windows. Furthermore, the Classroom model showed that it could also be very accurate for glare caused mainly by high luminances through vertical windows. The model-based method also avoids overestimating the glare from skylights which, while bright, are at the



**Figure 5-12. Error scatter plot (top) and histogram (below) for the Simple Corbusier model, showing DGPs errors in blue and DGPm errors in pink.**

edge of the visual field. Finally, the model-based method's tendency towards more positive error makes it a more conservative method than the DGPs, which tends to underestimate the DGP.

The biggest limitation of the DGPm is that it currently ignores all non-window glare sources, such as bright sun spots on diffuse surfaces. Furthermore, the refinement of glare source size and location for any scenario depends on the size and discretization of the object-file mesh grid (the glare sources found will be as biased toward the size and position of the glass patches). Both considerations are also beyond the scope of DGPs.

## 5.5 Definition of a Temporal Glare Metric

It is just as important to understand the annual occurrence of glare as it is to understand the annual performance based on illuminance. Similar to illuminance simulations, analyzing glare moment by moment and view by view would give a disjointed picture of the whole performance and would make analysis unnecessarily complicated. Fortunately, with the existence of a reasonable approximation which relies only on illuminance simulations and geometric information, annual Daylight Glare Probability can be simulated as quickly as annual illuminance data. The data reduction method used to find annual illuminances in Chapter 3 involves a weighted sum of the illuminances simulated under four discrete sky types. Because of this, it's important to note that the DGPM should be calculated *before* this weighted summation is performed. The vertical illuminance and the sky dome luminance are both included in the DGP equation (5.1), so the relationship must be kept intact to find an accurate DGPM. Thus, the DGPM represents the glare from a real sky condition.

From this point, there are a couple directions in which one can go. The DGP values for each period of the year can be, like the annual illuminance values in the data reduction method, weighted according to the frequency of each sky type. Alternatively, the maximum glare value among the four sky types could be selected to represent each time period. The former method would indicate the likely glare occurrence as dictated by local climate, while the latter would be a type of worst case scenario. This worst-case logic could be even extended from temporal to spatial variation by taking the maximum glare perceived by any sensor point. This would be useful in situations where no glare can be tolerated, such as the museum example of Section 3.5. The method in which the DGP is weighted according to sky type frequency is demonstrated in the next section, but the graphs showing maximum glare would be a useful alternative to have available. There is no reason why an analysis tool could not offer both options.

Finally, it is likely that a designer is interested in the whole room, not just selected positions and view directions. In the earliest stages of design, the programmatic layout of a space may not be fully defined, making the important locations and view directions uncertain. Like Acceptable Illuminance Extent, drawing all related data points into one graph reduces the mental processing required to understand multiple graphs while drawing out general trends, reducing unnecessary details, and making the data concise and readable. The proposed metric, called the Glare Avoidance Extent (GAE), is also goal-based and is defined as the portion of glare sensors which perceive a DGP less than a certain threshold.

The most common design goal for glare is to avoid it completely. At the very least, the designer should be told when glare occurs, so the DGP data points should be categorized according to DGP thresholds indicating glare perception. In a private communication with Jan Wienold, he indicated that 35% DGP and 40% DGP were rough thresholds for "perceptible glare" and "disturbing glare" respectively. Therefore, a point representing less than 35% DGP would be given "full credit" for avoiding glare, which in the AIE analogy, is equivalent to being within the prescribed illuminance range. Above 35% DGP, the scale of credit decreases until it hits zero at 40% DGP, after which there is no credit given for avoiding glare. On a temporal map, a large number of sensors perceiving glare, would appear as oranges and reds, or "too much glare" in the goal-based lexicon. A yellow color with very little orange in it might represent a lot of sensors perceiving "just perceptible" glare, or a few sensors perceiving disturbing glare.



It would be left up to the designer to group glare sensor planes according to the information desired. For instance, in a classroom model, with all desks facing the same direction, the designer might set up an array of vertical sensor planes at a seated student's head height facing the chalkboard. If the model represents a hospital room which has a very restricted layout, the designer might want to know the glare risk in very specific spots representing the head of the patient bed. On the other hand, if the designer wants a more general understanding of the glare potential in a space, an array of sensors facing in several different directions could provide that view. The most useful view directions to model would be those which are directly normal to windows. Figure 5-13 illustrates two of these options.

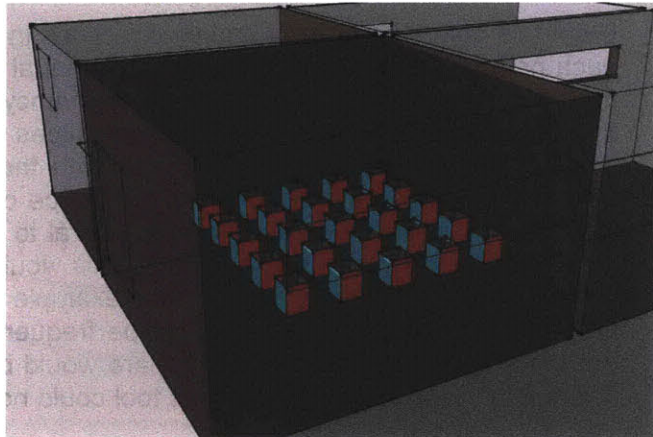
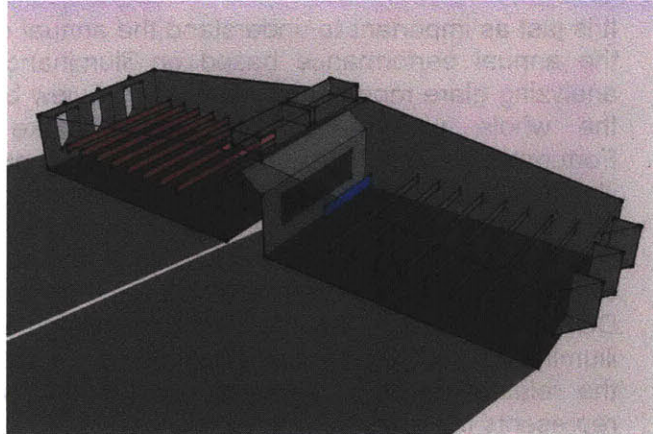


**Figure 5-13.** The top model shows a classroom in which glare arrays have been set up at student head height and single planes at teacher head height. A different glare material is used for each, so a different temporal map will be made for each. The bottom model shows an array of sensors, each facing a cardinal direction and grouped by material

## 5.6 Visual Comparisons Using Glare Avoidance Extent

Two ways to represent glare data variation over time and over space were suggested above – a comprehensive scenario and a worst-case scenario for each dimension. The comprehensive scenario for both temporal and spatial variation is the one demonstrated in the following comparisons – the DGP values for each period were made into a weighted sum according to sky type occurrence, and the value represented on the temporal map represents the percent of sensors which do or do not perceive glare. Of the comparison cases for single glare measurements in Section 5.3, only the Classroom and Skylights models were simulated over enough sensor points to provide a comprehensive view of the room.

### 5.6.1 Classroom Model Comparisons

The first comparison case for the comprehensive glare metric (weighted according to sky type occurrence and given as a percent of the sensors perceiving glare) is the Classroom model. In section 5.3.1, the individual DGP comparisons showed a large amount of agreement between the DGP, the DGPs, and the DGPM. Therefore the



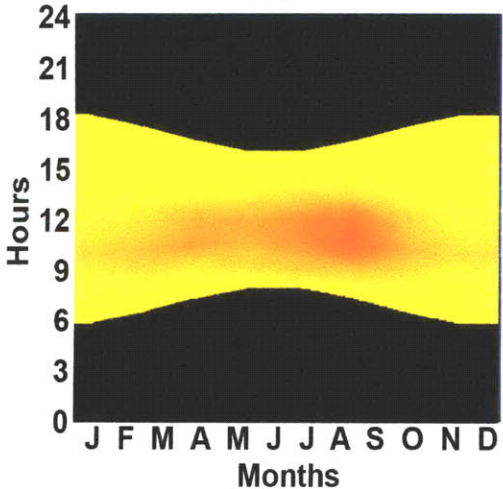
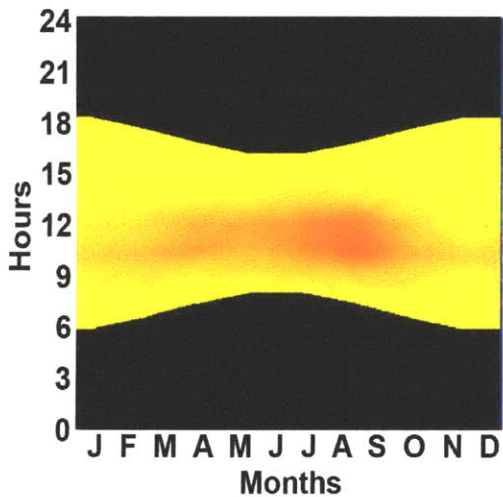
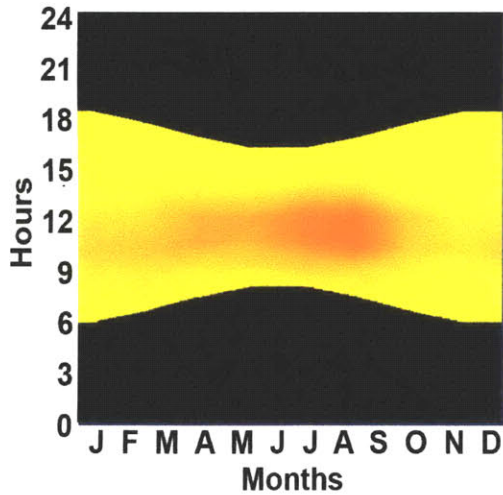


Figure 5-14. No sun GAE temporal maps restricted to points facing towards north and south windows in the Classroom model in Sydney: From top to bottom, *Evalglare* DGP, DGPm, simplified DGPs.

graphs of Glare Avoidance Extent (GAE) in figure 5-14 should show good visual agreement.

The graphs in Figure 5-14 include only no-sun DGP from the sensors directly facing the north and south windows. As expected based on the results from section 5.3.1, the graphs are virtually identical for all three cases. The equivalent full sun cases look almost exactly the same, since the severity of the glare is not recorded in the GAE – only whether or not there is glare – and there was already significant glare caused by the bright diffuse sky.

Figure 5-15 shows the high frequency, full-sun case of the GAE calculated using the DGPm approximation method. This graph was produced by interpolating the no-sun DGP at many points within the 56 periods, and then adding the effect of a direct sun glare source to the existing DGP value at any sensor which receives direct sun. The equation for the luminance of the sun can be found in Appendix B, the solid angle of the sun is 0.009 steradians, and the position index was found geometrically.

Although the direct sun does not significantly change the occurrence of glare in this example,

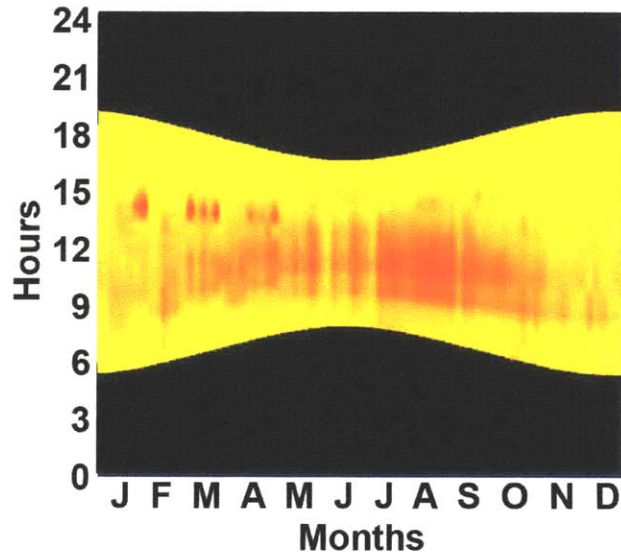


Figure 5-15. Full sun GAE temporal map restricted to those points facing towards the north and south windows in the Classroom model in Sydney. This figure was produced using the DGPm method and the high-frequency direct sun overlay.

the addition of high frequency solar points is still noticeable. There is no temporal map of similar frequency produced using *evalglare* to compare this map to, however it serves as an example of the final format of the GAE temporal maps which will be used in Lightsolve.

### 5.6.2 Frame Model Comparisons

The single DGP errors in section 5.3.3 revealed a greater discrepancy between the DGPs and the DGPm for low-illuminance contrast glare. Since there is only one sensor point in the Frame model, it is not representative of the situation for the whole space, and high (but not perfect) GAE will indicate barely perceptible glare rather than glare for a small portion of the room. The GAE was weighted by the frequency of the four sky types.

The left hand temporal maps in figure 5-17 represent the simulations done with no sun, so that the comparison with the DGPs would be valid. Even in these graphs, there is a faint indication of glare on summer mornings for both the *evalglare* DGP results and for the model-based method, however there is no sign of glare on the DGPs temporal map. The right hand temporal maps in figure 5-17 represent the simulations done with full sun. Despite the low illuminance levels, the sun is a small very bright point which still causes disturbing glare, which as been picked up by the DGP and the model-based approximation, but not the DGPs. This is unsurprising given Wienold's own conclusions about the inaccuracy of the DGPs in full-sun situations [Wienold & Christoffersen, 2006; Wienold, 2009].

Again, because glare is so very dependant on direct sun, a very bright point source which is constantly moving, it is preferable to include the high frequency sun overlay in the visual temporal representation of the GAE. Figure 5-16 shows the direct sun overlay for the frame model, and it is evident that several moments of glare have been missed completely in the 56 periods graph, and the ones caught have been misrepresented in

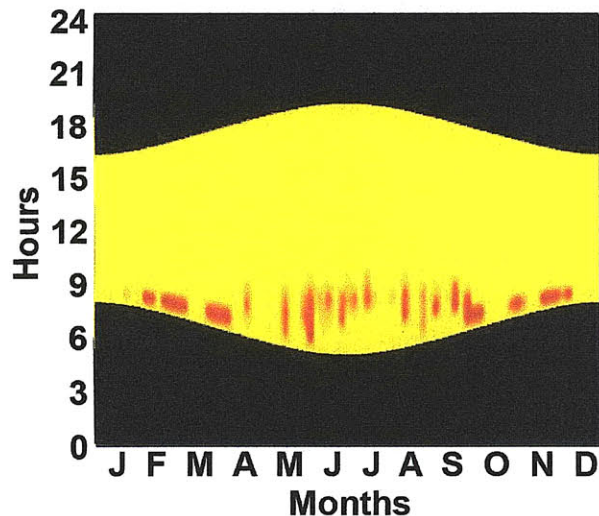


Figure 5-16. Full sun, high frequency direct sun overlay GAE temporal map for the Frame model in Boston.

both temporal area and position. The high frequency overlay gives a much better idea of the true glare times.

### 5.7 Summary of New Temporal Glare Metric

The DGPm method described in this chapter performs comparably with the DGPs in situations with large vertical windows and lots of light, and it performs better in low-illuminance situations (in both full sun and no sun situations), because it is better able to perceive contrast glare. The model-based approximation can also be done using only simulated illuminance and known geometry, eliminating the need for pixel analysis in annual glare situations. Currently, the DGPm is limited to window-



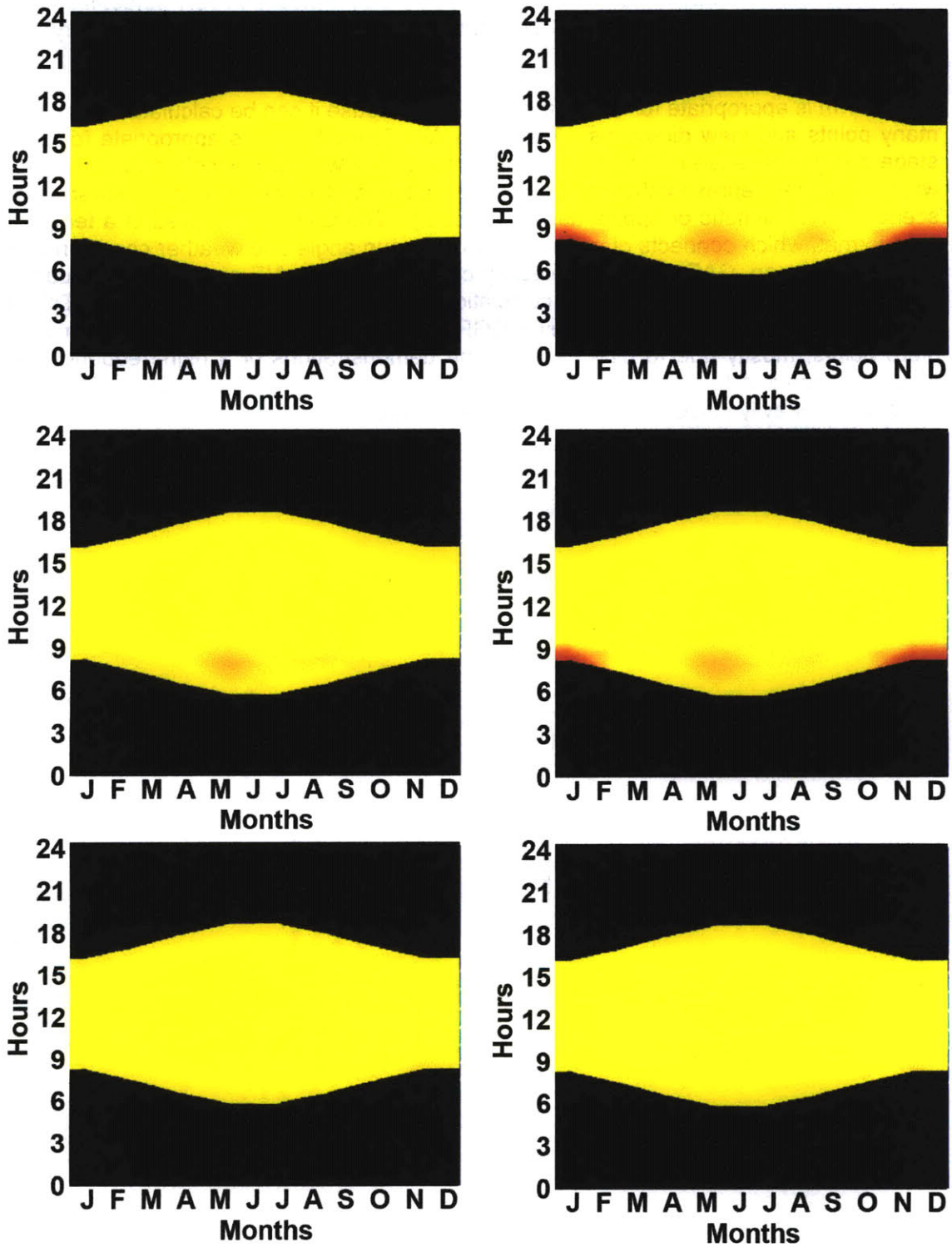


Figure 5-17. No-sun (left) and full-sun (right) GAE temporal maps restricted for a single point facing the window in the Frame model in Boston: From top to bottom, *Evalglare* DGP, DGPm, simplified DGPs.

size. It is also limited by the DGP equation itself, which is invalid at very object-file mesh size. It is also limited by the DGP equation itself, which is invalid at very low illuminances.

The DGPM is appropriate for early stage design, because it can be calculated quickly for many points and view directions. The Glare Avoidance Extent is appropriate for early stage design, because it can incorporate all related views into a single readable graph which is either representative of the whole space and climate, or is a worst- case scenario in its climatic or spatial aspect (or both). The GAE is displayed in a temporal map format, which connects glare performance to sun angle and weather conditions. In the temporal map, GAE can also be easily compared with a AIE and any other quantity displayed in that format. The visual correlation between the GAE maps for DGP, DGPs, and DGPM are all very close, however DGPM had an easier time accounting for peak glare points, mostly due to direct solar. The demonstrations of a high-frequency sun overlay showed it to be especially necessary in glare calculations, since direct sun penetration heavily influences the occurrence of glare.



# Chapter 6

## Solar Heat Surplus and Scarcity

Even though solar heat gain is not a photometric quantity, it is one of the tradeoffs associated with daylighting, and therefore it should be considered in any holistic analysis of daylighting. Unfortunately, as discussed in Section 2.1.6, it is difficult to understand the impact of solar heat gain on a space's temperature difference or HVAC loads without doing some kind of energy analysis. Since energy and daylighting analyses require very different model inputs and types of simulation, most existing daylighting analysis solutions that include solar heat gain are ones which either include or have easy exports to energy analysis tools [Urban & Glicksman, 2007; Reinhart *et al.*, 2007; Ecotect web; IES web]. The few existing analysis methods that do not require simulation are usually only applicable to certain restricted climate locations and use the existing results from previous energy simulations in their application [de Groot *et al.*, 2003; Hui, 1997]. Very few of these methods or tools parse the solar heat gain contribution out from the general energy analysis and present it separately as a tradeoff to incoming daylight [Ecotect web; de Groot *et al.*, 2003].

Like daylighting, the solutions for energy analysis range from algorithms which can be calculated manually to physically based algorithms which require computer simulation. If the energy consequences of solar heat gain are to be portrayed as a daylighting tradeoff for schematic design, it may be possible to use energy simulation results that are only accurate enough to provide a ballpark estimate – an indication of the benefits or disadvantages. Also, because few building materials are defined in the earliest stages of design, variable input defaults can be provided based on building type. It is therefore possible, although not ideal, to use a less accurate calculation of solar heat gain when making decisions in the early design stage.

It is beyond the scope of this thesis to focus on energy simulation techniques, however solar heat gain is an important aspect of daylighting. For this reason, a simple existing energy balance equation, the balance point method, was chosen for solar energy calculation, and the errors that one might expect when employing this method were analyzed against energy use data from the program Energy Plus. The data from the balance point method was then used in a proof of concept for a solar heat gain metric similar in form to the AIE and GAE metrics discussed in previous chapters. This metric, named Solar Heat Scarcity/Surplus (SHS) provides an indication of the urgency for shading windows during the cooling season or allowing more solar gain during the heating season. The Energy Plus energy use data, balance point data produced with complex equipment and occupancy schedules, and balance point data produced using simpler schedules are visually compared as SHS quantities in the temporal map format.

### 6.1 Balance Point Method

As part of the Vital Signs program run by the University of California – Berkeley, Utzinger and Wasley, of the University of Wisconsin – Milwaukee, produced a very thorough document describing the balance point method of building energy analysis. A building's balance point is defined as “the outdoor air temperature required for the indoor

temperature to be comfortable without the use of any mechanical heating or cooling,” [Uttinger & Wasley, 1997]. In essence, when outdoor conditions reach the balance point, building heat gains are equal to the heat loss through the façade, and for this reason, the balance point temperature is always lower than the target indoor temperature. If the outdoor temperature is higher than the balance point, the building will require cooling, if lower, the building will require heating.

The balance point temperature is found through the application of steady-state energy balance equations. The basic equation for the balance point is as follows:

$$T_{BP} = T_{set} - \frac{Q_{SHG} + Q_{IHG}}{(UA)_{building} + (\rho c_p V^*)_{vent}} \quad (6.1)$$

where  $T_{BP}$  is the balance point temperature ( $^{\circ}C$ ),  $T_{set}$  is the thermostat set point temperature ( $^{\circ}C$ ),  $Q_{SHG}$  and  $Q_{IHG}$  are the solar heat gain (from windows) and internal heat gain (W),  $U$  is the heat transfer coefficient of the façade ( $W/m^2K$ ),  $A$  is the area of the façade,  $\rho$  is the density of air ( $kg/m^3$ ),  $c_p$  is the heat capacity of air ( $kJ/kg^{\circ}K$ ), and  $V^*$  is the ventilation volume flow rate ( $m^3/s$ ). (Because the balance point equation involves a temperature difference, rather than an absolute temperature, it is possible to define  $T_{BP}$  and  $T_{set}$  in Celsius rather than Kelvin.) The full building product of  $U$  and  $A$  is defined as:

$$(UA)_{building} = \sum_i (UA)_i \quad (6.2)$$

where  $i$  represents each building façade element with a different  $U$ -value.  $Q_{IHG}$  is the sum of heat gain from occupants, equipment, electric lights, and any other heat source internal to the building, and  $V^*$  includes both infiltration and outdoor air ventilation supplied either through windows or the HVAC system. Every input given above can also be normalized by the total floor area of the building, so that buildings of different sizes may be compared to each other.

The other useful operation is to turn the balance point into a predicted heat load. The temperature difference between the outdoor air and the balance point is not a heat load in itself, but a load can be found by multiplying by the heat transfer rate of the building:

$$Load = (T_{out} - T_{BP}) \left[ (UA)_{building} + (\rho c_p V^*)_{vent} \right] \times t \quad (6.3)$$

where the load is in Joules (and is positive for cooling, and negative for heating loads), and  $t$  represents the appropriate time step in seconds, given the data available.

The balance point and outdoor temperature over the course of a day can be graphed in opposition for an immediate visual representation of heating and cooling load potential. Figure 6-1a shows a schematic graph of the balance point temperature which assumes a static internal heat gain during occupied hours and no internal heat gain during unoccupied hours; Figure 6-1b illustrates a more detailed occupancy and internal gains schedule. In this simple representation of a single day, the red line is the thermostat temperature, the green line is the balance point temperature due to internal heat gain only, and the orange line is the balance point temperature due to both internal heat gain and solar heat gain. The temperature differences between the balance point and the outdoor temperature must be addressed by the heating system (shaded in blue) or the

cooling system (shaded in orange). The yellow shaded portion represents the additional cooling load (or lesser heating load) due to the existence of solar gain through windows. The temperature differences themselves are not a load, but with the assistance of equation (6.3), they are instrumental to calculating the predicted load.

The graphs in Figure 6-1 show how the balance point loads can be found over the course of a day; the next step is to make it annual. One simply calculates the changing load using equation (6.3) for many days during the year, and this data could easily populate a temporal HVAC load map. The biggest visual difference between a load map and other maps presented in this thesis is that it would not be bounded by sunrise and sunset times – because solar gain is not the only contribution to building heat load, the temporal map would necessarily continue over all 24 hours.

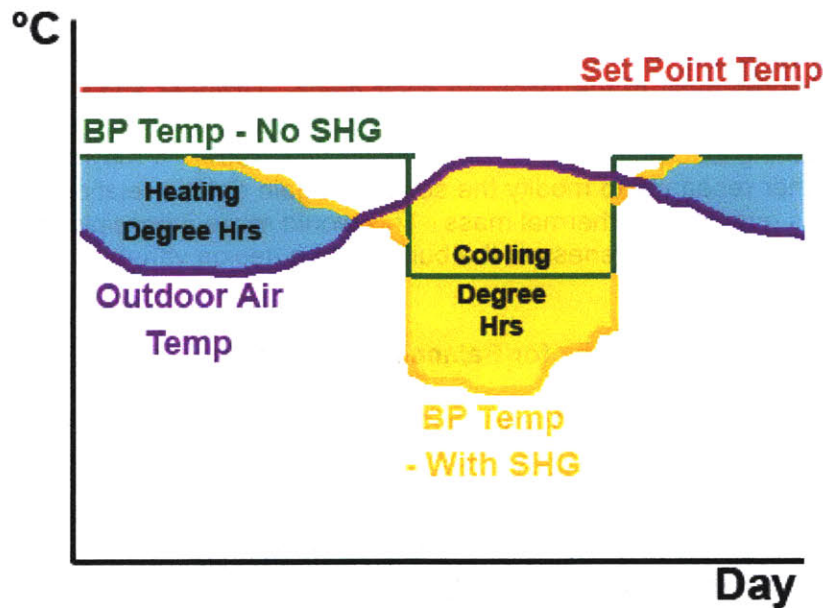


**Figure 6-1. Schematic diagram of how to find heating and cooling degree hours by comparing Balance Point temperatures to the outdoor air temperature.**

The greatest weakness of the balance point method as a temporally-based energy analysis is that it cannot handle the transient properties of solar heat absorption and re-radiation by a building's thermal mass. The interaction of solar heat gain with thermal mass vastly complicates an energy analysis, because the rates of absorption and re-radiation are dependent not only on the mass thickness and exposure to direct sunlight, but also on the temperature difference between the mass and its immediate surroundings. The practical result of this interaction is an inevitable delay of the effects of solar heat gain on the building's thermal loads.

The most noticeable effect of disregarding thermal mass is that the actual chronology of the thermal consequence will be misrepresented on a temporal map. Because thermal mass also serves to spread the release of heat gain over a longer period of time, it is also probable that the peak severity of solar gain (and its benefits during night time hours) will be misrepresented to the user. These inaccuracies would increase as the thermal mass increases.

For the particular application of displaying the solar heat gain tradeoffs associated with daylight, there is one possible advantage to disregarding thermal mass. If all solar gain is treated as if it has immediate consequence, the resulting temporal map would accurately show the chronology and severity of the *source* of solar gain, which is mostly due to the amount of direct solar penetration to the building. By understanding the times of day and year when solar influx is most severe, the designer can better make decisions to block these solar angles in the summer or preserve them in the winter. In this way, the heat influx caused by daylighting is more closely associated with more relevant illuminance and glare measurements in the mind of the designer.

It is also possible to assess the results of a balance point analysis in terms of whether the building would benefit from thermal mass. For instance, if the blue and orange shaded regions in Figure 6-1 are close in size, we know that the building is a better candidate for benefiting from exposed thermal mass, especially if the mass is placed such that it absorbs most of the incoming solar gains. Utzinger and Wasley provide a more detailed guide to the basic conclusions one can draw from the relative sizes of the cooling and heating load potentials [Utzinger & Wasley, 1997]. It may also be possible, after some further research, to modify the solar heat gain data in relation to an idealized effect of various quantities of thermal mass. This would make it possible for the architect to explore the general massiveness of the building as a design variable.

## **6.2 User Inputs and Defaults for Balance Point Analysis**

Because energy and daylighting simulations require different variable inputs, new information will be required from the designer. However, in deference to the need for analysis interactivity, and because very few specifics are firmly set in early stage analyses, it is preferable to offer as many variable defaults as possible – although with the option of editing these defaults. The analysis method presented here will offer the designer defaults based on building type and either ASHRAE recommendations [ASHRAE, 2007] or those used in the sixteen benchmark commercial building models recently released by the United States Department of Energy (DOE) [Torcellini *et al.*, 2008; DOE, 2008]. Some defaults suggestions for infiltration are also taken from the Vital Signs paper on balance point analysis [Utzinger & Wasley, 1997]. The ASHRAE defaults are most useful in situations where the designer has modeled a single part of the building, while the defaults listed for the sixteen DOE benchmark buildings are average values for the full building.

The feasibility study for the metric described in this chapter is done using those DOE benchmark models (see Section 6.4), and the tables in Appendix C list the suggested default values. The designer will be asked to provide the occupancy hours of the space and the building type. The designer is then asked to chose from defaults or assign a new value for occupancy per square meter, ventilation per person, ventilation per square meter, infiltration (in terms of air change rate per hour), heat gain due to equipment, and heat gain due to lights, as well as confirming the average room height (with a default set at 3 meters).

Because the required inputs for an energy calculation do not exist in the current Lightsolve modeling process, it is important to know what will be required from the user in the final application. In SketchUp (the CAD program from which one can run



Lightsolve), the model itself will have certain material tags indicating different façade materials, which should be only assigned to surfaces with a connection to the exterior. Each unique material with these tags will have its area automatically totaled, and the designer will have to enter U-values and Solar Heat Gain Coefficients or choose from the defaults listed in Appendix C. The model will also have a material designation for the floor in order to total the overall area of the space. If any of these material tags do not appear in the model, the designer will be prompted to enter the appropriate surface areas.

A few variables are assumed by the balance point calculation without the designer's input. Each occupant is assumed to radiate 75 Watts of sensible heat, which is the ASHRAE default for an adult doing light office work [ASHRAE, 2001], however convective heat gain should probably be included in similar future calculations. The density of air,  $\rho$ , is assumed to be  $1.2 \text{ kg/m}^3$ , and the heat capacity of air,  $c_p$ , is assumed to be  $1.005 \text{ kJ/kg}^\circ\text{K}$ . The exact form of the menus with which this information will be gathered from the user is a work in progress.

### 6.3 Definition of a Temporal Solar Energy Metric

Although it is useful to know the heat loads and the temperature difference between the balance point and the outdoor air, it is preferable for the solar energy information to be presented to the designer in the same format as the glare and illuminance information. If all three daylighting quantities are in the same format, the designer can more easily understand the heat load consequences of meeting the illuminance goals, or see how much illuminance is reduced when all glare is blocked. No single aspect of daylighting can be changed without affecting the other two, but many existing analyses solutions treat illuminance as if it occurred in a vacuum (see Section 2.3). For a truly comprehensive analysis, all three daylighting quantities should be comparable and readily available to the designer.

In the context of this thesis, that means that solar energy should be presented to the designer on a temporal map representative of the whole model and in terms of a goal-oriented metric which highlights the times when there is too much solar gain, when there is just the right amount of solar heat gain, or when there is not enough solar gain to offset heating. Using the balance point analysis described above, a building could be said to have excessive solar gain when the outdoor temperature is greater than the building balance point and be lacking in solar gain when the building balance point temperature is greater. The "right" amount of solar gain would be however much is required for the outdoor temperature to equal the balance point (or to fall between the two building balance points found using the cooling and heating set point respectively).

To apply the above reasoning mathematically, the solar heat gain metric is split into two parts, called Solar Heat Scarcity and Solar Heat Surplus (SHS), based on whether heating or cooling is required by the building:

$$\begin{array}{llll}
 \text{If} & T_{\text{out}} - T_{\text{BP,S}} \geq 0 & \rightarrow & \text{Solar Heat Surplus (cooling)} \\
 \text{If} & T_{\text{out}} - T_{\text{BP,S}} < 0 & \rightarrow & \text{Solar Heat Scarcity (heating)}
 \end{array} \tag{6.4}$$

Solar Heat Surplus (cooling)

$$= 2 \times \frac{\Delta T_{SHG}}{\Delta T_{SHG} + \Delta T_{IHG}} \times \max \left[ \frac{\Delta T_{load,S}}{\Delta T_{SHG}}, 1 \right] = 2 \times \left( \frac{T_{BP,NS} - T_{BP,S}}{T_{set} - T_{BP,NS}} \right) \times \max \left[ \left( \frac{T_{out} - T_{BP,S}}{T_{BP,NS} - T_{BP,S}} \right), 1 \right] \quad (6.5)$$

$$\text{Solar Heat Scarcity (heating)} = \frac{\Delta T_{load,S}}{\Delta T_{load,NS}} = \frac{-(T_{BP,S} - T_{out})}{T_{BP,NS} - T_{out}} \quad (6.6)$$

where  $T_{BP,S}$  is the balance point temperature ( $^{\circ}\text{C}$ ) based on both internal and solar heat gain,  $T_{BP,NS}$  is the balance point temperature ( $^{\circ}\text{C}$ ) based only on internal heat gain,  $T_{set}$  is the heating or cooling thermostat set point ( $^{\circ}\text{C}$ ), and  $T_{out}$  is the outdoor temperature ( $^{\circ}\text{C}$ ).

The Solar Heat Scarcity ranges from 0% to -100% and is the percent of the heating load *not* offset by solar gain, as illustrated in Figure 6-2. The Solar Heat Surplus is based on the same idea. It ranges from 0% to 100% and is partially defined by the percent of

solar heat gain which needs to be eliminated to bring the cooling load to zero, with a maximum value of 100%, as illustrated in Figure 6-3. However, because the balance-point based cooling load often exceeds the load due only to solar heat gain, if one defined Solar Heat Surplus using this simple equation, it would too often saturate at 100% SHS, and half the metric would become meaningless. Therefore, this value is also weighted by twice the ratio of the solar heat gain over the total heat gain of the building or space. In other words, because internal heat gain is

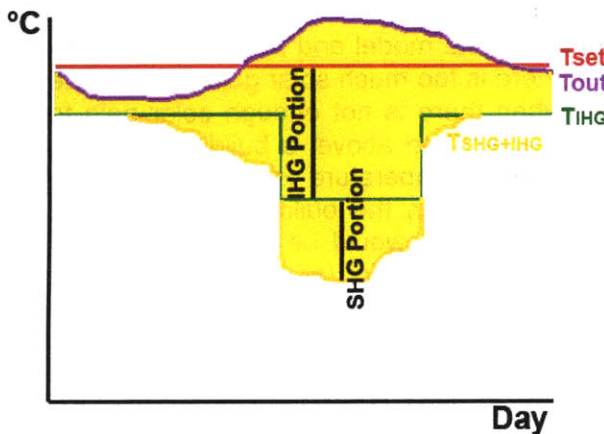
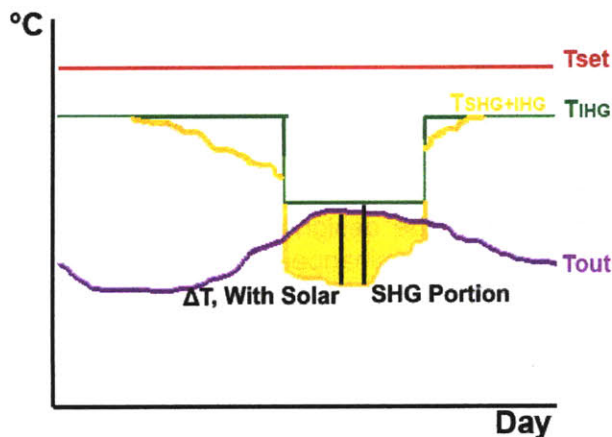


Figure 6-2. Schematic Example of Solar Heat Surplus. In the top example, the cooling required is less than the Solar Heat Gain alone. In the bottom example, that ratio is greater than 1, so the SHS depends on the ratio of SHG to IHG

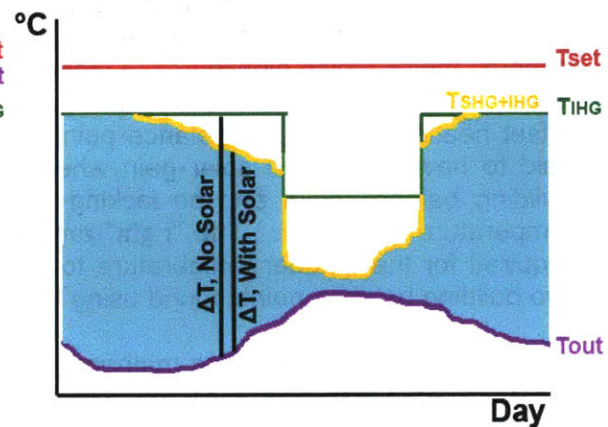
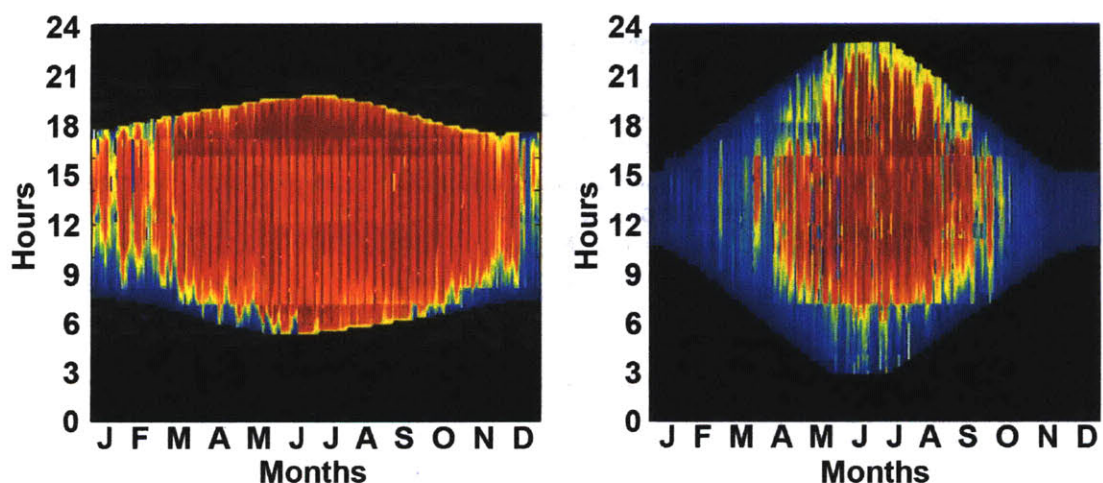


Figure 6-3. Schematic Example of Solar Heat Scarcity.

partially responsible for the cooling load, the measured “surplus” of the solar heat gain is weighted at two times its percent contribution to the total heat gain. The factor of two is included to put a greater weight on the solar heat gain when it equals or exceeds the internal heat gain. In practical terms, this means that buildings with large internal loads may always have a low Solar Heat Surplus, however since most of the cooling load in this example is due to internal gain, it would be a misrepresentation to attribute too much of the cooling load to solar heat gain.

For both Solar Heat Surplus and Solar Heat Scarcity (SHS), the closer a value is to 0% the better, because 0% SHS represents the perfect amount of solar heat gain to match the building balance point and the outdoor air temperature. In this case, 0% SHS is analogous to 100% Glare Avoidance Extent (GAE) (Chapter 5) or 100% Acceptable Illuminance Extent (AIE) (Chapter 4). Because SHS is a single percentage which represents the whole model, it is ideally suited to be displayed on a temporal map, in which case 0% SHS would be yellow, fading towards red for 100% (Surplus) and towards blue for negative 100% (Scarcity) (see Figure 6-4). Although it may seem that 0% SHS is a transition point from cooling to heating and would rarely occur, one must recall that there are often several degrees between the cooling and heating set points, making that transition area broader than it might initially appear. In the temporal maps in figure 6-4, and the rest of this chapter, the hours are in civil rather than solar time because of the output format from Energy Plus. In the implemented version, the hours would be in solar time to match the AIE and GAE outputs discussed in Chapters 4 and 5. Also, the night-times are blacked out, because talking about “too much solar gain” becomes meaningless when the sun is not even up.



**Figure 6-4. The SHS temporal maps for the Small Office in Phoenix and Fairbanks. The scale ranges from -100% Solar heat Scarcity (blue) to 100% Solar Heat Surplus (red) with yellow representing 0% SHS.**

Finally, because solar heat gain depends on highly changeable factors such as direct solar radiation and outdoor temperature, it is likely to benefit more from the high-frequency solar simulations than from the 56 annual periods. SHS can therefore be found using the high frequency direct sun calculations – which is also required also for greater accuracy in AIE and GAE. Due to the small temporal regions between high frequency annual moments, average representative outdoor temperatures can



calculated without too much trouble, and incident direct sun (which has a much greater effect on solar gain than diffuse light) can be acquired from the exterior of all glass patches. Besides occupancy or operation schedules, which are given by the user, all other variables are static over time.

#### 6.4 Solar Heat Surplus/Scarcity Feasibility Study

The feasibility of the Solar Heat Surplus/Scarcity metric was explored using the sixteen benchmark commercial building models made recently available by the U.S. Department in order to provide a more consistent baseline performance for commercial energy models [Torcellini *et al.*, 2008; DOE, 2008]. These buildings were released as Energy Plus models with an accompanying Excel spreadsheet giving building information and energy results, and each of the sixteen buildings was set up to be simulated in sixteen U.S. cities of different climates. (A few model variables, like U-values, were different in different climates, but on the whole the building was unchanged – see Appendix C.) The building models and locations used are listed in Table 6-1 below, and more information about the climate designations can be found in [Briggs *et al.*, 2002].

**Table 6-1. A list of the sixteen building types and the sixteen locations (including climate descriptions) used in the DOE benchmark commercial buildings program.**

Building Type	Location	Climate Type	Climate Description
Fastfood	Miami, FL	1A	Very Hot - Humid
Hospital	Houston, TX	2A	Hot - Humid
Large Hotel	Phoenix, AZ	2B	Hot - Dry
Large Office	Atlanta, GA	3A	Warm - Humid
Medium Office	Los Angeles, CA	3B	Warm - Dry
Midrise Apartment	Las Vegas, NV	3B	Warm - Dry
Outpatient	San Francisco, CA	3C	Warm - Marine
Primary School	Baltimore, MD	4A	Mixed - Humid
Retail	Albuquerque, NM	4B	Mixed - Dry
Secondary School	Seattle, WA	4C	Mixed - Marine
Sit Down Restarant	Chicago, IL	5A	Cool - Humid
Small Hotel	Denver, CO	5B	Cool - Dry
Small Office	Minneapolis, MN	6A	Cold - Humid
Strip Mall	Mt. Helena, MT	6B	Cold - Dry
Supermarket	Duluth, MN	7	Very Cold
Warehouse	Fairbanks, AK	8	Subarctic

The feasibility study was performed by comparing the actual simulated energy use of each Energy Plus model to a balance point load calculation with as similar inputs as possible. Each of the 256 simulation files was modified slightly to extract the necessary inputs for the balance point model from the stepwise variable output of Energy Plus; the Energy Plus outputs used in the subsequent analysis were “Outdoor Dry Bulb”, “Zone Total Internal Total Heat Gain”, “Zone Transmitted Solar Energy”, “Zone Infiltration Total Heat Loss”, “Zone Infiltration Total Heat Gain”, “Zone Mechanical Ventilation Mass Flow Rate”, “Cooling:Electricity”, and “Heating:Gas”. All energy quantities were output in



joules and outputs for heating and cooling energy were normalized by the given COP of the cooling systems or the given heating efficiency where appropriate.

If the ultimate goal is to compare energy use data with the balance point load calculations, the portion of the energy load due to solar heat gain must somehow be parsed from the whole. Therefore, after each building and city combination was simulated, the window properties of each building were modified so that the visible transmission and the SHGC were nearly zero (the program wouldn't run with all windows completely opaque), while the U-value of the glass was kept intact. The difference between the normal building energy use and the opaque building energy use was found, and this difference was attributed to the load effects of solar gain. With this information, the simulated energy use data can be compared with the loads approximated using the balance point method.

The balance point method was applied to the Energy Plus models in two ways. The more detailed calculation used the heat gains, ventilation rates, and other variables which are output at each time step. In essence, this is purely a test of the heat balance equation itself, assuming more accurate information than the designer is likely to have during schematic design. The most important feature of these inputs is the detailed schedules for occupancy, heat gains, and the ventilation system required by Energy Plus (see Figure 6-6). The second balance point calculation was done using the design

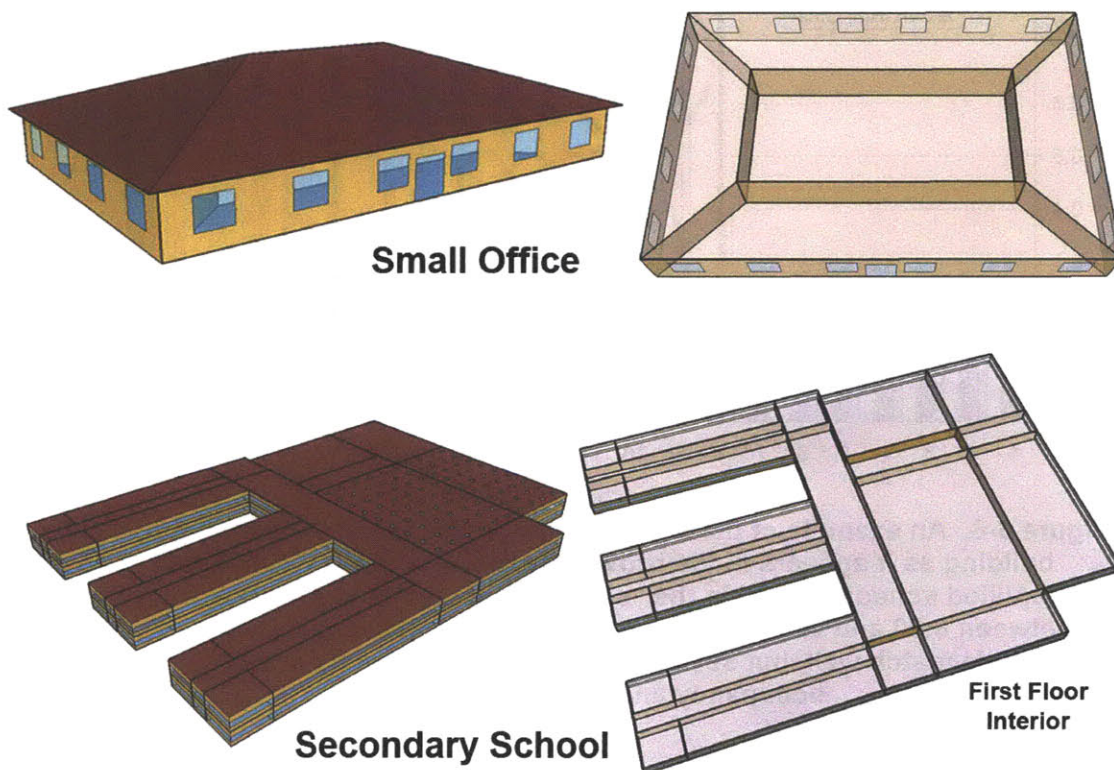


**Figure 6-5. Pictures of two of the energy plus building models as they appear in the provided excel workbooks: Top) Small Office, bottom) Secondary School [DOE, 2008].**

information for internal heat gain, ventilation, and infiltration which came with the Energy plus models – and a very simple schedule based on occupancy.

The complex occupancy schedule was distilled down to a start and stop time with no accounting for occupant variation, which is closer to the kind of generalization which might be made by a designer in the early stages of design. All other variables which depend on occupancy, most notably internal gain and ventilation, were given a value of 80% of the design value when the building was occupied and 30% of the design value when it was not. (In one extreme case, the sit-down restaurant model, occupied variables were set at 40% of design value and unoccupied variables were set at 15% of design value – see below.) These weights, visual average occupancy and non-occupancy values as perceived by the author, were a concession to the fact that the given variables rarely reached the peak design value and there was usually some building activity outside “normal” occupancy times. In sections 6.4.1 and 6.4.2, these two balance point calculations are named “detailed” or “simple” based on the schedule type it represents.

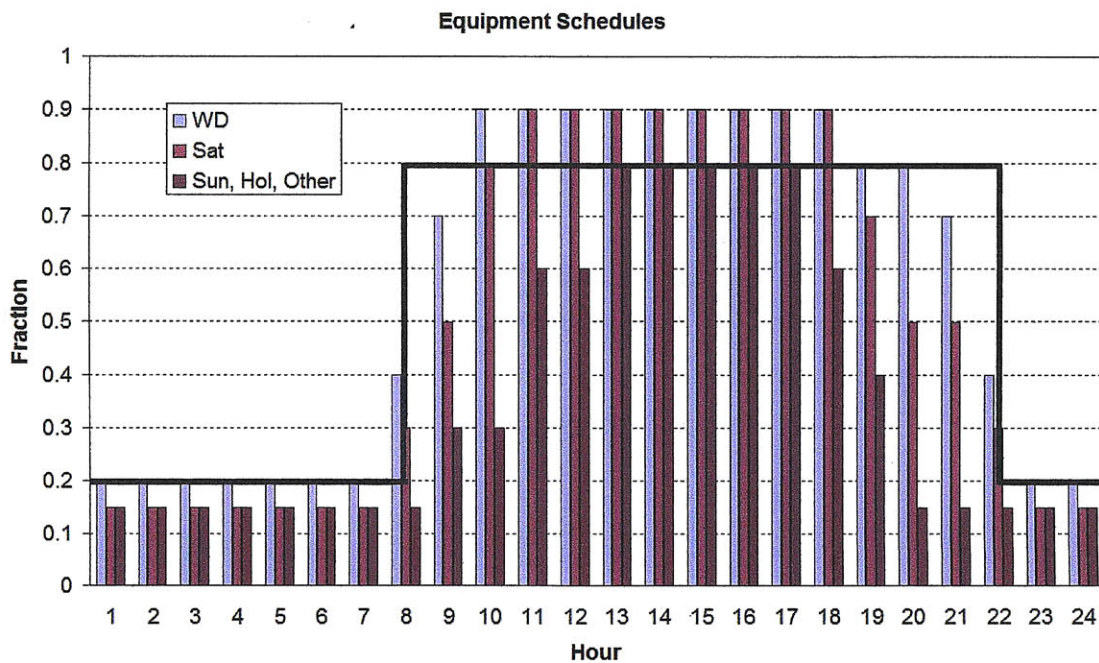


**Figure 6-6. An example of the detailed Equipment schedule for the Small Office building as it appears in the provided excel workbook [DOE, 2008]. The simplified schedule used in the “simple” calculation is 80% of design loads between 8:00 and 22:00. In this example, the real schedule and the simple schedule match well, but several other building types have more variance in occupancy and equipment schedules.**

#### 6.4.1 Comparison of Daily Total Loads

Because the Balance Point method is used in what is really a proof of concept of the SHS metric, the results of the balance point calculations will not be as rigorous as the Energy Plus simulations. However, it is still important to consider the quantities and causes of existing inaccuracies. Aside from the obvious differences in rigor between a



manual calculation and a physically-based simulation, there are at least two reasons why the balance point results will not precisely mirror those from Energy Plus.

First, as mentioned earlier, the balance point method disregards thermal mass. This causes all heat gain to have an instantaneous effect on the building loads, whereas in reality, the effects of thermal mass could delay the effects of heat gain for hours (depending on the size and layout of the mass). Second, one should be aware that the outputs from Energy Plus are in the form of energy use, not energy load. While the energy load of a building will rise and fall smoothly and sometimes gradually, a real HVAC system does not have infinite settings between on and off. Instead, the energy levels at which it can operate more closely resemble a disjointed stepwise curve, and to meet energy demands between these levels, the system might cycle on and off. This can cause a realistic system to consume a different amount of instantaneous energy, which can sometimes sum to a different amount of total energy, than an idealized system with an infinite variety of settings. It is still important to keep total energy use as a comparison value, however, because it takes into account the effects of thermal mass.

Both thermal mass and the stepwise behavior of the HVAC system will contribute to discrepancies between the simulated energy use and the balance point based energy load. Because of both chronological discrepancies, the daily load totals, rather than the instantaneous cooling and heating loads, will be compared to the daily total simulated energy use. The results from both the “detailed” and “simple” balance point calculations were converted from temperature differences into loads using the equation (6.3) and were then compared with the simulated energy use from Energy Plus. However, this comparison is not done in the form of conventional error (the ratio of the difference in results divided by the control value).

Heating and cooling loads can be considered part of the same spectrum of heat transfer conditions, and at the zero point between “positive” cooling and “negative” heating conditions, any conventional error is blown wildly out of proportion. In the comparisons shown below, the absolute load difference was more consistent than the conventional error. Because of this, the ratio used for comparison is the difference between balance point load and simulated energy use, divided by the *maximum* simulated heating or cooling energy use (whichever is appropriate):

$$\text{Maximum Load Ratio (MLR)} = \frac{Q_{BP} - Q_{sim}}{Q_{sim,MAX}} \quad (6.7)$$

where  $Q_{BP}$  is the daily total balance point load,  $Q_{sim}$  is the daily total simulated energy use, and  $Q_{sim,MAX}$  is either the maximum heating or the maximum cooling daily total energy use for that particular building and climate. The maximum load was chosen as a means of error comparison because it is a representative and a recognizable energy quantity associated with each particular building.

The results can be categorized by how closely they agree, using the annual average MLR – between the balance point daily total loads and the simulated energy use daily total – as an indicator. To help give an idea of the overall distribution of results, correlation categories have been assigned based on annual average MLR, as shown in Table 6-2. The thresholds shown in that table were determined after a visual analysis of many annual energy use and load graphs (such as the ones in figures 6-8 through 6-12).

The thresholds defining “very good” and “good” specifically are meant to represent a very close correlation between balance point loads and simulated energy use.

The percent of the 256 detailed and simple balance point simulations which fall into each of these categories are shown in Figure 6-7, and a detailed look at what each of these categories means in terms of the MLR daily correlation is illustrated in Figures 6-8 through 6-12. Tables of average, median and the standard deviation of MLR for all 256 building and climate combinations are in Appendix D. They are given in the form of cooling loads/use only, heating loads/use only, and cooling minus heating loads/use. This last form was deemed the most necessary comparison, especially considering that larger buildings often heat and cool at the same time, and because the ultimate goal is the accurate prediction of loads rather than energy use.

**Table 6-2. The assigned categories of correlation quality, based on average MLR.**

	Very Good	Good	Moderate	Poor	Very Poor
<b>Annual Average MLR, Cooling - Heating</b>	< 10%	10%-30%	30%-50%	50%-100%	> 100%

The Retail model in Chicago, shown as an annual plot of balance point loads and simulated energy use in Figure 6-8, is a typical result showing a very good correlation. Both balance point load calculations predict almost the same amount of daily energy load as the more rigorous Energy Plus simulation, which generally means that the building has a lower thermal mass, an uncomplicated schedule, an envelope which is responsive to external conditions, or all three. In contrast, the Warehouse Model in Houston, in Figure 6-10, represents moderately correlated balance point loads which rise and fall with the simulated energy use, but over-estimate both cooling and heating loads.

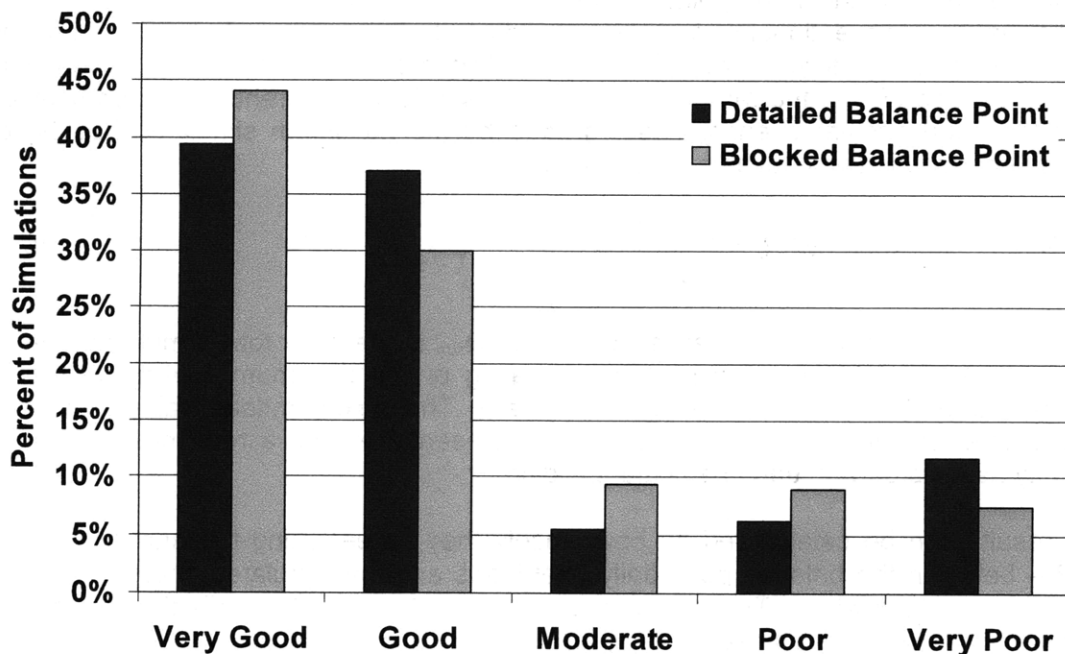


**Figure 6-7. The distribution of the 256 detailed and blocked balance point calculations in terms of the correlation quality with the simulated energy use.**



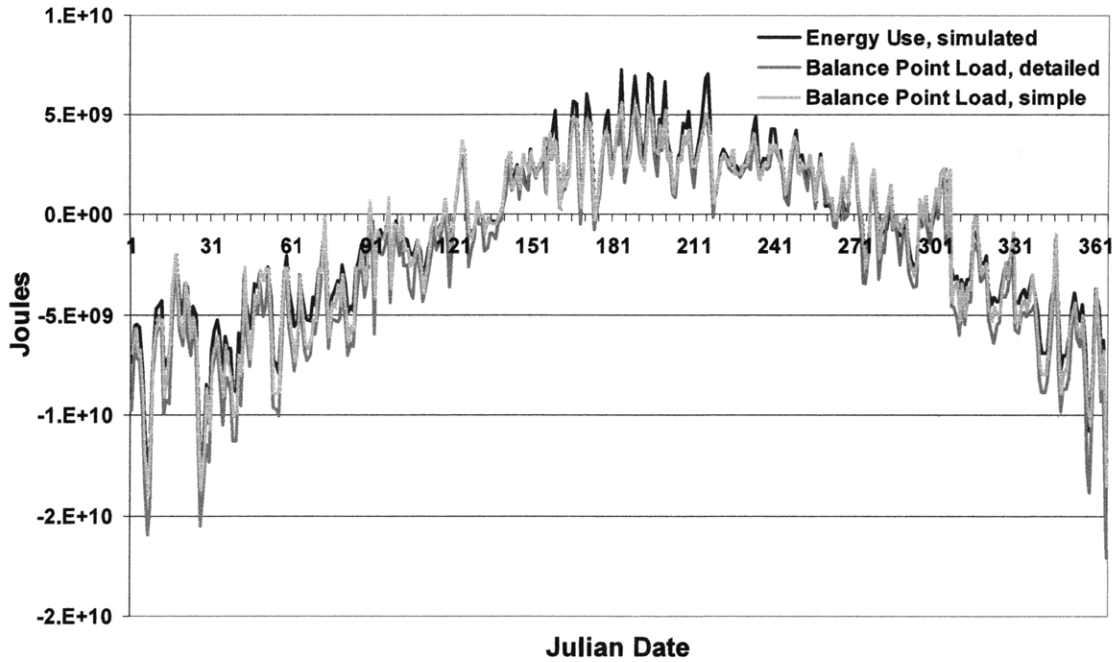


**Figure 6-8. The annual variation in Energy Plus simulated energy use and the two calculations of balance point load for the Retail model in Chicago. This graph shows a very good agreement between the Energy Plus simulation and both balance point loads.**

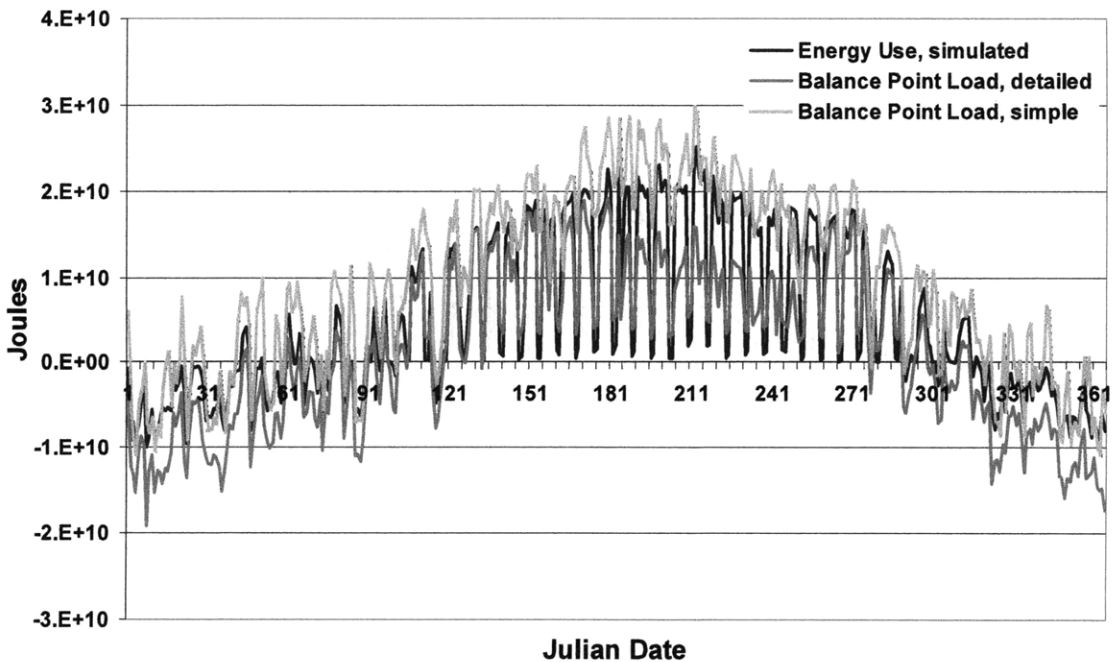


**Figure 6-9. The annual variation in Energy Plus simulated energy use and the two calculations of balance point load for the Primary School model in Albuquerque. This graph shows a good agreement between the Energy Plus simulation and both balance point loads.**

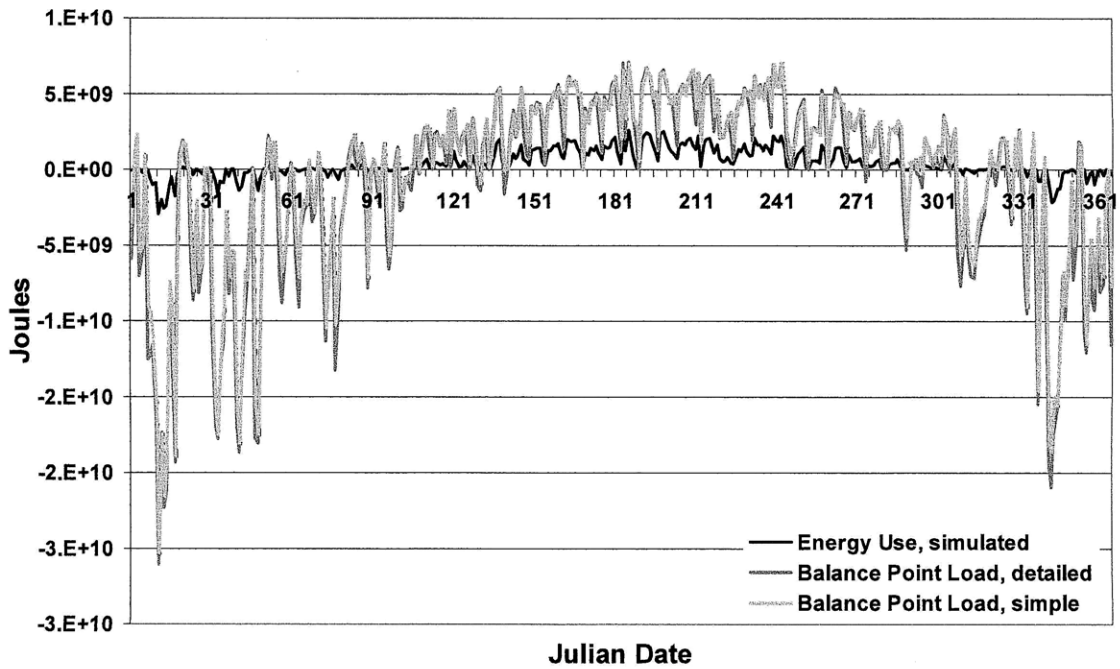


**Figure 6-10.** The annual variation in Energy Plus simulated energy use and the two calculations of balance point load for the Warehouse model in Houston. This graph shows a moderate agreement between the Energy Plus simulation and both balance point loads.

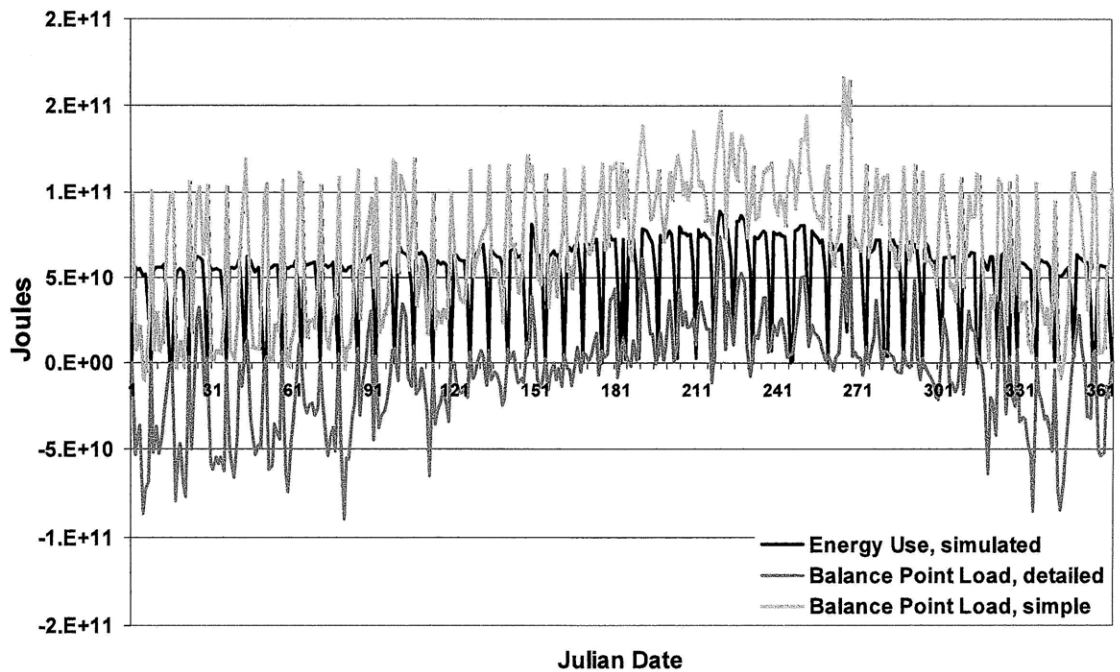


**Figure 6-11.** The annual variation in Energy Plus simulated energy use and the two calculations of balance point load for the Large Office model in Los Angeles. This graph shows a poor agreement between the Energy Plus simulation and the detailed balance point load.

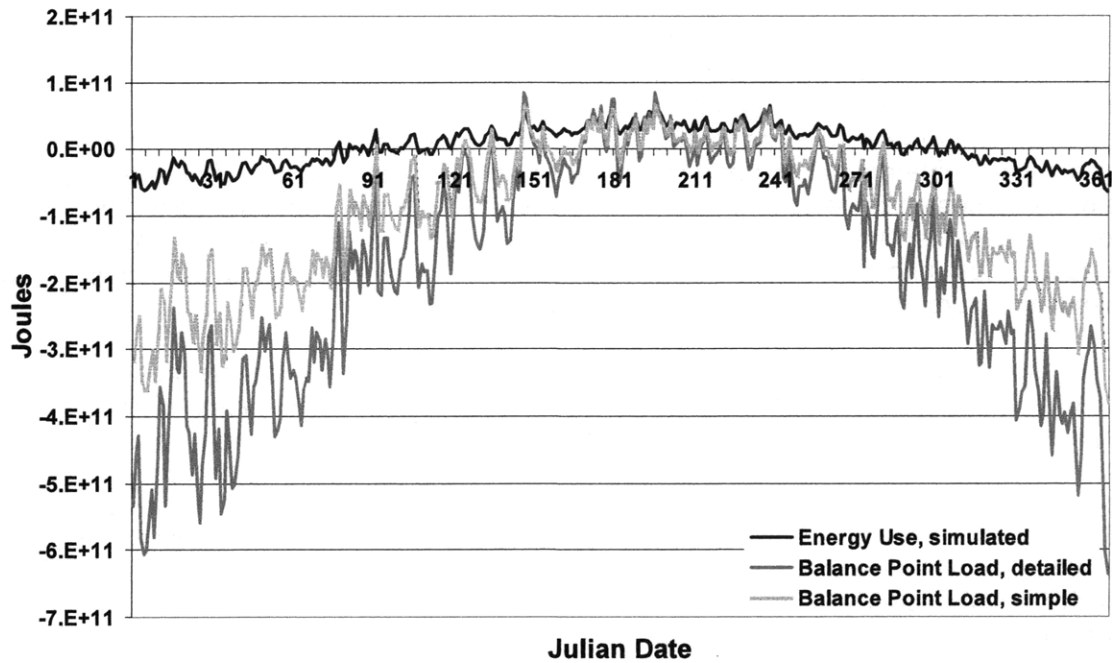


**Figure 6-12. The annual variation in Energy Plus simulated energy use and the two calculations of balance point load for the Large Hotel model in Minneapolis. This graph shows a very poor agreement between the Energy Plus simulation and both balance point loads.**

The “poor” and “very poor” correlations for the Large Office in Los Angeles (Figure 6-11) and the Large Hotel in Minneapolis (Figure 6-12) grow wider and wider apart. It is not a coincidence that the larger, internal gains-driven buildings are the ones representing poor correlations in balance point load data. Among other things, the Hospital, Large Office, and Large Hotel are more affected by their larger thermal mass, which makes them less suited to the balance point calculation.

From an overall performance standpoint, the simulated energy use of the Retail, Midrise Apartment Building, and Fastfood models were very well represented by both balance point analyses. The Outpatient, Small Hotel, and Small Office models showed “very good” correlation for one of the balance point analyses, and “good” for the other. These are all envelope-dominated buildings, based on their larger surface to volume ratio and moderate internal heat gain [Lechner, 2001]. As mentioned above, the three building models which are most internally dominated are the Hospital, the Large Office, and the Large Hotel, which had the worst correlations in general, especially the Large Hotel. In these cases, thermal mass acted as a dampener of the peak energy loads, allowing the heating system to remain off for a far greater amount of time and the cooling system work less hard.

The two other groups models which exhibit moderate to poor correlation are the simple balance point analyses of the Sit Down Restaurant and both balance point analyses for the Warehouse. In the restaurant’s case, the balance point analysis with a simple schedule vastly overestimated the cooling required all year. Another look at the kitchen

equipment schedule showed that it never goes above 30% of its capacity (and thus 30% of its heat output) at any time, and the peak uses are tied not to the work day, but to meal times. A re-simulation with an adjusted internal gain weight solved some of the problem, but the uneven schedule between meal times still meant that the simple case overestimated the load in general.) The Warehouse, on the other hand, is a building with several different heating and cooling set point temperatures for the different types of storage zones or office space. The analysis was unfortunately not set up to handle this level of detail, so the correlation between energy use and the calculated balance point loads varies unpredictable from “very good” to “very poor”, with the majority of simulations producing “moderate” to “poor” correlations.

The situations with the Sit Down Restaurant and the Warehouse are not a problem overall, but more a reminder that one must model the behavioral inputs of the building (like schedule and zone setpoint) as carefully as possible. Fortunately, most buildings (at least within the sixteen benchmarks set) have a much simpler occupancy and equipment schedule and are well-represented by the simple balance point calculation. The issues surround the three more massive buildings are more systematic, but not unexpected when using the balance point method. Again, it is worth considering that the designer may actually be more interested in assessing solar heat gain at its source than the chronological distribution of actual energy use.

#### **6.4.2 Visualizing Solar Heat Scarcity/Surplus**

Aside from a numerical comparison of daily totals, the temporal map showing SHS calculated using balance point loads and those calculated using simulated energy use should be nominally comparable – although because of the reasons given in the previous section, they will not look identical. The thermal mass effects are visible in the energy use graphs of Figures 6-14b and 6-15b and the cycling patterns of the HVAC system are noticeable in all models. The greatest visual differences, however, are generally caused by the internal load assumptions and actual energy use. Figures 6-13, 6-14, and 6-15, discussed individually below, are the temporal maps corresponding to the numerical data in Figures 6-8, 6-9, and 6-12 above.

The Retail model in the Chicago climate is an example of a situation in which the daily total MLR of both balance point calculations showed very good correlation with the simulated energy use. The temporal extents of detrimental and beneficial SHS are virtually identical for all three methods (Figures 6-13a, 6-13c, and 6-13e), as are the load and use graphs themselves (Figures 6-13b, 6-13d, and 6-13f). These load graphs are shown for all 24 hours of every day, whereas the SHS graphs are blacked out at night. This is largely due to the impossibility of judging the solar heat gain during hours when there is no solar heat gain and no consideration for thermal mass.

The most notable difference in the load and use graphs for the Primary School in Albuquerque (Figure 6-14) is a slight thermal mass shift from morning gain energy use in the afternoon (Figures 6-14a and 6-14b). This is more noticeable in the SHS graph than the load graph, but although the correlation is not perfect, it is still good. On the other hand, the simple balance point graphs definitely show the influence of an overestimated, un-nuanced solar energy gain during occupied hours. Because the internal heat gain is so high, less of the problem is attributed to solar gain, and the resulting Solar Heat Surplus is lower (Figure 6-14e).



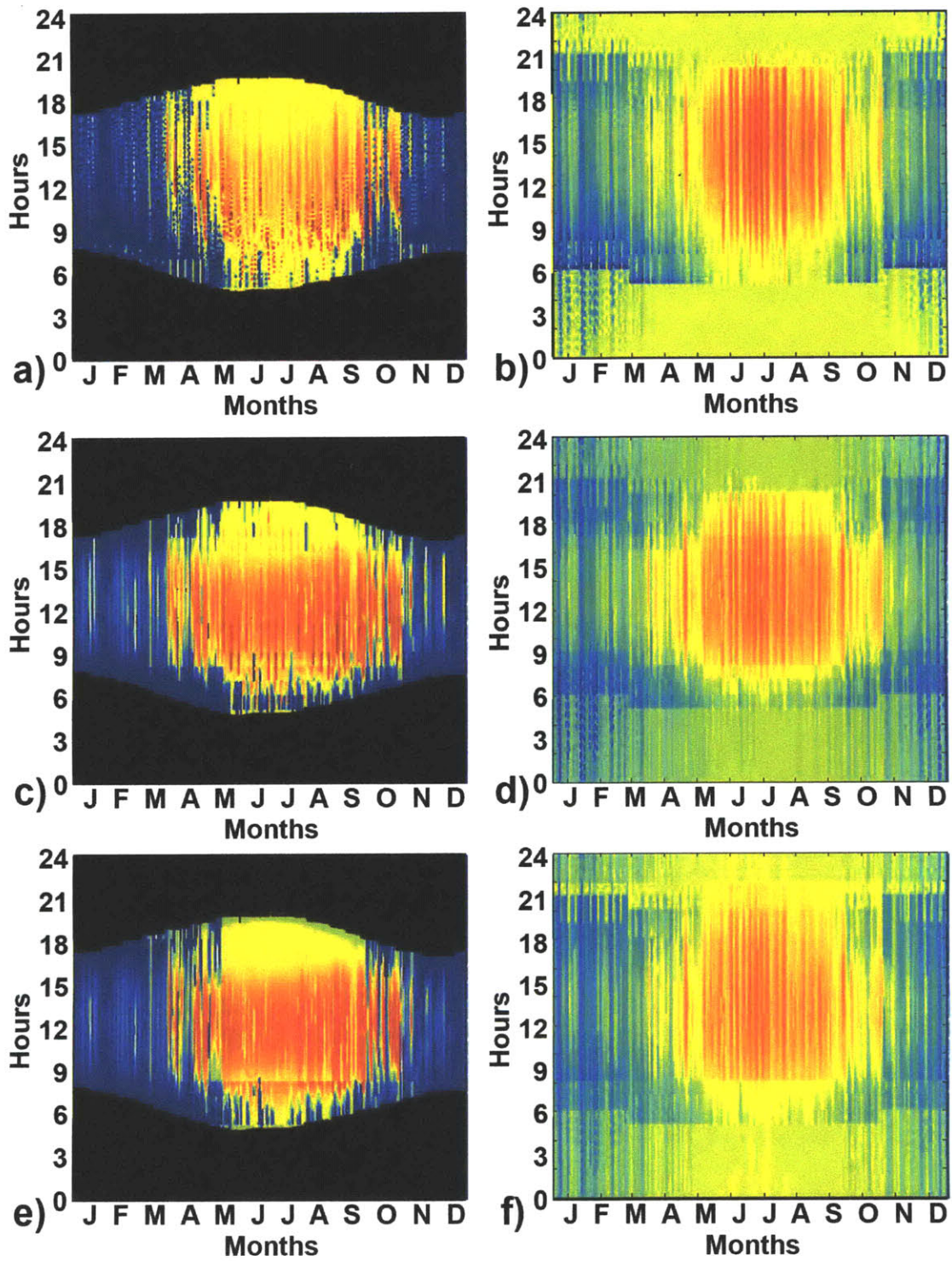


Figure 6-13. Temporal maps for the Retail model in Chicago. The SHS graphs are on the left and load/use graphs are on the right. Top) Energy plus energy use, middle) detailed balance point, bottom) simple balance point.



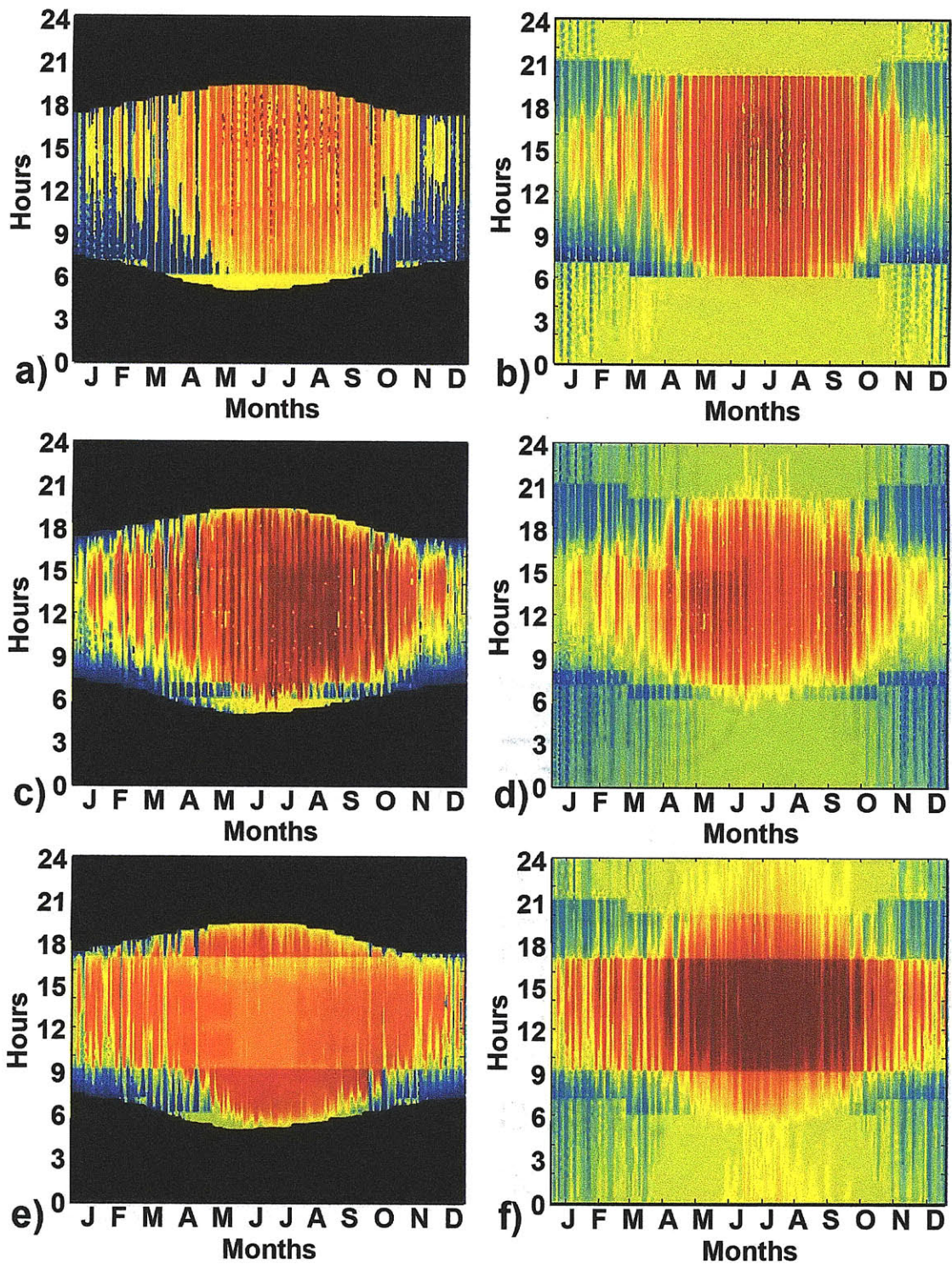


Figure 6-14. Temporal maps for the Primary School model in Albuquerque. The SHS graphs are on the left and load/use graphs are on the right. Top) Energy plus energy use, middle) detailed balance point, bottom) simple balance point.



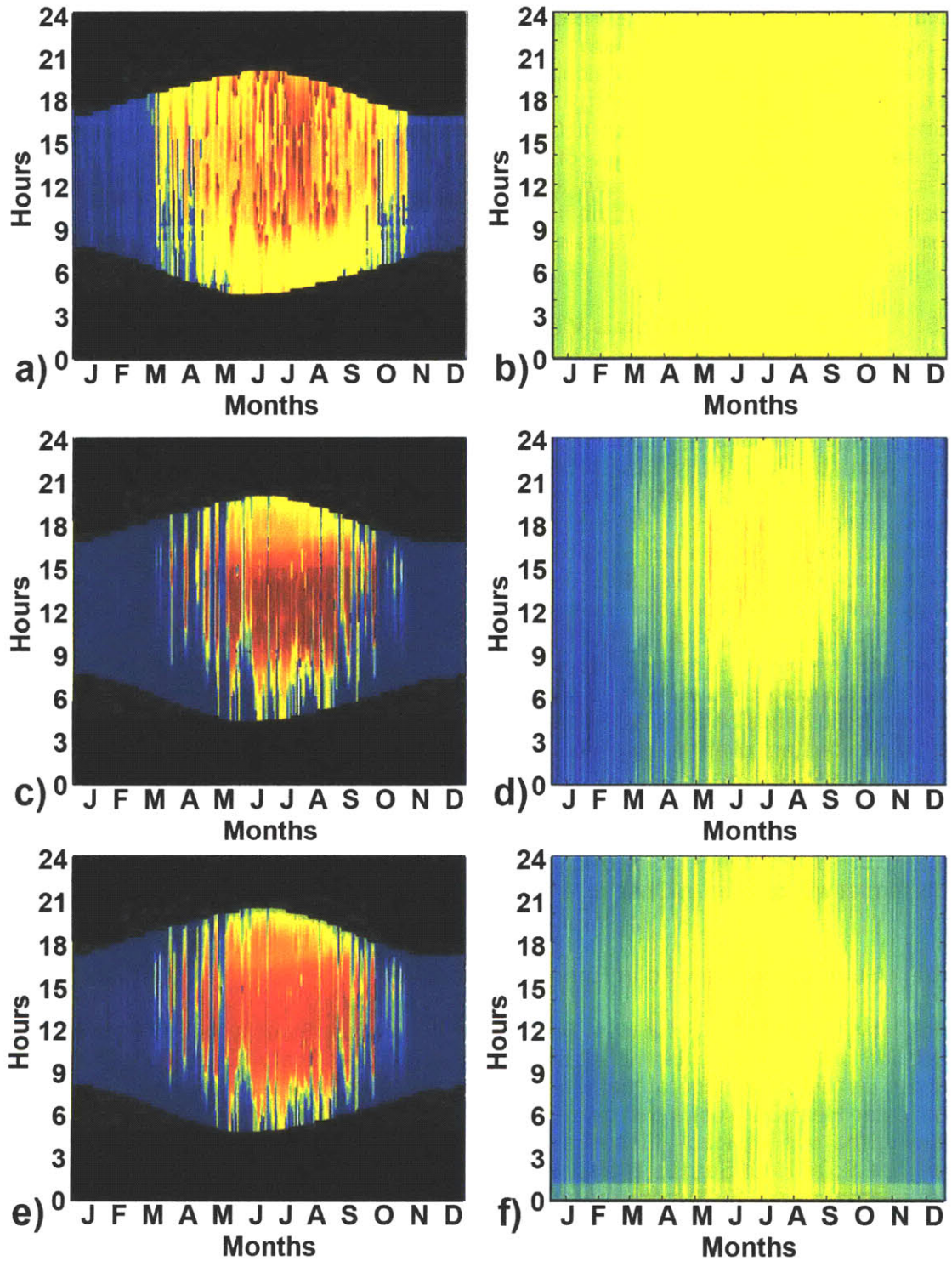


Figure 6-15. Temporal maps for the Large Hotel model in Minneapolis. The SHS graphs are on the left and load/use graphs are on the right. Top) Energy plus energy use, middle) detailed balance point, bottom) simple balance point.

Finally, the graphs for the Large Hotel in Minneapolis (Figure 6-15) illustrate the effect of a high internal gain coupled with high thermal mass. Although the summer loads predicted by the balance point calculations are reasonably accurate, there is much less heating energy used in the Energy Plus simulation than one might predict (Figure 6-15b). Because of this, the extent of 0% SHS is much larger for Figure 6-15a than it is in Figures 6-15c and 6-15e. Many of the simulations done for the Large Hotel, Large Office, and Hospital exhibit these tendencies, because high thermal mass dampens peak energy loads and shifts some solar from the warmer day to be released during the cooler night. In general, this affects heating loads more than cooling loads.

### 6.5 An Alternate Daily Totals Visualization

Because the balance point equation cannot take thermal mass into account, and because the comparisons made in Section 6.4.1 were between daily total loads, it is worth suggesting an alternate, less detailed visualization of the SHS. In the earliest stages of design, when accurate detailed information is not available, SHS could be found using daily total solar energy and internal loads in the place of hourly loads. The SHS percentage derived from these daily totals would be displayed in temporal maps in solid bands of color, since the value would be constant over the day (see Figure 6-16). The result is a look at seasonal, rather than hourly trends of SHS, but it is more representative of the accuracy of the data involved in balance point calculations. This format will be used in Chapter 7.

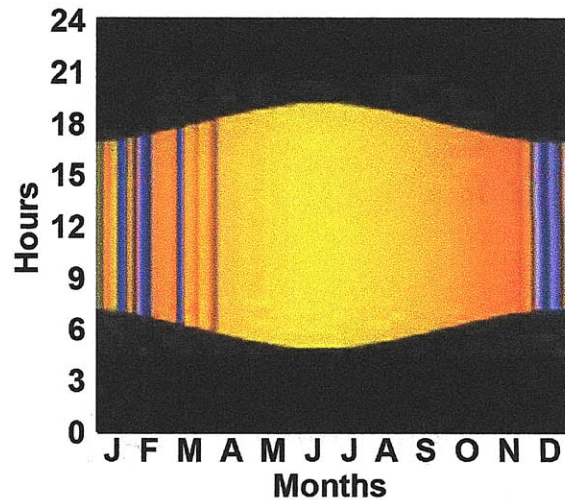


Figure 6-16. Solar Heat Scarcity/Surplus temporal map displayed in the form of daily totals rather than hourly data.

### 6.6 Summary of New Solar Energy Metric

SHS, which is split into Solar Heat Surplus and Solar Heat Scarcity, is a measure of the need for, or the need to get rid of, solar heat gain. Specifically, Solar Heat Scarcity is defined as the percentage of the heat load *not* being met by solar energy from windows, and Solar Heat Surplus is the percent of existing solar energy from windows which is causing the cooling load. Because internal heat gain also contributes to the cooling load, the Solar Heat Surplus is also weighted by the part solar gain plays in comparison with internal gain. SHS exists on a linear scale between -100% (Scarcity) and 100% (Surplus) and is displayed on temporal maps where 100% is red, -100% is blue and 0% is yellow. 0% SHS is the point at which there is just enough solar energy from windows for the building balance point to equal the outdoor air temperature.

SHS is found using the balance point method as a simple energy calculation and is analyzed against data gathered using the 16 Commercial Benchmark Buildings released recently by Energy Plus. A detailed balance point load is calculated using the Energy Plus variable outputs for each time step, and a simple balance point load is calculated



using a much simpler schedule. These two energy loads are compared with the energy use outputs of Energy Plus simulations. The numerical comparison was made using a Maximum Load Ratio in order to prevent errors near zero energy load from blowing out of proportion.

For the most part, the correlations were either “very good” or “good”. The two main causes of bad correlation between the balance point loads and the Energy Plus energy use are large thermal mass, and for the simple balance point calculation, inadequate representation of the model – especially internal loads, variable schedules, and multiple zone set points. It is important to note that while the balance point method was chosen as the simple energy calculation in Lightsolve, the SHS metric could even be used in conjunction with a far more complex energy simulation. In general, however, the main body of simulations performed reasonably well, when judged by the daily total energy use.

Although chronological shifts based on thermal mass are expected in some of the SHS graphs, even the worst results show some level of visual correlation. Mostly, however, this chapter demonstrated that it is possible to put solar heat gain information into a goal-based temporal format and thus make it easily comparable with illuminance- and glare-based data. Finally, it is possible to show less detailed data in a “daily totals” temporal map format which better represents the accuracy of the balance point equation.

# Chapter 7

## Temporal Maps and Design Analysis

Temporal maps have great potential for aiding early-stage design analysis. They have the ability to convey a full annual data set within a single graphic, which instantly connects daylighting performance with important time-based design influences like sun angle, seasonal climate, and occupancy hours. Although they are stronger in partnership with spatially-based data or renderings, a survey given by the author found that architects could answer simple analysis questions based only on Acceptable Illuminance Extent (AIE) temporal maps with no spatial references given at all (see Section 7.4).

In the following sections, several examples are given which illustrated the analysis potential of the temporal data and metrics described in Chapters 3 through 6: a simple mock design process, a comparison of spatial and temporal information for a classroom and other models, and an options analysis for the orientation and window shades in a single hospital room. Although this thesis provides a solar heat gain metric and recommends a comparison of all three aspects of daylighting for a complete analysis (light quantity, glare, and solar heat gain), these examples focus on AIE and GAE (Glare Avoidance Extent), because the solar gain analysis capabilities of Lightsolve have yet to be implemented.

### 7.1 Iterative Example of Improving Illuminance Performance

To illustrate a design process of several iterations, a simple box-like room was created in Radiance, located in Sydney, Australia, and given an arbitrary illuminance range goal of 400-1000 lux on the work plane (with partial credit given down to 200 and up to 2000 lux). This test illuminance range was not chosen for any particular reason, other than to keep relatively even light appropriate for reading available on the work plane. No occupancy hours are given for this model, so we are concerned with all sunlight hours. Radiance was used to perform the rendering rather than the LSV engine so that these models could be used as visual validation models for AIE (see Section 4.2.1), and the parameters used are similar to those considered in the validation of the data reduction method in Section 3.x: `-ab 5, -ar 128, -aa .1, -ad 2048, -as 256, -dp 1024, -ds .15, -dt .05, -dc .75, -dr 3, -ms 0.066, -sj 1, -st .01, -lr 12, -lw .0005, -l+, -h.`

The model (see Figure 7-1) is not much more complicated than the shoebox model from Chapter 3. It is 7.5m by 10m by 3m, with the short façade on the north and south faces. Two punch windows, each 2m wide by 1.5m tall, are located on the north (sunny) façade with 1.5m between them and a sill height of 1m. All objects are grayscale and opaque objects are lambertian; the ceiling reflectance is 83%, the wall reflectance is 65%, the floor reflectance is 20%, and the visible transmittance of the glass is 80%. Because there was initially going to be a classroom, there is a 6m by 1.5m chalkboard on the east wall with a 5% reflectance. The walls have a thickness of 25cm. An array of twelve work plane sensors were placed 1m from the floor at 2m, 3.5m, and 5m east of the west wall and 1m, 3.5m, 6m, and 8.5m north of the south wall.

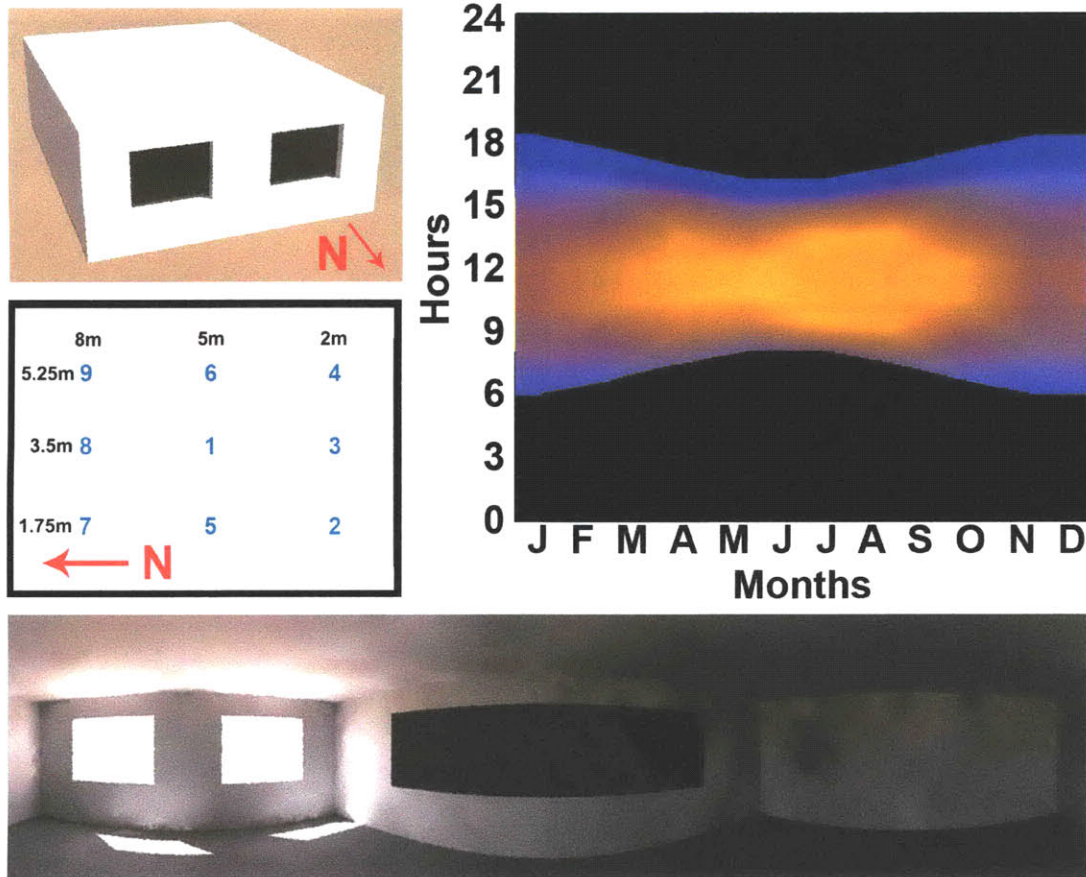


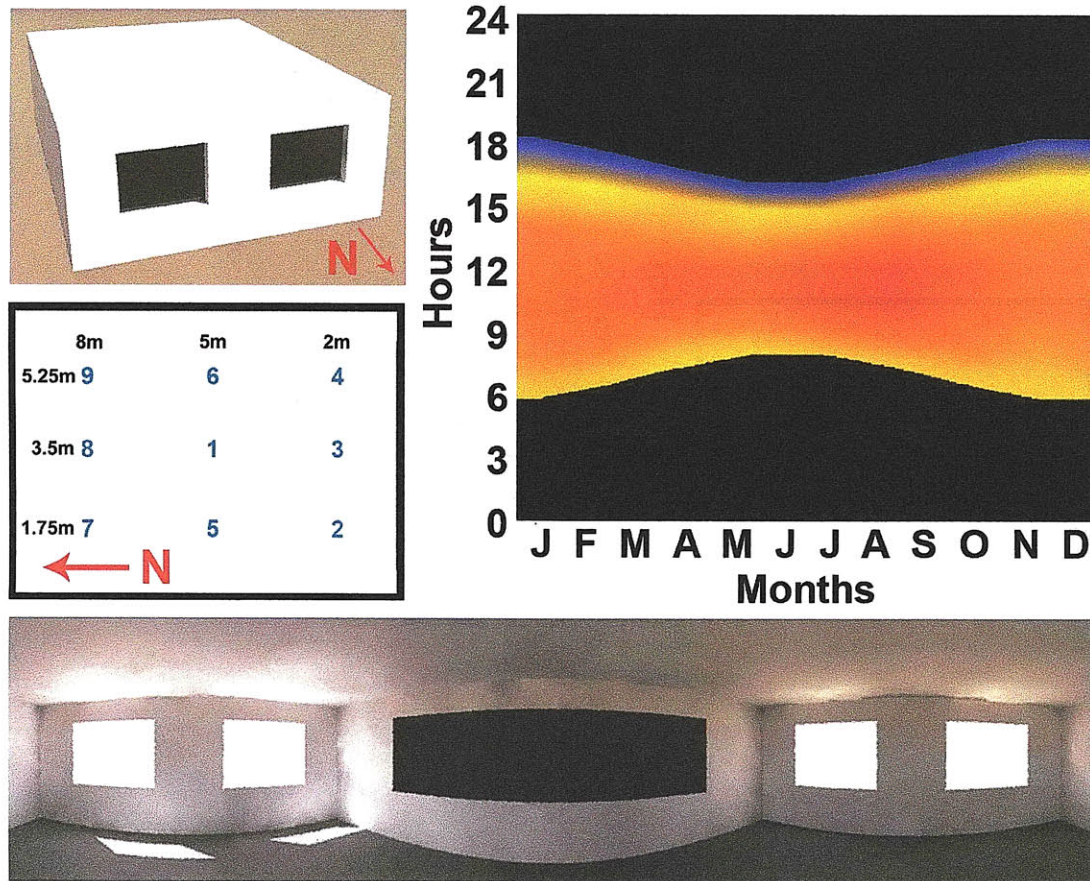
Figure 7-1. Cylindrical interior rendering, exterior rendering, points diagram, and temporal map of the work plane AIE for iteration 1 of the simple model.

Figure 7-1 shows some representative renderings of this simple model as well as a temporal map of the work plane AIE. Disregarding the very early morning and evening, the purple color during most of the day in the four or five warmest months of the year suggests a work plane which is partially too high, partially too low, and very little in range: a very low Acceptable Illuminance Extent. During the winter months (the center of the temporal map), more of the work plane is within the acceptable illuminance range, making the AIE higher, but there are still tinges of orange and blue over the whole temporal map. This suggests that at all times, at least part of the work plane is below acceptable illuminance, and part is above. By referencing the renderings, we can guess that the back of the room is where the low illuminances are, and the area next to the windows is sometimes hit by direct sun, which would cause very high illuminances.

The second design iteration of this simple model deals with the low illuminances by adding two identical windows to the south façade and raising the wall reflectance to 75%. All other model variables (and Radiance simulation parameters) remain the same. Figure 7-2 shows renderings and an AIE temporal map of this design iteration.

While the low illuminance problem has been virtually eliminated from the model, the high illuminance problem has not yet been dealt with, and has in fact been increased with the addition of extra windows. The temporal map in Figure 7-2 suggests that at least half





**Figure 7-2. Cylindrical interior rendering, exterior rendering, points diagram, and temporal map of the work plane AIE for iteration 2 of the simple model.**

the work plane nearly always has a higher than acceptable illuminance, making the AIE 50% or less, and this problem is exacerbated during winter mid-days, when the direct sun would reach further into the room. The object for the next design iteration, therefore, is to maintain a high level of diffuse illuminance while cutting off as much direct sun as possible.

Iteration three of this simple model actually represents a couple design steps, all with the objective of maintaining an even, but lower, illuminance level all year round. The wall reflectance is taken back down to 65%. All windows are made smaller to reduce illuminance; the south windows are reduced in height by half a meter each, and the north windows are made into three narrowly separated windows with a combined dimension of 1.1m by 5 m. Next, an exterior overhang and diffuse light shelf just over 1.25m deep are added to the north façade windows to cut out direct sunlight on the work plane but bounce some of it to the ceiling. Finally, the north windows are moved up the façade (and the north façade was heightened to four meters) to make sure the center of the room still receives enough light – the new window sill height is 2.4m.

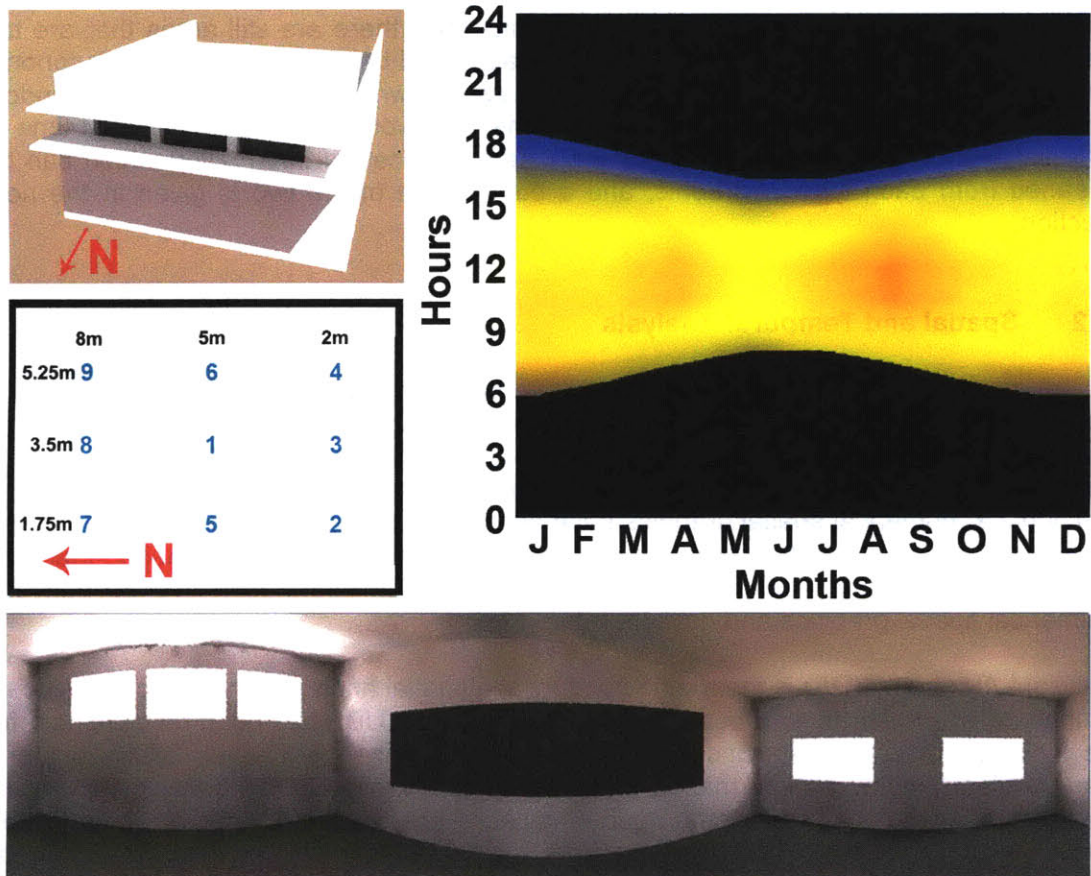


**Figure 7-3. Cylindrical interior rendering, exterior rendering, points diagram, and temporal map of the work plane AIE for iteration 3 of the simple model.**

As Figure 7-3 shows, this combination of design changes produces a vast performance improvement for this simple model. The work plane is at 100% AIE nearly all year round, with a few low illuminances at the daily extremes and a few pale orange spots in midwinter which might represent some winter sun escaping past the overhang or a general illuminance that is just slightly too high.

The decisions in this mock design process were made using the temporal AIE data, renderings of the space, and previous knowledge of how different design changes might affect daylight behavior. The analysis helps decide the objectives for the next design iteration, and the designer must use prior knowledge, logic, or trial and error to determine what steps to take. One reason that an early stage design analysis tool must be quick and interactive is that designers without experience must use a combination of logic and trial and error, although this process will also help the designer gain that experience, lessening the necessary number of design iterations in the future.

In these examples, logic and inference took the place of annual spatial data. For instance, it is logical to assume that high illuminances happen either near the window or as a result of direct sun penetration (or both), just as it is logical to assume that the darkest places in the room are furthest from existing windows. The temporal data in Figure 7-1 shows that during the summer, there are parts of the work plane that are both



too high and too low, and during the winter mid-days, there are still areas that are too high, but also more that are in range. If the graphs had been spatial Daylight Autonomy grids rather than temporal maps, they would have shown a higher DA near the window and lower towards the back of the room, but the user would have to guess what time of day and year problems occur. There are different pieces of information which can be gleaned from each type of graphic, and a comparison of the two is given in the next section.

## **7.2 Spatial and Temporal Analysis**

In the previous section, design decisions were based on both the temporal AIE data and renderings. Although it may seem obvious that spatial graphics show *where* daylighting problems occur while temporal maps show *when* they occur, it is good to take a more in depth look at the different conclusions one may draw from each. As discussed in section 2.x, numerical spatial graphics have dominated daylighting analysis for decades, and are, at the very least, more recognizable to the design world. This means that they are far more common, despite the fact that there is an information overlap between numerical spatial graphics and daylight renderings.

Daylight Autonomy (DA) is the metric used for the spatial analysis in this section, since it is the one which AIE most resembles. DA (and similarly UDI) has been revolutionary for its inclusion of climate-specific annual data sets [Reinhart & Herkel, 2000], but one cannot clearly show all information in one graphic. While DA condenses the annual performance results to a single number – indicating the percent of occupied hours when the illuminance is above a given threshold – AIE takes the complementary route by condensing spatial data to a percent of the area of interest which is within a given illuminance range. Essentially DA condenses temporal performance and displays it spatially, while AIE condenses spatial performance and displays it temporally. Additionally, thanks to the three-color scheme devised for the AIE temporal maps, each graph simultaneously shows the percent area of interest which is too high and too low as well as that which is in range.

### **7.2.1 Classroom Example**

The first spatial-temporal comparison involves two classroom models with the same basic size, orientation, and location. Both classrooms models consist of two 34 ft by 22 ft by 8 ft classrooms on a double-loaded corridor with windows facing either Southeast or Northwest. The given goal is to keep the work planes of both classrooms between 400 and 2000 lux (with no partial credit buffer zone) from 8am to 4pm between September 1<sup>st</sup> and June 30<sup>th</sup>. The reflectance of the walls is 65%, the floor is 30%, the ceiling is 80%, and the windows are 80% transmissive. The models, shown in Figure 7-4, are located in Boston. The daylight source for the first is a set of inadequate unilateral punch windows, and the second includes an indirect skylight over the corridor for bilateral lighting and some slightly modified window shading which make the sky access directly east (to limit the hours of possible direct sun in the absence of an overhang) and directly north (to entirely occlude direct sun).



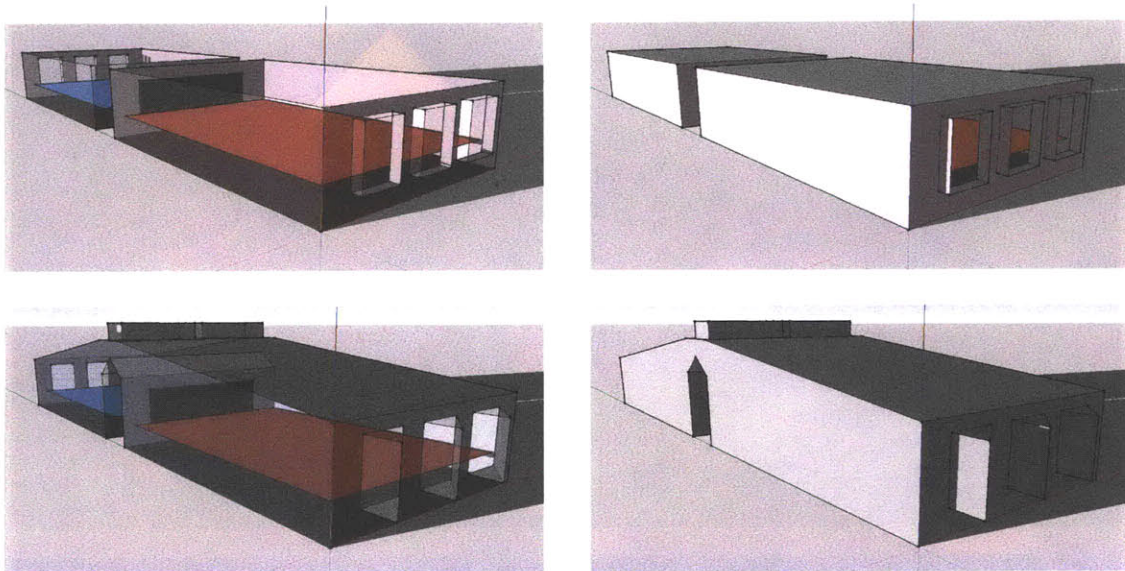


**Figure 7-4. Exterior and interior views of SketchUp models (including sensor planes) for classroom 1 (top) and classroom 2 (bottom).**

The classrooms were modeled in SketchUp and the temporal maps were made using Lightsolve. The SketchUp models were then imported into Ecotect and exported into Daysim to produce the appropriate DA data, which was then imported back into Ecotect where it was displayed graphically in two parts, the first showing the DA with a 400 lux threshold, and the second showing the DA with a 2000 lux threshold. In all instances, the color scheme of the Daylight Autonomy graphics was made to match that of the temporal maps as closely as possible: The DA graph with a 400 lux threshold fades from blue (0% DA) to yellow (100% DA), and the graph with a 2000 lux threshold fades from yellow (0% DA) to red (100% DA). In each case, yellow is more desirable. Figure 7-5. shows all graphics associated with the first basic classroom, and figure 7-6 shows those relating to the second modified classroom.

The most noticeable feature of the DA graphs is that a large portion of the back of each room never reaches 400 lux. They also tell us that a small area near each window is sometimes too bright. This in itself is not unexpected; the most interesting information given in the DA graphs is the extent of the space with very low DA, and that the area nearest the window on the southeast side, which is approximately 70-80% DA at 400 lux threshold, corresponds almost exactly with a similar area between 30% and 60% DA in the 2000 lux threshold graphs. This suggests that the area near the window actually is only 20-40% within the prescribed range. The most obvious design decision to make based on these graphs is to add another light source at the back of the classroom.

The temporal maps give slightly different information. Again the first noticeable feature is that the work plane is always partially too dim – and the whole plane is too dim every afternoon on the southeast side and nearly all the time on the northwest side. It is also interesting to note that the southeastern room receives similarly bright light in the morning regardless of season, and that this light places part of the work plane in range and simultaneously makes part too high. This suggests that it is difficult to keep any significant percent AIE without also incurring direct sunlight – a circumstance which

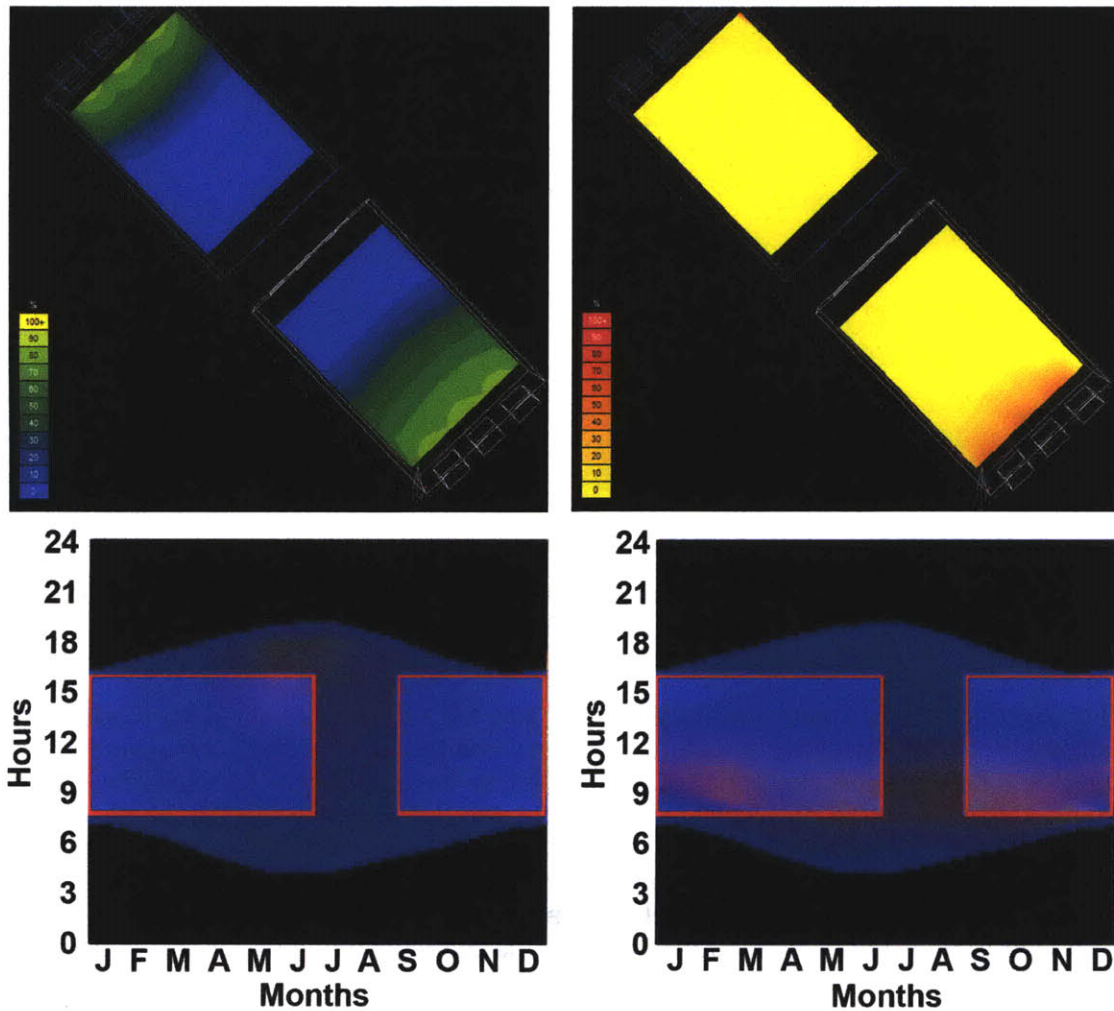


**Figure 7-5. Daylight Autonomy data (top) and temporal maps (bottom) for classroom 1. The occupied hours have been outlined (and the rest of the hours shaded) in the temporal maps.**

would make most teachers close the blinds in the morning, most likely making the whole work plane too dim again.

It is also important to realize that Daysim does not allow the option of seasonal occupancy schedules, which means that the summer days between 8am and 4pm are included in the calculation of Daylight Autonomy, even though they are not part of the given occupancy. This is not inherent to DA itself, but is a feature of the program which calculates it.

In the second classroom model, shown in figure 7-6, the addition of the light wells increases the 400 lux threshold DA while the window shade adjustments decrease the 2000 lux threshold DA by decreasing the direct sun penetration. The new minimum DA is 40% in the northwestern room and 50% in the southeastern room, which means that each part of the room is within the correct illuminance range over half the time. What we



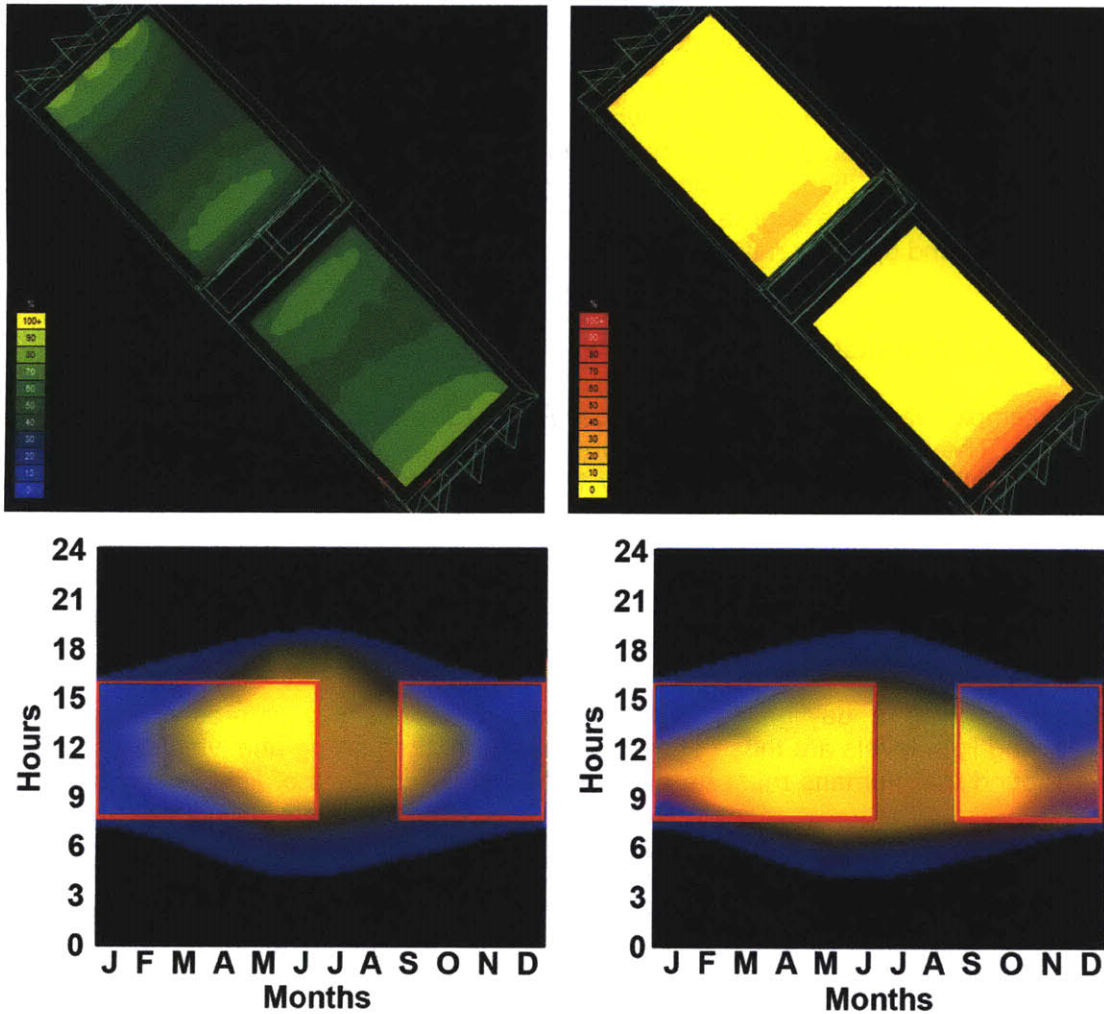


Figure 7-6. Daylight Autonomy data (top) and temporal maps (bottom) for classroom 2. The occupied hours have been outlined (and the rest of the hours shaded) in the temporal maps.

don't know from the daylight autonomy graphs is whether there are any times when the whole room is autonomous. This would be particularly important to know when dealing with traditional light switches, which either switch all light on or all lights off; the only time when the lights will be turned off is when the whole space is bright enough.

In looking at the temporal maps, one can see that there are significant portions of bright yellow – indicating 100% (or nearly 100%) AIE – within the occupied zones of both rooms. During these times, even traditional lighting arrangements can stay off. Both classrooms will need supplemental lights in the winter, particularly in the afternoons for the southeast room, and all day for the northwest room. As suggested by the 2000 lux threshold DA graph, both rooms avoid large areas of high illuminances most of the time, although there may be a small issue with direct sun on some winter mornings in the southeast room.



Because different information is gained from each, spatial and temporal graphics are very complementary, and analyzing both types of data gives a more complete picture than analyzing only one. Temporal maps are particularly rich in diurnal and seasonal performance information, however, which is arguably more important in the earliest stages of design, when the decisions pertaining to orientation and general building form must be made. It is those aspects of building design, most pertinent to daylight access, which will determine the degree to which the building will work with the climatic and solar environment and optimize natural light resources.

### 7.2.2 Hospital Room Example

This example was inspired by Christopher Pechacek's work on daylight in health care facilities. The model proportions conform to health care codes [Pechacek *et al.*, 2008]: the main part of the room is 16 ft wide by 13 ft deep, and the bed, which has a clearance of at least 3ft on each side, is 7ft 10in by 3ft 4in by 3ft 1in. The ceiling reflectance is 80%, the wall reflectance is 60%, the floor reflectance is 30%, and the visible transmittance of the window is 73% and is meant to represent double-pane low-e glass. The location of this model is Phoenix, Arizona, and several orientations of this room were studied, including the south and east orientations shown below.

When designing a daylighting scheme focused on health and recovery, the most interesting light levels are those at the patient's face, both sitting and lying down. It has been found that humans must be exposed to certain amounts of light to regulate their

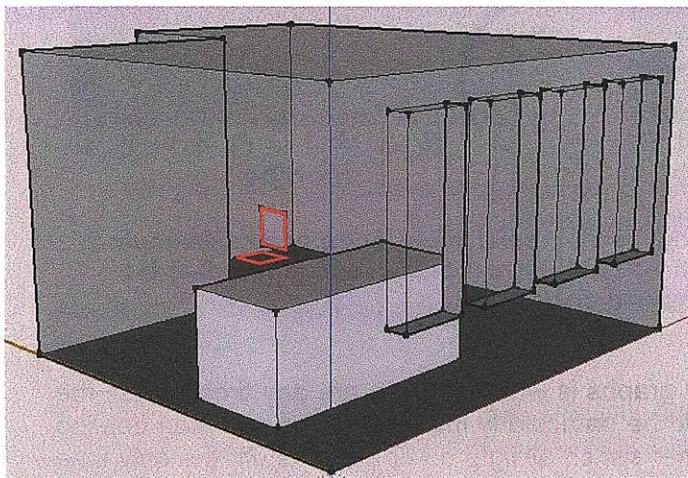


**Figure 7-7. SketchUp model and several renderings of the hospital room. The sensor planes are outlined in red.**

endogenous circadian rhythms and maintain a healthy hormonal balance [Rea *et al.*, 2002; Cajochen *et al.*, 2000; Küller & Lindsten, 1992]. By applying the particular spectrum of daylight to preliminary night-time findings by Cajochen *et al.* [Cajochen *et al.*, 2000], Pechacek argued that a natural light level of at least 192 lux was necessary for alertness [Pechacek *et al.*, 2008]. The goal, therefore, is to keep the light on the patient's face above 192 lux (with no partial credit buffer) while the sun is up. For the sake of the DA, an occupancy schedule of 6am to 6pm was implemented, so that there would be very few night hours included in the calculations.

Despite the very different behavior of daylight on a southern and eastern façade, the Daylight Autonomy graphs look almost identical. In fact, the slightly higher DA of the east-facing room

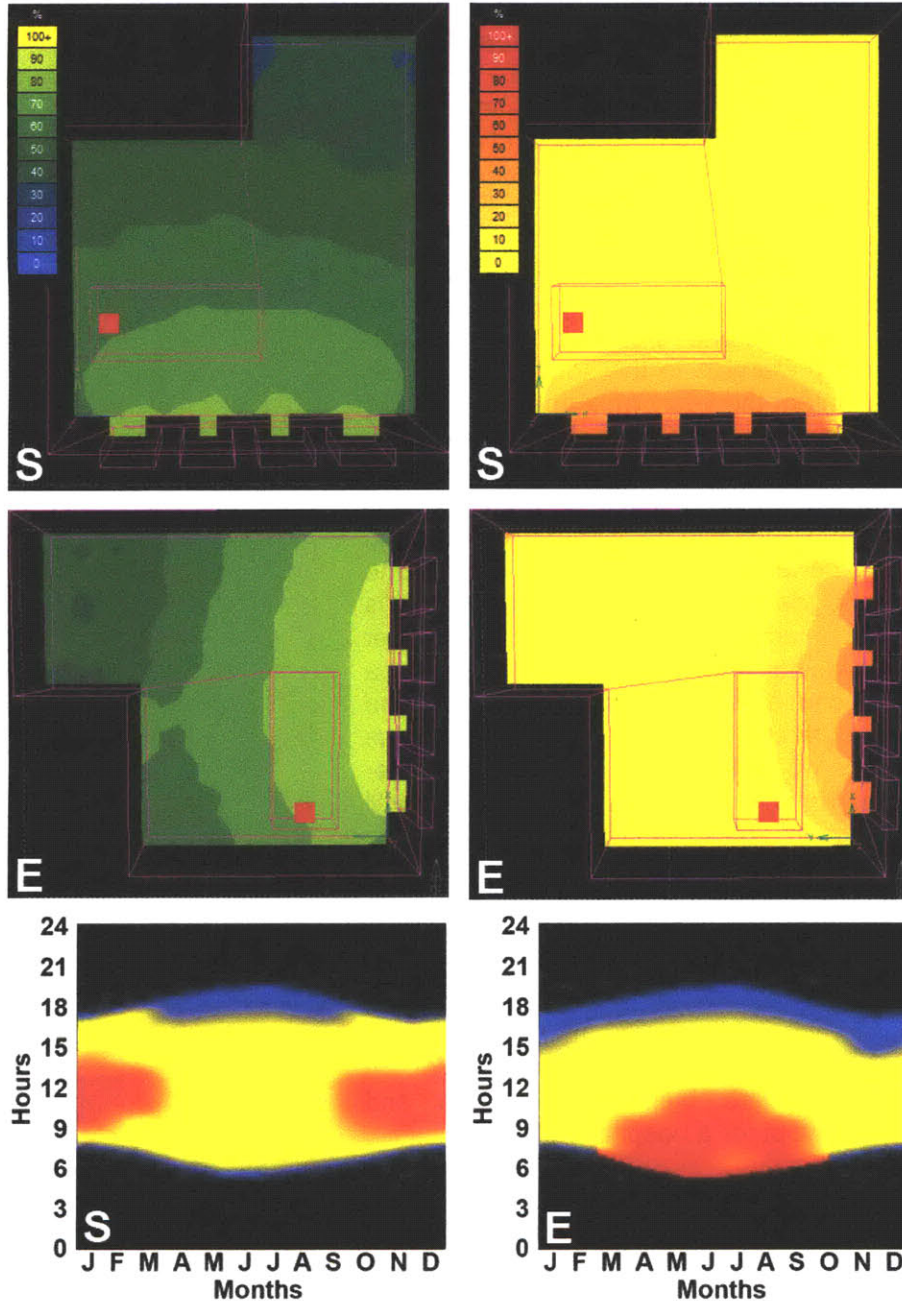


Figure 7-8. Daylight Autonomy data over 400 lux (top left) and 2000 lux (top right), and AIE temporal maps of a reclining patient (bottom) for both south and east facing hospital rooms.

is the only noticeable difference, and the only other conclusion that can be drawn is that there is (unsurprisingly) more light closer to the window. The fact that the DA is 60%-70% at the patient's head does not tell us when or why this is so, nor does it show us whether the patient will be alert all day. (The actual DA is probably a bit higher, due to a few night-time hours included in the occupancy schedule.)

Although the DA for the whole hospital room is shown in a horizontal grid for reference, the patient's face is the only area of real interest, so the horizontal and vertical sensor



planes associated with the temporal maps are approximately the size of the red square shown in Figure 7-8. Because the planes are small, they tend to be a uniform illuminance, and thus the temporal map moves from blue to yellow to red without any gradations in between. The maps show that although both orientations give the patient *enough* light for most of the day, the glare-potential times (when shades might need to be drawn) are very different. For instance, the east-facing room is preferable to the south-facing room in the colder half of the year, while the south-facing room is just the opposite. This is probably because the only eastern sun-angles which can hit that part of the bed occur on early summer mornings, and the southern sun-angles in the winter are lower and can therefore penetrate further into the room. One strategy this suggests for the hospital, therefore, is to fill the south-facing rooms first in the summer and the east-facing rooms first in the winter. On a side note, because this is a smaller sensor, and occurrence of direct sunlight is important, these temporal maps would have been more refined after a high-frequency direct sun simulation, which will be implemented in Lightsolve in the near future.

In this example, orientation makes a difference in when the room is bright enough for patients, while the DA of each room does not have a significantly different distribution. These and further temporal explorations, which might include more orientations and bed positions could help an architect decide on the most appropriate building orientation and programmatic layout for a hospital building.

### 7.2.3 Church of Light Example

Other than the renderings or photographs used to do image-based assessment, glare does not lend itself well to spatial analysis. Glare is usually analyzed at a limited number of points and view directions because of the simulation time involved, so it does not often get displayed in grid-format. The example discussed below will demonstrate the difference between existing glare graphics attached to the program *evalglare* with a temporal map display of Glare Avoidance Extent (see Chapter 5).

The model used in this example (see Figure 7-9) is a detailed replica of the main worship space in Tadao Ando's Church of Light in Osaka, Japan, which was made using

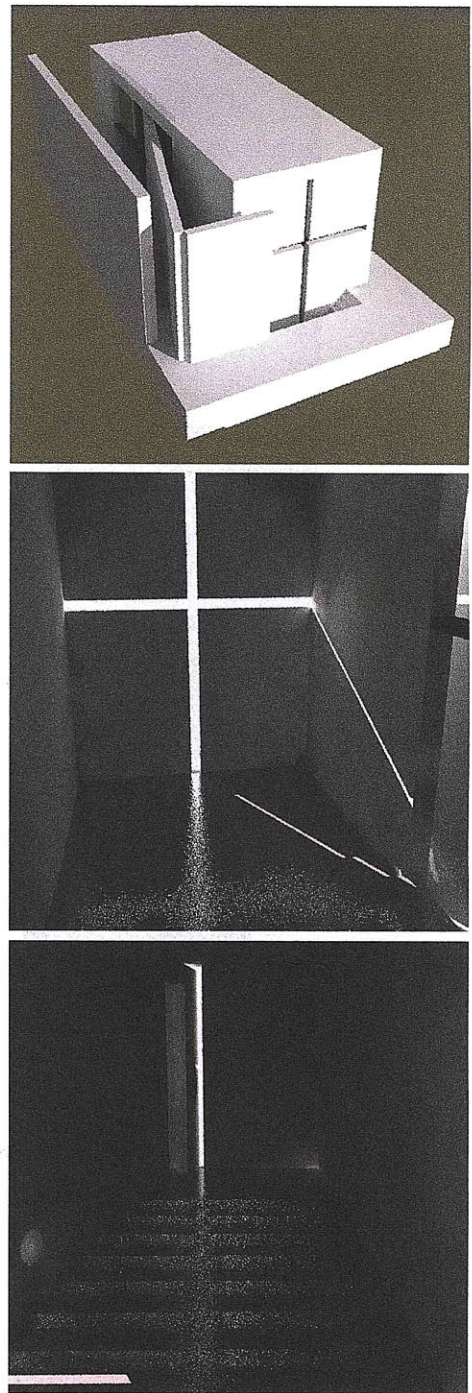


Figure 7-9. Radiance renderings of Ando's Church of Light in Osaka, Japan.



both Radiance (for *evalglare*) and SketchUp (for Lightsolve). The model is offset about 26 degrees from north, the walls and ceiling are 75% reflective, and the floor is 10% reflective. There is a large system of walls on the exterior which has also been modeled. Because the illuminances in this model tend to be very low, the numerical results in the temporal map are not necessarily valid, but they are still a good illustration of that type of analysis.

Unfortunately, there is no existing glare analysis or metric which attempts to incorporate both spatial and temporal data in a single number, so the Glare Avoidance Extent (GAE) outlined in Chapter 5 must be compared with single point - single view - single moment data. This would be like comparing AIE to illuminance rather than to DA, so the available graphics consist of rendered pictures which have been processed to determine glare. *Evalglare* outputs pictures with glare sources depicted in different colors, and the ones shown in figure 7-10 represent moments in winter, spring, and summer from top to bottom, and morning, noon, and afternoon from left to right. All nine pictures also represent a single point and view position and a single sky type (clear). In looking at these pictures and the data along side them, it is evident that one would have to analyze and synthesize many moments to get an accurate picture of the performance of the church.

As was demonstrated in Chapter 5, single-point glare data like DGP values can be placed in a temporal map in a weighted or maximum glare format according to sky type. However, each temporal map would represent only one sensor position and view direction and still might not give an impression of the performance of the space as a whole. GAE, on the other hand, summarizes an entire space (or area of interest) by displaying the percent of sensors which perceive glare. Figure 7-11 represents the GAE of an array of sensors set up at the adult head height of people sitting in pews and facing the altar. Although the very low illuminances of the situation make the numerical values shown in the graph less valid (see Chapter 5), it is still an example of the richness of temporal and spatial information which can be acquired in a single glance.

#### **7.2.4 Combining Temporal Maps with Renderings**

Because temporal and spatial graphics provide different kinds of information, it would be preferable to make both available to the designer – if it can be done without overwhelming him with information. For Lightsolve, a coupling of quantitative temporal maps and qualitative spatial renderings was thus chosen as the primary source of data graphics. Aside from the usefulness of temporal information in design decisions, Chapters 4, 5, and 6 showed that illuminance, glare, and solar gain information could all be conveyed via temporal graphics, and would therefore provide an easy vehicle for comparison and weighing tradeoffs. It is certainly feasible to provide glare in a spatial format as well, since each sensor has a physical location and view direction. However, an array of glare sensors might not be located on a single plane and thus might be more difficult to display intuitively. Furthermore, solar gain is a single quantity which represents the model as a whole and cannot be displayed spatially.

Because the numerical data gathered is displayed in the temporal maps, renderings were chosen to provide feedback on spatial light distribution and an opportunity for qualitative assessment. Numerical spatial graphics could certainly be provided as an alternative, but the qualitative information gained from renderings can be conveyed in no

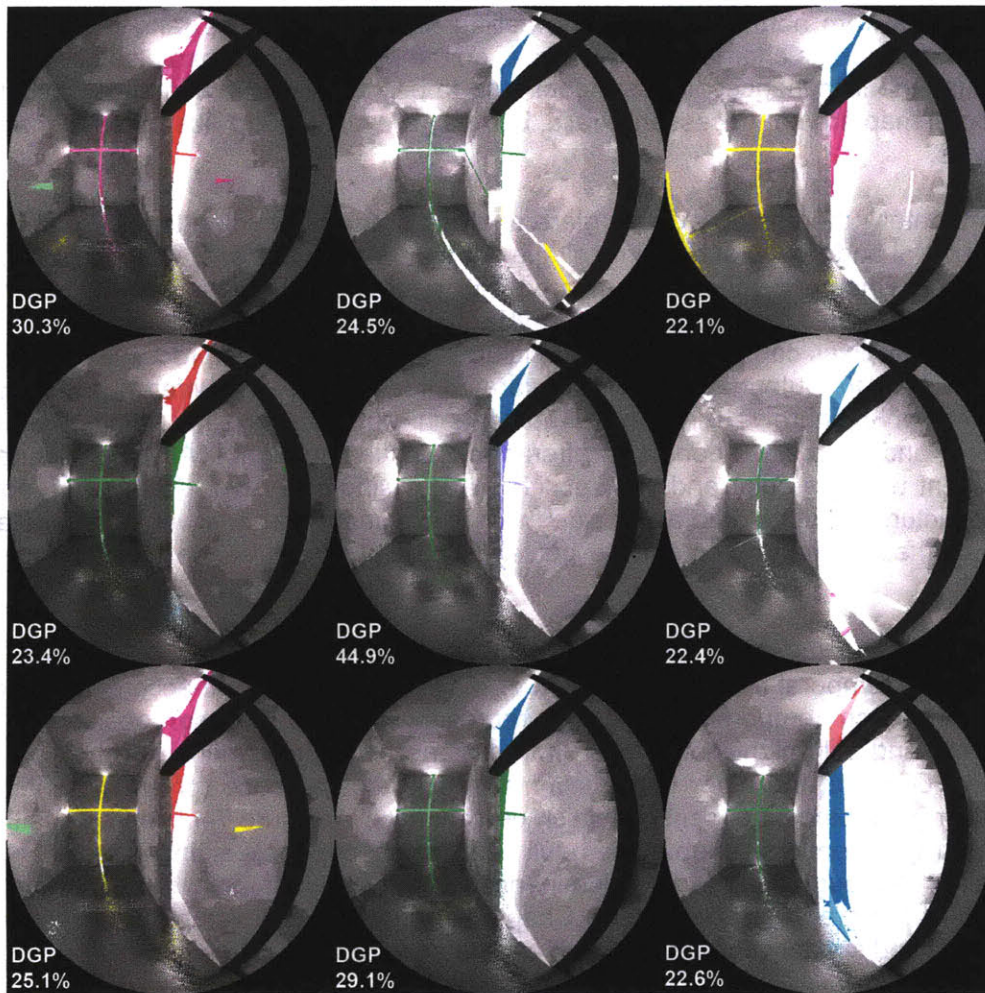


Figure 7-10. Evalglare pictures showing glare sources in the Church of Light in Osaka, Japan. Morning, noon, and afternoon are represented from right to left, and moments in winter, spring, and summer are displayed from top to bottom.

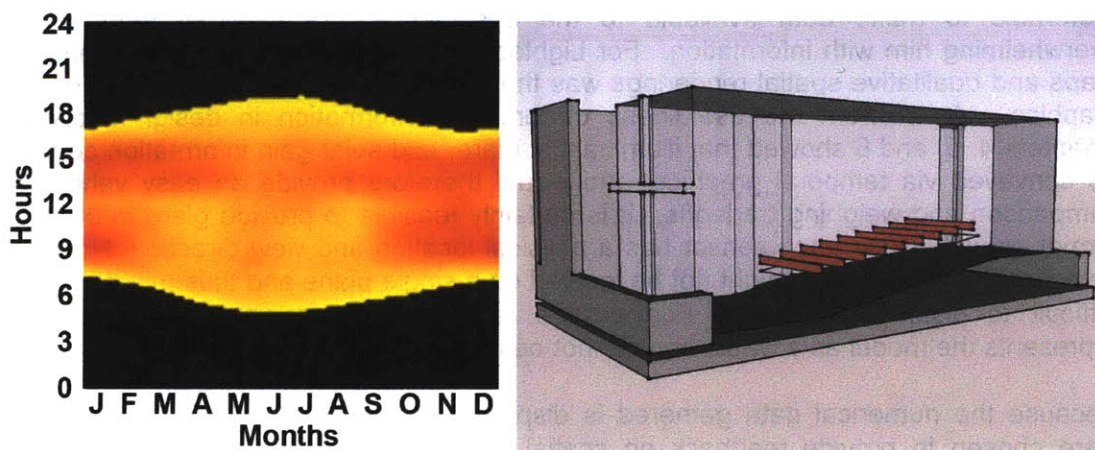
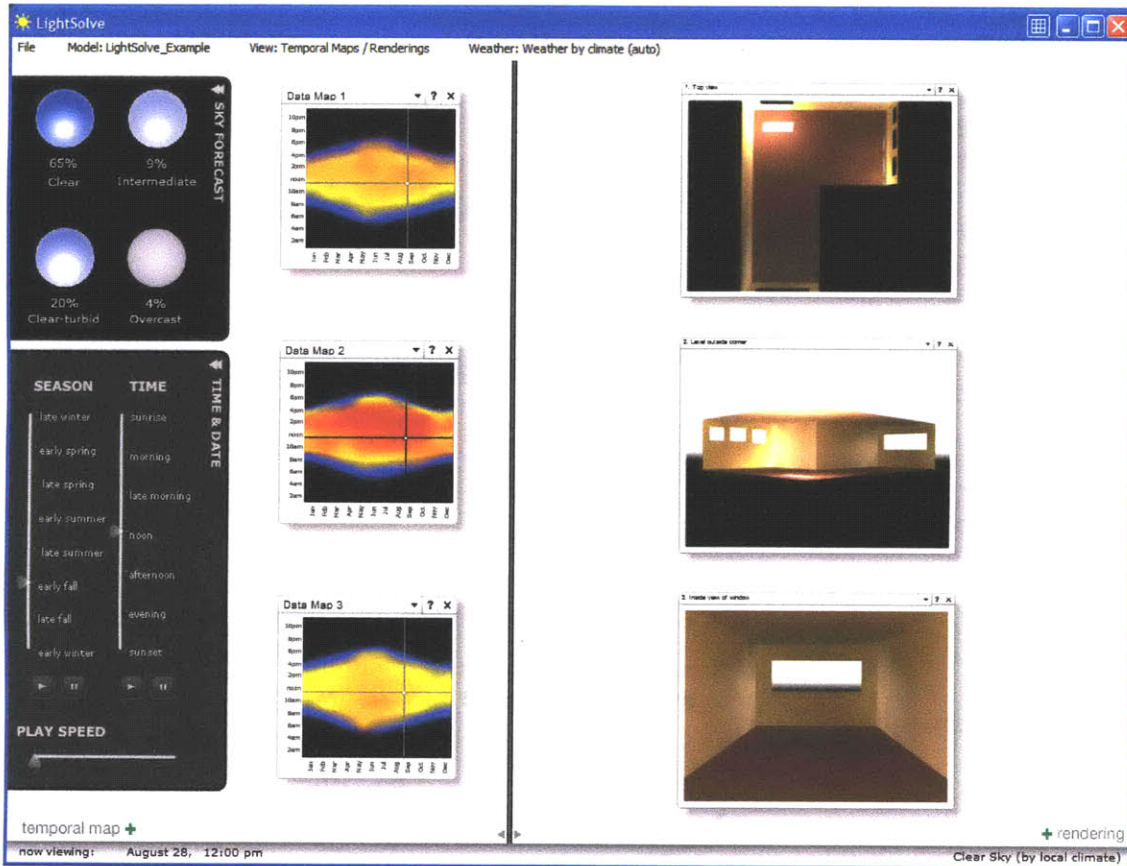


Figure 7-11. A GAE temporal map for the Church of in Osaka and a SketchUp image of the array of pew sensors on which the temporal map is based.



other way, and the designer merely needs an indication of the spatial distribution of light to complement the quantitative data in the temporal map.

Figure 7-12 shows the main features of the Lightsolve interface, in which the renderings update when the user scrolls over the temporal maps, similar to the “brushing and linking” method described by Glaser [Glaser & Ubbelohde, 2001; Glaser & Ubbelohde, 2002]. In this way, the user can connect the time-based performance of the space with a realistic depiction of sun penetration and light distribution for a single weather type, or for the dominant conditions at that particular time of day and year.



**Figure 7-12. A screenshot of the data page from the main Lightsolve interface. The crosshairs in the temporal maps determine the time and date of the renderings shown next to them. The user can choose to show a particular weather type or the dominant weather type of each time period**

### 7.3 Analyzing Options Using All New Metrics

Design involves a great many choices, and the most informed way to make choices is often by comparing options, so this section will examine the use of temporal maps to compare orientation and shading options for a single room. The model used in this example is the hospital model discussed in section 7.2.2, and it has been simulated for three orientations – South, East, and West – with two shading options – no shading and fixed horizontal louvers. Again, the illuminance goal range is 192 – 2000 lux with no



buffer intervals, although being above 192 lux is more important than avoiding illuminance greater than 2000 lux. The temporal maps illustrating the AIE and GAE at the patient's face are shown in figures 7-13 and 7-14 for a patient who is lying down, and in figures 7-15 and 7-16 for a patient who is sitting up. SHS temporal maps created using daily load totals are shown in Figure 7-17. The horizontal louvers in this example are fixed, wider-spaced permanent louvers rather than Venetian blinds.

For the reclining patient in the option without shades, the illuminance stays greater than 192 lux nearly all the time for all orientations (with the west slightly outperforming the south, which slightly outperforms the east in the evening). There are correlating glare problems for all orientations; in the summer midmorning in the east-facing room, in the winter mid-day in the south-facing room, and in a large portion of sunset times in the west-facing room.

If fixed horizontal louvers are added, there is a reduction, but not elimination, of glare for the reclining patient, and all orientations gain times when the patient is not receiving enough light. The south-facing room still maintains good illuminance levels in the winter, but both east and west drop too low in the afternoons and mornings respectively.

The patient who is sitting up receives good illuminance through more of the day, but also more instances of glare. The south-facing room is very glarey during the colder half of the year without shades, and the horizontal louvers mitigate the problem, but do not fix it in winter mornings. The horizontal louvers improve the glare situation in the east- and west-facing rooms slightly, but not much, which is not surprising considering horizontal

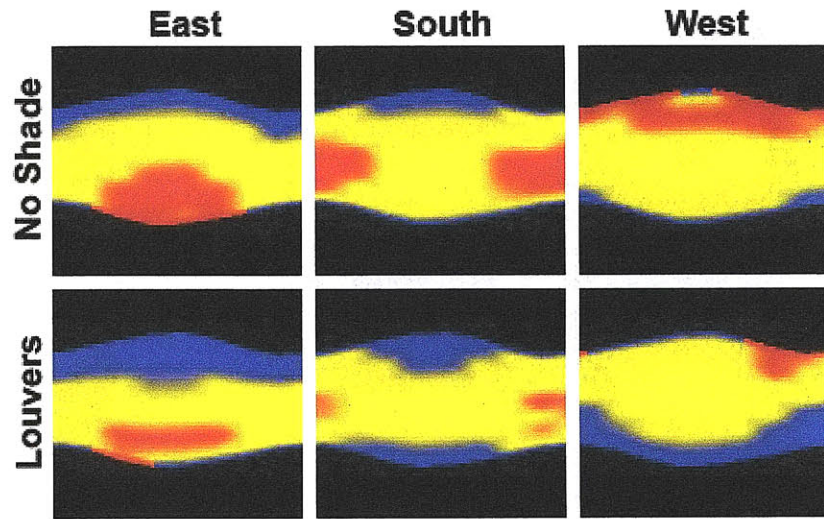


Figure 7-13. A comparison of different orientation and shading options. All temporal maps represent AIE for the reclining patient.

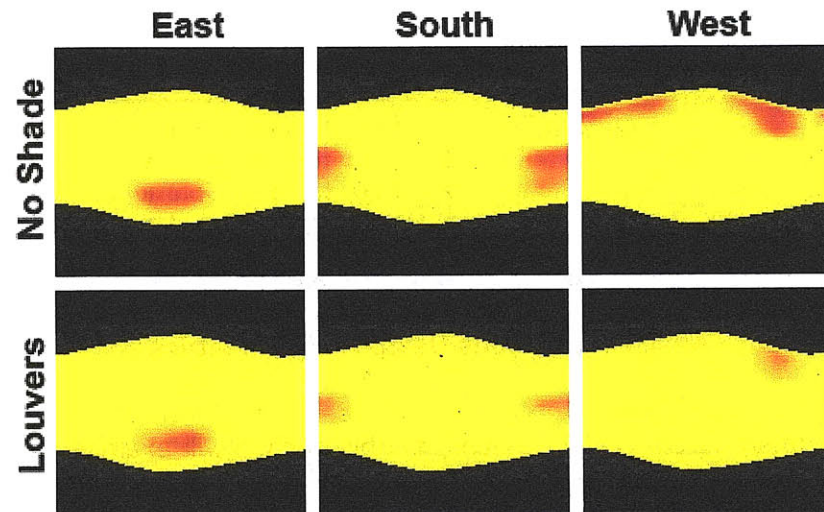


Figure 7-14. A comparison of different orientation and shading options. All temporal maps represent GAE for the reclining patient.

louvers are not optimal on east and west façades. Although it has the benefits of bright mornings with which to wake the patient up, the east facing room loses the most illuminance overall. On reviewing the weather type frequencies at different times of day, this seems to happen because a greater occurrence of intermediate and overcast skies in the afternoon.

Taking the SHS maps into account (Figure 7-17) is another point in favor of including horizontal louvers. Although the balance point is not really accurate enough to identify hourly problems in solar energy influx, the SHS maps bear out the previous seasonal conclusions – the unshaded south facing room incurs more solar gain when the sun is more normal to the windows in the winter, and phoenix is a hot enough climate so that the solar gain is still an issue in cooler months. The east and west-facing unshaded

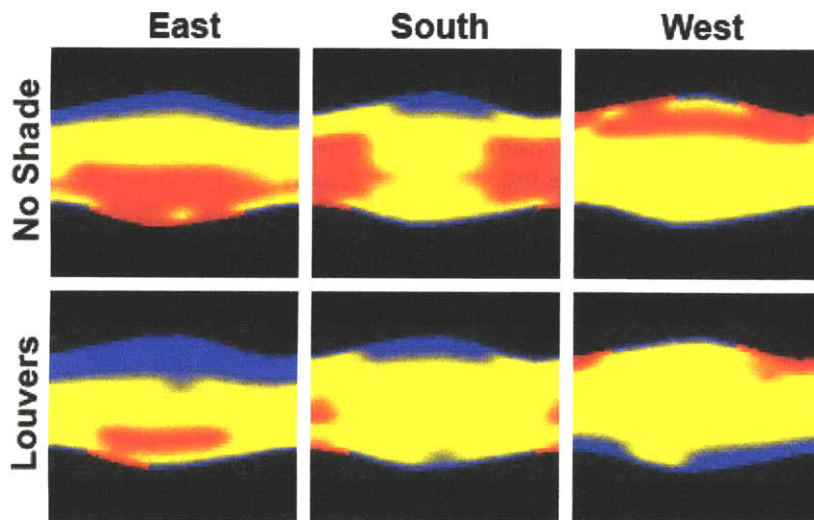


Figure 7-15. A comparison of different orientation and shading options. All temporal maps represent AIE for the seated patient.

rooms have problems with excess solar energy throughout most of the year, and this problem is slightly greater for the east-facing window than for the west. When all orientations are shaded by horizontal louvers, the excess solar gain is largely mitigated, although this is done to the detriment of desirable illuminance.

Unsurprisingly, the horizontal louvers cut out slightly more solar gain on the south-facing orientation.

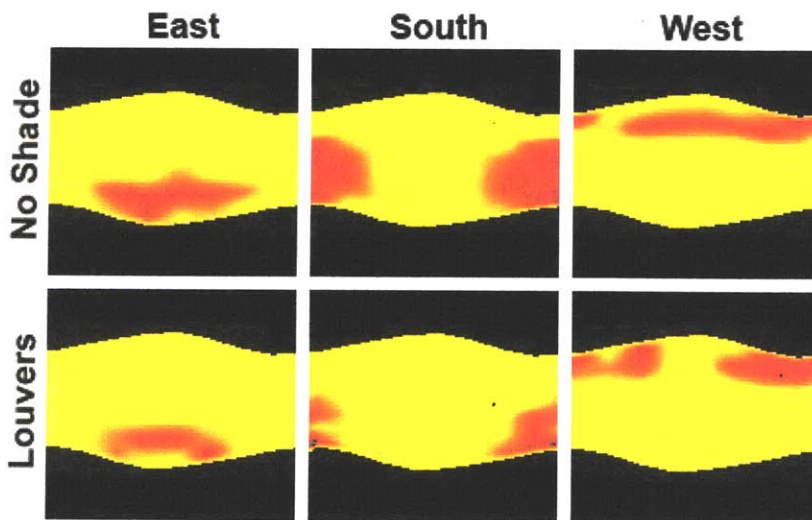


Figure 7-16. A comparison different orientation and shading options. All temporal maps represent GAE for the seated patient.

The values used in the balance point equation for the hospital room were all derived using the information in Appendix C. The U-value of the exterior walls and windows were 0.856  $[W/m^2K]$  and 3.24  $[W/m^2K]$  respectively, the SHGC of the glass was 0.60 (which is the SHGC of a good double-glazed, low-e window glass according to [ASHRAE, 2001]), and the total ventilation rate was 0.1  $[m^3/s]$ . The occupancy rate was 0.1  $[people/m^2]$



and 130W was used to represent the heat gain of a human. The general equipment heat gain assumption was 500 [W], and the occupancy was assumed to be continuous with 72 [°C] and 69 [°C] as the cooling and heating setpoint temperatures.

The temporal maps allow one to compare the simultaneous performance of both illuminance and glare for different orientation and shading options of the hospital room. Given both sets of data, the tradeoff between maintaining illuminance levels and lowering glare can be quantified as periods of time when the room is sub-optimal. The architect could use similar comparisons to choose the best shading system for the climate and orientation, and to design a higher number of patient recovery rooms on the best-performing orientations. Strategies can also be suggested involving timing and control of automatic blinds, moving the beds, or filling the best rooms first according to the time of year.

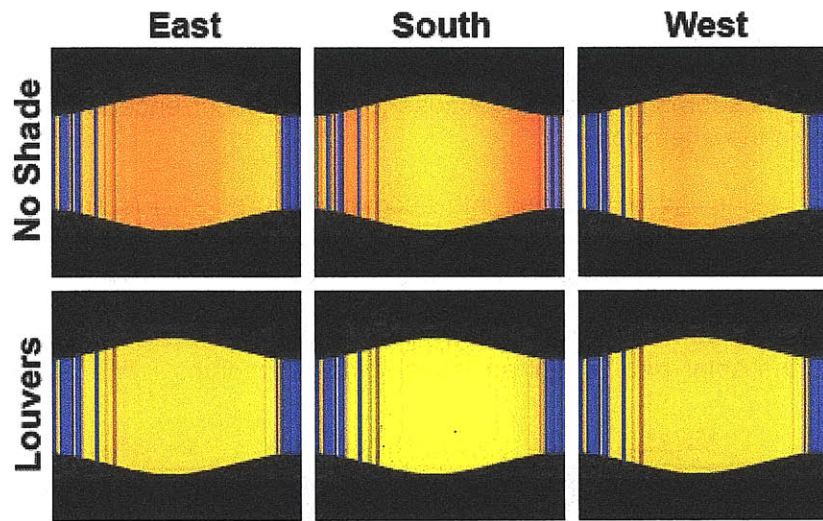


**Figure 7-17. A comparison different orientation and shading options. All temporal maps represent daily total SHS for the seated hospital room.**

#### 7.4 Daylight Analysis Surveys

Since one purpose of Lightsolve is to find more intuitive ways of presenting daylighting data to architects, it was essential to get some feedback from the intended audience. Therefore, a formal survey was given to complement informal feedback already received.

In May 2009, a survey comparing data formats was given mainly to student architects at MIT. Given a basic model, daylighting goals, and resulting data in both spatial and temporal graphs, participants were asked to assess how well the model had achieved the desired goals. The model consisted of two 34 ft by 22 ft by 8 ft classrooms on a double-loaded corridor with punch windows facing either Southeast or Northwest. A second iteration of this model included an indirect skylight which gave some bilateral lighting to both classrooms. Both classroom models were used in a previous example in this chapter and are shown in figure 7-4.

The given goal was to keep the work planes of both classrooms between 400 and 2000 lux from 8am to 4pm between September 1<sup>st</sup> and June 30<sup>th</sup> in Boston. Spatial data was given as an array of falsecolor illuminance graphs for CIE clear skies at 9am, 12pm, and 3pm on December 21<sup>st</sup>, March 21<sup>st</sup>, and June 21<sup>st</sup>, for one 10,000 lux CIE overcast sky, and for Daylight Autonomy (with occupancy hours set as 8am-4pm and the illuminance threshold at 400 lux). Temporal data was given in the form of one temporal map for



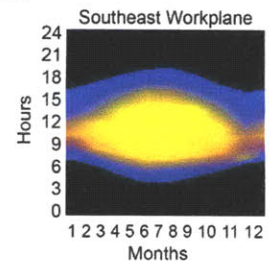
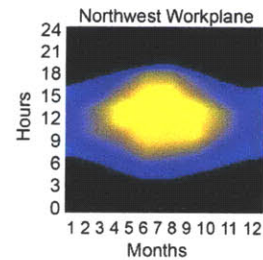
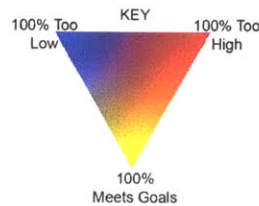
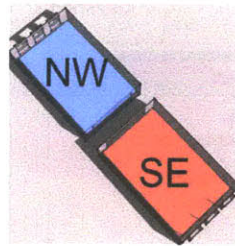
each classroom's work plane, showing the percent of the work plane which achieved the given goals (see figure 4-17). Before the survey, a very brief introduction to work plane illuminance, daylight autonomy, and temporal maps was given by the survey administrator. Photorealistic renderings were not given for either data format. Participants were not told which model they were assessing, and neither were they informed that there were only two iterations of the basic model. Finally, the survey was strictly timed – participants were given 3 minutes to answer questions about the first scenario and 2 minutes 15 seconds to answer the same questions for each following scenario. The restrictive time limits, enforced by the survey administrator, forced participants to rely on intuition and put a special emphasis on the speed of the analysis.

#### 7.4.1 Survey Results

Through queries about software experience, and familiarity with a number of daylighting terms, the 58 participants of the data analysis survey (mostly student or practicing architects) were shown to have little daylighting experience in general. However, one third was familiar with the term “temporal maps” and 22% said they could explain it. This is unusual, but unsurprising given that some students were familiar with the author, and that a few lighting specialists were also surveyed.

The main body of the survey asked 6 questions about each of four scenarios (see Figure 7-18 for two of them). Paraphrasing, these questions were 1) did the scenario meet the goals during occupied hours, 2) if not, what was the biggest problem, 3) when do problems occur, 4) where in the room do problems occur, 5) how confident are you in your analysis, and 6) what other information do you want? The tallied responses to all scenario and follow-up questions are given as bar charts in figure 7-19.

### SCENARIO B



### SCENARIO C

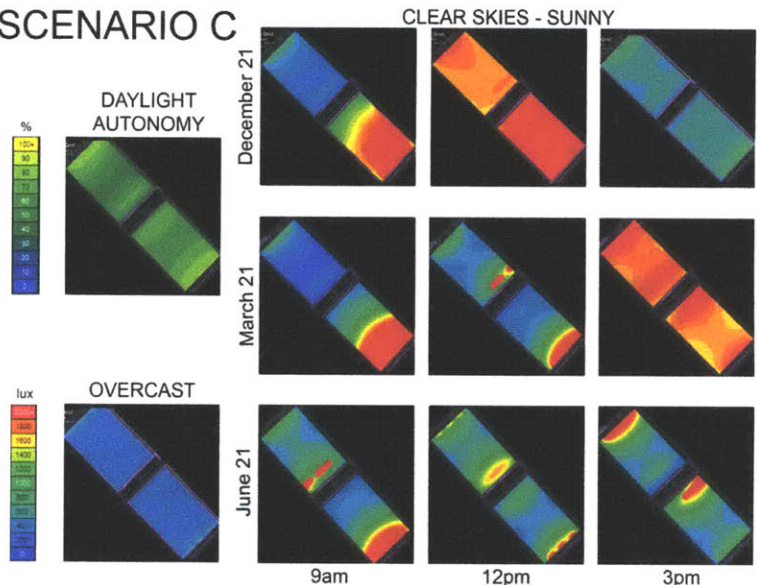


**Figure 7-18: This is an example of the data given to survey participants to compare available temporal and spatial data. Both scenarios represent the better of the two models (the original model very obviously did not let in enough daylight).**

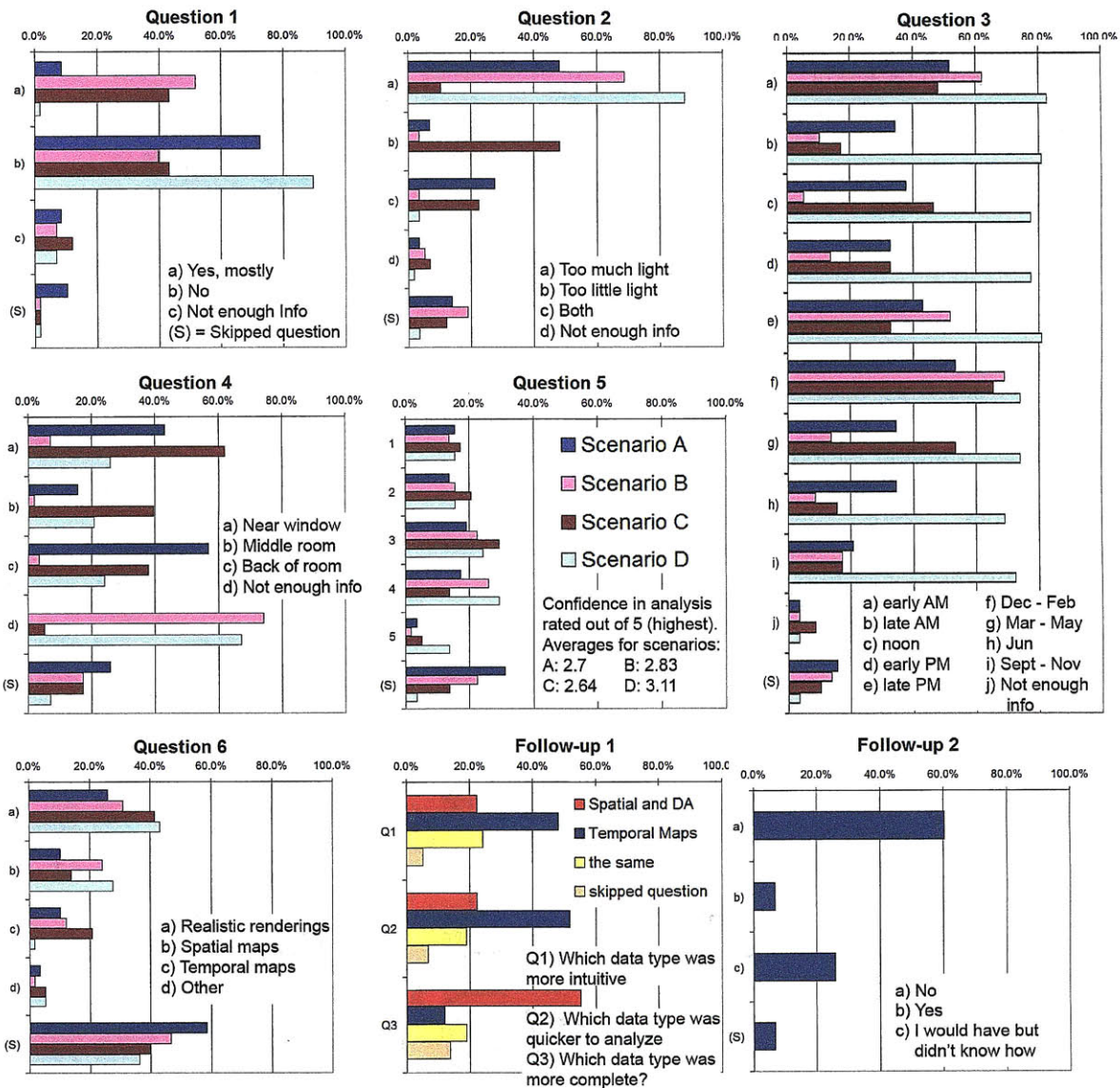


**Figure 7-19: The results from the bulk of the data formats survey. Scenario A is the original model spatial data, B is the improved model temporal data, C is the improved model spatial data, and D is the original model temporal data. The original model data is depicted in blues and the improved model in pinks. Spatial scenarios are represented by dark bars and temporal scenarios by light colored bars.**

## 7.4.2 Survey Discussion

The consistency in responses to the temporal data (scenarios B and D) – especially questions 2 and 3 regarding what the problem was and when it happened – and the first follow-up question show that temporal maps are both readable to the untrained eye and quick, intuitive methods for displaying comprehensive daylighting data. Also, several participants commented on the “at-a-glance” nature of temporal data and the intuitive



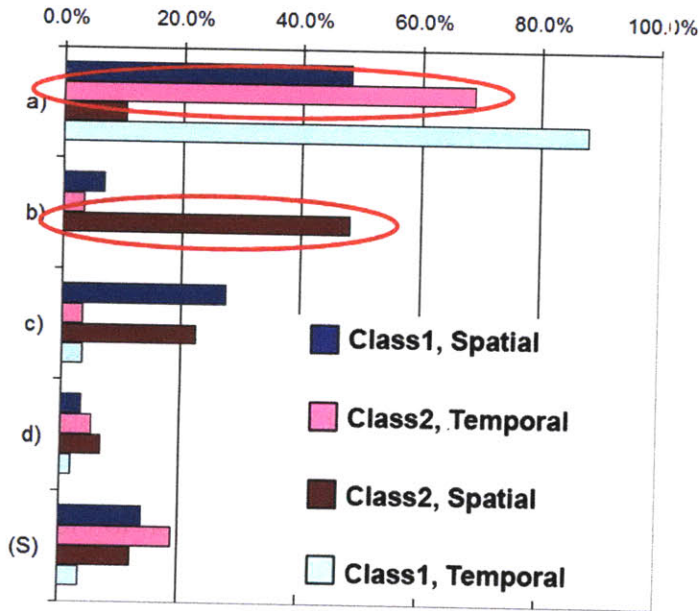


**Figure 7-20.** The results to question 2 show that the same people drew very different conclusions regarding the main fault of the same space depending on which data they were viewing. The letters on the bar graph represent the answers a) Too much light, b) Too little light, c) Both, and d) Not enough info.

nature of the “goal-range” color scheme, although another comment unfavorably mistook the temporal maps as a collection of average illuminances. Both surveys, interestingly, revealed the architects’ attachment to spatial graphics. Renderings and spatial graphics were the most requested pieces of “extra information” in question 6, and a surprising number of people revealed – through comments and confidence levels – an abiding faith in traditional single-moment illuminance graphs. The spatial data was also considered more complete, as the single-moment illuminance graphs gave an illusion of temporal information. This can also be seen in the fact that very few participants considered the spatial data “not enough information” to judge *when* problems occurred in question 3 (although the participants could not agree which judgement was correct), but the vast majority recognized there was not enough information in

temporal maps to answer the spatial-dependant question 4. Finally, for the improved model, participants decided that the biggest problem was “too much light” when given spatial data, and either no problem or “not enough light” when given temporal data (see Figure 7-20). In essence, when reading different data formats for the same model, participants made opposite judgements about what that data was telling them. This is most likely because too much attention was paid to the clear-skies illuminance data over the climate-specific daylight autonomy, while the temporal maps also took Boston weather (which is often overcast) into account. When asked at the end of the survey, the majority of participants admitted that they did not take weather into account when considering single-moment spatial data.

It should be noted that there were a couple complaints about the ambiguity of the time designations in question 3 and that the spatial data page was found to be a little ‘crowded’ and ‘confusing’. Of course, the analysis of many different illuminance-based graphs could also be seen as mind-clutteringly confusing. It is finally the author’s suspicion that most participants ignored the daylight autonomy data in favor of the 3x3 clear sky illuminance graphs, despite the fact that the daylight autonomy graphs should have been the focus. In retrospect, a better survey would be one which compared AIE temporal maps with only Daylight Autonomy data and not single-moment illuminance data. It was not the authors’ intention to show that either data format was superior; rather, it was to show the weaknesses of either without the other and to prove that temporal maps are intuitive enough for designers to use.



## **7.5 Design Analysis Summary**

In this chapter, examples were shown highlighting the benefits of displaying data in a temporal format. The simple mock design process demonstrated the ability of goal-based temporal maps to convey the degree of design-goal success and the degree and type of failure to meet goals. The classroom and hospital room comparisons between goal-based temporal maps and DA spatial graphs emphasized the different types of information which could be gathered from each. In the temporal maps, the effects of building orientation and general light access were more pronounced than in the spatial graphs, as was information pertaining to the instantaneous performance of the whole space (in other words, whether there are simultaneous highs and lows or if the whole space is in range at once). The hospital room was also employed in a demonstration using temporal maps to compare orientation and window shading options; both AIE and GAE metrics were involved in the comparison, giving more than one dimension to the results.

Finally, a small-scale survey about reading daylighting data was given to architectural students at MIT. The goal of the survey was to prove the usability and usefulness of temporal daylighting graphs and to show that they improve an architect's understanding of daylighting performance. While the former claim is well supported by the results above, this section has relied on examples rather than surveys to show the latter.

This chapter included a discussion on the merits of coupling qualitative spatial renderings with quantitative temporal maps, given that this is the chosen information pairing in the Lightsolve interface. Since there is a slight redundancy between renderings and spatial graphs, temporal maps could give daylighting data new depth. However, the choice should not be spatial versus temporal data – both should be used to create the greatest understanding of daylight performance.

# Chapter 8

## Conclusion

Daylighting analysis is under-used in the earliest stages of design, but unfortunately, that is precisely the time at which it could do the most good. There may be several reasons for this, including the current design culture and educational practices, but there is also a lack of interactive yet accurate design analysis methods which give the architect all necessary information in a form that is clear and concise. This thesis has focused on the simulation, pre-processing, and presentation of light quantity, glare, and solar heat gain data for the purpose of making good design decisions in the earliest stage of daylighting design.

### 8.1 Main Achievements

The overarching objective for the research presented here was to forge a daylighting analysis process for early stage design which interactively and effectively communicates complete and accurate information to the designer. This process has incorporated existing research when it fits the agenda, however new work has also been done, especially in the design of goal-based dynamic metrics suitable for temporal graphics.

To achieve this goal, five questions were asked in the introduction:

- 1) What daylighting information is necessary for informed design decisions?
- 2) How can that information be calculated quickly, but with reasonable accuracy?
- 3) How, if at all, should that information be pre-processed for the designer?
- 4) What output formats should be used to convey the information?
- 5) What metrics are appropriate for those output formats?

First, based on the research of others it was determined that designers require dynamic, climate-inclusive information to fully understand the daylighting performance of a space. Arguments were also made in the introduction and in Chapter 3 for using a format which preserves the performance variation over time (a choice which also address question 4). The temporal map was thus chosen to be the basic vehicle for communicating daylighting information of all sorts. As a graphic, it emphasizes the time-based variation of daylighting performance, which automatically ties this performance to many of the greatest influences on daylighting collection, transmission, and distribution – in particular, to climate considerations and weather type and to solar angles.

Because interactivity is important, and because it reduces the “clutter” of highly detailed annual information, a method was developed to reduce the necessary simulations while still keeping the authenticity of realistic sky conditions. The ASRC-CIE sky model was used to calculate illuminances under four different sky conditions for each of 56 periods of the year. The sum of these illuminances, weighted by the occurrence of each sky type during the period in question, becomes the single illuminance which represents the whole period. These illuminances were used to populate temporal maps, which in Chapter 3 were then compared to temporal maps made using detailed illuminance data

extracted from the program Daysim. The numerical and pixel comparison results were generally good and the data reduction method aided the emphasis of general illuminance trends and patterns. Furthermore, the overlay of high-frequency direct solar data compensated for the inability of a more complex model to capture the highly dynamic nature of direct solar irradiance. This method addresses the questions concerning quick, accurate calculation, as does the subsequent development of the DGPm approximation (Chapter 5). The question of pre-processing is handled as part of the development of appropriate metrics. Three metrics for communicating three main aspects of daylight design, light quantity, glare, and solar heat gain, were introduced and validated against existing data and processes.

In order to more easily understand the performance of an entire area of interest – be it a work plane in a single or multiple zones, a museum wall, a chalkboard, or other self-contained area to which the same design goals apply – a method was devised for reducing each area to a single temporal map. This metric, called the Acceptable Illuminance Extent (AIE), gives the percent of the area of interest which is within a user-defined illuminance goal range. Thanks to a triangular temporal map color scale which uses and mixes the three primary colors, the areas of low AIE can be visually divided into those areas which are too high and those which are too low. Thus, problem times can not only be identified but understood as a certain type of issue. Chapter 4 provides a comparison between AIE temporal maps created using the above data reduction method and those created using very high frequency Daysim data. The visual correlation between these temporal maps is stronger in general even than the single point illuminance comparisons in Chapter 3. The only circumstance under which the visual correlation is less strong is when the desired illuminance range is very tight and the model complex.

Chapter 5 examined Daylight Glare Probability (DGP) as a promising glare metric and looked at the available simplified DGP method (DGPs) for the purpose of annual calculations. The results show that, while DGPs is a great approximation method for high luminance glare, it does not adequately represent contrast-based glare. An alternate model-based DGP approximation method (DGPm) was proposed which uses simulated illuminances, sky distribution equations, and geometric model information to find the DGP. Both DGPs and DGPm performed very well in the Classroom model, which has large vertical windows and glare caused mostly by the quantity of light hitting the eye. In the Skylights model, DGPs overestimated the glare a little, probably due to the bright space combined with the position of the glare sources. In the Frame model and the Simple Corbusier model, the DGPs approximation underestimated the DGP to nearly the greatest extent allowed by the DGPs equation. This is likely due to the lower-illuminance situations in which glare was largely due to luminance contrast. Conversely, the DGPm method performed within 10% of the DGP nearly all the time, and within 5% of the DGP most of the time. The only model in which this is not true is the Frame model, where some of the error extended past -10%.

Again, in order to present all available information in as few temporal maps as possible, the glare information at separate sensors was compiled into a single metric, called Glare Avoidance Extent (GAE), which indicates the percent of a group of glare sensors (usually a vertical array) that does *not* perceive glare – in other words, the portion of the space at which glare is avoided. In visual comparisons between GAE temporal maps showing the true DGP, DGPs, and DGPm, the two approximations performed similarly well for the Classroom model, and DGPm outperformed DGPs for the Frame model.



Chapter 6 discussed the application of the Balance Point load calculation method to a solar heat gain metric called Solar Heat Surplus or Solar Heat Scarcity (SHS). The intention of SHS is to give a ballpark indication whether the current solar gain is acceptable, or whether it should be decreased or increased. Because SHS or any solar heat gain metric must involve some kind of energy analysis, and because the balance point was chosen for its simplicity, not its rigor, the resulting comparison between Energy Plus and the balance point calculated SHS is not expected to be as close as the validations required for AIE and GAE. However, when examined in terms of the ratio of the difference between methods and the maximum seasonal energy load, the daily total energy use calculated by the balance point method was reasonably correlated to the actual simulated energy use. In some cases, the balance point method with a blocked occupancy schedule, thought to be closer to the information the designer could supply during schematic design, performed better than the detailed balance point method. The SHS calculated using the balance point method was less accurate when the building had either a lot of thermal mass, or a complex occupancy, equipment, or zoning schedule.

The most important goal is not the understanding of each metric separately, but to be able to understand at a glance how they complement and contradict each other – and to be able to use that knowledge in the design process. This ability is especially useful when choices and tradeoffs must be made between fulfilling conflicting objectives. For this purpose, the metrics based on the temporal map format are ideally suited. Some examples emphasizing the type of data one can gather from sets of complementary temporal graphics were presented in Chapter 7, along with the results of a small-scale survey. The survey was given largely to architecture students at MIT and was an attempt to gauge their intuitive understanding of temporal graphics. The results of that survey indicated that temporal maps were indeed intuitive enough for architects, many of whom had never seen them before. The survey also found that architects are uncomfortable without a connection between temporal graphics and some kind of spatial anchor like renderings or spatial data. This further strengthens the claim that both temporal and spatial information should be used in design analysis. The survey also concluded that designers will not generally take the variation of climate and sky type into account unless this is done already for them by the preprocessing of data.

## **8.2 Applications**

While some of the components of these data processing and display methodologies have been in existence for years, it is their unique combination that holds great promise in the capacity of helping architects to make design decisions. The ability to see – in one glance – the variation in annual performance of a building design via temporal maps adds an extra and important dimension to the design process. With this information, one could modify a design according to seasonal or daily trends without drowning in data noise, and without having to rely on single renderings representing only a few somewhat arbitrary moments during the year. This pre-processing of annual data and its linking to both temporal maps and spatial renderings, an approach designed for a program named Lightsolve, is what the author sees as the next development phase of a research effort meant to help architects make the correct daylighting design decisions early in the process.

Lightsolve, is a work in progress which has already involved a diverse group of researchers and projects [Andersen *et al.*, 2008; Cutler *et al.*, 2007; Yi, 2008; Seaton, 2009]. Aside from the current rendering engine and interface, there are also plans to include an interactive design optimization consultant [Lee *et al.*, 2009], and the ultimate goal is for Lightsolve to become an early-stage design analysis tool which exemplifies the interactivity, accuracy, communication, and intuition discussed in Section 8.1.

Beyond Lightsolve, the author hopes that this research has an impact on the way daylighting data is analyzed and communicated. Temporal maps are a valuable design tool and are underused in the daylighting analysis process, however, with the development of goal based illuminance, glare, and solar gain metrics suitable for them, perhaps they will not be underused for long. In the end, a successful analysis depends on how effectively data is communicated to the designer or whomever makes decisions.

### 8.3 Future Work

Although the theory of every part of this thesis has been tested and verified, there are certain aspects which have not yet been implemented in Lightsolve. The high-frequency direct sun overlay for all metrics is one which will be incorporated in the near future. Similarly, the author would like to include HDR rendering capability and the option for displaying numerical spatial graphics as well as renderings.

For the GAE metric, Chapter 5 was generally rectangular in nature. To use this method for any situation in which the view of the sky or the window may be masked from the sensor point, such as in “L” or “E” shaped buildings, the rendering engine would need to indicate that the line of sight to the sky is blocked. While this is not yet implemented in the Lightsolve program, it will be in the near future. The real test of the model-based approximation method would be very low illuminance situations with high luminance contrasts. These scenarios are common in religious architecture and in rooms with lower-reflectance walls (such as dark wood panelling) and can’t be ignored. Unfortunately, they cannot be rigorously tested until the DGP equation is modified to include lower illuminance situations. Also, the SHS metric is not yet implemented in Lightsolve.

The simulations in this thesis have not involved models representing occupant behavior in the form of predicted blind use, citing the argument that it is important to explore the full daylighting potential of the design in question [Mardaljevic *et al.*, 2009]. While this may be a reasonable position, it does not preclude the future incorporation of a predictive blinds model into this method or the Lightsolve program. Research on integrating blinds control into daylight simulation programs has been done [Reinhart, 2004; Bourgeois *et al.*, 2006] and could be included in this case. Similarly, algorithms to predict and account for the use of operable windows and natural ventilation could be incorporated into the balance point calculation. In this vein, Lightsolve could eventually become part of a suite of tools which might include a dedicated, early stage energy simulation tool. One such tool is the MIT Design Advisor mentioned in Chapter 2 [Lehar & Glucksman, 2007].

Beyond the quantitative aspects of daylighting, there are aesthetic and psychological goals that need to be met by the designer. These things, by their nature, defy quantification, and it was partially for this reason that so much thought was given to

associating realistic renderings with quantitative metrics. However, there are more peripheral things related to aesthetics which could be quantified, such as the amount of outdoor views long lines of sight available in the space. Long lines of sight allow the eyes to relax, and outdoor views give occupants a psychological connection to the outdoors and the passing of the day. Quantities such as the gradient of light levels could also be measured and related in some way to an aesthetic goal.

Climate-based, time-variable data are very valuable to the design process because they are able to reveal the nature of the environmental conditions in which a design performs well or poorly, to make visual comfort predictions, and because they encourage the designer to address the most important issues in daylighting with an annual perspective, such as building orientation, position and size of openings, and shading strategies. It is critical for an architect to have such data in hand early in the design process, before the overarching design strategies have been solidified. Ultimately, it is also critical for an architect to connect such numerical data to visualizations of a space so as to reconcile performance criteria with aesthetic considerations. These concerns are the motivation behind the Lightsolve project and this thesis, and the author hopes that the research presented here will go some way towards addressing them.



# References

- [Adeline web] Adeline website: <http://www.ibp.fraunhofer.de/wt/adeline/>, last accessed October 2009.
- [Altmann & Apian-Bennewitz, 2001] Altmann K, Apian-Bennewitz P. "Report on an Investigation of the Application and Limits of Currently Available Programme types for Photorealistic Rendering of Light and Lighting in Architecture." 2001. Online source: [http://www.pab-opto.de/radiance/render\\_vergleich/](http://www.pab-opto.de/radiance/render_vergleich/), last accessed November 2009.
- [AGI32 web] AGI32 website: <http://www.agi32.com/>, Data sheet: [http://www.agi32.com/Products/AGI32/AGi32\\_brief\\_datash eet.pdf](http://www.agi32.com/Products/AGI32/AGi32_brief_datash eet.pdf), last accessed October 2009.
- [Andersen *et al.*, 2008] Andersen M, Kleindienst S, Yi L, Lee J, Bodart M, Cutler B. "An intuitive daylighting performance analysis and optimization approach." *Building Research and Information*, Vol 36 (6), pp 593-607, 2008.
- [ASHRAE, 2001] *ASHRAE Handbook, Fundamentals*, ASHRAE, Atlanta, GA, 2001.
- [ASHRAE, 2007] *ANSI/ASHRAE Standard 62.1.2007, Ventilation for Acceptable Indoor Air Quality*, ASHRAE, Atlanta, GA, 2007.
- [Autodesk, 2009] Autodesk. "Daylight Simulation in 3ds Max Design 2009 – Getting Started." Online source: [http://resources.autodesk.com/Architecture/3ds\\_Max\\_Design/White\\_Papers](http://resources.autodesk.com/Architecture/3ds_Max_Design/White_Papers), last accessed October 2009.
- [BBC web] BBC World Weather city guides. Online source: [http://www.bbc.co.uk/weather/world/city\\_guides/](http://www.bbc.co.uk/weather/world/city_guides/), last accessed November 2009.
- [Bodart & De Herde, 2002] Bodart M, De Herde A. "Global energy savings in offices buildings by the use of daylighting." *Energy and Buildings*, Vol 34, pp 421-429, 2002.
- [Bourgeois & Reinhart, 2006] Bourgeois D, Reinhart CF. "An intermodel comparison of DDS and Daysim daylight coefficient models." Proceedings of the 4<sup>th</sup> European Conference on Energy Performance & Indoor Climate in Buildings, Lyons, November 20-22, pp 1-6, 2006.
- [Bourgeois *et al.*, 2008] Bourgeois D, Reinhart CF, Ward G. "A standard daylight coefficient model for dynamic daylighting simulations." *Building Research and Information*, Vol 36 (1), pp 68-82, 2008.

- [Boyce, 2004] Boyce P. "Reviews of Technical Reports on Daylight and Productivity." Daylight Dividends Program. 2004. Online source: [http://www.lrc.rpi.edu/programs/daylighting/pdf/BoyceHMG\\_Review.pdf](http://www.lrc.rpi.edu/programs/daylighting/pdf/BoyceHMG_Review.pdf), last accessed: October 2009.
- [Briggs *et al.*, 2002] Briggs R, Lucas R, Taylor ZT. "Climate Classification for Building Energy Codes and Standards." Technical paper final review draft, Pacific Northwest National Laboratory, March 26, 2002. Online Source: [http://www.energycodes.gov/implement/pdfs/climate\\_paper\\_review\\_draft\\_rev.pdf](http://www.energycodes.gov/implement/pdfs/climate_paper_review_draft_rev.pdf), last accessed, October 2009.
- [Building Authority, 1995] *Code of Practice for Over-all Thermal Transfer Value in Buildings*, Building Authority, Hong Kong, 1995.
- [Bund & Do, 2005] Bund S, & Do EYL. "Spot! Fetch Light Interactive navigable 3D visualization of direct sunlight." *Automation in Construction*, Vol 14 (2), pp 181-188, 2005.
- [Cannon-Brookes, 1997] Cannon-Brookes SWA. "Simple scale models for daylighting design: Analysis of sources of error in illuminance prediction." *Lighting Research and Technology*, Vol 29 (3), pp 135-142, 1997.
- [Carroll & Hitchcock, 2005] Carroll WL, Hitchcock RJ. "DElight2 daylighting analysis in energy plus: integration and preliminary user results." Proceedings of the 9<sup>th</sup> International IBPSA Conference, Montréal, August 15-18, pp 139-144, 2005.
- [Cajochen *et al.*, 2000] Cajochen C, Zeitzer JM, Czeisler CA, Dijk DJ. "Dose-response relationship for light intensity and ocular and electroencephalographic correlates of human alertness." *Behavioral Brain Research*, Vol 115, pp 75-83, 2000.
- [CIE, 1926] Commission internationale de l'Eclairage. *Commission internationale de l'Eclairage proceedings, 1924*. Cambridge University Press, Cambridge, 1926.
- [CIE, 1973] Commission internationale de l'Eclairage. *Standardization of luminous distribution on clear skies*. CIE Publication 22, Paris, 1973.
- [Collins, 1984] Collins, JB., "The development of daylighting – a British view." *Lighting Research and Technology*, Vol 16 (4), pp 155-170, 1984.
- [Cutler *et al.*, 2007] Cutler B, Sheng Y, Martin S, Glaser D, Andersen M. "Interactive Selection of Optimal Fenestration Materials for Schematic Architectural Daylighting Design." *Automation in Construction*, Vol 17 (7), pp 809-823, 2008.

- [Chynoweth, 2004] Chynoweth P. "Progressing the rights to light debate – Part 1: a review of current practice." *Structural Survey*, Vol 22 (3), pp 131-137, 2004.
- [Darula & Kittler, 2002] Darula S, Kittler R. "CIE general sky standard defining luminance distributions." Proceedings of eSim 2002 Conference, Montréal, Canada, 2002.
- [DOE, 2008] "Net Zero Energy Commercial Buildings Initiative." United States Department of Energy website: [http://www1.eere.energy.gov/buildings/commercial\\_initiative/benchmark\\_models.html](http://www1.eere.energy.gov/buildings/commercial_initiative/benchmark_models.html), last accessed, October 2009.
- [DOE-EIA, 2008] "Table E5. Electricity Consumption (kWh) by End Use for Non-Mall Buildings." United States Department of Energy, Energy Information Administration website: [http://www.eia.doe.gov/emeu/cbecs/cbecs2003/detailed\\_tables\\_2003/detailed\\_tables\\_2003.html](http://www.eia.doe.gov/emeu/cbecs/cbecs2003/detailed_tables_2003/detailed_tables_2003.html), last accessed, November 2009.
- [Eble-Hankins & Waters, 2004] Eble-Hankins ML, Waters CE. "VCP and UGR Glare Evaluation Systems: A Look Back and A Way Forward." *LEUKOS*, Vol 1 (2), pp 7-38, 2004.
- [Ecotect web] Ecotect website: <http://ecotect.com/products/ecotect/features/>, last accessed: October 2009.
- [Erhorn *et al.*, 1997] Erhorn H, Stoffel J, Szerman M. "Adeline 2.0 – Using Computer Tools to Evaluate Daylighting and Electric Lighting Applications in Buildings." Proceedings of the Right-Light 4 Conference Copenhagen, Denmark, 1997.
- [Erhorn *et al.*, 1998] Erhorn H, de Boer J, Dirksmöller M. "Adeline – An integrated approach to lighting simulation." Proceedings of Daylighting '98, Ottawa, Canada, pp 21-28, 1998.
- [FormZ web] FormZ website: <http://www.formz.com/>, last accessed October 2009.
- [Galasiu & Reinhart, 2008] Galasiu AD, Reinhart CF. "Current daylighting desing practice: a survey." *Building Research & Information*, Vol 36 (2), pp 159-174, 2008.
- [Glaser & Hearst, 1999] Glaser DC, Hearst MA. "Space Series: simultaneous display of spatial and temporal data." Proceedings of IEEE Symposium on Information Visualization 1999, San Francisco, October 24-26, 1999.
- [Glaser & Ubbelohde, 2001] Glaser DC, Ubbelohde MS. "Visualization for time dependent building simulation." Proceedings of the 7<sup>th</sup> International IBPSA Conference, Rio de Janeiro, August 13-15, 2001.



- [Glaser & Ubbelohde, 2002] Glaser DC, Ubbelohde MS. "Techniques for managing planar daylight data." *Building and Environment*, Vol 64, pp 825-831, 2002.
- [Glaser *et al.*, 2003] Glaser DC, Voung J, Xiao L, Tai B, Ubbelohde MS, Canny J, Do EYL. "LightSketch: A sketch-modelling program for lighting analysis." CAAD Futures 2003 Conference, Tainan, Taiwan, 2003.
- [Glaser *et al.*, 2003a] Glaser DC, Tan R, Canny J, Do EYL. "Developing Architectural Lighting Representations." *Proceeds of the IEEE Symposium on Information Visualization 2003*, Seattle, October 19-22, pp 241-248, 2003.
- [GmbH, 2009] GmbH. "DIALux Version 4.7: The software standard for calculatin lighting layouts: User manual." Online source: [http://www.dial.de/CMS/English/Articles/DIALux/Download/Download d e fr it es cn.html](http://www.dial.de/CMS/English/Articles/DIALux/Download/Download%20de%20fr%20it%20es%20cn.html), last accessed October 2009.
- [de Groot *et al.*, 2003] de Groot E, Zonneveldt L, Paule B. "Dial Europe: A decision support tool for early lighting design." *Proceedings of the 8<sup>th</sup> International IBPSA Conference*, Eindhoven, The Netherlands, August 11-14, 2003.
- [Herkel, 1997] Herkel S. "Dynamic link of light- and thermal simulation: on the way to integrated planning tools." *Proceedings of the 5<sup>th</sup> International IBPSA Conference*, Prague, September 8-10, pp 307-312, 1997.
- [Heschong *et al.*, 1999] Heschong L, Mahone D, Kuttaiah K, Stone N, Chappell C, McHugh J, Burton J, Okura S, Wright R, Erwin B, Digert N, Baker K.. *Daylighting in Schools: An Investigation into the Relationship Between Daylighting and Human Performance*. Submitted to the Pacific Gas and Electric Company. The Heschong Mahone Group, Fair Oaks, California, 1999.
- [Hitchcock & Carroll, 2003] Hitchcock RJ, Carrol WL. "DElight: A daylighting and electric lighting simulation engine." *Proceedings of the 8<sup>th</sup> International IBPSA Conference*, Eindhoven, August 11-14, pp 483-490, 2003.
- [Hopkinson, 1957] Hopkinson RG. "Evaluation of Glare." *Illuminating Engineering*, pp 305-316, June, 1957.
- [Hopkinson, 1963] Hopkinson RG, *Architectural Physics: Lighting*. HMSO, London, 1963.
- [Hopkinson *et al.*, 1966] Hopkinson RG, Petherbridge P, Longmore J. *Daylighting*. William Heinemann, Ltd., London, 1966.
- [Hopkinson, 1972] Hopkinson RG. "Glare from daylighting in buildings." *Applied Ergonomics*, Vol 3 (4), pp 206-215, 1972.

- [Houghton Mifflin web] Houghton Mifflin Company. *World Climate*. An outline map of world climates. Online source: [http://www.eduplace.com/ss/maps/pdf/world\\_clim.pdf](http://www.eduplace.com/ss/maps/pdf/world_clim.pdf), last accessed November 2009.
- [Hui, 1997] Hui SCM. "Overall Thermal Transfer Value (OTTV): How to Improve Its Control in Hong Kong." Proceedings of the One-day Symposium on Building, Energy, and Environment, Hong Kong, October 16, pp12-1 – 12-11, 1997.
- [Ibrahim & Krawczyk, 2003] Ibrahim M, and Robert Krawczyk. "The Level of Knowledge of CAD Objects within the Building Information Model." *Connecting: Crossroads of Digital Discourse*, Proceedings of the 2003 Annual Conference of the Association for Computer Aided Design In Architecture, Indianapolis Indiana, October 24-27, pp 173-177, 2003.
- [IES web] IES Virtual Environment website: <http://www.iesve.com/>, last accessed October 2009.
- [IESNA, 2000] Illuminating Engineering Society of North America. *The IESNA Lighting Handbook: reference and application*. 9th edition. Edited Mark S. Rea. Pub: IESNA, New York, 2000.
- [Igawa *et al.*, 1999] Igawa N, Nakamura H, Matsuura K. "Sky luminance distribution model for simulation of daylight environment." Proceedings of the 6<sup>th</sup> International IBPSA Conference, Kyoto, Japan, Vol 2, pp 969- 975, 1999.
- [Igawa *et al.*, 2004] Igawa N, Koga Y, Matsuzawa T, Nakamura H. "Models of sky radiance distribution and sky luminance distribution." *Solar Energy*, Vol 77 (2), pp 137-157, 2004.
- [Inspirer web] Inspirer website: <http://www.integra.jp/en/inspirer/index.html>, last accessed October 2009.
- [Iwata & Tokura, 1998] Iwata T, Tokura M. "Examination of the limitations of predicted glare sensation vote (PGSV) as a glare index for a large source: Towards a comprehensive development of discomfort glare evaluation." *Lighting Research and Technology*, Vol 30 (2), pp 81-88, 1998.
- [Jameson & Hurvich 1961] Jameson D, Hurvich LM. "Complexities of Perceived Brightness." *Science*, Vol 133 (3447), pp174-179, 1961.
- [Joseph, 2006] Joseph A. "The Impact of Light on Outcomes in Healthcare Settings." The Center for Health Design, Concord, CA, Issue Paper #2, August 2006.

- [Jung *et al.*, 2002] Jung T, Gross MD, Do EYL. "Sketching annotations in a 3D Web environment." *Proceeds of CHI 2002, Conference on Human Factors in Computing Systems*, ACHM Press, Minneapolis, pp 618-619, 2002.
- [Koenigsberger *et al.*, 1975] Koenigsberger OH, Ingersoll TG, Mayhew A, Szokolay SV. *Manual of Tropical Housing and Building: Climatic Design (Part I)*. Orient Longman, 1975.
- [Küller & Lindsten, 1992] Küller R, Lindsten C. "Health and Behavior of Children in Classrooms with and without Windows." *Journal of Environmental Psychology*, Vol 12, pp 305-317, 1992.
- [Lambert *et al.*, 2002] Lambert GW, Reid C, Kaye DM, Jennings GL, Esler MD. "Effect of sunlight and season on serotonin turnover in the brain." *The Lancet*, Vol 360, pp 1840-1842, December 7th, 2002.
- [Lawrence, 2005] Lawrence M. "Integration of Lighting Early in the Design Process: evaluations of tools and methodologies." 4.481 Building Technology Seminar, Massachusetts Institute of Technology, December, 2005.
- [LBNL, 2001] *User's Guide to the Building Design Advisor Version 3.0*. Building Technologies Department, Lawrence Berkeley National Laboratory, University of California, 2001.
- [Lechner, 2001] Lechner, N. *Heating, Cooling, Lighting: Design methods for architects*. 2nd Ed. John Wiley & Sons, New York, NY, 2001.
- [Lee *et al.*, 2009] Lee J, Andersen M, Sheng Y, Cutler B. "Goal-Based Daylighting Design Using an Interactive Rendering Method." *Proceedings of the 11<sup>th</sup> International IBPSA Conference*, Glasgow, Scotland, July 27-30, pp 936-943, 2009.
- [Lehar & Glicksman, 2007] Lehar MA, Glicksman LR. "Rapid Algorithm for Modeling Daylight Distributions in Office Buildings." *Building and Environment*, Vol 42 (8), pp 2908-2919, 2007.
- [Leslie, 2003] Leslie RP. "Capturing the daylight dividend in buildings: Why and How?" *Building and Environment*, Vol 38, pp 381-385, 2003.
- [Levitt *et al.*, 2002] Levitt AJ, Lam RW, Levitan R. "A comparison of open treatment of seasonal major and minor depression with light therapy." *Journal of Affective Disorders*, Vol 71, pp 243-248, 2002.
- [Li & Lam, 2001] Li DHW, Lam JC. "Evaluation of lighting performance in office buildings with daylighting controls." *Energy and Buildings*, Vol 33, pp 793-803, 2001.



- [Li *et al.*, 2002] Li DHW, Lam JC, Wong SL. "Daylighting and its implications to overall thermal transfer value (OTTV) determinations." *Energy*, Vol 27, pp 991-1008, 2002.
- [Littlefair, 2001] Littlefair PJ. "Daylight, sunlight, and solar gain in the urban environment." *Solar Energy*, Vol 70 (3), pp 177-185, 2001.
- [Lynes, 1968] Lynes, JA. *Principals of Natural Lighting*. Applied Science Publishers, Ltd., London, 1968.
- [Mardaljevic, 1995] Mardaljevic, J. "Validation of a lighting simulation program under real sky conditions." *Lighting Research and Technology*, Vol 27 (4), pp 181-188, 1995.
- [Mardaljevic & Lomas, 1998] Mardaljevic J, Lomas KJ. "A Simulation Based Method to Evaluate the Probability of Daylight Glare Over Long Time Periods and its Application." CIBSE National Lighting Conference, Lancaster University, April 5-8, pp 282-291, 1998.
- [Mardaljevic, 2000] Mardaljevic J. "Simulation of annual daylighting profiles for internal illuminance." *Lighting Research and Technology*, Vol 32 (3), pp 111-118, 2000.
- [Mardaljevic, 2001] Mardaljevic J. "Taking daylight modeling out of the dark ages." *International Daylighting RD&A #2*, 2001.
- [Mardaljevic, 2002] Mardaljevic J. "Quantification of parallax errors in sky simulator domes for clear sky conditions." *Lighting Research and Technology*, Vol 34 (4), pp 313-332, 2002.
- [Mardaljevic, 2003] Mardaljevic J. "Precision modeling of parametrically defined solar shading sytems: pseudo-changi." *Proceeds of the 8<sup>th</sup> International IBPSA Conference*, Eindhoven, August 11-14, 2003.
- [Mardaljevic, 2004] Mardaljevic, J. "Verification of program accuracy for illuminance modeling: assumptions, methodology and an examination of conflicting findings." *Lighting Research and Technology*, Vol 36 (3), pp 217-242, 2004.
- [Mardaljevic, 2009] Mardaljevic J. "Applicaation of the Useful Daylight Illuminance Metric: A Parametric Evaluation Covering 480 Combinations of Building Type, Climate and Orientation." *Proceedings of Lux Europa 2009*, Istanbul, Sept 9-11, 2009.
- [Mardaljevic *et al.*, 2009] Mardaljevic J, Heschong L, Lee E. "Daylight metrics and energy savings." *Lighting Research and Technology*, Vol 41 (3), pp 261-283, 2009.
- [Maxwell web] Maxwell Render website: <http://www.maxwellrender.com/>, last accessed October 2009.

- [McQuiston *et al.*, 2005] McQuiston FC, Parker JD, Spitler JD. "Heating, Ventilation, and Air Conditioning." John Wiley & Sons, New York, 2005.
- [MIT Design Advisor web] MIT Design Advisor website: <http://designadvisor.mit.edu/design/>, last accessed October 2009.
- [Mitanchey *et al.*, 1997] Mitanchey R, LaForgue P, Fontoynt M, Marolles O, Avouac-Bastie P, Dumortier D, Duport JM, Kenny P, Badinier C, Demé C. "Lighting Calculations on the Internet Using Genelux-Web." Proceedings of Right Light 4 Conference, Vol 1, pp 125-130, 1997.
- [Moon & Spencer, 1942] Moon P, Spencer D. "Illumination from a nonuniform sky". Illuminating Engineering, Vol 37 (10), pp 707-726, 1942.
- [Nabil & Mardaljevic, 2005] Nabil A, Mardaljevic J. "Useful daylight illuminance: a new paradigm for assessing daylight in buildings." *Lighting Research and Technology*, Vol 37 (1), pp 41-59, 2005.
- [Nabil & Mardaljevic, 2006] Nabil A, Mardaljevic J. "The Useful Daylight Illuminance Paradigm: A Replacement for Daylight Factors." *Energy and Buildings*, Vol 38 (7), pp 905-913, 2006.
- [Nakamura *et al.*, 1985] Nakamura H, Oki M, Hayashi Y. "Luminance distribution of Intermediate Sky." *Journal of Light and Visual Environment*, Vol 9 (1), pp 6-13, 1985.
- [Nazzal, 2001] Nazzal AA. "A new daylight glare evaluation method: Introduction of the monitoring protocol and calculation method." *Energy and Buildings*, Vol 33, pp 257-265, 2001.
- [Nazzal & Chutarat, 2001] Nazzal AA, Chutarat A. "A new daylight glare evaluation method: A comparison of the existing glare index and the proposed method and an exploration of daylighting control strategies." *Architectural Science Review*, 44: pp 71-82, 2001.
- [Newsham, 1994] Newsham, GR. "Manual control of windows blinds and electric lighting: implications for comfort and energy consumption." *Indoor Environment*, Vol 3 (3), pp 135-144, 1994.
- [Nicklas & Bailey, 1996] Nicklas MH, Bailey GB. *Energy Performance of Daylit Schools in North Carolina*. Innovative Design Architectural Firm, Raleigh, NC, 1996.
- [Österhaus, 2005] Österhaus WKE. "Discomfort glare assessment and prevention for daylight applications in office environments." *Solar Energy*, Vol 79, pp140-158, 2005.
- [Painter *et al.*, 2009] Painter B, Fan D, Mardaljevic J. "Evidence-based daylight research: Development of a new visual comfort monitoring

- method.” Proceedings of Lux Europa 2009, Istanbul, Sept 9-11, 2009.
- [Papamichael *et al.*, 1997] Papamichael K, La Porta J, Chauvert H. “Decision Making through Use of Interoperable Simulation Software.” Proceedings of the 5<sup>th</sup> International IBPSA Conference, Vol II, Prague, Czech Republic, September 8-10, 1997.
- [Papamichael *et al.*, 1998] Papamichael K, La Porta J, Chauvert H. “Building Design Advisor: automated integration of multiple simulation tools.” *Automation in Construction*, Vol 6 (4), pp 341-352, 1998.
- [Paule & Scartezzini, 1997] Paule B, Scartezzini JJ. “‘Leso-DIAL’, a new computer-based daylighting design tool.” *Right Light*, Vol 4 (1), pp93-97, 1997.
- [Pechacek, 2008] Pechacek CS. *Space, Light, and Time: Prospective Analysis of Circadian Illumination for Health-Based Daylighting with Applications to Healthcare Architecture*. Masters Thesis, Massachusetts Institute of Technology, 2008.
- [Pechacek *et al.*, 2008] Pechacek CS, Andersen M, Lockley SW. *Preliminary Method for Prospective Analysis of the Circadian Efficacy of (Day)Light with Applications to Healthcare Architecture*. LEUKOS, Vol 5 (1), pp 1-26, 2008.
- [Perez *et al.*, 1990] Perez R, Ineichen P, Seals R. “Modeling daylight availability and irradiance components from direct and global irradiance.” *Solar Energy*, Vol 44 (5), pp 271-289, 1990.
- [Perez *et al.*, 1992] Perez R, Michalsky J, Seals R. “Modeling Sky Luminance Angular Distribution for Real Sky Conditions: Experimental Evaluation of Existing Algorithms.” *Journal of the Illuminating Engineering Society*, Vol 21 (2), pp 84-92, 1992.
- [Perez *et al.*, 1993] Perez R, Seals R, Michalsky J. “All-Weather model for sky luminance distribution – preliminary configuration and validation.” *Solar Energy*, Vol 50 (3), pp 235-245, 1993.
- [Prescription Act, 1832] *Prescription Act 1832*. Imperial Act 71, 1 August, 1832.
- [Radiance web] *gensky.c*. C code for Radiance simulation program sky generation. Online source: <http://radsite.lbl.gov/radiance/>, last accessed November 2009.
- [Rea, 1984] Rea MS. “Window Blind Occlusion: a Pilot Study.” *Building & Environment*, Vol 19 (2), pp 133-137, 1984.
- [Rea *et al.*, 2002] Rea MS, Figueiro MG, Bullough JD. “Circadian photobiology: an emerging framework for lighting practice



- and research." *Lighting Research and Technology*, Vol 34 (3), pp 177-190, 2002.
- [Reinhart & Herkel, 2000] Reinhart CF, Herkel S. "The simulation of annual daylight illuminance distributions – a state-of-the-art comparison of six RADIANCE-based methods." *Energy and Buildings*, Vol 32, pp 167-187, 2000.
- [Reinhart & Walkenhorst, 2001] Reinhart CF, Walkenhorst O. "Validation of dynamic RADIANCE-based daylight simulations for a test office with external blinds." *Energy and Buildings*, Vol 33, pp 683-697, 2001.
- [Reinhart *et al.*, 2003] Reinhart CF, Morrison M, Dubrous F. "The Lightswitch Wizard – Reliable daylight simulations for initial design investigation." Proceedings of the 8<sup>th</sup> International IBPSA Conference, Eindhoven, The Netherlands, August 11-14, pp1093-1100, 2003.
- [Reinhart, 2004] Reinhart CF. "Lightswitch-2002: a model for manual and automated control of electric lighting and blinds." *Solar Energy*, Vol 77 (1), pp 15-28, 2004.
- [Reinhart & Fitz, 2004] Reinhart CF, Fitz A. "Key findings from an online survey in the use of daylight simulation programs." Proceedings of eSim 2004, Vancouver, June 10-11, pp 1-8, 2004.
- [Reinhart, 2005] Reinhart CF. "Tutorial on the Use of Daysim/Radiance Simulations for Sustainable Design." National Research Council of Canada, Institute for Research in Construction. Ottawa, February 8, 2005.
- [Reinhart, 2005a] Reinhart CF. "A Simulation-based review of the ubiquitous window-head-height to daylight zone depth rule-of-thumb." Proceedings of Building Simulation 2005, Montreal, Canada, August 15-18, pp 1-8, 2005.
- [Reinhart & Fitz, 2006] Reinhart CF, Fitz A. "Findings from a survey on the current use of daylight simulations in building design." *Energy and Buildings*, Vol 38 (7), pp 824-835, 2006.
- [Reinhart *et al.*, 2006] Reinhart CF, Mardaljevic J, Rogers Z. "Dynamic daylight performance metrics for sustainable building design." *Leukos*, Vol 3 (1), pp 1-25, 2006.
- [Reinhart *et al.*, 2007] Reinhart CR, Bourgeois D, Dubrous F, Laouadi A, Lopez P, Stelescu O. "Daylight 1-2-3 – A state-of-the-art daylighting/energy analysis software for initial design investigations." Proceedings of the 10<sup>th</sup> International IBPSA Conference, Beijing, September 3-6, pp 1669-1676, 2007.

- [Reinhart & Breton, 2009] Reinhart CF, Breton PF. "Experimental Validation of 3ds Max® Design 2009 and Daysim 3.0." Proceedings of the 11<sup>th</sup> International IBPSA Conference, Glasgow, Scotland, July 27-30, pp 1514-1521, 2009.
- [Reinhart & Breton, 2009a] Reinhart CF, Breton PF. "Experimental Validation of 'Autodesk® 3ds Max® Design' 2009 and Daysim 3.0." NRC Project #B3241 Report. January 29, 2009
- [Rogers, 2006] Rogers Z. "Daylighting Metric Development Using Daylight Autonomy Calculations In the Sensor Placement Optimization Tool: Development Report and Case Studies." Boulder, Colorado, USA: Architectural Energy Corporation, March 17, 2006. Online source: <http://www.archenergy.com/SPOT/download.html>
- [Rubifio *et al.*, 1994] Rubifio M, Curz A, Garcia JA, Hita E. "Discomfort glare indices: a comparative study." *Applied Optics*, Vol 33 (34), pp 8001-8008, 1994.
- [Sarawgi, 2006] Sarawgi, T. "Survey on the Use of Lighting Design Software in Architecture and Interior Design Undergraduate Education." *International Journal of Architectural Computing*, Vol 4 (4), pp 91-108, 2006.
- [Simon, 1969] Simon H. *The Sciences of the Artificial*. MIT Press, Cambridge, Massachusetts, 1st edition, 1969.
- [Stephenson, 1957] Stephenson DG. "Thermal radiation and its effect on the heating and cooling of buildings." National Research Council of Canada, Division of Building Research, Report No. 121, Ottawa, 1957.
- [Stephenson, 1965] Stephenson DG. "Equations for solar heat gain through windows." *Solar Energy*, Vol 9 (2), pp 81-86, 1965.
- [Thanachareonkit *et al.*, 2005] Thanachareonkit A, Scartezzini JL, Andersen M. "Comparing daylighting performance assessment of buildings in scale models and test modules." *Solar Energy* Vol 79, pp 168-182, 2005.
- [Tobler, 1999] Tobler W. "World population by latitude." Slide in *Unusual Map Projections* slideshow. UC Santa Barbara. Used with permission, stylistically reformatted. 1999. Online source: <http://www.ncgia.ucsb.edu/projects/tobler/Projections/sld075.htm>, last accessed November 2009.
- [Torcellini *et al.*, 2008] Torcellini P, Deru M, Griffith B, Benne K, Halverson M, Winiarski D, Crawley DB. "DOE Commercial Building Benchmark Models." Proceedings of the 2008 ACEEE Summer Study on Energy Efficiency in Buildings, Pacific Grove, California, August 17-22, 2008. Online source: <http://www.nrel.gov/docs/fy08osti/43291.pdf>, last accessed October 2009.

- [Tregenza, 1980] Tregenza PR. "The daylight factor and actual illuminance ratios." *Lighting Research and Technology*, Vol 12 (2), pp 64-68, 1980.
- [Tregenza & Waters, 1983] Tregenza PR, Waters IM. "Daylight coefficients." *Lighting Research and Technology*, Vol 15 (2), pp 65-71, 1983.
- [Tregenza, 1987] Tregenza PR. "Subdivision of the sky hemisphere for luminance measurements." *Lighting Research and Technology*, Vol 19 (1), pp 13-14, 1987.
- [Tuft, 1983] Tuft E. *The Visual Display of Quantitative Information*. Graphics Press, Cheshire, Connecticut, 1983.
- [Ubbelohde, 1998] Ubbelohde MS. "Comparative Evaluation of Four Daylighting Software Programs." Proceedings of ACEE Summer Study on Energy Efficiency in Buildings, 1998.
- [University of Oregon web] University of Oregon. Solar Radiation Monitoring Laboratory. Sun path chart program online source: <http://solardat.uoregon.edu/SunChartProgram.html>, last accessed November 2009.
- [Urban & Glicksman, 2007] Urban BJ, Glicksman LR. "A Simplified Rapid Energy Model and Interface for Nontechnical Users." Proceedings of Oak Ridge National Laboratory, Buildings Conference X, 2007.
- [Uttinger & Wasley, 1997] Uttinger M, Wasley JH. "Building Balance Point." Vital Signs Curriculum Materials Project, University of California – Berkeley, and University of Wisconsin – Milwaukee. August, 1997. Online source: <http://arch.ced.berkeley.edu/vitalsigns/res/rps.html>, last accessed October, 2009.
- [Vine, 1998] Vine E, Lee E, Clear R, DiBartolomeo D, Selkowitz S. "Office worker response to an automated venetian blind and electric lighting system: a pilot study." *Energy and Buildings*, Vol 28, pp 205-218, 1998.
- [Vos, 2003] Vos JJ. "Reflections on glare." *Lighting Research and Technology*, Vol 35 (2), pp163-176, 2003.
- [Walkenhorst et al., 2002] Walkenhorst O, Luther J, Reinhart C, Timmer J. "Dynamic annual daylight simulations based on one-hour and one-minute means of irradiance data." *Solar Energy*, Vol 72 (5), pp 385-395, 2002.
- [Ward & Shakespeare, 1998] Ward G, Shakespeare RA. *Rendering with Radiance*. Morgan Kaufmann Publishers, 1998.
- [Wienold & Christoffersen, 2006] Wienold J, Christoffersen J. "Evaluation methods and development of a new glare prediction model for



- daylight environments with the use of CCD cameras.”  
*Energy and Buildings*, Vol 38, pp743-757, 2006.
- [Wienold, 2007] Wienold J. “Dynamic simulation of blind control strategies for visual comfort and energy balance analysis.”  
Proceedings of the 10<sup>th</sup> International IBPSA Conference, Beijing, September 3-6, pp 1197-1204, 2007.
- [Wienold, 2009] Wienold J. “Dynamic daylight glare evaluation.”  
Proceedings of the 11<sup>th</sup> International IBPSA Conference, Glasgow, July 27-30, pp 944-951, 2009.
- [Wienold, IP] Wienold J. *Daylight Glare in Offices*. Ph.D. Thesis, Fraunhofer Institute for Solar Energy Systems, In Progress.
- [Winkelmann & Selkowitz, 1985] Winkelmann F, Selkowitz S. “Daylighting simulation in the DOE-2 building energy analysis program.”  
*Energy and Buildings*, Vol 8, pp 271-286, 1985.
- [Wittkopf *et al.*, 2006] Wittkopf SK, Yuniarti E, Soon LK. “Prediction of energy savings with anidolic integrated ceiling across different daylight climates.” *Energy and Buildings*, Vol 38, pp1120-1129, 2006.
- [Wu & Ng, 2003] Wu W, Ng E. “A review of the development of daylighting in schools.” *Lighting Research and Technology*, Vol 35 (2), pp 111-125, 2003.
- [Yi, 2008] Yi L. *A New Approach in Data Visualization to Integrate Time and Space Variability of Daylighting in the Design Process*. Masters Thesis, Massachusetts Institute of Technology, 2008.
- [Yik & Wan, 2005] Yik FWH, Wan KSY. “An evaluation of the appropriateness of using overall thermal transfer value (OTTV) to regulate envelope energy performance of air-conditioned buildings.” *Energy*, Vol 30, pp 41-71, 2005.

# Appendix A

There have been several glare metrics developed over the latter half of the last century, and these were briefly discussed in section 2.1.3. The formulae are listed below in the order of the chronology of their development.

British Glare Index (BGI):

$$BGI = 10 \log_{10} 0.478 \sum_{s=1}^n \frac{L_s^{1.6} \omega_s^{0.8}}{L_b P^{1.6}} \quad (A.1)$$

Discomfort Glare Rating (DGR):

$$DGR = \left( \sum_{s=1}^n \frac{0.5 L_s \Psi}{P E_a^{0.44}} \right)^\alpha \quad (A.2)$$

( $E_a$  = ave illum over direct field of view,  $\Psi = 20.4 \omega_s + 1.52 \omega_s^{0.2} - 0.075$ )

Visual Comfort Probability (VCP):

$$VCP = \frac{100}{\sqrt{2\pi}} \int_{-\infty}^{6.374 - 1.3227 \ln DGR} e^{-t^2/2} dt \quad (A.3)$$

Daylight Glare Index (Cornell Formula) (DGI):

$$DGI = 10 \log_{10} 0.48 \sum_{s=1}^n \frac{L_s^{1.6} \Omega_s^{0.8}}{L_b + 0.07 \omega_s^{0.5} L_s} \quad (A.4)$$

CIE Glare Index (CGI):

$$CGI = 8 \log_{10} 2 \frac{[1 + (E_d/500)]}{E_d + E_i} \sum_{s=1}^n \frac{L_s^2 \omega_s}{P^2} \quad (A.5)$$

( $E_d$  = direct vertical illum at the eye,  $E_i = \pi L_b$  = indirect illum at eye)

Unified Glare Rating (UGR):

$$UGR = 8 \log_{10} \frac{0.25}{L_b} \sum_{s=1}^n \frac{L_s^2 \omega_s}{P^2} \quad (A.6)$$

## Appendix B

In order to encourage as close an agreement as possible between the Daylight Glare Probability found using *evalglare* and the new approximation, the numerical validations of the DGPM (see Section 5.2) incorporated the same equations for sky, sun, and ground luminance distribution as the Radiance program. These luminance equations are listed below. The variables in the equations are defined here:

- $L_x$  (where  $x$  is clear, clear-turbid, intermediate, or overcast) is the sky luminance of any point in the sky dome.
- $L_{sol}$  is the sun's luminance
- $L_g$  is the ground luminance ( $L_{g,ov}$  is the ground luminance for overcast skies)
- $L_z$  is the zenithal sky luminance.
- $k$  is the angle between the sun and the sky position of interest
- $\delta$  is the angle between the zenith and the sky position of interest
- $\gamma$  is the angle between the zenith and the sun
- $\rho_g$  is the ground reflectance (generally taken to be 20%)
- $\alpha$  is the solar altitude

$$\frac{L_{clear}}{L_z} = \frac{(0.91 + 10e^{-3k} + 0.45 \cos^2(k)) (1 - e^{-0.32 \sec(\delta)})}{(0.91 + 10e^{-3\gamma} + 0.45 \cos^2(\gamma)) \times 2.74} \quad (B.1)$$

$$\frac{L_{clear-turbid}}{L_z} = \frac{(0.856 + 16e^{-3k} + 0.3 \cos^2(k)) (1 - e^{-0.32 \sec(\delta)})}{(0.91 + 10e^{-3\gamma} + 0.45 \cos^2(\gamma)) \times 2.74} \quad (B.2)$$

$$\frac{L_{intermediate}}{L_z} = \frac{((1.35 \sin(5.631 - 3.59\delta) + 3.12) \sin(4.396 - 2.6\delta) + 6.37 - \delta) \left( e^{-0.563((2.629 - \delta)^2 + 0.812)k} \right)}{2.326(2.739 + 0.9891 \sin(0.3119 + 2.6(90 - \delta))) \left( e^{\gamma(-0.4441 - 1.48(90 - \delta))} \right)} \quad (B.3)$$

$$\frac{L_{overcast}}{L_z} = \frac{1 + 2 \sin(\phi)}{3} \quad (B.4)$$

$$L_g = \rho_g \left( \frac{0.00006}{\pi} L_{sol} \sin(\alpha) + L_z \right) \quad (B.5)$$

$$L_{sol} = 1.5 \times 10^9 \left( 1.147 - \frac{0.147}{\max[\sin(\alpha), 0.16]} \right) \quad (B.6)$$

$L_{g,ov}$  for overcast skies is a simpler equation which does not involve the sun.

$$L_{g,ov} = 0.778 \rho_g L_z \quad (B.7)$$



# Appendix C

Table C.1: The default balance point calculation values options from the 16 DOE Commercial Building Benchmark Models [Torcellini et al., 2008; DOE, 2008]

Building Type:	Occupancy [Person/m <sup>2</sup> ]	Ventilation [L/s/person]	Ventilation [L/s/m <sup>2</sup> ]	Infiltration [ACH]	Equipment Heat Gain [W/m <sup>2</sup> ]	Lights Heat Gain [W/m <sup>2</sup> ]	U-value [W/m <sup>2</sup> K] - Wall - Very Hot	U-value [W/m <sup>2</sup> K] - Wall - Warm Temperat	U-value [W/m <sup>2</sup> K] - Wall - Cool Temperate	U-value [W/m <sup>2</sup> K] - Wall - Very Cold	U-value [W/m <sup>2</sup> K] - Roof	U-value [W/m <sup>2</sup> K] - Roof - Very Cold	U-value [W/m <sup>2</sup> K] - Window - Very Hot	U-value [W/m <sup>2</sup> K] - Window - Temperate	U-value [W/m <sup>2</sup> K] - Window - Very Cold	SHGC [%] - Window - Very Hot	SHGC [%] - Window - Warm Temperate	SHGC [%] - Window - Cool Temperate	SHGC [%] - Window - Very Cold
Fastfood	0.386	9.000	0.000	0.640	215.20	17.75	0.505	0.505	0.505	0.29	0.194	0.154	6.88	3.24	2.62	0.25	0.25	0.39	0.49
Hospital	0.070	5.853	0.044	0.088	42.17	11.31	2.61	0.856	0.698	0.454	0.357	0.273	6.88	3.24	2.62	0.25	0.25	0.39	0.49
Large Hotel	0.123	0.707	0.248	0.115	32.58	10.76	1.285	1.285	1.285	1.285	0.564	0.564	6.88	3.24	2.62	0.25	0.25	0.39	0.49
Large Office	0.517	10.000	0.000	0.074	7.82	10.76	0.704	0.704	0.477	0.364	0.357	0.273	6.88	3.24	2.62	0.25	0.25	0.39	0.49
Medium Office	0.054	2.500	0.300	0.167	8.07	10.76	0.704	0.704	0.477	0.364	0.357	0.273	6.88	3.24	2.62	0.25	0.25	0.39	0.49
Midrise Apartment	0.025	6.180	0.300	0.251	4.22	5.06	0.704	0.477	0.364	0.313	0.357	0.273	6.88	3.24	2.62	0.25	0.39	0.39	0.49
Outpatient	0.054	2.500	0.300	0.300	8.07	10.76	0.704	0.477	0.364	0.313	0.357	0.273	6.88	3.24	2.62	0.25	0.39	0.39	0.49
Primary School	0.205	3.401	0.454	0.372	51.21	13.71	0.704	0.704	0.477	0.364	0.357	0.273	6.88	3.24	2.62	0.25	0.25	0.39	0.49
Retail	0.078	3.800	0.600	0.270	5.22	16.65	2.61	0.856	0.698	0.454	0.357	0.273	6.88	3.24	2.62	0.25	0.25	0.39	0.49
Secondary School	0.301	2.706	0.628	0.205	30.68	12.37	0.704	0.704	0.477	0.364	0.357	0.273	6.88	3.24	2.62	0.25	0.25	0.39	0.49
Sit Down Restarant	0.537	2.764	0.655	0.550	636.61	19.95	0.704	0.704	0.477	0.364	0.194	0.154	6.88	3.24	2.62	0.25	0.25	0.39	0.49
Small Hotel	<sup>a</sup>	<sup>a</sup>	<sup>a</sup>	<sup>a</sup>	22.29	19.96	0.704	0.704	0.477	0.364	0.357	0.273	6.88	3.24	2.62	0.25	0.25	0.39	0.49
Small Office	0.054	10.000	0.000	0.449	8.07	10.76	2.61	0.856	0.698	0.454	0.194	0.154	6.88	3.24	2.62	0.25	0.25	0.39	0.49
Strip Mall	0.086	0.000	15.169	11.611	4.30	17.46	0.704	0.704	0.477	0.364	0.357	0.273	6.88	3.24	2.62	0.25	0.25	0.39	0.49
Supermarket	0.078	0.215	0.137	0.247	13.65	16.71	2.61	0.856	0.698	0.454	0.357	0.273	6.88	3.24	2.62	0.25	0.25	0.39	0.49
Warehouse	0.001	0.122	0.300	0.196	2.09	11.34	0.641	0.641	0.641	0.324	1.627	1.627	6.88	3.24	2.62	0.25	0.39	0.39	0.49

NOTES: a) This Data was not available in the files provided by the DOE [DOE, 2008].

**Table C.2: The default balance point calculation values options from the ASHRAE Handbook [ASHRAE, 2000]**

Building Type : Sub-Type	Occupancy [Person/m <sup>2</sup> ]	Ventilation [L/s/person]	Ventilation [L/s/m <sup>2</sup> ]
Food Service : Fastfood/Cafeteria/Bar	1.0	3.8	0.9
Food Service : Restaurant Dining Room	0.7	3.8	0.9
Office	0.1	2.5	0.3
Hotel : Room	0.1	2.5	0.3
Hotel : Lobby	0.3	3.8	0.3
Hotel : Multipurpose	1.2	2.5	0.3
School : Classroom	0.3	5.0	0.6
School : Lecture Hall	1.5	3.8	0.3
School : Science Lab	0.3	5.0	0.9
Retail : Mall Common Area	1.0	3.8	0.9
School : Gymnasium	a	a	1.5
Auditorium	1.5	2.5	0.3
Residential : House/Apartment	0.1	2.5	0.3
Health Care : Patient Room	0.1	13.0	b
Health Care : Medical Procedure	0.2	8.0	b
Health Care : Operating Room	0.2	15.0	b
Health Care : Recovery/ICU	0.2	8.0	b
Retail : Sales Area	0.2	3.8	0.6
Supermarket	0.8	3.8	0.9
Religious	1.2	2.5	0.3
Library	0.1	2.5	0.3
Warehouse	a	a	0.3

NOTES:

- a) No recommendations were made by ASHRAE 62.1-2007 [ASHRAE, 2007].
- b) Specific codes for the locality and the medical procedure should be used [ASHRAE, 2007].

**Table C.3: The default balance point calculation values options from "Building Balance Point" [Uttinger & Wasley, 1997]**

	Infiltration (ACH)
Residential Loose	2
Residential Medium	0.5
Residential Tight	0.2
Residential Too Tight	< 0.2
Commercial Loose	3.5
Commercial Medium	2
Commercial Tight	0.5
Economizer Cycle	5

## Appendix D

The tables in this appendix represent the Maximum Load Ratio (MLR, as defined in Section X) between the measured energy use from Energy Plus and the detailed balance point load (white) or the blocked balance point load (gray). A positive MLR means that balance point load exceeds the measured energy use, and a negative MLR means that it is less than the measured energy use. Average, median, and standard deviations are presented for annual data sets of cooling energy, heating energy, and cooling energy-heating energy (since realistic HVAC systems sometimes cool and heat at the same time). All values are displayed in the tables as percents, rather than decimals, for ease of reading.

**Table D.1: Annual average MLR, cooling – heating.**

	Fastfood		Hospital		Lg Hotel		Lg Office		Med Office		Midrise Apt		Outpatient		Prim. Sch.	
<b>Miami</b>	-16%	1%	-32%	-20%	-9%	-15%	-15%	44%	-20%	-15%	-17%	-19%	-20%	-13%	-22%	-2%
<b>Houston</b>	-11%	1%	-35%	-18%	-60%	-42%	-38%	22%	-19%	-13%	-13%	-14%	-18%	-9%	-20%	-1%
<b>Phoenix</b>	4%	21%	-14%	5%	-10%	-8%	-7%	61%	-8%	-2%	-5%	-9%	-10%	1%	-7%	15%
<b>Atlanta</b>	-6%	1%	-39%	-11%	-124%	-75%	-66%	7%	-16%	-8%	-12%	-10%	-14%	-4%	-15%	6%
<b>Los Angeles</b>	20%	57%	-45%	-8%	-161%	-95%	-65%	20%	-20%	-11%	-19%	-7%	-6%	29%	-18%	17%
<b>Las Vegas</b>	6%	22%	-19%	12%	-64%	-41%	-42%	21%	-9%	-2%	-4%	-8%	-9%	5%	-7%	20%
<b>San Francisco</b>	6%	21%	-73%	-5%	-302%	-169%	-127%	-29%	-26%	-13%	-14%	-8%	-27%	9%	-26%	18%
<b>Baltimore</b>	-6%	-4%	-36%	-9%	-153%	-88%	-82%	-13%	-16%	-6%	-7%	-6%	-13%	-3%	-14%	6%
<b>Albuquerque</b>	5%	5%	-54%	3%	-191%	-112%	-90%	-14%	-16%	-6%	-9%	-8%	-14%	5%	-14%	18%
<b>Seattle</b>	0%	6%	-77%	-4%	-328%	-182%	-145%	-36%	-21%	-5%	-8%	-4%	-18%	9%	-16%	23%
<b>Chicago</b>	-3%	-6%	-43%	-8%	-219%	-124%	-110%	-28%	-18%	-4%	-8%	-4%	-12%	-3%	-13%	8%
<b>Boulder</b>	2%	-8%	-58%	0%	-304%	-171%	-121%	-30%	-19%	-5%	-8%	-5%	-14%	1%	-14%	15%
<b>Minneapolis</b>	-3%	-9%	-53%	-12%	-262%	-148%	-133%	-45%	-11%	-1%	-5%	0%	-10%	-3%	-10%	6%
<b>Mt. Helena</b>	0%	-11%	-51%	-4%	-286%	-160%	-156%	-56%	-15%	-3%	-4%	0%	-11%	-1%	-10%	9%
<b>Duluth</b>	-3%	-16%	-66%	-13%	-332%	-185%	-201%	-83%	-16%	-1%	-4%	3%	-10%	-4%	-10%	7%
<b>Fairbanks</b>	-4%	-21%	-62%	-15%	-290%	-161%	-96%	-47%	-6%	2%	-1%	8%	-7%	-2%	-5%	9%
	Retail		Second. Sch.		Restaurant		Sm Hotel		Sm Office		Strip Mall		Supermarket		Warehouse	
<b>Miami</b>	-24%	-24%	-12%	2%	-15%	57%	-23%	-59%	-15%	-10%	-20%	-17%	-1%	-1%	41%	50%
<b>Houston</b>	-18%	-15%	-13%	3%	-7%	55%	-17%	-44%	-15%	-8%	-11%	-7%	4%	11%	-40%	-23%
<b>Phoenix</b>	-8%	-5%	-4%	13%	7%	72%	-6%	-36%	-4%	3%	-1%	6%	14%	18%	18%	34%
<b>Atlanta</b>	-10%	-3%	-10%	11%	1%	57%	-11%	-32%	-10%	1%	-7%	-1%	12%	27%	-87%	-73%
<b>Los Angeles</b>	-2%	14%	-11%	34%	37%	175%	-11%	-49%	10%	26%	6%	16%	41%	80%	-297%	-177%
<b>Las Vegas</b>	-7%	2%	-4%	17%	10%	75%	-5%	-32%	0%	10%	-3%	5%	23%	35%	-25%	-9%
<b>San Francisco</b>	-14%	17%	-25%	25%	33%	135%	-10%	-33%	-16%	11%	-6%	11%	25%	58%	-263%	-208%
<b>Baltimore</b>	-9%	0%	-11%	10%	3%	45%	-8%	-20%	-15%	-1%	-6%	0%	9%	25%	-104%	-92%
<b>Albuquerque</b>	-12%	-1%	-11%	24%	18%	92%	-7%	-33%	-13%	1%	-7%	4%	19%	39%	-188%	-169%
<b>Seattle</b>	-9%	13%	-14%	44%	31%	110%	-5%	-20%	-20%	7%	-5%	6%	21%	49%	-192%	-166%
<b>Chicago</b>	-7%	-2%	-11%	16%	9%	49%	-6%	-14%	-19%	-5%	-5%	1%	7%	23%	-105%	-95%
<b>Boulder</b>	-9%	2%	-10%	18%	16%	65%	-6%	-24%	-20%	-5%	-4%	2%	10%	25%	-132%	-124%
<b>Minneapolis</b>	-6%	3%	-10%	14%	7%	35%	-8%	-10%	-16%	-3%	-5%	1%	5%	21%	-102%	-95%
<b>Mt. Helena</b>	-7%	2%	-10%	15%	12%	42%	-5%	-13%	-17%	-5%	-4%	1%	7%	23%	-112%	-106%
<b>Duluth</b>	-7%	4%	-10%	16%	8%	27%	-7%	3%	-19%	-4%	-5%	2%	5%	23%	-146%	-136%
<b>Fairbanks</b>	-5%	7%	-9%	14%	3%	6%	-9%	16%	-17%	-3%	-3%	3%	4%	25%	-105%	-97%



**Table D.2: Annual average MLR, cooling only.**

	Fastfood		Hospital		Lg Hotel		Lg Office		Med Office		Midrise Apt		Outpatient		Prim. Sch.	
<b>Miami</b>	-16%	2%	-31%	-20%	-1%	-12%	-13%	44%	-20%	-16%	-17%	-18%	-19%	-13%	-22%	-3%
<b>Houston</b>	-10%	4%	-25%	-16%	-4%	-12%	-16%	28%	-17%	-15%	-11%	-13%	-9%	-4%	-19%	-3%
<b>Phoenix</b>	4%	23%	0%	7%	44%	19%	11%	64%	-8%	-4%	-4%	-9%	-2%	5%	-7%	13%
<b>Atlanta</b>	-4%	7%	-23%	-11%	-14%	-17%	-27%	20%	-15%	-11%	-10%	-9%	-3%	1%	-14%	2%
<b>Los Angeles</b>	22%	61%	-33%	-8%	-46%	-43%	-48%	19%	-20%	-14%	-16%	-6%	17%	34%	-18%	13%
<b>Las Vegas</b>	8%	27%	0%	12%	22%	3%	-21%	25%	-9%	-4%	-4%	-8%	0%	9%	-5%	17%
<b>San Francisco</b>	12%	31%	-25%	-5%	-31%	-30%	-60%	-17%	-22%	-20%	-4%	0%	21%	29%	-24%	2%
<b>Baltimore</b>	-3%	5%	-14%	-7%	-10%	-12%	-25%	8%	-13%	-10%	-5%	-5%	-1%	2%	-12%	1%
<b>Albuquerque</b>	10%	29%	-10%	6%	-17%	-21%	-45%	-2%	-12%	-7%	-5%	-4%	6%	16%	-8%	15%
<b>Seattle</b>	8%	23%	-19%	-5%	-24%	-23%	-53%	-8%	-20%	-16%	-3%	-1%	13%	21%	-11%	11%
<b>Chicago</b>	1%	9%	-12%	-5%	-10%	-12%	-25%	8%	-12%	-10%	-5%	-4%	1%	3%	-10%	4%
<b>Boulder</b>	10%	26%	-10%	6%	-14%	-17%	-47%	-5%	-12%	-8%	-4%	-3%	10%	18%	-8%	15%
<b>Minneapolis</b>	1%	8%	-12%	-5%	-12%	-13%	-26%	8%	-12%	-9%	-5%	-4%	1%	3%	-10%	4%
<b>Mt. Helena</b>	9%	24%	-10%	4%	-16%	-17%	-45%	-11%	-14%	-11%	-3%	-2%	9%	18%	-8%	11%
<b>Duluth</b>	3%	9%	-10%	-4%	-15%	-15%	-32%	-4%	-11%	-9%	-5%	-3%	5%	5%	-9%	5%
<b>Fairbanks</b>	5%	14%	-12%	-2%	-21%	-21%	-34%	-2%	-12%	-8%	-5%	-1%	7%	9%	-10%	13%
	Retail		Second. Sch.		Restaurant		Sm Hotel		Sm Office		Strip Mail		Supermarket		Warehouse	
<b>Miami</b>	-23%	-24%	-11%	2%	-15%	57%	-23%	-58%	-13%	-9%	-19%	-17%	-1%	-1%	53%	58%
<b>Houston</b>	-11%	-12%	-11%	1%	-8%	52%	-16%	-43%	-4%	-2%	-7%	-6%	4%	4%	56%	60%
<b>Phoenix</b>	-3%	-3%	-1%	12%	7%	70%	-6%	-34%	4%	7%	2%	5%	13%	12%	69%	76%
<b>Atlanta</b>	-3%	-3%	-8%	7%	-2%	50%	-12%	-34%	3%	5%	-1%	-1%	9%	14%	30%	33%
<b>Los Angeles</b>	9%	12%	-9%	31%	35%	171%	-12%	-45%	26%	28%	15%	12%	43%	91%	82%	75%
<b>Las Vegas</b>	-1%	2%	-1%	15%	9%	71%	-5%	-32%	9%	13%	2%	4%	17%	21%	49%	55%
<b>San Francisco</b>	10%	12%	-14%	15%	26%	119%	-10%	-29%	25%	23%	12%	8%	28%	68%	29%	28%
<b>Baltimore</b>	-2%	-2%	-7%	4%	-1%	36%	-9%	-24%	3%	5%	-1%	0%	7%	11%	27%	29%
<b>Albuquerque</b>	4%	4%	-3%	22%	14%	82%	-8%	-35%	10%	13%	6%	7%	23%	33%	55%	63%
<b>Seattle</b>	5%	6%	-4%	30%	17%	83%	-11%	-26%	14%	16%	6%	5%	16%	38%	31%	32%
<b>Chicago</b>	0%	0%	-5%	7%	4%	39%	-9%	-24%	2%	4%	1%	1%	9%	15%	25%	26%
<b>Boulder</b>	5%	10%	-4%	21%	16%	79%	-9%	-33%	11%	12%	8%	8%	23%	35%	44%	48%
<b>Minneapolis</b>	0%	1%	-5%	7%	4%	37%	-8%	-22%	3%	4%	0%	0%	8%	16%	21%	22%
<b>Mt. Helena</b>	3%	9%	-6%	15%	16%	77%	-10%	-29%	8%	9%	6%	5%	19%	33%	28%	31%
<b>Duluth</b>	2%	2%	-6%	10%	7%	40%	-9%	-21%	5%	6%	3%	3%	9%	20%	13%	13%
<b>Fairbanks</b>	5%	8%	-11%	17%	18%	76%	-12%	-25%	5%	8%	8%	8%	23%	57%	34%	32%

**Table D.3: Annual average MLR, heating only.**

	Fastfood		Hospital		Lg Hotel		Lg Office		Med Office		Midrise Apt		Outpatient		Prim. Sch.	
<b>Miami</b>	2%	5%	21%	2%	183%	81%	184%	26%	0%	-2%	11%	7%	53%	25%	-1%	-4%
<b>Houston</b>	3%	6%	26%	4%	153%	80%	63%	18%	4%	-3%	5%	3%	15%	9%	2%	-4%
<b>Phoenix</b>	5%	12%	48%	7%	291%	148%	102%	21%	0%	-7%	8%	6%	30%	15%	2%	-10%
<b>Atlanta</b>	3%	10%	36%	1%	278%	145%	114%	37%	3%	-5%	5%	3%	17%	8%	2%	-6%
<b>Los Angeles</b>	11%	27%	126%	-3%	1356%	612%	90%	-6%	-2%	-13%	43%	22%	100%	23%	-4%	-20%
<b>Las Vegas</b>	6%	18%	56%	1%	449%	229%	262%	47%	2%	-7%	11%	10%	47%	18%	5%	-8%
<b>San Francisco</b>	10%	18%	95%	0%	783%	401%	172%	29%	5%	-9%	32%	23%	55%	23%	2%	-24%
<b>Baltimore</b>	4%	11%	47%	4%	299%	158%	117%	44%	5%	-6%	4%	1%	15%	6%	3%	-6%
<b>Albuquerque</b>	8%	38%	69%	5%	558%	292%	279%	73%	11%	-3%	11%	11%	35%	18%	13%	-5%
<b>Seattle</b>	8%	18%	80%	-1%	623%	324%	264%	81%	2%	-15%	11%	6%	29%	8%	6%	-14%
<b>Chicago</b>	4%	13%	46%	5%	276%	148%	152%	65%	6%	-6%	3%	-1%	13%	6%	5%	-5%
<b>Boulder</b>	5%	25%	51%	5%	319%	170%	136%	45%	8%	-3%	5%	3%	21%	12%	7%	-2%
<b>Minneapolis</b>	4%	16%	45%	7%	260%	140%	110%	52%	5%	-3%	2%	-3%	10%	5%	4%	-4%
<b>Mt. Helena</b>	4%	20%	46%	6%	276%	148%	127%	52%	6%	-4%	3%	-1%	15%	9%	5%	-3%
<b>Duluth</b>	4%	20%	58%	10%	320%	173%	169%	78%	8%	-6%	2%	-4%	12%	6%	6%	-4%
<b>Fairbanks</b>	5%	24%	60%	15%	284%	154%	88%	46%	4%	-4%	1%	-8%	9%	4%	4%	-6%
	Retail		Second. Sch.		Restaurant		Sm Hotel		Sm Office		Strip Mall		Supermarket		Warehouse	
<b>Miami</b>	12%	4%	4%	-2%	0%	-2%	2%	8%	35%	17%	7%	1%	0%	-4%	293%	195%
<b>Houston</b>	11%	4%	5%	-2%	-2%	-7%	1%	2%	19%	11%	5%	1%	0%	-7%	89%	76%
<b>Phoenix</b>	17%	6%	8%	-4%	-2%	-8%	3%	8%	31%	17%	8%	0%	-1%	-11%	120%	101%
<b>Atlanta</b>	9%	0%	4%	-6%	-5%	-12%	-3%	-5%	21%	7%	6%	0%	-6%	-16%	105%	93%
<b>Los Angeles</b>	40%	-8%	9%	-12%	-4%	-13%	-1%	19%	72%	12%	22%	-9%	-16%	-26%	420%	280%
<b>Las Vegas</b>	17%	1%	8%	-5%	-4%	-11%	-2%	-1%	34%	12%	10%	0%	-8%	-19%	173%	148%
<b>San Francisco</b>	24%	-6%	14%	-13%	-8%	-20%	-1%	11%	40%	11%	17%	-4%	-14%	-31%	270%	214%
<b>Baltimore</b>	8%	-1%	5%	-8%	-6%	-14%	-3%	-11%	21%	7%	6%	0%	-5%	-18%	116%	104%
<b>Albuquerque</b>	19%	7%	12%	-4%	-6%	-15%	-3%	-5%	48%	24%	14%	3%	-6%	-19%	217%	203%
<b>Seattle</b>	13%	-8%	9%	-15%	-14%	-28%	-12%	-11%	33%	7%	9%	-3%	-14%	-34%	197%	171%
<b>Chicago</b>	7%	2%	6%	-10%	-6%	-11%	-4%	-16%	21%	8%	5%	0%	-3%	-17%	112%	103%
<b>Boulder</b>	11%	3%	7%	-4%	-4%	-8%	-4%	-11%	28%	15%	8%	2%	-3%	-15%	143%	135%
<b>Minneapolis</b>	6%	-3%	6%	-10%	-3%	-4%	0%	-17%	18%	6%	5%	-1%	-2%	-16%	106%	99%
<b>Mt. Helena</b>	8%	0%	7%	-7%	-5%	-7%	-4%	-15%	21%	10%	6%	1%	-4%	-16%	115%	110%
<b>Duluth</b>	8%	-3%	8%	-11%	-4%	-4%	-3%	-24%	22%	7%	6%	-1%	-3%	-19%	148%	137%
<b>Fairbanks</b>	6%	-6%	7%	-12%	0%	6%	4%	-27%	18%	4%	4%	-2%	-3%	-22%	105%	98%

**Table D.4: Annual median MLR, cooling – heating.**

	Fastfood		Hospital		Lg Hotel		Lg Office		Med Office		Midrise Apt		Outpatient		Prim. Sch.	
<b>Miami</b>	-18%	1%	-32%	-20%	-4%	-13%	-11%	49%	-23%	-21%	-16%	-15%	-21%	-15%	-26%	-14%
<b>Houston</b>	-8%	1%	-35%	-17%	-34%	-28%	-21%	35%	-21%	-16%	-8%	-6%	-18%	-9%	-20%	-4%
<b>Phoenix</b>	5%	25%	-19%	2%	-10%	-9%	0%	74%	-8%	-4%	-3%	-2%	-9%	2%	-7%	10%
<b>Atlanta</b>	-5%	3%	-38%	-9%	-91%	-57%	-48%	21%	-17%	-9%	-7%	-5%	-14%	-4%	-13%	4%
<b>Los Angeles</b>	23%	68%	-46%	-9%	-146%	-89%	-69%	8%	-22%	-15%	-17%	-6%	-3%	29%	-15%	17%
<b>Las Vegas</b>	8%	28%	-30%	2%	-87%	-57%	-27%	35%	-9%	-5%	-3%	-2%	-9%	5%	-8%	15%
<b>San Francisco</b>	6%	20%	-74%	-5%	-292%	-162%	-126%	-45%	-27%	-16%	-15%	-7%	-24%	9%	-26%	15%
<b>Baltimore</b>	-6%	-1%	-34%	-6%	-130%	-76%	-60%	-8%	-17%	-5%	-4%	-2%	-13%	-3%	-12%	6%
<b>Albuquerque</b>	8%	20%	-59%	-3%	-175%	-108%	-78%	-4%	-17%	-9%	-8%	-6%	-13%	10%	-15%	11%
<b>Seattle</b>	-3%	-1%	-75%	-3%	-315%	-174%	-136%	-50%	-23%	-7%	-8%	-3%	-21%	7%	-14%	20%
<b>Chicago</b>	-5%	-1%	-38%	-7%	-187%	-105%	-85%	-25%	-19%	-3%	-5%	-3%	-13%	-3%	-12%	6%
<b>Boulder</b>	3%	-3%	-57%	-3%	-280%	-163%	-111%	-37%	-20%	-9%	-8%	-5%	-14%	3%	-15%	9%
<b>Minneapolis</b>	-5%	-6%	-42%	-9%	-222%	-123%	-101%	-37%	-12%	-1%	-4%	-2%	-10%	-3%	-10%	4%
<b>Mt. Helena</b>	-2%	-11%	-46%	-3%	-263%	-147%	-144%	-67%	-16%	-6%	-4%	-2%	-12%	-1%	-9%	7%
<b>Duluth</b>	-5%	-13%	-50%	-9%	-287%	-158%	-174%	-77%	-16%	-1%	-4%	-2%	-10%	-4%	-9%	5%
<b>Fairbanks</b>	-4%	-16%	-52%	-8%	-249%	-138%	-82%	-37%	-6%	2%	-1%	0%	-8%	-2%	-5%	8%
	Retail		Second. Sch.		Restaurant		Sm Hotel		Sm Office		Strip Mall		Supermarket		Warehouse	
<b>Miami</b>	-24%	-23%	-12%	-5%	-17%	57%	-24%	-61%	-17%	-15%	-20%	-16%	0%	1%	58%	62%
<b>Houston</b>	-18%	-12%	-14%	0%	-5%	57%	-14%	-44%	-12%	-9%	-11%	-5%	4%	14%	24%	36%
<b>Phoenix</b>	-7%	-4%	-4%	4%	10%	74%	-4%	-31%	-2%	2%	0%	6%	15%	22%	27%	38%
<b>Atlanta</b>	-10%	1%	-10%	10%	6%	61%	-7%	-28%	-7%	0%	-7%	1%	13%	26%	-23%	-16%
<b>Los Angeles</b>	-1%	14%	-13%	27%	38%	180%	-10%	-48%	15%	24%	7%	13%	39%	80%	-197%	-93%
<b>Las Vegas</b>	-8%	2%	-5%	10%	11%	73%	-4%	-25%	3%	9%	-2%	5%	23%	38%	-19%	-7%
<b>San Francisco</b>	-13%	16%	-28%	23%	32%	133%	-10%	-33%	-13%	11%	-6%	10%	25%	57%	-231%	-176%
<b>Baltimore</b>	-9%	3%	-10%	9%	8%	49%	-4%	-15%	-10%	-2%	-6%	1%	10%	24%	-70%	-54%
<b>Albuquerque</b>	-7%	-1%	-14%	18%	18%	92%	-6%	-29%	-5%	2%	-2%	5%	18%	40%	-142%	-126%
<b>Seattle</b>	-10%	13%	-13%	44%	31%	103%	-5%	-20%	-19%	6%	-6%	6%	21%	48%	-180%	-146%
<b>Chicago</b>	-7%	-2%	-10%	17%	13%	50%	-4%	-11%	-12%	-4%	-5%	1%	7%	21%	-80%	-66%
<b>Boulder</b>	-9%	2%	-11%	14%	16%	66%	-4%	-22%	-13%	-3%	-2%	2%	10%	24%	-114%	-104%
<b>Minneapolis</b>	-6%	3%	-7%	15%	11%	39%	-5%	-6%	-11%	-3%	-4%	1%	5%	18%	-81%	-70%
<b>Mt. Helena</b>	-7%	2%	-7%	14%	13%	42%	-3%	-12%	-12%	-3%	-5%	1%	7%	20%	-99%	-93%
<b>Duluth</b>	-7%	3%	-7%	17%	11%	31%	-4%	4%	-14%	-3%	-5%	1%	5%	19%	-123%	-114%
<b>Fairbanks</b>	-5%	3%	-5%	14%	8%	18%	-3%	19%	-14%	-2%	-4%	3%	5%	21%	-89%	-87%

Table D.5: Annual median MLR, cooling only.

	Fastfood		Hospital		Lg Hotel		Lg Office		Med Office		Midrise Apt		Outpatient		Prim. Sch.	
Miami	-18%	1%	-31%	-20%	-4%	-13%	-11%	49%	-23%	-21%	-16%	-15%	-21%	-15%	-26%	-14%
Houston	-7%	4%	-29%	-17%	-8%	-12%	-14%	36%	-20%	-17%	-7%	-5%	-8%	-2%	-19%	-9%
Phoenix	6%	26%	-7%	4%	18%	5%	4%	74%	-8%	-5%	-2%	-1%	0%	6%	-6%	6%
Atlanta	0%	6%	-22%	-8%	-14%	-18%	-28%	23%	-15%	-12%	-5%	-2%	0%	1%	-11%	-1%
Los Angeles	23%	70%	-36%	-9%	-46%	-44%	-59%	6%	-23%	-20%	-14%	-4%	17%	34%	-14%	10%
Las Vegas	8%	30%	-6%	2%	-11%	-12%	-24%	35%	-9%	-7%	-2%	0%	1%	9%	-5%	12%
San Francisco	12%	29%	-25%	-4%	-33%	-32%	-74%	-37%	-24%	-24%	-4%	0%	22%	30%	-21%	2%
Baltimore	0%	3%	-11%	-3%	-7%	-9%	-28%	0%	-12%	-11%	-1%	0%	0%	0%	-9%	0%
Albuquerque	12%	32%	-9%	0%	-19%	-21%	-48%	1%	-12%	-11%	-3%	-1%	6%	15%	-6%	9%
Seattle	3%	11%	-15%	-1%	-21%	-21%	-62%	-30%	-22%	-19%	-2%	0%	9%	13%	0%	0%
Chicago	0%	5%	-8%	-1%	-6%	-7%	-26%	0%	-13%	-10%	-1%	0%	0%	0%	-5%	0%
Boulder	10%	24%	-5%	0%	-14%	-15%	-53%	-18%	-13%	-11%	-1%	0%	9%	18%	-6%	7%
Minneapolis	0%	1%	-6%	-1%	-7%	-9%	-24%	0%	-12%	-10%	-1%	0%	0%	0%	-7%	0%
Mt. Helena	3%	5%	-1%	0%	-12%	-13%	-48%	-23%	-15%	-12%	-1%	0%	4%	9%	-7%	3%
Duluth	0%	0%	0%	0%	-8%	-8%	-35%	-5%	-11%	-8%	-1%	0%	1%	0%	-4%	0%
Fairbanks	0%	0%	0%	0%	-8%	-8%	-20%	0%	-6%	-2%	0%	0%	0%	0%	-9%	1%
	Retail		Second. Sch.		Restaurant		Sm Hotel		Sm Office		Strip Mall		Supermarket		Warehouse	
Miami	-23%	-23%	-11%	-5%	-17%	57%	-24%	-61%	-15%	-13%	-20%	-16%	0%	1%	59%	62%
Houston	-7%	-7%	-10%	-4%	-6%	57%	-14%	-42%	-1%	0%	-3%	-2%	3%	6%	50%	55%
Phoenix	0%	0%	0%	2%	9%	73%	-4%	-29%	3%	5%	3%	5%	14%	15%	51%	56%
Atlanta	0%	0%	-7%	4%	0%	59%	-9%	-26%	1%	3%	0%	0%	9%	15%	0%	6%
Los Angeles	9%	11%	-10%	21%	37%	178%	-11%	-43%	26%	27%	14%	8%	46%	94%	0%	0%
Las Vegas	0%	3%	-1%	8%	10%	72%	-4%	-23%	9%	11%	2%	4%	20%	22%	17%	19%
San Francisco	10%	12%	-15%	10%	28%	122%	-10%	-28%	24%	22%	13%	6%	23%	72%	0%	0%
Baltimore	0%	0%	-8%	1%	0%	45%	-7%	-15%	1%	2%	0%	0%	4%	11%	0%	0%
Albuquerque	3%	2%	-4%	14%	16%	88%	-9%	-27%	10%	11%	6%	5%	24%	37%	0%	0%
Seattle	1%	2%	-1%	25%	19%	87%	-11%	-23%	8%	9%	1%	0%	6%	38%	0%	0%
Chicago	0%	0%	-3%	5%	2%	42%	-8%	-16%	0%	0%	0%	0%	2%	13%	0%	0%
Boulder	3%	7%	-5%	16%	18%	81%	-9%	-26%	9%	8%	8%	5%	20%	43%	0%	0%
Minneapolis	0%	0%	-4%	5%	1%	35%	-7%	-14%	0%	0%	0%	0%	3%	12%	0%	0%
Mt. Helena	0%	2%	-6%	15%	18%	70%	-9%	-23%	3%	3%	2%	0%	6%	31%	0%	0%
Duluth	0%	0%	-4%	9%	1%	21%	-9%	-16%	0%	0%	0%	0%	0%	10%	0%	0%
Fairbanks	0%	0%	-12%	8%	0%	1%	-10%	-20%	0%	0%	0%	0%	0%	13%	0%	0%



Table D.6: Annual median MLR, heating only.

	Fastfood		Hospital		Lg Hotel		Lg Office		Med Office		Midrise Apt		Outpatient		Prim. Sch.	
Miami	0%	0%	0%	0%	-5%	-5%	0%	0%	0%	0%	0%	0%	0%	0%	0%	-1%
Houston	0%	0%	2%	0%	22%	5%	3%	0%	0%	0%	0%	0%	3%	0%	0%	-1%
Phoenix	1%	2%	23%	0%	124%	52%	24%	0%	0%	-1%	3%	1%	21%	5%	0%	-3%
Atlanta	0%	3%	18%	0%	141%	63%	20%	0%	0%	-1%	2%	0%	13%	2%	0%	-3%
Los Angeles	5%	17%	98%	0%	1129%	493%	49%	-3%	-1%	-7%	31%	7%	95%	13%	-5%	-14%
Las Vegas	2%	7%	38%	0%	277%	121%	45%	0%	0%	-1%	7%	2%	48%	9%	0%	-2%
San Francisco	8%	13%	89%	0%	750%	367%	126%	13%	3%	-7%	31%	24%	55%	23%	2%	-28%
Baltimore	2%	6%	36%	0%	228%	116%	40%	2%	0%	-3%	4%	0%	16%	4%	0%	-4%
Albuquerque	5%	21%	57%	2%	421%	206%	90%	3%	3%	-2%	10%	8%	39%	15%	5%	-5%
Seattle	8%	14%	75%	0%	587%	298%	177%	17%	0%	-10%	11%	5%	29%	9%	5%	-12%
Chicago	3%	8%	38%	0%	222%	114%	61%	6%	1%	-4%	3%	0%	14%	4%	3%	-4%
Boulder	5%	17%	45%	2%	267%	140%	70%	9%	4%	-2%	5%	4%	23%	12%	6%	-3%
Minneapolis	3%	8%	37%	0%	217%	114%	53%	8%	1%	-3%	.2%	0%	11%	4%	2%	-3%
Mt. Helena	4%	15%	42%	1%	243%	129%	74%	15%	2%	-3%	3%	1%	15%	8%	4%	-3%
Duluth	5%	13%	49%	2%	278%	150%	117%	31%	3%	-5%	2%	0%	12%	6%	4%	-4%
Fairbanks	4%	16%	52%	7%	249%	136%	68%	30%	2%	-3%	1%	0%	9%	4%	2%	-6%
	Retail		Second. Sch.		Restaurant		Sm Hotel		Sm Office		Strip Mall		Supermarket		Warehouse	
Miami	0%	0%	0%	0%	0%	0%	0%	0%	0%	0%	0%	0%	0%	0%	0%	0%
Houston	1%	0%	0%	0%	0%	0%	0%	1%	2%	0%	1%	0%	0%	-1%	5%	3%
Phoenix	8%	2%	2%	0%	0%	-1%	0%	9%	12%	5%	5%	0%	-1%	-6%	34%	22%
Atlanta	6%	0%	0%	-1%	0%	-2%	0%	0%	9%	1%	4%	0%	-4%	-8%	37%	26%
Los Angeles	35%	0%	7%	-5%	0%	-5%	-1%	20%	59%	7%	19%	-5%	-13%	-20%	283%	140%
Las Vegas	14%	0%	3%	0%	0%	-2%	0%	0%	22%	3%	7%	0%	-6%	-12%	81%	47%
San Francisco	24%	-3%	12%	-15%	-4%	-15%	1%	12%	39%	10%	17%	-3%	-12%	-28%	233%	176%
Baltimore	7%	0%	1%	-1%	-1%	-6%	0%	-1%	16%	3%	5%	0%	-4%	-12%	73%	55%
Albuquerque	18%	3%	7%	-1%	0%	-7%	0%	0%	40%	14%	12%	0%	-4%	-14%	151%	131%
Seattle	12%	-6%	5%	-9%	-8%	-18%	-9%	-8%	29%	5%	8%	-2%	-14%	-30%	180%	146%
Chicago	6%	0%	3%	-2%	-2%	-6%	-2%	-8%	16%	4%	5%	0%	-3%	-13%	80%	66%
Boulder	11%	2%	5%	-2%	-1%	-5%	-1%	-5%	24%	11%	8%	0%	-2%	-11%	116%	107%
Minneapolis	5%	-1%	2%	-3%	-1%	-2%	0%	-10%	14%	4%	4%	0%	-2%	-12%	81%	70%
Mt. Helena	7%	0%	3%	-3%	-2%	-6%	-3%	-11%	17%	8%	6%	0%	-4%	-14%	99%	93%
Duluth	7%	-1%	3%	-8%	-4%	-4%	-3%	-20%	17%	5%	5%	0%	-2%	-16%	123%	114%
Fairbanks	5%	-3%	2%	-11%	-2%	-1%	-1%	-27%	15%	3%	4%	-1%	-3%	-20%	89%	87%

**Table D.7: Annual standard deviation of MLR, cooling – heating.**

	Fastfood		Hospital		Lg Hotel		Lg Office		Med Office		Midrise Apt		Outpatient		Prim. Sch.	
<b>Miami</b>	11%	8%	6%	7%	39%	19%	23%	28%	11%	19%	10%	14%	6%	10%	18%	24%
<b>Houston</b>	11%	10%	8%	8%	93%	47%	54%	50%	10%	16%	11%	16%	9%	11%	16%	21%
<b>Phoenix</b>	6%	13%	34%	20%	127%	70%	78%	78%	7%	11%	3%	14%	6%	8%	11%	17%
<b>Atlanta</b>	9%	14%	10%	9%	125%	64%	68%	64%	10%	15%	9%	12%	9%	10%	14%	17%
<b>Los Angeles</b>	10%	26%	8%	9%	77%	38%	41%	58%	13%	18%	8%	6%	17%	16%	20%	18%
<b>Las Vegas</b>	6%	23%	36%	20%	144%	78%	70%	70%	7%	11%	3%	14%	7%	9%	9%	16%
<b>San Francisco</b>	13%	29%	14%	12%	109%	58%	74%	76%	11%	14%	3%	5%	22%	22%	17%	16%
<b>Baltimore</b>	7%	15%	12%	8%	132%	69%	76%	64%	9%	14%	8%	11%	9%	10%	13%	14%
<b>Albuquerque</b>	12%	49%	37%	16%	162%	87%	70%	64%	10%	14%	3%	7%	14%	19%	14%	21%
<b>Seattle</b>	15%	37%	21%	12%	158%	84%	98%	89%	10%	15%	3%	4%	16%	21%	15%	20%
<b>Chicago</b>	6%	21%	19%	8%	174%	93%	100%	79%	11%	14%	7%	11%	9%	9%	11%	13%
<b>Boulder</b>	9%	39%	36%	15%	234%	129%	95%	80%	14%	16%	3%	8%	13%	20%	13%	19%
<b>Minneapolis</b>	6%	23%	27%	10%	215%	116%	121%	89%	7%	9%	5%	12%	7%	8%	9%	10%
<b>Mt. Helena</b>	7%	28%	31%	12%	200%	110%	114%	88%	9%	10%	1%	9%	9%	13%	8%	10%
<b>Duluth</b>	5%	24%	34%	13%	215%	117%	154%	109%	9%	11%	3%	12%	7%	7%	8%	8%
<b>Fairbanks</b>	8%	26%	40%	17%	191%	105%	74%	51%	4%	5%	1%	13%	5%	5%	5%	4%
	Retail		Second. Sch.		Restaurant		Sm Hotel		Sm Office		Strip Mall		Supermarket		Warehouse	
<b>Miami</b>	10%	13%	16%	27%	11%	5%	10%	18%	10%	16%	10%	12%	8%	14%	62%	52%
<b>Houston</b>	11%	13%	15%	24%	14%	10%	11%	26%	18%	17%	9%	11%	8%	16%	181%	168%
<b>Phoenix</b>	6%	6%	10%	20%	8%	19%	6%	21%	13%	14%	5%	5%	7%	10%	128%	126%
<b>Atlanta</b>	8%	11%	12%	18%	13%	15%	9%	26%	17%	14%	7%	8%	5%	16%	150%	142%
<b>Los Angeles</b>	11%	11%	15%	21%	7%	26%	6%	16%	23%	16%	11%	10%	9%	15%	461%	369%
<b>Las Vegas</b>	6%	8%	9%	18%	5%	26%	5%	23%	15%	15%	6%	5%	7%	14%	136%	133%
<b>San Francisco</b>	14%	7%	14%	15%	6%	26%	3%	13%	34%	23%	12%	8%	6%	8%	165%	162%
<b>Baltimore</b>	8%	9%	11%	15%	11%	17%	9%	26%	21%	15%	6%	6%	4%	15%	130%	125%
<b>Albuquerque</b>	14%	10%	16%	21%	5%	40%	4%	25%	26%	22%	13%	11%	8%	10%	242%	241%
<b>Seattle</b>	10%	6%	16%	20%	4%	34%	5%	23%	32%	21%	8%	6%	5%	11%	138%	136%
<b>Chicago</b>	6%	5%	12%	15%	9%	27%	8%	29%	22%	14%	5%	4%	3%	12%	113%	109%
<b>Boulder</b>	9%	8%	13%	14%	4%	37%	7%	29%	28%	23%	7%	6%	5%	7%	137%	139%
<b>Minneapolis</b>	5%	5%	11%	11%	9%	31%	10%	31%	18%	11%	4%	3%	3%	11%	107%	104%
<b>Mt. Helena</b>	6%	4%	11%	9%	6%	33%	11%	34%	20%	14%	5%	3%	4%	8%	98%	98%
<b>Duluth</b>	6%	5%	12%	9%	9%	32%	12%	35%	19%	10%	4%	3%	3%	11%	116%	115%
<b>Fairbanks</b>	4%	6%	11%	6%	9%	32%	16%	30%	15%	7%	3%	3%	3%	13%	80%	76%

**Table D.8: Annual standard deviation of MLR, cooling only.**

	Fastfood		Hospital		Lg Hotel		Lg Office		Med Office		Midrise Apt		Outpatient		Prim. Sch.	
<b>Miami</b>	11%	8%	7%	7%	25%	13%	17%	27%	12%	19%	10%	15%	9%	11%	18%	24%
<b>Houston</b>	12%	8%	12%	9%	23%	12%	22%	40%	11%	16%	12%	17%	12%	11%	18%	22%
<b>Phoenix</b>	5%	10%	22%	18%	72%	42%	57%	73%	8%	12%	4%	15%	8%	7%	11%	18%
<b>Atlanta</b>	9%	7%	16%	10%	17%	12%	22%	47%	11%	15%	11%	12%	12%	10%	16%	18%
<b>Los Angeles</b>	9%	22%	12%	9%	16%	14%	27%	58%	14%	18%	10%	7%	13%	13%	21%	18%
<b>Las Vegas</b>	4%	16%	22%	20%	68%	40%	49%	66%	7%	12%	4%	14%	9%	8%	10%	17%
<b>San Francisco</b>	9%	23%	16%	11%	18%	16%	32%	68%	14%	18%	3%	4%	13%	17%	24%	17%
<b>Baltimore</b>	8%	7%	13%	8%	17%	12%	21%	41%	10%	13%	9%	11%	10%	9%	14%	15%
<b>Albuquerque</b>	8%	24%	12%	13%	25%	17%	27%	52%	9%	14%	6%	8%	8%	11%	15%	23%
<b>Seattle</b>	9%	25%	19%	11%	20%	18%	27%	63%	13%	17%	4%	4%	13%	21%	19%	25%
<b>Chicago</b>	6%	9%	13%	7%	17%	13%	21%	41%	11%	14%	8%	9%	9%	9%	15%	17%
<b>Boulder</b>	9%	26%	14%	14%	26%	18%	30%	55%	11%	17%	6%	8%	9%	16%	17%	26%
<b>Minneapolis</b>	6%	10%	14%	8%	15%	13%	23%	41%	11%	14%	9%	10%	10%	9%	15%	18%
<b>Mt. Helena</b>	11%	29%	14%	13%	24%	18%	31%	49%	12%	16%	5%	7%	11%	19%	13%	22%
<b>Duluth</b>	5%	14%	15%	8%	18%	16%	27%	42%	11%	13%	9%	8%	8%	9%	15%	19%
<b>Fairbanks</b>	9%	25%	19%	10%	25%	24%	35%	49%	15%	16%	9%	4%	12%	14%	17%	28%
	Retail		Second. Sch.		Restaurant		Sm Hotel		Sm Office		Strip Mall		Supermarket		Warehouse	
<b>Miami</b>	12%	14%	16%	27%	11%	5%	11%	19%	11%	16%	12%	12%	8%	13%	39%	34%
<b>Houston</b>	13%	14%	15%	24%	13%	16%	12%	26%	10%	13%	11%	11%	7%	12%	55%	54%
<b>Phoenix</b>	6%	7%	9%	20%	8%	22%	7%	22%	7%	11%	5%	5%	7%	8%	71%	76%
<b>Atlanta</b>	9%	10%	12%	19%	11%	23%	9%	23%	9%	12%	8%	8%	8%	10%	41%	42%
<b>Los Angeles</b>	9%	10%	16%	22%	8%	31%	7%	17%	18%	16%	9%	10%	22%	16%	138%	131%
<b>Las Vegas</b>	5%	7%	7%	18%	6%	31%	5%	22%	8%	12%	4%	4%	10%	8%	60%	66%
<b>San Francisco</b>	9%	9%	16%	17%	12%	38%	3%	11%	21%	20%	10%	9%	25%	27%	103%	106%
<b>Baltimore</b>	8%	9%	11%	16%	9%	25%	8%	21%	9%	11%	7%	7%	8%	11%	46%	46%
<b>Albuquerque</b>	6%	7%	12%	22%	8%	50%	5%	22%	10%	13%	6%	7%	17%	18%	80%	87%
<b>Seattle</b>	6%	7%	13%	22%	14%	57%	3%	15%	16%	19%	7%	7%	20%	29%	94%	100%
<b>Chicago</b>	7%	7%	10%	15%	8%	33%	6%	20%	9%	11%	7%	7%	10%	15%	46%	44%
<b>Boulder</b>	6%	10%	13%	25%	11%	58%	6%	20%	11%	14%	8%	9%	21%	24%	75%	81%
<b>Minneapolis</b>	6%	8%	10%	16%	8%	34%	7%	20%	9%	12%	6%	6%	10%	16%	43%	42%
<b>Mt. Helena</b>	4%	11%	11%	22%	15%	69%	5%	20%	10%	13%	7%	8%	23%	29%	64%	69%
<b>Duluth</b>	5%	7%	11%	18%	10%	43%	5%	17%	8%	10%	6%	6%	13%	21%	42%	41%
<b>Fairbanks</b>	9%	12%	17%	37%	24%	99%	8%	20%	10%	15%	13%	13%	40%	69%	131%	129%

**Table D.9: Annual standard deviation of MLR, heating only.**

	Fastfood		Hospital		Lg Hotel		Lg Office		Med Office		Midrise Apt		Outpatient		Prim. Sch.	
<b>Miami</b>	9%	21%	61%	7%	519%	260%	614%	136%	7%	8%	33%	25%	138%	80%	6%	10%
<b>Houston</b>	5%	12%	40%	8%	235%	129%	126%	52%	14%	8%	7%	6%	21%	14%	9%	7%
<b>Phoenix</b>	8%	18%	59%	11%	375%	202%	165%	47%	12%	12%	10%	8%	31%	18%	14%	15%
<b>Atlanta</b>	5%	15%	43%	5%	319%	175%	173%	78%	11%	9%	6%	6%	17%	11%	10%	8%
<b>Los Angeles</b>	16%	36%	117%	6%	1018%	533%	105%	11%	13%	16%	43%	31%	62%	26%	17%	21%
<b>Las Vegas</b>	8%	24%	62%	3%	501%	268%	391%	104%	11%	12%	12%	12%	43%	21%	12%	13%
<b>San Francisco</b>	8%	14%	43%	3%	342%	194%	142%	39%	12%	11%	12%	12%	14%	10%	16%	19%
<b>Baltimore</b>	4%	14%	45%	8%	281%	155%	146%	71%	11%	9%	4%	5%	12%	7%	8%	7%
<b>Albuquerque</b>	8%	42%	62%	7%	507%	281%	337%	124%	17%	10%	10%	11%	22%	17%	19%	8%
<b>Seattle</b>	6%	15%	47%	6%	351%	200%	247%	112%	15%	16%	6%	6%	10%	10%	12%	12%
<b>Chicago</b>	4%	15%	40%	9%	238%	133%	178%	95%	12%	8%	2%	7%	9%	7%	8%	5%
<b>Boulder</b>	4%	25%	39%	8%	256%	144%	164%	81%	11%	7%	4%	7%	10%	11%	9%	4%
<b>Minneapolis</b>	4%	18%	41%	12%	231%	129%	128%	73%	8%	5%	1%	9%	7%	5%	7%	4%
<b>Mt. Helena</b>	3%	20%	35%	10%	203%	115%	139%	76%	10%	6%	2%	8%	6%	7%	7%	4%
<b>Duluth</b>	4%	20%	41%	14%	224%	127%	167%	97%	11%	6%	1%	11%	6%	5%	7%	4%
<b>Fairbanks</b>	7%	23%	43%	17%	197%	111%	79%	50%	5%	4%	1%	13%	4%	4%	5%	6%
	Retail		Second. Sch.		Restaurant		Sm Hotel		Sm Office		Strip Mall		Supermarket		Warehouse	
<b>Miami</b>	34%	13%	12%	7%	3%	10%	8%	16%	102%	58%	18%	6%	4%	11%	928%	701%
<b>Houston</b>	16%	8%	11%	8%	6%	14%	8%	5%	30%	20%	8%	3%	4%	11%	151%	137%
<b>Phoenix</b>	21%	10%	15%	12%	6%	14%	7%	7%	39%	24%	9%	3%	4%	13%	173%	155%
<b>Atlanta</b>	9%	3%	11%	12%	8%	16%	9%	12%	26%	12%	6%	3%	6%	18%	135%	126%
<b>Los Angeles</b>	31%	13%	12%	18%	9%	17%	6%	8%	66%	15%	17%	11%	10%	20%	428%	333%
<b>Las Vegas</b>	17%	4%	12%	12%	8%	17%	6%	7%	39%	16%	11%	3%	7%	20%	209%	191%
<b>San Francisco</b>	8%	7%	15%	16%	10%	17%	8%	7%	19%	9%	7%	4%	8%	17%	156%	153%
<b>Baltimore</b>	7%	3%	11%	13%	8%	16%	11%	16%	21%	9%	5%	2%	5%	18%	118%	113%
<b>Albuquerque</b>	16%	8%	17%	13%	9%	17%	6%	12%	46%	27%	11%	6%	4%	17%	213%	208%
<b>Seattle</b>	7%	8%	13%	19%	14%	25%	12%	16%	22%	10%	5%	4%	8%	22%	132%	130%
<b>Chicago</b>	6%	4%	11%	13%	8%	16%	10%	18%	20%	10%	4%	3%	3%	15%	106%	102%
<b>Boulder</b>	7%	4%	10%	9%	6%	12%	10%	15%	24%	15%	5%	3%	3%	13%	126%	126%
<b>Minneapolis</b>	5%	4%	10%	12%	7%	16%	13%	19%	17%	7%	4%	2%	2%	15%	103%	100%
<b>Mt. Helena</b>	5%	3%	10%	10%	7%	17%	12%	15%	17%	10%	4%	2%	3%	12%	94%	94%
<b>Duluth</b>	5%	5%	11%	12%	8%	20%	14%	20%	17%	7%	3%	2%	3%	14%	114%	112%
<b>Fairbanks</b>	3%	7%	11%	10%	8%	23%	17%	21%	14%	5%	2%	3%	2%	16%	79%	75%